Drug delivery to the female reproductive tract to prevent sexually transmitted infection and unwanted pregnancy

Hannah M. VanBenschoten

A dissertation submitted in partial fulfillment of the

requirements for the degree of

Doctor of Philosophy

University of Washington

2023

Reading Committee:

Kim Woodrow, Chair

Patrick Stayton

Jeffrey Jensen

Program Authorized to Offer Degree:

Bioengineering

University of Washington

Abstract

Drug delivery to the female reproductive tract for prevention of sexually transmitted infection and unwanted pregnancy

Hannah M. VanBenschoten

Chair of the Supervisory Committee:
Kim A. Woodrow
Department of Bioengineering

Strategies to prevent HIV infection in the female reproductive tract that offer local drug delivery, long-term efficacy, and high user acceptability are critical in pursuit of alleviating the global burden of HIV among people with female reproductive anatomy. Current pre-exposure prophylaxis (PrEP) regimens demand daily oral administration and fall short in terms of their adherence, discretion, and accessibility. Long-acting reversible contraception (LARC) modalities demonstrate sustained delivery of active pharmaceutical agents that partition to the female reproductive tract and therefore provide a technological premise for sustained, adherence independent antiretroviral (ARV) drug delivery. Here, we develop a novel multipurpose prevention technology (MPT) that incorporates ARV delivery onto a copper intrauterine device (IUD). In the first aim of this dissertation, we evaluate global access and utilization of family planning and STI/HIV prevention services in order to motivate the demand for a long-acting MPT device. This work informs the design criteria of an integrated ARV-releasing copper IUD that can deliver drug at relevant clinical doses to the vaginal mucosa to protect against HIV for at

least one year. In the second aim, we describe the fabrication and characterization of matrix and reservoir drug delivery systems (DDS) for sustained release of multiclass ARVs. We demonstrate an in-vitro-in-silico workflow to rationally design long-acting DDS for tunable release of physicochemically distinct agents. Lastly, we assess the safety and pharmacokinetics of novel MPT upon intrauterine installation in a non-human primate model and provide evidence for local drug transport from the upper to lower female reproductive tract (FRT). This work motivates the further development of long-acting MPT for prevention of unwanted pregnancy, HIV, and other prophylactic and therapeutic targets within the FRT.

TABLE OF CONTENTS

LIST OF FIGURES

LIST OF TABLES

ACKNOWLEDGMENTS

I'd like to thank my wonderful advisor, Dr. Kim Woodrow, for her invaluable guidance and unwavering support throughout my PhD. Kim is a truly brilliant, creative, and ambitious researcher whose rigorous intellectual guidance has been instrumental in shaping the quality and direction of this work. Thank you for cultivating a warm and collaborative research environment motivated by scientific curiosity. I've found my purpose and passion in research because of the work you've trusted me with, and I can never thank you enough for believing in me as you have.

I'd like to acknowledge the members of my committee: Patrick Stayton, Jen Balkus, and Jeffrey Jensen. Thank you for volunteering your time and expertise to this work. Your input has inspired deeper thinking about translating preclinical discoveries and global barriers to accessing biomedical innovations. Thank you also to my reading committee for reviewing this thesis.

This work was supported by an NIH/NIAID grant to Kim (RO1AI150325), a Gates Foundation grant to Kim and Jeff (OPP1006248), and by the Fulbright US Scholars Program.

I'd like to thank all of the Woodrow lab members who have made this journey possible through scientific and moral support. Thank you to Hannah Frizzell, Rachel Creighton, and Jamie Hernandez who offered guidance and mentorship when I first joined the lab. Ian Suydam, thank you for all of your support; your immense expertise as a chemist and researcher has benefitted this work enormously. Lastly, thank you to Peter Chien, My-Anh Doan, Ioana Tobos, Duru Tasman, Joyce Chen, and Estelle Nguyen – I'm so grateful to have had the opportunity to get to know you all as scientists and as friends. I can't wait to see everything that all of you accomplish (hopefully that involves winning trivia one day).

I would like to thank all of my collaborators in Portland and in Stockholm. Specifically, I owe endless thanks to Jeff Jensen. Some of my fondest early memories of my PhD are driving

down to OPERM to work on the guinea pig procedures. Thank you for your insightful discussions, personable mentorship, and for being a champion of reproductive health. Thank you also to Kristina Gemzell-Danielsson and my colleagues in Sweden; I never imagined such a warm working environment could exist in such a cold place! I appreciate all of the opportunities for learning and exploration I was entrusted with at Karolinska.

Thank you to all of my friends who supported me unconditionally throughout this process. To name a few – Aimee Manderlink and Doug Lescarbeau, thank you for being my family in Seattle. I can't put into words how much I owe to you both. There is no chance I would have finished this dissertation without your constant support. Thank you for bringing me on your adventures, making me laugh, and always telling me to "try harder" at the climbing gym. To my K9 family, my time in Stockholm shared with you all was the happiest of my life. Erin Ronald, thank you for being my Fulbright companion, I am forever grateful for all of our sunny memories together. Finally, thank you to Tara Martin-Chen for being my kindred spirit – I'm so proud to know you and I'm eternally grateful to have you in my corner.

Thank you to my partner, Felix, for being a source of endless support and love. Your infectious positivity, wonder, and excitement is a force of good in this world. Thank you for all of the adventures so far and all of the adventures to come. I thank my family for supporting me on this long journey and encouraging me to make it to the finish line. To my brother, Nathan, thank you for being my role model and always encouraging me to think deeper. I could get five more PhDs and you'd still be the more successful sibling. To my parents, Wayne and Susan, I am so grateful to you both. You have taught me how to work hard and never give up on my goals. This dissertation would never have even started without your lifelong support. Also, thank you for adopting Charlie, my furry four-legged soulmate.

Chapter 1. SUMMARY AND SPECIFIC AIMS

The syndemics of human immunodeficiency virus (HIV)/acquired immunodeficiency syndrome (AIDS) and unintended pregnancy pose significant health burdens globally among people who can become pregnant and people with female reproductive anatomy. Ensuring universal access to modern contraception as well as methods to prevent, diagnose, and treat HIV is critical to ameliorating these dual health burdens. Effective utilization of medical resources requires both acceptance and adherence, two factors that motivate policy and practice adaptations as well as biomedical innovations to expand the available toolbox of technology to combat HIV and unintended pregnancy. Towards preventing HIV transmission, pre-exposure prophylaxis (PrEP) is a powerful tool in which antiretroviral (ARV) drugs are formulated into a daily oral pill and taken by individuals prior to viral exposure. Despite global initiatives that have expanded its use, oral PrEP has several drawbacks, particularly for people with female reproductive anatomy, as it requires near-perfect daily adherence to effectively prevent HIV transmission in the vaginal mucosa due to poor partitioning to female genital tissue [1–3]. Clinical trials of daily oral PrEP use among women have shown adherence as low as 40% [4,5]. Issues of adherence along with side effects, cost, service delivery challenges, and lack of awareness have significantly limited global PrEP coverage [6].

Several alternative technologies have been developed in an effort to meet the demand for PrEP, including vaginal gels [7–9] and films [7,10,11], long-acting injectables (LAI) [12–14], and intravaginal rings [15–17]. Vaginal films and rings offer on-demand, local delivery of drugs directly to genital tissue, providing superior protection over oral PrEP; however, these approaches face similar issues regarding low adherence. LAIs have potential to address issues of adherence due to their low dosing frequency on the order of one injection every two months.

However, injectables are not reversible, require an oral lead-in period, and their use is often associated with pain at the injection site; thus, their clinical acceptability is lacking. In pursuit of long-acting, adherence independent, reversible PrEP that can target drug to tissue in the female reproductive tract, there is significant potential for integration with long-acting reversible contraception (LARC). LARC, defined as any method with a dosing frequency less than once per cycle or month, includes injectables, subdermal implants, and intrauterine devices (IUDs). IUDs specifically offer local delivery of active pharmaceutical agents, either spermicidal copper ions or steroidal hormones, in addition to adherence-independent use for three to ten years, discretion, cost efficiency, immediate efficacy, reversibility, and few contraindications. Despite their benefits, LARCs are not widely used in regions with the highest rates of unintended pregnancy; indeed, IUD use in sub-Saharan Africa is the lowest in the world [18].

Due to these dual needs, we propose to improve the clinical efficacy, adherence, and utilization of PrEP while also bolstering the perceived benefits of LARC by combining HIV prevention with a copper-releasing IUD. This approach, called multipurpose prevention technology (MPT), has the potential to revolutionize sexual and reproductive health by simultaneously preventing HIV and unwanted pregnancy without the need for regular user adherence. We propose to investigate two well-characterized polymeric drug delivery systems, the conventional monolithic matrix and the core-sheath reservoir, to offer long-acting delivery of physicochemically distinct ARVs to the female reproductive tract with the goal of achieving at least one year of protection against HIV. Ultimately, this device may significantly increase the incidence of PrEP and contraception in settings where both are in high demand for at-risk populations. As such, the goal of this thesis is to characterize the potential for MPT to improve access and utilization of sexual and reproductive healthcare, to develop a novel, long-acting

MPT that offers sustained delivery of multiple ARVs integrated onto an existing LARC method, and to assess its clinical potential in an *in vivo* non-human primate pharmacokinetic model.

1.1 AIM 1

Aim: Investigate the demand and potential for improved and combined family planning and HIV-prevention technologies.

Gap: Existing needs in sexual and reproductive health (SRH) care for people capable of pregnancy and people with female reproductive anatomy are well understood and point to a demand for discreet, long-acting, user-controlled multipurpose prevention technology (MPT). However, the acute demand for improved SRH services and technology during major public health emergencies, specifically the COVID-19 pandemic, has not been synthesized on a global scale. Here, we provide context for the relevance of developing MPT in the wake of the pandemic by systematically reviewing original literature pertaining to the impact of the COVID-19 pandemic on access to and utilization of SRH services. We identified geographical and demographical differences in access to and utilization of SRH services – including family planning and STI prevention methods – and synthesized global barriers to SRH caused by the pandemic.

Impact: This work premises research, policy, and practice adaptations in the context of SRH to remediate gaps in our understanding of populations that were and continue to be significantly affected by the COVID-19 pandemic and to address barriers to accessing and utilizing care. We identified regions where impacted access to contraception, particularly LARC methods, correlated with significant barriers to STI/HIV prevention and care, thus motivating MPT. We also found that marginalized groups with distinct SRH needs, such as adolescents and sex

workers, faced exacerbated challenges to accessing family planning and PrEP. These findings strongly motivate the development of MPT that can combine contraception and HIV prevention into a single, discreet, female-controlled, and long-acting technology that minimizes identified barriers to care.

Thesis Chapter(s): Chapter 3

1.2 AIM 2

Aim: Design and characterization of drug delivery strategies for sustained release of contraceptive and antiretroviral agents.

Gap: Long-acting drug delivery systems (DDS) that offer sustained release of active pharmaceutical agents (API) in the female reproductive tract have potential to improve the contraceptive and pre-exposure prophylactic toolbox. Here, we demonstrate the development of two DDS designed for nonsurgical permanent contraception and for multipurpose prevention technology, leveraging local and targeted delivery to the FRT to achieve sustained durations of use. No medical device is currently available that provides permanent contraception nonsurgically, representing a major gap for people capable of pregnancy who have reached their desired family size. We used electrospun fiber technology to generate drug-eluting microparticles that can be perfused transcervically into the fallopian tubes to cause tubal occlusion via scar tissue formation. Moreover, multipurpose prevention technology that integrates prevention of unwanted pregnancy with protection against HIV is limited in its duration of use, with the longest window of protection being 6-months for one modality in preclinical development. We investigated two long-acting polymeric drug delivery systems

(DDS), the conventional matrix and the core-sheath reservoir, for sustained delivery of single and triple-ARV combinations for at least one year.

Impact: Capitalizing on the tunability of polyester electrospun fiber formulations, we developed microparticles that can release physicochemically distinct sclerosing agents on acute and sustained release timescales. In a novel guinea pig model, we demonstrated the potential of this platform to generate scar tissue and inflammatory requisites to tubal occlusion. This biomaterial strategy represents progress towards expanding the permanent contraception toolbox with implications for expanding access to contraception globally and domestically. Insofar as MPT development, we demonstrated an in-vitro-in-silico workflow that permits rapid design and optimization of matrix and reservoir DDS for tuned release of physicochemically unique active agents. The design and characterization of modular ARV-IUDs that can release multi-class ARVs on one- to three-year timescales potentiates future development translation of this MPT device. This device will be highly impactful for individuals at risk of vaginal HIV transmission and unwanted pregnancy as an adherence independent, long-acting, discreet, and reversible modality.

Thesis Chapter(s): Chapter 4, Chapter 5

1.3 AIM 3

Aim: Evaluate the safety and pharmacokinetics of an ARV-releasing intrauterine device in nonhuman primates.

Gap: The ability to target antiretroviral drugs safely and effectively to the lower female reproductive tract via intrauterine delivery is not known, nor are the pharmacokinetics of intrauterine delivery of any drug other than the hormone levonorgestrel. As such, we determined

the *in vivo* release behavior of novel, long-acting DDS formulations integrated onto an IUD frame and evaluated the safety of local delivery of ARVs to the upper female reproductive tract. We determined partitioning behavior of the NNRTI dapivirine into plasma, vaginal secretions, and reproductive tract tissue to assess whether DDS candidates can achieve sustained protective drug concentrations in genital tissue.

Impact: This pharmacokinetic study showed protective levels of ARV in vaginal fluid and tissue upon *in utero* ARV-IUD instillation, potentiating further clinical translation of this novel MPT. Moreover, drug content retained in ARV-IUDs evidences the long-acting potential of this delivery system for up to one-year of protection against HIV. Significantly, this work demonstrates the feasibility of intrauterine delivery of drugs targeted for action in the vaginal tract and sheds light on the existence of a local drug transport mechanism from the upper to lower FRT. The implications of this aim premise further development of the ARV-IUD system with efficacy studies against a SHIV challenge in a rhesus macaque model. More generally, the ability to deliver drugs via an IUD that are intended for purposes beyond contraception has significant implications for treatment of various pathologies in the FRT, such as endometriosis and ovarian cancer, and prophylaxis of other STIs such as chlamydia and gonorrhea.

Thesis Chapter(s): Chapter 6

Chapter 2. INTRODUCTION TO RESEARCH

Partially adapted from: **VanBenschoten, H.,** Woodrow, KA: Vaginal Delivery of Vaccines. Advanced Drug Delivery Reviews. 178 (2021).

2.1 ABSTRACT

Individuals with female reproductive anatomy (commonly referred to as women*) are disproportionately burdened with syndemic effects of HIV/AIDS and unwanted/unplanned pregnancy. Here, we will review the current global incidence of HIV/AIDs and discuss its disproportionate impact on subpopulations including women and girls. The prevailing strategy to prevent HIV infection, called pre-exposure prophylaxis (PrEP), is a daily oral pill that is effective at inhibiting viral transmission when adhered to strictly. We will discuss the mechanisms of oral PrEP including its partitioning to the female reproductive tract (FRT) and review alternative drug delivery modalities to prevent vaginal HIV infection. We will also review the burden of unplanned and unwanted pregnancy in people who can become pregnant and discuss available contraceptive methods. We will review the state of emerging multipurpose prevention technology, devices that offer dual protection against STIs and unwanted pregnancy. Informed by design criteria for sustained and targeted drug delivery to the FRT, we will discuss two major classes of long-acting drug delivery systems – the monolithic matrix and the core-sheath reservoir– and discuss the influence of material properties on drug dissolution and clinical use. Lastly, we will briefly review female reproductive physiology as it relates to evidence that describes drug transport mechanisms in the FRT. The synthesis of this background information informs the design and development of next-generation multipurpose prevention technology.

* We acknowledge that not all individuals who identify as women have female reproductive anatomy and not all people with female reproductive anatomy identify as women.

2.2 HIV INFECTION IN WOMEN

2.2.1 Global burden of HIV infection in women

Human immunodeficiency virus (HIV) has infected 79.3 million people and has caused 36.3 million deaths since the beginning of the epidemic. In 2020 it was estimated that 37.7 million people aged 15-49 years old were living with HIV, representing 0.7% of the adult population [19]. HIV has a disproportionate impact on marginalized populations and is unequally distributed throughout various regions of the world. The Southern Africa region is the most severely affected by the HIV epidemic, where approximately 3.6% of adults are living with HIV. This population accounts for nearly two thirds of the people living with HIV worldwide. HIV is the leading disease burden in sub-Saharan Africa, with the highest HIV-seropositive population residing in Eswatini (27% prevalence) [20].

The HIV epidemic disproportionately impacts women. In 2020, the WHO estimated that 19.3 million women were living with HIV; compared to the 16.7 million men living with HIV, this represents nearly 54% of the adult population [19]. Every week, 6000 young women (aged 15-24) become infected with HIV. In sub-Saharan Africa, young women are twice as likely as men to be living with HIV and women accounted for 63% of new infections in 2020 [20]. Figure 2.1 illustrates the disparate share of women in populations living with HIV and the disproportionate prevalence among women in sub-Saharan Africa. Reasons for the high burden of HIV among women are myriad and relate to gender inequalities, differential access to services, sexual violence which increases social and biological vulnerability, and physiological susceptibility to viral acquisition. These issues are exacerbated for individuals who face multiple forms of discrimination. Indeed, the incidence of HIV is 10-times higher among female sex workers than the general population. As a consequence, HIV is the leading cause of death

globally for women aged 15-49 [21]. This enormous global burden has detrimental impacts on the health, economic status, and overall well-being of individuals, communities, and nations.

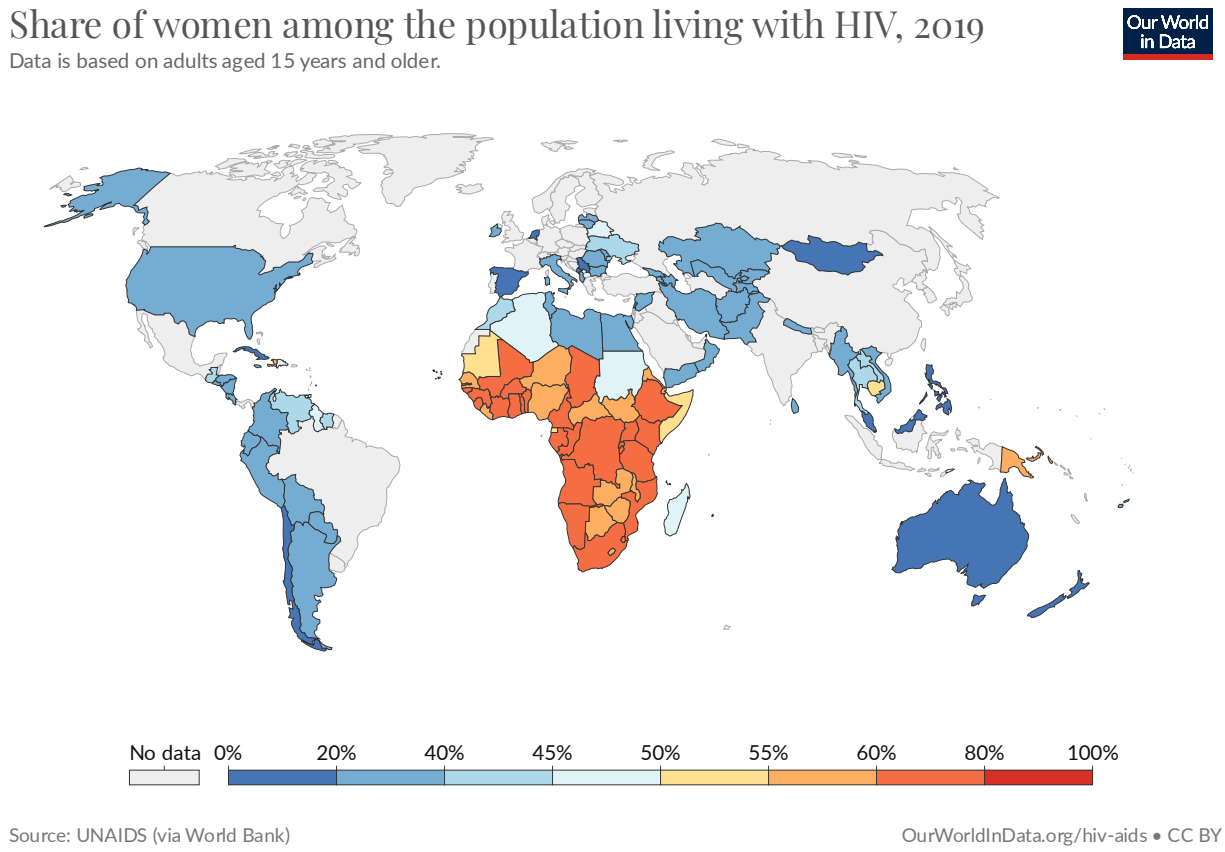

FIGURE 2.1. **Map of the proportion of women among the HIV-positive population aged 15 and older.** Estimates made for 2019 by UNAIDS with data from the World Bank Group [4,5].

2.2.2 HIV Infection and Pathology in the Female Reproductive Tract

In order to make progress towards reducing the incidence of HIV in women, it is necessary to understand the physiology of the vaginal mucosa and molecular mechanisms of HIV infection. HIV-1 is a lentivirus composed of two copies of single-stranded RNA enclosed by a capsid containing viral protein p24 and glycoproteins gp120 and gp41. The virus is adept at efficiently infecting mucosal surfaces throughout the body. It is estimated that the female genital tract (FGT) is the most common route of HIV transmission, followed by the male genital tract,

the rectum, direct blood stream contact, and vertical transmission from mother to child [22]. The human vagina is lined by a non-keratinized stratified squamous epithelium that is covered apically by a layer of cornified cells that are permeable to microbes as well as cellular and molecular mediators of immunity [23]. The type II mucosa of the lower genitourinary tract is rich in innate and adaptive immune cells, but lacks organized mucosa-associated lymphoid tissue (MALT) found in the type I mucosa of the upper FRT. The organizational and immunological differences between the upper and lower FRT are illustrated in Figure 2.2.

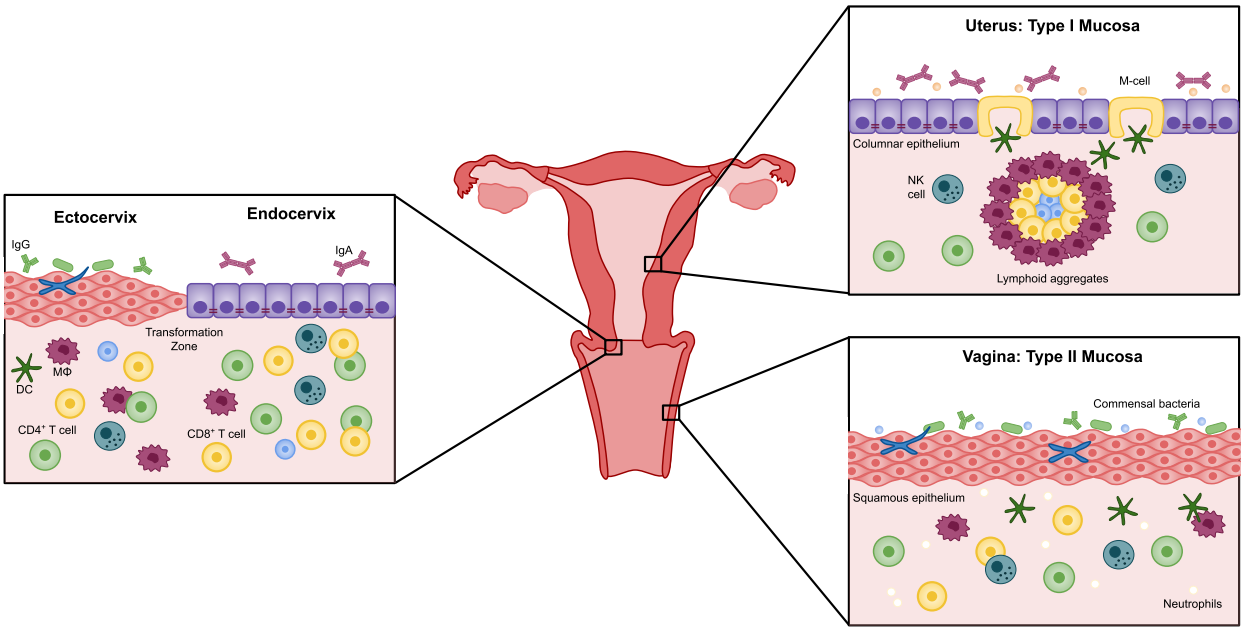

FIGURE 2.2. **Structural and cellular differences in the immunological milieu of the upper and lower female reproductive tract** [24].

Primary HIV infection in the FGT was previously thought to occur only in the endocervix, which is lined by a vulnerable single layer of cuboidal epithelial cells. However, hysterectomized women and macaques lacking a cervix can be infected with HIV and simian immunodeficiency virus (SIV), respectively; thus, it is evident that HIV can and does penetrate

the stratified squamous epithelium of the vagina, though it does so relatively inefficiently [25]. Estimates suggest that heterosexual intercourse results in transmission in only 0.1% of exposures, and transmission is highly correlated with viral load in seminal fluid [26]. Much of this inefficiency is thought to be the result of innate physical barriers such as the presence of multiple cell layers in the vaginal epithelium which form a formidable obstacle to accessing the lamina propria, wherein cells targeted for infection reside. This effect is enhanced during the follicular and ovulatory stages of the menstrual cycle when a decrease in progesterone drives epithelial thickening [27,28]. Additionally, cervicovaginal mucus has been shown to impair the mobility of HIV molecules [29].

Despite these innate mechanisms of defense, there are numerous probable routes of transmission across an intact vaginal epithelium. Langerhans cells (LCs), which patrol the cervicovaginal mucosa, have dendritic cytoplasmic processes that extend into the vaginal lumen and sample antigens. Though they do not express CD4 or CCR5, LCs express surface HLA-DR, CD1a, and mannose-dependent C-type lectin receptors that may be involved in DC-mediated HIV transmission [30,31]. Upon capture of virions, immature DCs in the epithelium migrate and present virus to $CD4^{+}CCR5^{+}$ T cells abundant in the lamina propria, thus permitting viral amplification. The precise dynamics of this antigen-presentation cascade are unclear, though it is thought to occur rapidly and results in transport of virus to underlying cells in a matter of minutes. Evidence also points to direct primary infection of $CD4^{+}CCR5^{+}$ T cells as a mechanism of HIV transmission, wherein viral particles can access T cells typically residing in deeper layers of tissue via tears, inflammation, and hormone-induced thinning of the stratified epithelium. Coinfection with other STI's can also increase susceptibility to vaginal HIV infection through epithelial weakening and immunogenic T cell recruitment [25]. Upon entry into the lamina

propria via LC-mediated transport or direct contact, HIV enters $CD4^+CCR5^+$ target cells and generates a "nidus" of infection, infecting more and more recruited cells that eventually travel to secondary lymphatic tissue and systemic circulation. Thus, the vaginal mucosa serves as an effective portal of entry for systemic HIV infection, a process that can be exacerbated by adverse coincidental conditions of the mucosal microenvironment.

Depletion of $CD4^+$ T cells is a hallmark of early HIV infection, as these cells express HIV-receptor CCR5 and are transcriptionally active. Primary HIV/SIV infection is marked by extreme follicular hyperplasia as B cells in secondary lymphoid tissues become activated and expand; however, as infection becomes chronic, this initial activity is replaced by lymphoid depletion caused by follicular fibrosis and involution, culminating in destruction of germinal centers [32]. B cell and T follicular helper (Tfh) cell impairment is consistent with a weak or ineffective neutralizing antibody response to HIV/SIV infection. One strategy to prevent vaginal HIV transmission involves inhibiting $CD4^+$ T cell infection by preventing APC uptake and direct $CD4^+$ T cell contact with virions. Preventing viral replication by enhancing antiretroviral activity and bolstering immunity through vaccination are other means by which the viral mucosa may be protected. These antiviral strategies will be discussed in depth in section 2.2.3.

2.2.3 Pre-Exposure Prophylaxis for Preventing HIV Infection in Women

2.2.3.1 Overview of Pre-Exposure Prophylaxis Prevalence

Pre-exposure prophylaxis refers broadly to medicine taken before exposure to a disease-causing agent to prevent acquisition of that disease. In the context of HIV, PrEP involves administration of antiretroviral (ARV) drugs that inhibit viral entry and/or replication in vulnerable cell types. Currently, there are two medications approved for use as PrEP – Truvada®

and Descovy® – that are 99% and at least 74% effective at reducing the risk of acquiring HIV through sex and injection drug use, respectively [4,33]. PrEP was included on the WHO Essential Medicines List in 2017 and over 70 countries have expanded normative recommendations for its use since 2019 [34]. Despite its clinical potential and global initiatives promoting its implementation, substantial barriers to PrEP access and use exist including dosing frequency and adherence, side effects, cost, service delivery, and awareness [35]. As such, less than 500,000 people globally were estimated to have initiated PrEP as of 2019. Figure 2.3 depicts total PrEP initiations by country as of March 2022 according to aggregate data from PrEP programs and clinical trials from over 78 countries. In the US, the CDC estimates that only 10% of women who could benefit from PrEP were prescribed it in 2019 [36]. In order to increase PrEP coverage, improvements must be made across the spectrum of biomedical innovation to program implementation. From a biomedical engineering perspective, providing a longer duration of protection via alternative drug delivery modalities is the highest priority to shift away from the daily or event-driven (coitally dependent) models of PrEP administration [34].

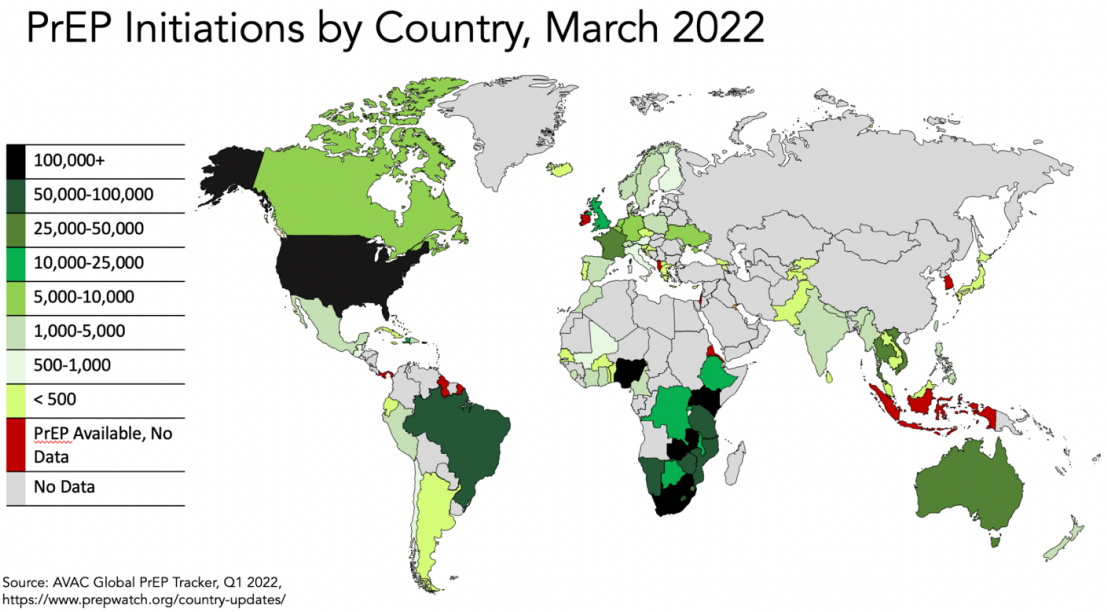

FIGURE 2.3. **PrEP initiations by country as of March 2022**. Data collected from AIDS Vaccine Advocacy Coalition Global PrEP Tracker initiative [6].

2.2.3.2 Antiretroviral Drugs

Antiretroviral drugs fall into eight main classes according to the mechanism by which they prevent HIV (Table 2.1). NRTIs, NNRTIs, and integrase inhibitors work intracellularly to prevent viral replication and maturation by interfering with the reverse transcriptase process (NRTIs and NNRTIs) and by inhibiting integration of viral genetic material with host DNA (integrase inhibitors) [37,38]. Protease inhibitors prevent cleavage of viral polyproteins into functional subunits that are necessary for viral assembly and escape from a host cell [38]. Extracellular ARVs prevent the entry of HIV virions into and from target cells. These drugs either bind to receptors on host cells (CCR5 agonists, post-attachment inhibitors) or the HIV envelope protein (fusion inhibitors, attachment inhibitors) [39].

TABLE 2.1. Classes of antiretroviral drugs and FDA approved ARVs.

Class	Mechanism of action	Drugs (Abbrv.)
Nucleoside/ nucleotide reverse transcriptase inhibitors (NRTI)	Inhibit the construction of proviral DNA during the reverse transcriptase process to stop viral replication	Abacavir (ABC) Didanosine (ddl) Emtricitabine (FTC) Lamivudine (3TC) Stavudine (d4T) Tenofovir (TDF, TAF) Zidovudine (AZT, ZDV)
Non-nucleoside reverse transcriptase inhibitors (NNRTI)	Binds to the reverse transcriptase enzyme to stop viral replication	Delavirdine (DLV) Doravirine (DOR) Efavirenz (EFV) Dapivirine (DPV) Etravirine (ETR) Nevirapine (NVP) Rilpivirine (RPV)

Integrase inhibitors	Targets HIV integrase protein to prevent viral genomic DNA insertion into host DNA	Bictegravir (BIC) Dolutegravir (DOL) Raltegravir (RAL) Elvitegravir (EVG) Cabotegravir (CBG)
Fusion inhibitors	Binds to gp41 subunit of the HIV envelope to prevent the fusion of the HIV envelope protein with CD4 cell membranes	Enfuvirtide (ENF)
CCR5 agonist	Binds to CCR5 co-receptor on $CD4^+$ cells and blocks viral entry	Maraviroc (MVC)
Protease inhibitors	Blocks the activity of protease enzymes used by HIV to break down polyproteins to use for assembly of new viral particles, resulting in neutralized virions	Atazanavir (ATZ) Darunavir (DRV) Lopinavir (LPV) Fosamprenavir (FPV) Nelfinavir (NFV) Ritonavir (RTV) Indinavir (IDV) Tipranavir (TPV)
Attachment inhibitors	Binds to gp120 spike protein on HIV envelope to prevent attachment to host cells	Fostemsavir (FTR)
Post-attachment inhibitors	Binds to $CD4^+$ receptors to prevent conformational change of the HIV gp120 protein upon binding prohibiting co-receptor interaction	Ibalizumab (IBA)

It is necessary to understand the pharmacodynamics (PD) and pharmacokinetics (PK) of ARVs in genital tissue in order to define dosing strategies that may confer protection at these anatomical sites. Key metrics of the potency of a given ARV is its half maximal effective concentration (EC_{50}) or half maximal inhibitory concentration (IC_{50}); these values refer to the concentration of drug required for 50% inhibition of viral infectivity *in vitro*. Clinically, ARVs are employed at concentrations well above the IC_{50}; commonly reported values are the protein-adjusted inhibitory concentration for 90 and 99% viral inhibition (PA-IC_{90}/PA-IC_{99}). These values account for the concentration of drug that is bound and functionally inactivated by plasma proteins and are considered more predictive of ARV potency [40,41]. A low IC_{50} or PA-IC_{90}/PA-

IC_{99} indicates a highly potent drug or drug combination. The terminal half-life ($t_{1/2}$) in plasma is another important consideration that informs the frequency of dosing required to maintain sufficient inhibitory drug concentrations. A longer terminal half-life indicates a drug delivery regimen that requires less frequent dosing.

Administering multiple ARVs in combination is a well-established strategy to increase the efficacy of PrEP. Studies have shown that combination PrEP that incorporates ARVs of the same class [42] and multiclass ARVs have synergistic effects in inhibiting HIV infection and therefore have lower IC_{50} values in combination than upon single-drug administration [43]. Monoclass combination ARV PrEP is effective because it can account for viral mutations that confer resistance of HIV to one or more ARV with the same inhibition mechanism [44]. There is virtually no cross-resistance in HIV mutations between ARV drug classes, therefore multiclass ARVs administered in combination can account for drug-resistant HIV strains and bolster the efficacy of less potent ARVs. For instance, NRTIs are characteristically less potent than NNRTIs and PIs, therefore it is common for NRTIs to be administered in combination with an NNRTI. NNRTIs have been shown to increase the potency of NRTIs because NNRTIs can inhibit removal of NRTIs by mutated viral reverse transcriptase [45]; conversely, NNRTI hyper-susceptibility has been observed for NRTI-resistant viruses [46].

2.2.3.3 Oral PrEP

Evidence that antiretroviral PrEP is effective at preventing HIV transmission during receptive heterosexual intercourse derives from two multinational, randomized, placebo-controlled clinical trials of daily oral emtricitabine-tenofovir disoproxil fumarate (TDF-FTC) [47,48]. The Partners PrEP trial was conducted between July 2008 and November 2010; 4758

serodiscordant heterosexual couples were enrolled in Kenya and Uganda and assigned to one of three treatment arms: once-daily oral tenofovir (TDF), combination daily oral tenofovir-emtricitabine (TDF-FTC), or placebo [47]. For 48% of the couples followed, the seronegative partner was female. In total, 82 seroconversions occurred during the study period – 17 in the TDF group, 13 in the TDF-FTC group, and 52 in the placebo group; this indicates a relative reduction in HIV incidence of 67% and 75% with TDF and TDF-FTC, respectively. In the TDF-2 study, 1219 high risk men and women in Botswana were administered daily oral TDF-FTC or placebo [48]. The treatment group saw a 62.2% reduction in the relative risk of HIV infection; however, this study raised questions of the safety of daily oral TDF-FTC as participants who received PrEP had a significant decline in bone mineral density.

Despite promising findings among serodiscoordinant couples, these results were not substantiated in studies conducted only among women. Two studies, FEM-PrEP and VOICE, demonstrated no benefit of oral PrEP among heterosexual women at risk of HIV. The FEM-PrEP study enrolled 2120 women at risk of HIV in sub-Saharan Africa and administered daily oral TDF-FTC or placebo [49]. TDF-TDC had no significant effect on HIV prevention and was associated with increased side effects. This result is likely the effect of adherence to the daily oral regimen, which was estimated to be as low at 40%. The VOICE trial was conducted in South Africa, Uganda, and Zimbabwe, enrolling 5029 HIV-negative women who were assigned to once daily oral TDF, TDF-FTC, 1% TFV vaginal gel, or placebo [50]. None of the study arms resulted in significant protection against HIV and similar to the FEM-PrEP trial, adherence was low among participants.

These unsuccessful clinical trials highlight several downsides to oral PrEP that limit its acceptability and use. To reach effective levels in the bloodstream and at vulnerable tissues,

PrEP must be taken in a daily oral formulation and adhered to strictly. Adherence has been identified as the most prohibitive challenge preventing more widespread use and adherence to PrEP is highly correlated with its efficacy [5,51]. The requirement for daily adherence is particularly stringent for women taking PrEP to prevent HIV infection from receptive heterosexual intercourse – women must adhere near-perfectly to daily oral PrEP in order to remain protected. This is in part due to limitations of the oral drug delivery route in achieving high drug accumulation at anatomical sites of infection necessary to prevent transmission. Drug partitioning to the female genital tract is limited upon oral drug delivery and certain classes of ARVs are particularly susceptible to low FGT partitioning. Indeed, orally administered NNRTIs and PIs achieve lower drug concentration in the FGT relative to plasma concentrations compared to less potent NRTIs [1,2,52]. Alternatives to oral PrEP for preventing vaginal HIV transmission have been explored in order to enhance FGT penetration, prolong the duration of action, reduce the frequency of dosing, and minimize adherence requirements. An overview of alternative strategies for PrEP delivery that have advanced to clinical trials is summarized in Table 2.2.

TABLE 2.2. Summary of alternatives to oral PrEP.

PrEP Method	**Route**	**ARVs Used**	**Dosing Frequency**	**Efficacy (relative reduction in HIV)**
Gels	Vaginal	Tenofovir, Dapivirine	Pericoitally	39-54% (vs. placebo)
Films	Vaginal	Tenofovir, Dapivirine	Pericoitally	Not reported
Injectables	Intramuscular	Rilpivarine, Cabotegravir	Every 8 weeks	34% (in MSM, vs. oral TVF-FTC)

Rings	Vaginal	Dapivirine, Maraviroc	4-13 weeks	27-37% (vs. placebo)

2.2.3.4 Topicals for PrEP

Vaginal gels have been investigated for their ability to target active agents to the FGT and offer on-demand protection against HIV. Gels containing the NRTI tenofovir (TVF) emerged as the first technology developed to address the issue of ARV partitioning to the FGT with oral dosing. The CAPRISA 004 clinical trial assessed the safety and efficacy of vaginal TVF gel. HIV-negative women in South Africa were enrolled in the trial and instructed to apply a 40 mg dose of gel containing 1% TVF with a prefilled vaginal applicator pericoitally [3]. In the high-adherence group, this strategy proved to reduce the incidence of HIV by 54% compared to the placebo arm and resulted in a 39% reduction in HIV acquisition overall. Vaginal gels have proven to be superior to oral PrEP at targeting and protecting the FGT. One clinical study of a vaginal TVF gel measured 10^3-10^4 ng/g and 10^5-10^6 ng/g of TVF in vaginal tissue and cervicovaginal fluid, respectively. These values represent a 1000 to 10,000-fold increase in vaginal tissue and CVF tenofovir concentrations compared to dosing with the oral formulation of the same drug [53]. Another cross-over study comparing vaginal TVF gel with oral tablets found that vaginal TDF was over 130-fold higher with vaginal compared to oral dosing [54]. Gels have practical advantages as they can be dosed on-demand, may offer lubrication during sex, can be discreet and can offer fewer systemic side effects than oral pills [55]. However, their use is patient-dependent and coital adherence remains a challenge translation into use at a larger scale. The “real-world” efficacy of vaginal gels is also in question; despite earlier clinical trials showing promising pharmacokinetic data, the VOICE trial showed that a 1% TVF gel was

ineffective at preventing HIV in study participants [36]. Due to conflicting reports on their efficacy, vaginal gels have not been prioritized as a PrEP modality in recent years and no vaginal gel is currently marketed for use in women.

Vaginal films have also been investigated as an alternative to vaginal gels. Films are dissolvable strips of ARV-containing material that are inserted 15 minutes prior to intercourse, offering rapid, on-demand protection against HIV. In a Phase 1 trial comparing dapivirine gel or film and placebo gel or film, the DPV gel and film resulted in 4 $\log_{10}$ higher [DPV] in cervical and vaginal tissues than plasma; however, tissue concentrations of DPV were 3-5 times higher among gel users than film users [9]. Despite this finding, 80% of film users compared to 68% of gel users noted that they would use a film if it ever became available to prevent HIV. In a subsequent two-arm crossover study, women received a single dose of 1.25 mg of vaginal DPV gel or film [56]. Concentrations of DPV in plasma, CVF, and cervical tissue were not statistically different among gel and film users and both the gel and film resulted in reduced cervical tissue infectivity upon *ex vivo* HIV challenge 5 hours post dose. Thus, vaginal films appear comparable to vaginal gels with respect to tolerability, pharmacokinetics, and antiviral activity. Similar results have been reported in studies with tenofovir-loaded films in the FAME-04 and FAME-05 clinical trials [7,10]. Vaginal films present a promising strategy for on-demand HIV PrEP due to their discretion, quick dissolvability, reduced tendency to leak, and smaller volume which may minimize side effects.

2.2.3.5 Long-Acting Injectables for PrEP

Long acting injectables are an ARV delivery approach that offers adherence-independent dosing with an intramuscular injection of a nanocrystalline suspension of either rilpivarine

(RPV-LA) or cabotegravir (CAB-LA). Rilpivirine, an NNRTI, and cabotegravir, an integrase inhibitor, are water insoluble drugs with long terminal half-lives that allow them to remain in circulation for an extended period of time. Two Phase 1 clinical trials have assessed the safety and PK of RPV-LA which demonstrated good tolerability and high plasma accumulation after administration [57,58]. Injections of 300, 600, and 1200 mg of RPV-LA were administered intramuscularly and showed plasma concentrations of 6.4, 16.2, and 30.2 ng/ml, respectively, 84 days after dosing. RPV was detectible in CVF 8-hours post-dose and attained higher concentrations than that measured in plasma, indicating favorable partitioning in the FGT. Treatment with the 1200 mg dose resulted in high antiviral activity in CVL samples between day 28 and 56 [57]. A follow up Phase 1 trial, the MWRI-01 study, assessed the PK and efficacy of RPV-LA i.m. injections in seronegative HIV patients. The study found that RPV partitioning to rectal tissue was two-fold higher than vaginal and cervical tissue and resulted in no viral suppression in the FGT [58]. Results from this study suggest that RPV-LA alone is insufficient to prevent HIV acquisition via the vaginal mucosa.

Cabotegravir is an integrase strand-transfer inhibitor (INSTI) that has also been investigated as an ARV candidate for long-acting injectables. CAB-LA has successfully shown safety and tolerability in clinical trials, although some patients reported experiencing mild to moderate local reactions at the injection site [12,13]. In a study of 8 male and female subjects, CAB-LA resulted in measurable plasma concentrations up to 52 weeks after a single dose and achieved plasma concentrations above the PA-IC_{90} for 16 weeks [12]. In a Phase 2A clinical trial in HIV-negative men and women, a 600 mg dose of CAB-LA was administered in a single 3 mL injection every 4-8 weeks and was highly tolerable, resulting in trough CAB concentrations above the PA- IC_{90} in 95% of participants [59]. In a large randomized noninferiority trial, an

intention-to-treat population of transgender women and men-who-have sex with men were administered either CAB-LA in a 600 mg dose i.m. every 8 weeks or daily oral tenofovir disoproxil fumerate—emtricitabine (TDF-FTC) and followed for 153 weeks [60]. Results from the first interim endpoint analysis showed that the incidence of HIV in the CAB-LA group was 0.41 per 100 person-years, while the incidence in the oral TDF-FTC group was 1.22 per 100 person years, representing significant superiority of CAB-LA compared to TDF-FTC at preventing HIV. However, in participants infected with HIV after CAB-LA treatment, INSTI resistance was noted in 4 of 9 incident cases, indicating a level of drug resistance that must be addressed with combination ARV strategies.

In a recent clinical trial, the LATTE-2 study, LAIs of ralpivirine and cabotegravir were tested in combination [14]. 309 treatment naïve adults with HIV were enrolled and randomly assigned to receive either 400 mg of CAB-LA plus 900 mg of RPV-LA at 4-week intervals, 600 mg of CAB-LA plus 900 mg of RPV-LA at 8-week intervals, or daily oral CAB plus abacovir-lamivudine. At 94 weeks, viral suppression was 84% in the oral group, 84% in the 4-week LAI group, and 94% in the 8-week LAI group. These findings suggest that 4- and 8-week intervals of LAI injections are noninferior to daily oral ART treatment and motivate PrEP strategies in which combination RPV-LA and CAB-LA could prevent infection from antiviral resistant HIV strains. Patient tolerance and acceptability of LAIs has generally been high; trial participants cited ease of use, long-term protection, discretion, and non-interruption of sex as benefits. Bekker et al. noted that in follow up to a Phase 1 trial of RPV-LA in African women, 68% of patients in the treatment arm reported interest in future injectable use, saying they would “definitely use it" [61]. Further clinical trials are necessary to assess the efficacy of LAIs to prevent vaginal HIV transmission. Moreover, the formulation and side-effect profile of LAIs has room for

improvement as pain upon injection is a noted downside. Most trials have included an oral lead-in period, which may also compromise the clinical acceptability of this PrEP modality [8]. Importantly, LAIs are not reversible, presenting a major drawback given a risk for negative reactions with no immediate course of remediation.

2.2.3.6 Intravaginal Rings for PrEP

ARV-releasing intravaginal rings (IVR), which parallel products currently in development for contraception, have been investigated for their potential as PrEP delivery vehicles. Rings are composed of a silicone-elastomer ARV-containing reservoir surrounded by a rate-controlling membrane that offers sustained release of microbicidal agent for a period of up to 4-weeks. In Phase 1 clinical trials, participants treated with vaginal rings noted that they are comfortable and have the advantage of being user-controlled and coitally-independent [62]. Two Phase 3 clinical trials of dapivirine vaginal rings have demonstrated the ability of the device to deliver DPV at a sustained rate to target tissue at concentrations that are highly protective against HIV. In a double-blind, randomized, placebo-controlled trial conducted among 16 HIV-negative women, a ring containing 25 mg of DPV was applied to the treatment arm group for 28 days [63]. On the day of ring removal, concentrations of DPV in vaginal fluid taken adjacent to the ring, from the cervix, and from the introitus exceeded the IC_{99} over 3900-fold. Adherence was near-perfect for all participants and treatment resulted in no product-related adverse side effects. Subsequently, in the ASPIRE clinical trial, 2629 African women were enrolled and treated with either a monthly DPV-releasing vaginal ring or a placebo ring [15]. The DPV ring reduced HIV incidence by 27% compared to the placebo group; when corrected for adherence and retention, this reduction amounted to 37%. This relatively low protective efficacy is potentially due to the

lack of multicompartment protection and low barrier to resistance of dapivirine. Recently, sustained release vaginal rings with 100 and 200 mg of DPV were investigated in a Phase 1 clinical trial [16]. Compared to 25 mg DV rings, the sustained release rings resulted in higher DPV concentrations in plasma and CVF that persisted out to 91 days. Vaginal rings with combination ARVs, such as DPV and maraviroc, have been investigated and require improvement in their formulations to stabilize release rates of both agents [17]. Multipurpose rings that can prevent HIV, other STIs, and/or unwanted pregnancy are also an attractive technological advancement that will be discussed further in section 2.4.

2.3 UNINTENDED PREGNANCY

2.3.1 Global Burden of Unintended Pregnancy

Unintended pregnancy, defined as a pregnancy that is wanted at a later date but not wanted at conception (mistimed) or a pregnancy that is not wanted at a later date or the time of conception (unwanted), is an imposing burden on people capable of pregnancy globally. Between 2015 and 2019 there were 121 million unintended pregnancies annually, corresponding to 64 unintended pregnancies per 1000 reproductive aged women [64]. In the US, unintended pregnancy is highest among women with an income less than 200% of the federal poverty level, young women (aged 18-24), cohabiting women and women of color [65]. On a global scale, unintended pregnancy occurs across all country income groups, however, it disproportionately affects women in low-income regions including sub-Saharan Africa (91/1000 women) and West Africa and North Africa (86/1000 women) [64]. Figure 2.4 depicts the global distribution of unintended pregnancy.

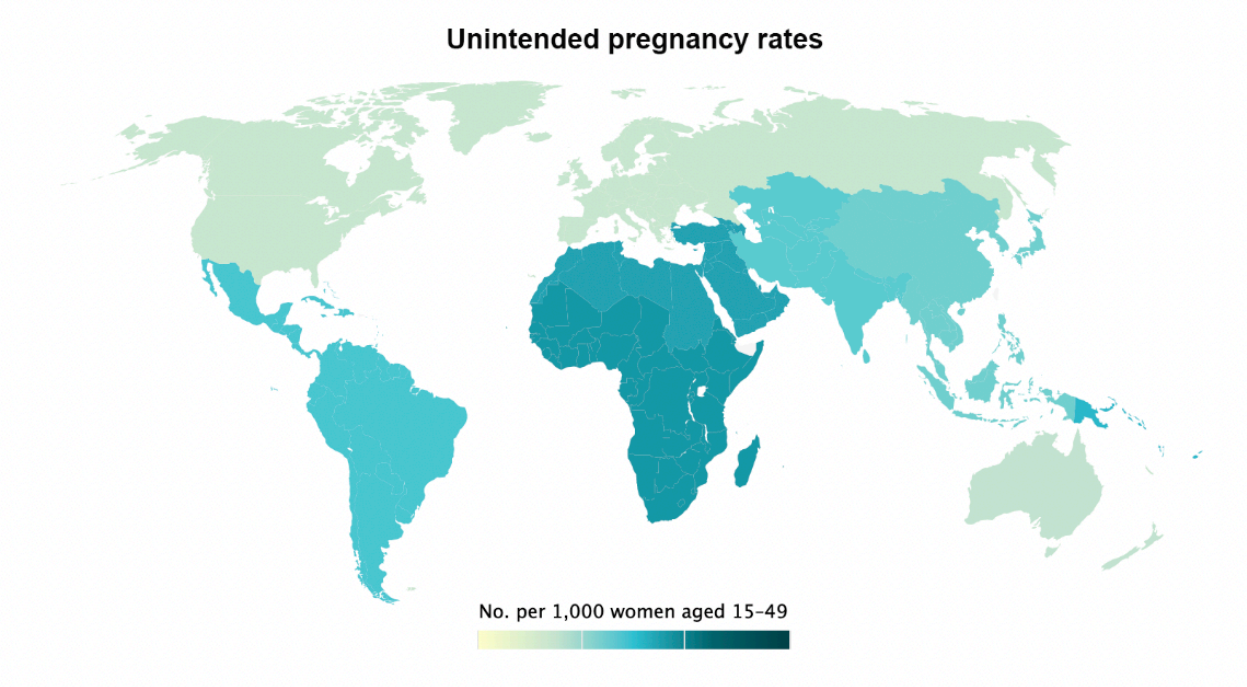

FIGURE 2.4. **World map of unintended pregnancy rates**. Values represent annual averages from 2015-2019; analyzed by Bearak et al. [64] and compiled by the Guttmacher Institute [66].

The consequences of unintended pregnancy disenfranchise and disempower women globally. On a national level, high rates of unintended pregnancy correlate with reduced quality of life and workforce efficacy, reduced economic growth, stifled socio-economic development, and worsened public health outcomes [67]. Concerning maternal and child health, unintended pregnancy is positively associated with maternal risk behaviors, delayed initiation of antenatal care and a decrease in the number of antenatal care visits, increased risk of congenital anomalies, spontaneous abortion, premature delivery, low birth weight, childhood mortality and abuse, maternal mortality, and negative maternal mental health outcomes [68]. It is estimated that 48% of all pregnancies are unintended and about 61% end in abortion [64]. This is troubling given the current landscape of abortion restrictions; indeed, 41% of women globally live under restrictive abortion laws that result in the persistent use of unsafe abortion methods. The WHO estimates

that 25 million unsafe abortions occur annually, and 23,000 women die because of unsafe abortion each year [69]. Tens of thousands more experience serious health complications. While universal access to safe abortion remains to be seen, it is critical that research and public health efforts prioritize reducing the incidence of unintended pregnancy.

The primary causes of unintended pregnancy are contraceptive failure, contraceptive misuse, and non-use of contraceptive services. Globally, 270 million women have an unmet need for contraception [70]. Factors that underly this unmet need include lack of access to family planning providers, gender-based barriers, cultural or religious opposition, unawareness of contraceptive options, inadequate sexual education leading to risky sexual behavior and misunderstandings about the risk of pregnancy, failure of available methods to meet patient needs and desires, and perceived or real side effects of available methods [71]. As such, preventing unwanted pregnancy is a matter of making available and accessible a mix of contraceptive methods that are acceptable to users and educating users about their options. Indeed, a multinational study of contraceptive use showed that for every one contraceptive method that is made accessible to at least half of a given population, the prevalence of contraceptive use in that population increases by 4-8%. Equipping all populations with a robust and expanding toolbox of contraceptive options is critical to reducing unintended pregnancy.

2.3.2 Existing Contraceptive Strategies

Modern contraceptive use has expanded significantly in the past several decades as the contraceptive prevalence rate has increased from 47.7% to 49% among women with a need for family planning since 2000; this represents an additional 188 million women using a modern contraceptive method [72]. Contraceptive methods include oral pills, implants, injectables,

patches, vaginal rings, intra-uterine devices, condoms, male and female permanent contraception, and fertility awareness. Methods are evaluated based on their efficacy given perfect use and their efficacy given common use, accounting for average rates of misuse and nonadherence. Table 2.3 summarizes the mechanisms of action, dosing frequency, global prevalence, and efficacy of contraceptive methods available today.

TABLE 2.3. Summary of available contraceptive methods [73].

Method	**Mechanism**	**Dosing**	**Efficacy - perfect use**	**Efficacy - common use**	**Prevalence** [74]
Combined oral contraceptives (COCs)	Estrogen and progestin prevent ovulation and fertilization	Daily (oral)	> 99%	93%	16%
Progestin-only pills (POPs)	Progestin prevents ovulation and fertilization	Daily (oral)	> 99%	93%	
Combined injectables	Estrogen and progestin prevent ovulation	Once per month	> 99%	97%	8%
Progestin-only injectables (DMPA/NET-EN)	Progestin prevents ovulation	2 – 3 months	> 99%	96%	
Dermal patch (Evra)	Estrogen and progestin prevent ovulation	Once per week	> 99%	93%	< 2%
Vaginal ring (NuvaRing)	Estrogen and progestin prevent ovulation	Once per month	> 99%	93%	< 2%
Subdermal implant (Nexplanon, Jadelle, Levoplant)	Levonorgestrel or etonogestrel prevent ovulation and fertilization	3-4 years	> 99%	> 99%	2%

Copper intrauterine device (IUD) (ParaGuard)	Creates hostile environment to sperm and egg	12 years	> 99%	> 99%	
Levonorgestrel intrauterine device (IUD) (Mirena, Liletta, Kyleena, Skyla, Jaydess)	Levonorgestrel prevents fertilization	3-8 years	> 99%	> 99%	17%
Female condom	Barrier prevents fertilization	Coitally	95%	79%	< 2%
Male condoms	Barrier prevents fertilization	Coitally	98%	87%	21%
Female sterilization (tubal ligation)	Prevents egg from meeting sperm	Permanent	> 99%	> 99%	24%
Male sterilization (vasectomy)	Prevents sperm from entering ejaculate	Permanent	> 99%	> 99%	2%
Spermicides	Capacitates sperm to prevent fertilization	Coitally	82%	72%	< 2%

Long-acting reversible contraception (LARC) is defined as any method with a dosing frequency less than once per cycle or month. As such, the progestin-only injectable, subdermal implants, and copper and levonorgestrel IUDs are characterized as LARC methods. LARC has many advantages over short-acting reversible contraceptives (SARC; COCs, POPs, combined injectables, dermal patch, vaginal ring) and coitally-dependent and barrier methods (male and female condoms, vaginal gels). LARCs are adherence-independent; because of this, common-use efficacy is nearly identical to perfect-use efficacy, and they do not require ongoing effort to maintain. Beyond contraceptive benefits, LARCs are more cost-effective than short acting or coitally-dependent methods [75]. LARCs are discrete and do not interfere with sexual or

menstrual activity. Many long-acting methods can treat menstrual related disorders such as anemia, fibroids, and endometriosis (LNG-IUD) and alleviate menstrual symptoms including dysmenorrhea and migraine headaches (progestin injectables). IUDs in particular are beneficial as they are immediately effective and reversible, have few contraindications, and the copper IUD is the most effective form of emergency contraception (EC) if inserted within 5 days of unprotected sex.

Despite the efficacy and convenience of LARC, these methods are not used widely in regions of the world with the highest rates of unintended pregnancy. The prevalence of IUDs in sub-Saharan Africa, a region with the highest rates of unintended pregnancy, is the lowest in the world at 0.8% [76]. A decrease or stagnation in IUD use has been attributed to concerns over adverse health outcomes, misconceptions about their use, and perceived costs. Addressing the underutilization of LARC including IUDs is critical to meeting development goals of reducing unwanted pregnancy. Policy and provider interventions, such as implementing comprehensive contraceptive counselling, are strategies towards this end. Moreover, technological advances that decrease discomfort and side effects and increase the acceptability and perceived benefits of these methods may bolster their use.

2.4 MULTIPURPOSE PREVENTION TECHNOLOGIES

Multipurpose prevention technology (MPT) is defined as any product that simultaneously prevents HIV, other STIs, and/or unintended pregnancy. MPTs have the ability to revolutionize the global sexual and reproductive health (SRH) landscape, particularly in regions with both high incidence of HIV and unintended pregnancy. Offering streamlined dosing for multiple indications, MPT could enhance uptake and adherence to PrEP and eliminate the need for

multiple clinic visits to address family planning and sexual health needs. The scientific and engineering complexities of developing MPT products have thus far delayed progress towards realizing their value. Currently, male and female condoms are the only available product that can prevent transmission of HIV, other STIs, and unwanted pregnancy. Condoms have numerous disadvantages, including coital dependency, lack of discretion, lack of female control and often negotiating power for their use, and sexual preferences that make them undesirable. Multiple end-user studies on MPT preference indicate a high level of support for female controlled, discrete, and long-acting products to prevent HIV and pregnancy [18,77]. It is clear that no single MPT option will be suitable to all women and a method mix for simultaneous HIV/STI prevention and contraception is desirable.

Existing contraceptive methods, especially LARC, are promising precursors as drug delivery platforms for MPT. Indeed, over the past decade, various contraceptive strategies have been adapted to include HIV and STI prevention functionalities. Nearly half of all MPTs currently in the development pipeline are vaginal rings; however, vaginal gels, vaginal inserts and films, subdermal implants, injectables, and oral tablets are also in early pre-clinical stages of investigation. Research on MPTs is primarily concerned with including diverse active pharmaceutical agents (APIs) into a single delivery modality, such as hormones, ARVs, non-hormonal contraceptives, and biologics like monoclonal antibodies. Delivering physiochemically distinct agents safely, effectively, and for the same duration poses an engineering challenge. Competing metabolic pathways and inconsistent drug dissolution patterns are two primary difficulties noted in many MPT development programs. To date, there are 14 MPTs designed to prevent HIV and pregnancy in preclinical stages of development, one in a Phase 1 clinical trial,

one in a Phase 2 clinical trial, and one in consideration for premarket approval. Features of these products are described in Table 2.4.

TABLE 2.4. Multipurpose prevention technology for HIV and unintended pregnancy.

Product	API	Duration of Use	Stage of Development	Reference
Copper IVR (Cu-IVR)	Copper	Unspecified	Preclinical	[78]
DPV + pritelivir + LNG IVR	Dapivirine, levonorgestrel, pritelivir	1 month	Preclinical	[79]
Islatravir + ENG-EE IVR	Etonogestrel, ethinyl estradiol, islatravir	90 days	Preclinical	[80]
Pod-type ENG-EE + Q-Griffithsin IVR	Etonogestrel, ethinyl estradiol, Q-Griffithsin	90 days	Preclinical	[81,82]
mAb contraceptive + TDF IVR	Monoclonal antibodies, tenofovir disoproxil fumerate	90 days	Preclinical	[82]
DOL+ RPV + acyclovir + ENG/EE IVR	Dolutegravir, rilpivirine, acyclovir, etonogestrel, ethinyl estradiol	30-90 days	Preclinical	[83]
Contraceptive antibody + VRC01+N6 IVR	Contraceptive antibody, VRC01+N6	1 month	Preclinical	[82,84]
DPV + LNG IVR	Dapivirine, levonorgestrel	90 days	Phase 1 Clinical Trial	[85]
TVF + LNG IVR	Tenofovir, levonorgestrel	90 days	Phase 2 Clinical Trial	[86]
Yaso-GEL	Polyphenylene carboxymethylene	Coitally	Preclinical	[87]

Amphora/Q-Griffithsin vaginal insert	Citric acid, L-lactic acid, potassium birtartrate, Q-Griffithsin	Coitally	Preclinical	[82]
Islatravir + progestin vaginal film	Islatravir, progestin	1 month	Preclinical	[88]
ARV/LNG Long-acting Injectable	Integrase inhibitors (TBD), levonorgestrel	3-6 months	Preclinical	[82]
Subcutaneous Contraceptive + HIV Implant Engineered for Long-Acting Delivery (SHIELD)	Unspecified	Unspecified	Preclinical	[89]
Ultra-Long Acting MPT In-situ Forming Implant (ISFI)	Hormonal contraceptive (TBD), ARV (TBD)	6 months	Preclinical	[82]
MPT Microarray Patch	Cabotegravir, norelgestromin	1 month +	Preclinical	[90]
Dual Prevention Pill (DPP)/TELE (oral)	Emtricitabine (FTC), ethinyl estradiol (EE), levonorgestrel, tenofovir disoproxil fumarate	Daily	Clinical: Bioequivalence Study	[91]

2.5 LONG-ACTING DRUG DELIVERY SYSTEMS

2.5.1 Overview of Diffusion-Controlled Drug Delivery Systems

Long-acting drug delivery systems have been developed and used clinically for a variety of indications including esophageal and prostate cancer, diabetes mellitus, neurological diseases, and eye diseases [92]. Drug release from a dosage form is controlled by a variety of mechanisms, including water penetration into the system, drug diffusion out of the system, swelling and erosion, osmotic effects, and drug dissolution [93]. Several of these processes may occur in one drug delivery system resulting in a sequence that is rate-limited by the slowest step. Non-

degradable polymeric devices composed of polyurethanes, silicone, and poly (ethylvinyl acetate) are the most common formulations for long-acting delivery and drug release is generally considered diffusion driven. Physicochemical properties of the encapsulated drug itself affect its diffusion and partitioning; as such, drug particle size, solubility in the drug delivery matrix, diffusion coefficient, and partitioning coefficient influence drug release to different extents depending on the type of long-acting delivery device [94]. For polymeric delivery systems, polymer properties such as crystallinity, glass transition temperature, molecular weight, hydrophilicity, degradation, and swelling can impact drug diffusion and the mechanism of drug release [95–97]. The shape and surface area of a device also plays a role in dissolution of drug into the surrounding media; characteristically, a larger surface area to volume ratio results in more rapid dissolution of encapsulated agent [98]. For the purposes of this thesis, two distinct classes of nondegradable, long-acting drug delivery systems, monolithic matrix devices (Section 2.5.2) and reservoir devices (Section 2.5.3), will be discussed here.

2.5.2 Monolithic Matrix Devices

In a monolithic matrix device, drug is homogenously dispersed or dissolved within a rate-controlling polymer matrix. Drug release is primarily driven by water penetration into the matrix and drug diffusion through the hydrated or dehydrated polymer medium in a nondegradable system. Insofar as describing matrix devices mathematically, it is critical to understand if a drug exists in the polymer as a solution, meaning it is molecularly dispersed, or as a suspension, meaning that the quantity of drug in the device is above the saturation solubility of the matrix polymer. In a monolithic dispersion, dissolved and undissolved drug exist in the matrix simultaneously, however, only dissolved drug is free to diffuse. A depiction of the geometries

and mathematical equations used to quantify drug release from monolithic matrices is presented in Figure 2.5.

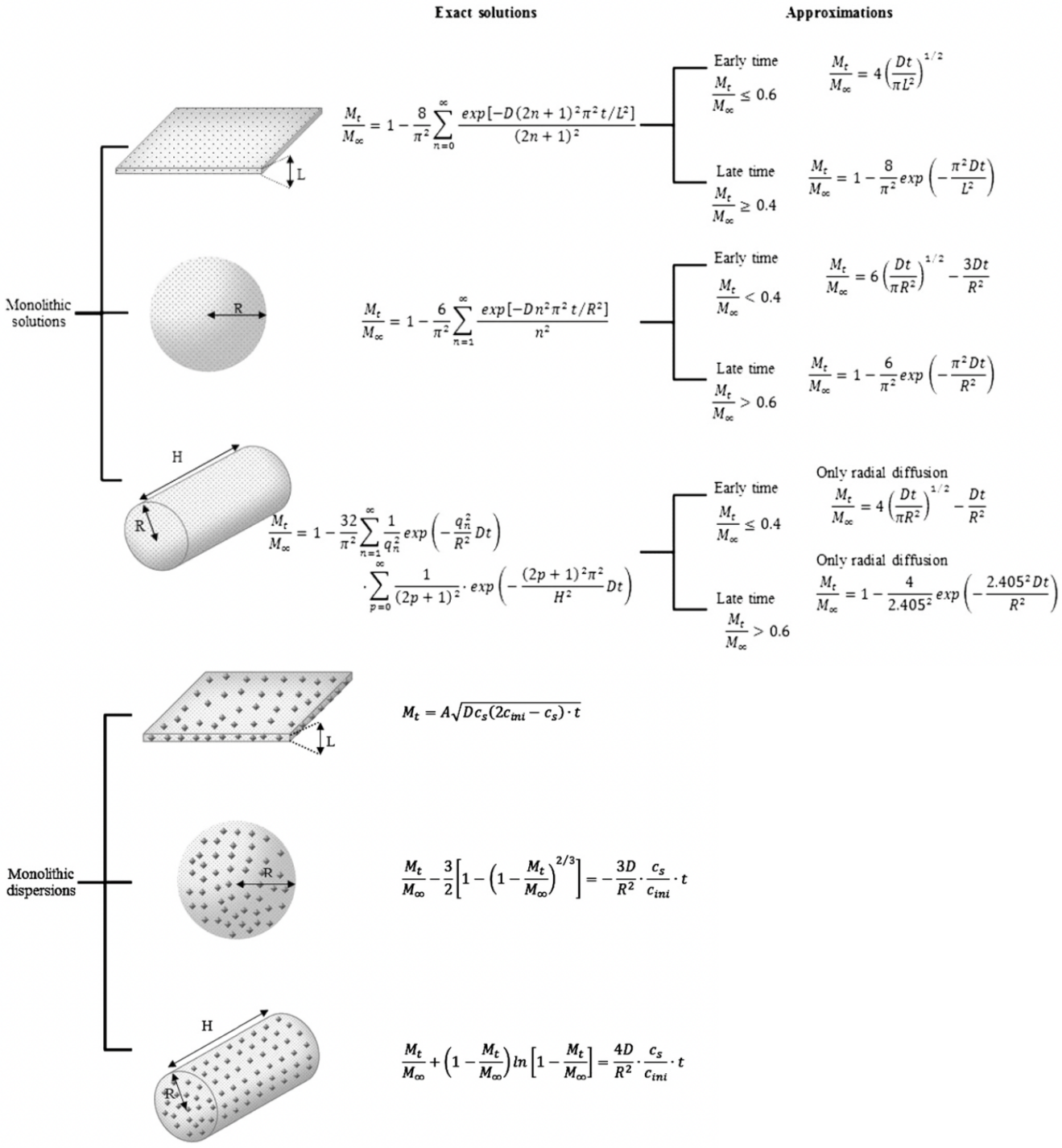

FIGURE 2.5. **Schematic by Siepmann and Siepmann depicting various geometries of monolithic solutions and dispersions**. Exact solutions are valid for the entire release period, while approximate solutions are valid for early and late time periods indicated. Variables not indicated in the schematic are diffusion coefficient (D), mass released (M_t) and total mass (M_∞), saturation solubility (c_s), initial concentration of drug (c_{ini}), and total amount of drug present in the matrix per unit volume (A) [93].

Fick's first and second law of diffusion inform the approximate solutions of drug dissolution depicted above. Fickian diffusion is based on several assumptions: (1) diffusional mass transport is rate-limiting, (2) the diffusion coefficient is constant, (3) dissolution occurs in perfect sink conditions, (4) swelling is not significant, or swelling occurs rapidly and quickly reaches equilibrium, (5) significant erosion does not occur, and (6) mass transfer resistance due to unstirred boundary layers on the surface of the device is negligible [93]. An important mathematical solution describes drug release from a monolithic solution with slab geometry: the Higuchi equation. In 1961, Takeru Higuchi derived a famously simple equation considering release of drug from a thin ointment film into the skin [99]:

$$M_t = A\sqrt{Dc_s(2c_{ini} - c_s) \cdot t}$$

Here, M_t is the mass of drug released at time t, A is the surface area, D is the diffusion coefficient, c_s is the saturation solubility of drug in the matrix, and c_{ini} is the initial concentration of drug in the matrix. Higuchi considered several conditions that are more or less congruent with the assumptions that define Fickian transport; diffusion is rate-limiting, the device is nonswellable, dissolution occurs in perfect sink conditions, drug is homogenously distributed, the diffusion coefficient is constant, and edge effects are negligible [100]. The simplified Higuchi equation makes use of a constant of proportionality, k_H, between drug release and the square root of time, that has a specific and physically realistic meaning [101]:

$$Q = k_H\sqrt{t} \text{ , where } k_H = A\sqrt{2c_{ini}Dc_s}$$

Here, Q is the amount of drug released after time t.

Higuchi also described drug release from a granular matrix, in which diffusion proceeds through granular vacancies in the matrix space. Compared to the classical Higuchi equation, the granular matrix equation is adjusted for the effective volume where diffusion can occur and the effective diffusional pathlength [102]:

$$Q = \sqrt{\frac{D\varepsilon}{\tau}(2A - \varepsilon C_s) \cdot C_s t}$$

Here, D represents the diffusivity of drug in the permeating fluid, ε is the porosity of the matrix, τ equals the tortuosity factor of the matrix system, and C_s is the solubility of the drug in the permeating fluid. All other variables are the same as defined above. This equation is based on the assumptions that drug particles are quite small relative to the average distance of diffusion, are relatively distributed throughout the matrix, and A is greater (3-4 times) than C_s and εC_s [103]. The effects of matrix swelling, porosity, and erosion are described by this modified Higuchi equation: an increase in these parameters results in an increase in the rate of dissolution. Conversely, and increase in the tortuosity of the matrix, which can be impacted by degree of crystallinity, chain relaxation, and glass-transition temperature of a polymer, decreases the rate of dissolution. Ultimately, the Higuchi equation and its variations provide a powerful and simple description of parameters that affect drug release from monolithic dispersions and the square-root of time relation is widely applicable to Fickian-diffusion in a matrix device.

Despite its simplicity and widespread use, the Higuchi equation does not describe all mechanisms of drug release from a polymeric system and specifically excludes swellable matrixes. In order to prevent misuse of Higuchi or other mechanistic models, Ritger and Peppas

[104,105] and Korsmeyer and Peppas [106] developed an equation to analyze Fickian and non-Fickian release of drug from swellable and nonswellable polymer delivery systems, given by:

$$\frac{M_t}{M_\infty} = kt^n$$

Where *k* is a rate constant and *n* is the release exponent indicative of the mechanism of transport of drug through the matrix. This equation is only valid for the first 60% of cumulative drug release from a device. Classification of drug release mechanisms based on the value of n is presented in Table 2.5.

TABLE 2.5. Korsmeyer-Peppas characterization of drug release [102,107].

Release exponent (n)			**Drug transport mechanism**	**Drug release mechanism**
Thin film	**Cylinder**	**Sphere**		
n < 0.5	n < 0.45	n < 0.43	Quasi-Fickian diffusion	Non-swellable matrix diffusion
n = 0.5	n = 0.45	n = 0.43	Fickian diffusion	
0.5 < n < 1.0	0.45 < n < 0.89	0.43 < n < 0.85	Anomalous (Non-Fickian transport)	Diffusion and matrix relaxation
n = 1.0	n = 0.89	n = 0.85	Case II transport	Zero-order release
n > 1.0	n > 0.89	n > 0.85	Super case II transport	Relaxation/ erosion

Understanding and mathematically describing the mechanism of drug release from a polymeric matrix device is a critical tool in identifying formulation parameters that affect drug release and predicting release timescales from dissolution data. This allows for rapid iteration and characterization of monolithic devices for long-acting drug release applications.

2.5.3 Core-Sheath Reservoir Devices

A reservoir system, also called a "core-sheath system," contains drug dissolved or dispersed within a core material that is surrounded by a release rate controlling membrane material. Like a monolithic device, it is critical to understand whether the drug is molecularly dispersed in the core material or if it is above the wetted material's saturation solubility [94]. A reservoir device with soluble drug in the core is said to have a "non-constant activity source," meaning that once drug dissolves out of the rate controlling membrane into surrounding sink conditions, it is not replenished by a depot of drug remaining in the core. The amount of drug remaining in the dosage form as a function of time is an exponentially decreasing curve, thus first order release kinetics are observed for reservoir devices with a nonconstant activity source. A reservoir system in which a drug is above the saturation solubility of the core material is said to have a "constant activity source" in which molecularly dispersed (soluble) drug molecules are available for dissolution through the membrane and are rapidly replaced by the partial dissolution of remaining drug in excess. In all cases of dissolution from a reservoir device with a constant activity source, the cumulative amount of drug released increases linearly with time, thus, zero-order release kinetics are observed. Mathematical descriptions of drug release from non-constant and constant activity source reservoir devices of varied geometries are depicted in Figure 2.6.

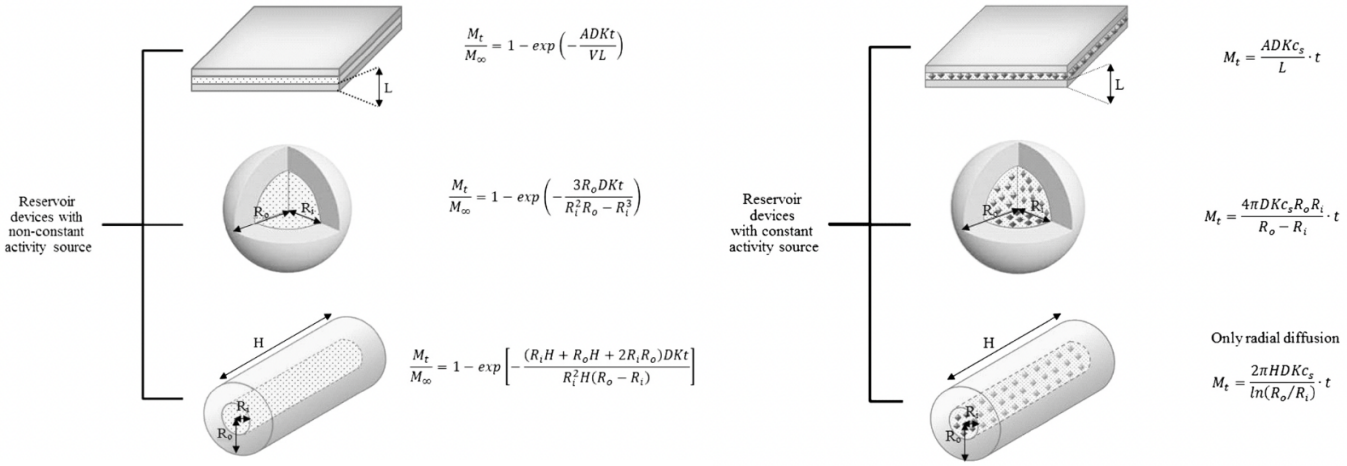

FIGURE 2.6. **Schematic by Siepmann and Siepmann depicting various geometries of reservoir devices with nonconstant and constant activity sources**. Variables not indicated in the schematic are the diffusion coefficient of the membrane (D), the partition coefficient between the core and the membrane (K), reservoir volume (V), mass released (M_t) and total mass (M_∞), and saturation solubility of drug in the core (C_s) [94].

A noteworthy equation for a cylindrical reservoir with a constant activity source was derived by Baker and Lonsdale; it highlights the dependency of drug release rate on the sheath membrane thickness, diffusivity in the sheath polymer, and solubility in the core polymer [108]. Such mathematical approximations are useful in determining design parameters for reservoir devices and predicting the duration of sustained release, which is particularly valuable for very long-acting reservoir systems in which the full duration of release is experimentally difficult to capture. Bao et al. demonstrated the use of zero-order and first-order model fitting to *in vitro* release data obtained from a levonorgestrel-releasing IUD reservoir device [109]. This work allowed for prediction of the half-lives of LNG-IUDs in various *in vitro* dissolution conditions and elucidated transport mechanisms underlying accelerated release.

A primary challenge in predicting drug release from a constant or non-constant reservoir system is obtaining values for diffusivity and saturation solubility of drug in sheath and core

polymers, respectively. These parameters can be determined experimentally, though the fidelity of determined values is often low [110]. Moreover, two confounding properties can cause deviations in the "ideal" behavior of reservoir devices at early time points. After the preparation of a reservoir dosage form, if the device is immediately subject to *in vitro* release testing or clinical use, the rate-controlling membrane can be devoid of drug; therefore, it takes some time for drug to diffuse through the membrane which leads to an underestimation of drug release. This is called the lag-time effect [94]. On the other hand, if a drug is allowed sufficient time to equilibrate into the rate controlling membrane during long-term storage, the membrane will become saturated with drug and result in concentration gradients that are not representative of steady state. This is called a burst effect and results in overestimation of drug release [94]. Despite these noted discrepancies, mathematical models are useful to understand and predict underlying factors that drive drug release from reservoir devices. Reservoir devices are highly amenable to long term drug delivery because of the ability to load high quantities of drug without affecting release kinetics given that drug is loaded above the saturation solubility. Applications of reservoir devices in contraception and PrEP will be further discussed (Section 2.5.4).

2.5.4 Review of Long-Acting Delivery Systems for Contraception and PrEP

From a technical perspective, many LARC methods provide a strong premise for sustained delivery of active agents to the female reproductive tract. These devices often combine one or more of the monolithic and reservoir DDS strategies, or variations of the two, to achieve innovative control over API stability and release. Two LARC modalities, the levonorgestrel IUD and subdermal implant, utilize core-sheath reservoirs to offer sustained, near-zero-order release of contraceptive agents. The Nexplanon and Implanon implants are 4 cm long and 2 mm in

diameter consisting of an ethylene vinyl acetate (EVA) copolymer core loaded with 68 mg of etonogestrel surrounded by an EVA sheath [111]. The implant releases 60-70 μg of etonogestrel per day in the first two months, decreasing to 20-30 μg/day at the end of the third year with serum concentrations around 153 ± 52 pg/mL at this terminal timepoint (36 months).

The Mirena IUD contains 52 mg of levonorgestrel in a silicone-based core surrounded by a drug-free silicone sheath that mediates the release of approximately 20 μg of LNG per day [112]. The release rate of LNG declines over time to approximately 10 μg/day after 5 years, at which point the IUD is typically replaced. Upon removal of the LNG-IUD, approximately half of the loaded drug content remains in the device. One published *in-vitro-in-vivo* correlation exists, reporting a 1.165 ratio between *in vitro* and *in utero* release of LNG from the Mirena IUD [113]. The pharmacokinetics of local, long-term, sustained release of LNG into the uterine cavity results in stable plasma concentrations ranging from 180.66 pg/mL (12 months of use) to 159.59 pg/mL (60 months of use); plasma levels do not display peaks and troughs like those seen with OCPs and implants [112].

Intravaginal rings are the most advanced stage delivery modality for MPT and represent various design strategies for sustained drug delivery. The standard IVR design involves a silicone matrix ring, in which contraceptive and/or microbicidal API is directly incorporated into the polymer matrix [86]. This approach poses formulation challenges, particularly for delivery of multiple agents, as control over drug stability, release kinetics, and drug-drug interactions can be difficult. Segmented, dual reservoir IVRs have also been described, in which two unique core-sheath reservoir configurations are combined into a single device for orthogonal delivery of both APIs [87]. Pod-type IVRs have also been investigated wherein a solid silicone ring is produced by injection molding and vacancies are introduced to the matrix to create “pods” where tablet-

like formulations of API are packaged. Pod-type IVRs can formulate biologics, such as monoclonal antibodies [114] as well as small molecule agents [115,116] for multipurpose prevention. Release of encapsulated agent is controlled by the number of pods, drug loading in the pods, and the type and amount of sealant that encloses the pod. Modular designs such as segmented and pod IVRs afford greater control over drug release of multiple APIs and inspire development of further iterations of long-acting MPT.

2.6 DRUG DELIVERY AND TRANSPORT IN THE FEMALE REPRODUCTIVE TRACT

In order to design drug delivery systems that achieve high API accumulation in the female reproductive tract, it is important to understand transport mechanisms that affect local pharmacokinetics. Perhaps the most studied FRT delivery phenomenon is the uterine first pass effect. In 1997, De Ziegler et al. first proposed that vaginally administered drugs are preferentially delivered to the uterus via a direct transport mechanism [117]. Researchers studying the effects and pharmacokinetics of progesterone (P) delivered vaginally discovered a paradox: P administered vaginally caused predictable and significant secretory transformation of the endometrium but resulted in sub physiological levels of the hormone in plasma. By contrast, orally administered P resulted in high plasma levels coupled with weak endometrial effects. In a direct comparison of intramuscular versus vaginally administered P, steady state plasma concentrations were 69.8 ± 5.9 ng/mL and 11.9 ± 1.2 ng/mL, respectively. However, endometrial tissue concentrations of P were 10-times greater after vaginal administration than intramuscular [118]. These findings have been replicated for a variety of active agents, including the androgen

danazol [119], estradiol [120], misoprostol for medical abortion [121], and mifepristone for treatment of uterine leiomyomata [122].

The physiological mechanism by which this occurs is linked to a local "portal" system between the vagina and the uterus that has been explained by four theories [123]. The first possible explanation is direct diffusion through local tissues. Bulletti et al. provided evidence for this theory in an *in vitro* extracorporeal perfusion non recycling system [124]. Labelled progesterone was placed on vaginal tissue that remained attached to the cervix after hysterectomy; output of P through the uterine vein was monitored in parallel with endometrial tissue concentrations of P. Absorption in the uterine vein peaked after 1-2 hours before declining, while endometrial P peaked at 5 hours. Due to the open perfusion system, endometrial P could not have been the product of circulatory distribution, thus the existence of a passive diffusion mechanism was suspected. The second theory involves passage of drug through the cervical lumen (aspiration) by way of uterine peristalsis. Wildt et al. demonstrated this theory utilizing sperm-sized aggregates of labelled human serum albumin that, upon vaginal placement, migrated within minutes to the utero-tubal junction [125]. Upon thoroughly washing the cervical canal, labelled albumin activity immediately disappeared, suggesting that intraluminal transport exists at least for sperm-sized particles. This is perhaps not surprising considering the natural movement of sperm up the cervical canal during the peri-ovulatory period, in which aspiratory peristaltic movements towards the fallopian tubes are at their peak. However, this finding is significant given particle movement in the absence of active propulsion present on spermatozoa. In the luteal phase, dominated by progesterone, uterine contractions favor movements radiating from the fundus to favor embryo implantation [126]. However, during menstruation, prostaglandin-mediated contractions propel endometrial layers from the uterus to the vaginal

canal. This pattern of pelvic contractility potentiates uterine-to-vaginal transport via the cervical lumen.

A third theory describes transport via the venous or lymphatic circulatory systems; this is premised by the anatomy of lymphatic vessels that run from the cranial part of the vagina towards the uterine cervix, which eventually join and meet the hypogastric lymph glands [123]. Much less is known about uterine-to-vaginal transport through the circulatory system, though bidirectional transport between the uterus and ovaries has been described and is understood by the endocrine influence of the endometrium on the ovaries. Here, prostaglandins, peptide- and steroid-hormones diffuse between venous and arterial vessels of the uterus and ovaries [123]. Given the proximity of uterine lymphatics to the vaginal tract and the fact that the uterine body, cervix, and upper third of the vaginal tract all drain to the external iliac lymph node, it is possible that direct transport of substances from the uterus to the vaginal tract via lymphatic circulation can occur. Finally, countercurrent exchange between the utero-ovarian vein and the ipsilateral ovarian artery is proposed due to the close proximity of afferent and efferent vessels in the upper third of the vagina and uterus. Indeed, the vaginal venous plexus tightly coils around branches of the uterine artery, creating a high surface area of contact that favors diffusion of substances. This theory was experimentally validated by the observation that upon vaginal administration of progesterone, P concentrations in the uterine artery were significantly higher than in the radial artery [127]. Countercurrent transport in the uterine-to-vaginal direction is also a possibility; the uterine veins coil tightly around the uterine artery, which branches into the superior vaginal arteries thus providing an opportunity for transport between efferent uterine vessels and afferent vaginal blood supply.

Despite a lack of information on uterine-to-vaginal transport, it is known that uterine delivery of drugs results in high local tissue concentrations within the upper FRT. Nilsson et al. measured the concentration of LNG in endometrial, myometrial, fallopian, and fat tissue in hysterectomized uteri in which either a hormonal IUD was inserted 36 to 49 days prior to surgery or oral LNG was administered for 7 days [128]. Endometrial tissue concentrations were significantly higher in the IUD group than the oral group, measuring approximately 808 ng/g of wet tissue versus 3.5 ng/g of wet tissue, respectively. LNG concentrations in plasma (202 vs 559 ng/g), myometrium (2.34 vs 1.42 ng/g), and the fallopian tubes (1.8 vs 1.7 ng/g) were not significantly different between IUD and oral groups, respectively. The accumulation of locally delivered drug to the anatomical site of action represents an advantage of local drug delivery in the FRT. This is the only study that provides evidence for local pharmacokinetics of intrauterinely delivered drugs reporting more than just plasma PK. Pursuant to studies on the uterine first-pass effect, the influence of drug diffusion in tissue and cervical lumen, as well as angio- and lymphatic architecture, on transport in the FRT and its clinical significance in developing local drug delivery systems remains to be fully realized.

2.7 CONCLUSION

The HIV/AIDS epidemic and the burden of unintended pregnancy pose major barriers to the health, economic, and social success of women globally. These burdens are exacerbated in regions such as sub-Saharan Africa, where HIV disproportionately affects women and where modern contraceptive prevalence, particularly long-acting reversible contraception, is low. Daily oral pre-exposure prophylaxis requires burdensome dosing regimens that must be adhered to perfectly to afford protection in the lower female reproductive tract. Innovations in multipurpose

prevention technology promise to offer protection against both HIV and unwanted pregnancy with discreet, acceptable, and long-acting delivery modalities. Despite their promise, MPTs face developmental barriers in formulating multiple physicochemically diverse agents into stable DDS that offer optimized release kinetics. Understanding the design and drug transport mechanisms of long-acting delivery systems and their current applications in contraception and PrEP offers insight into formulation strategies for next-generation MPT devices. Moreover, considering the physiology of the female reproductive tract and local drug transport phenomena informs topical drug delivery approaches that can favorably partition to the FRT. The synthesis of this knowledge into the development of long-acting MPT has the potential to alter the landscape of contraception and PrEP and improve the lives of women and girls globally.

Chapter 3. IMPACT OF THE COVID-19 PANDEMIC ON ACCESS TO AND UTILIZATION OF SERVICES FOR SEXUAL AND REPRODUCTIVE HEALTH (SRH): A SYSTEMATIC SCOPING REVIEW

Adapted from: Impact of the COVID-19 Pandemic on Access to and Utilization of Services for Sexual and Reproductive Health (SRH): A Systematic Scoping Review. **VanBenschoten H**, Kuganantham H, Larsson EC, Endler M, Thorson A, Gemzell-Danielsson K, Hanson C, Ganatra B, Ali M, Cleeve A. BMJ Global Health (2022).

3.1 ABSTRACT

Introduction: The COVID-19 pandemic has negatively impacted health systems globally and widened preexisting disparities. We conducted a scoping review on the impact of the COVID-19 pandemic on women and girls' access to and utilization of sexual and reproductive health (SRH) services for contraception, abortion, gender-based and intimate partner violence (GBV/IPV), and sexually transmitted infections (STIs).

Methods: We systematically searched peer reviewed literature and quantitative reports, published between December 2019 and July 2021, focused on women and girls' (15–49 years old) access to and utilization of selected SRH services during the COVID-19 pandemic. Included studies were grouped based on setting, SRH service area, study design, population, and reported impact. Qualitative data were coded, organized thematically, and grouped by major findings.

Results: We included 83 of 3067 identified studies and found that access to contraception, in-person safe abortion services, in-person services for GBV/IPV, and STI/HIV testing, prevention, and treatment decreased. The geographical distribution of this body of research was uneven and

significantly less representative of countries where COVID-19 restrictions were very strict. Access was limited by demand and supply side barriers including transportation disruptions, financial hardships, limited resources, and legal restrictions. Few studies focused on marginalized groups with distinct SRH needs.

Conclusion: Reports indicated negative impacts on access to and utilization of SRH services globally, especially for marginalized populations during the pandemic. Our findings call for strengthening of health systems preparedness and resilience to safeguard global access to essential SRH services in ongoing and future emergencies.

3.2 INTRODUCTION

Since the onset of the coronavirus disease 2019 (COVID-19) pandemic, direct and indirect effects of COVID-19 on health systems have been documented globally. Primary effects of infection with the coronavirus and secondary effects of public health and policy responses have exerted unequal health burdens among various populations [128,129]. Infectious disease outbreaks are known to negatively affect human, social, physical, and financial capital – livelihood assets that contribute to treatment seeking – leaving people more vulnerable to limited access and utilization of healthcare including sexual and reproductive health (SRH) services. Indeed, SRH care and outcomes have reportedly declined as a result of the COVID-19 pandemic and associated mitigation efforts such as lockdowns [130,131]. At its onset, the public health crisis threatened hard-won progress towards modern contraceptive coverage targets set by the Sustainable Development Goals (SDGs); the United Nations Population Fund (UNFPA) estimated that the pandemic interfered with contraceptive use for about 12 million women

resulting in as many as 2.7 million unintended pregnancies in its first year [132]. In addition, Marie Stopes International estimated that there were 1.2 million unsafe abortions in the first 6-months of the pandemic alone [133]. The ongoing threat to safe abortion access is perpetuated by an increase in circumstances that lead to unsafe abortions, such as restrictive abortion policies [134], increased poverty among women [135], and clinic closures caused by the pandemic [133]. Another vulnerable area of SRH is sexually transmitted infections (STIs) that continue to dominate the healthcare burden of many regions; indeed, HIV is a major global health issue with AIDS being leading cause of death among women of reproductive age [17]. At the beginning of the pandemic, it was estimated that in high-burden settings, there could be a 10% increase in deaths due to HIV over 5 years caused by the effect of the COVID-19 pandemic on HIV programs [137,138].

Reduced access to SRH services in the wake of the pandemic is of heightened concern considering the gendered impacts of the pandemic that aggravated existing health disparities for women and girls [133]. Containment measures established in response to the pandemic increased the incidence of negative SRH outcomes for women and girls, particularly in low-and-middle income countries. For instance, school closures resulted in increased risk and incidence of pregnancy among adolescent girls in regions of sub-Saharan Africa, thus exacerbating their SRH needs as far as contraception and safe abortion [139,140]. The COVID-19 pandemic also saw increased rates of domestic violence across the globe correlated with increased household economic insecurity, additional childcare work, loss of social networks, and isolation – each of which are risk factors for increased violence that disproportionately affects women and, in turn, hinder the ability of women to seek help [128,141]. As the pandemic drove an increase in certain SRH needs, the ability to access and utilize SRH services remains critical. Understanding where,

how, and for whom access to SRH services was most impacted is essential to ensuring continued restoration of SRH service coverage.

Several reviews have synthesized literature regarding the COVID-19 pandemic and its impact on the health of women and girls. These have primarily focused on maternal and perinatal health [142–145], sexual health and behavior [144,146], menstrual cyclicity and pregnancy intentions [147], and the adoption of practice recommendations for reproductive health services amid the pandemic [148]. In this current review, we sought to assess the impact of the COVID-19 pandemic on access to and utilization of four key SRH service areas that represent major health needs among women and girls of reproductive age: contraception, abortion, gender-based violence (GBV) and intimate partner violence (IPV), and sexually-transmitted infections (STIs), including HIV. These SRH services have, apart from contraception [144], not been included in aforementioned reviews [15,16, 18-21], nor have prior reviews reported evidence regarding the specific barriers imposed by the pandemic, included evidence beyond the first year of the pandemic, or synthesized both qualitative and quantitative data on a global scale. Here, we aimed to identify geographical, demographic, and thematic research gaps and to describe the findings of included research, including barriers to accessing SRH services and the impact of the COVID-19 pandemic on groups with distinct SRH needs.

3.3 MATERIALS AND METHODS

3.3.1 Study design

We adopted methods from a scoping review framework [149] and followed the Preferred Reporting Items for Systematic Reviews and Meta-Analysis extension for Scoping Reviews (PRISMA-ScR) checklist [150]. The study protocol was registered at the open science

framework and can be accessed via osf.io/2tk9j. The objectives were to: 1) describe the impact of the COVID-19 pandemic on access to and utilization of SRH services; 2) identify research and knowledge gaps in relation to how the COVID-19 pandemic has impacted access to and utilization of SRH services and 3) identify barriers to access and utilization. In order to successfully meet these objectives, we utilized the population, concept, and context (PCC) framework [151].

Population: Women and girls of reproductive age (15-49 years old) seeking SRH services. The term "women and girls" is used throughout this review and seeks to encompass all individuals seeking SRH services directed towards people who can become pregnant, have female reproductive anatomy, or may be victims of gender-based violence. We acknowledge that not all individuals who seek SRH services identify as women.

Concept: Access to and utilization of selected SRH services for women and girls. Access is defined as (any measure of) an individual's ability to seek, reach, and receive SRH services during the COVID-19 pandemic, which implicates measures of behavioral, logistic, infrastructural, organizational, or policy changes made in response to the pandemic including the impact of lockdowns on these functions [152]. We defined utilization as any measure of peoples' self-reported or provider's noted use of SRH services, either in-person or remote through telehealth approaches.

Context: Any country in which the COVID-19 pandemic impacted access to/utilization of selected SRH services.

3.3.2 Data sources and literature search

We conducted searches of peer reviewed journals and grey literature in five electronic databases: PubMed, Web of Science, CINAHL, Global Health, and WHO Global Index Medicus. Searches were conducted without any limitation with regards to geography, language, or year. Search terms related to COVID-19 were used as previously defined by Lazarus et al. [153]. A detailed description of our search strategy is available in Supplementary Material (Appendix 1). We also searched the reference list of all studies relevant to our research question for additional studies.

3.3.3 Study selection

Prior to screening, all references retrieved from searched databases were imported into Covidence (Covidence, Melbourne, Australia) and duplicates were removed. HV and HAK screened all abstracts and titles, excluding studies that did not pertain to the SRH focus areas or address the research question. Next, HV and HK screened the full texts of all studies remaining after the title/abstract screening phase. EL arbitrated conflicts at both stages of screening through mediated discussion.

3.3.4 Eligibility criteria

This study included original, English language, peer reviewed research studies presenting quantitative and/or qualitative data, and primary quantitative reports/letters on clinical/program data from service providers, published between December 2019 to July 2021. These include studies that investigated the impact of the COVID-19 pandemic in relation to four SRH focus

areas (contraception, safe abortion, GBV/IPV STIs including HIV), with data on SRH service access/utilization by women and girls of reproductive age (15–49 years old). We excluded any study that reported effects of the SARS-CoV-2 virus/disease and only included studies that considered impacts of the COVID-19 pandemic response and/or mitigation measures. We excluded studies that did not meet the inclusion criteria on the basis of language, study dates, study type, and SRH focus area. We also excluded studies on men as other reviews have focused on the SRH needs of this group during the COVID-19 pandemic [146].

3.3.5 Data extraction

Data was extracted by HVB using Covidence Data Extraction 2.0. Extracted information from each article included, country, study setting (urban vs. rural), SRH service subject area(s), subgroups with distinct SRH needs included in analysis, metrics (units of measurement), and impact of the COVID-19 pandemic. Country income group and geographical region were recorded and classification applied according to the World Bank list of economies (June 2020) [154].

3.3.6 Reporting the results

We synthesized a narrative account of the major findings of included studies regarding the impact of the COVID-19 pandemic on access and utilization of the four key SRH services. Studies were grouped by SRH focus area, study design, setting, study population and directionality (increase/decrease) in terms of the impact on access and/or utilization. Qualitative manifest data were coded inductively and grouped into themes representing the major findings relating to how the pandemic impacted access and utilization.

3.3.7 Patient and Public Involvement

Patients and the public were not involved in the design, conduct, reporting, or dissemination plans of this review.

3.4 RESULTS

3.4.1 Screening results

After the initial systematic search, a total of 4186 studies were identified with 1120 duplicates removed. The remaining 3079 studies were subject to title and abstract review; 2671 were excluded at this screening phase. Following the screening of 421 full texts, 83 studies were included in the review. The PRISMA flow-chart mapping the results of this screening process is displayed in Figure 3.1.

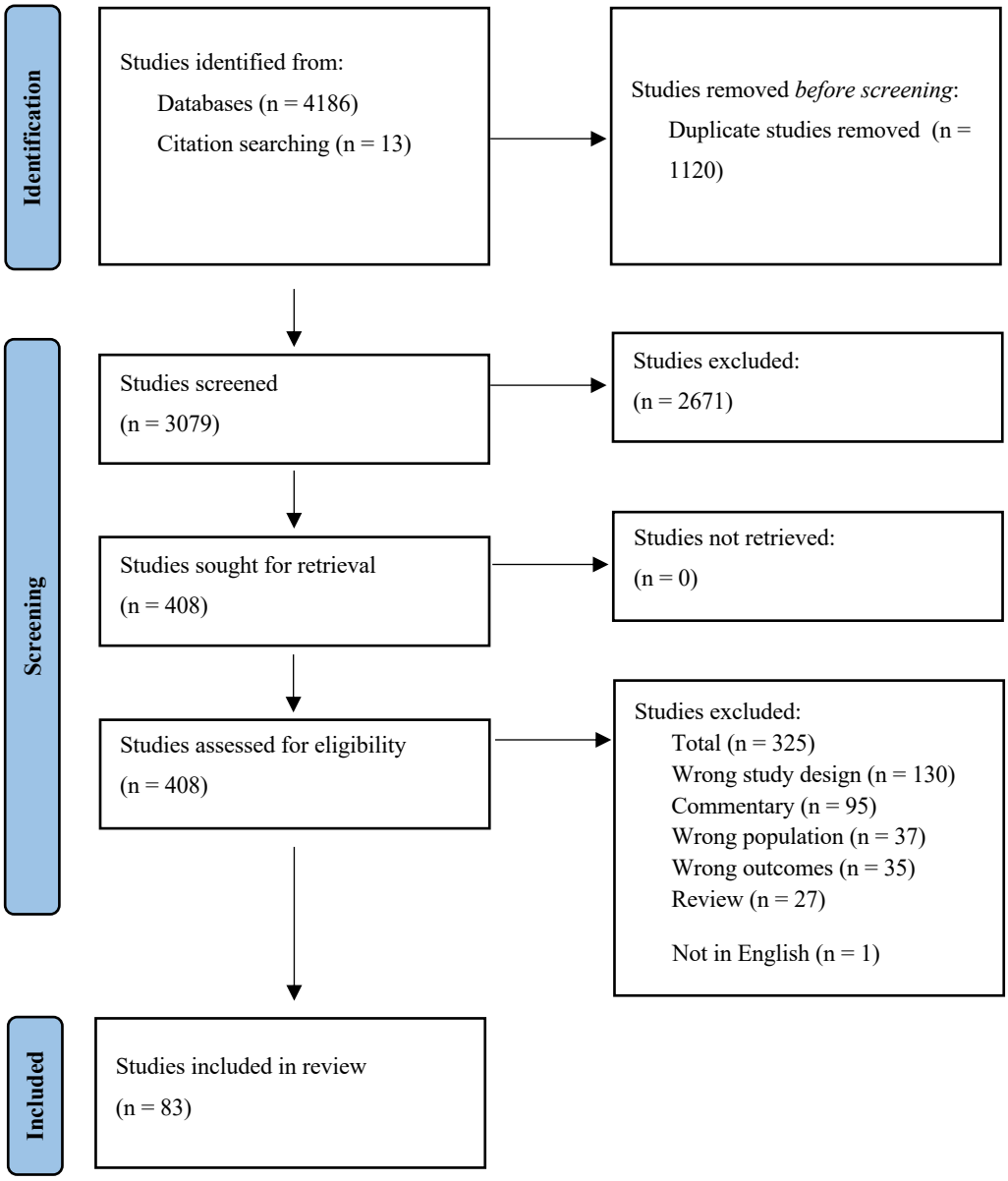

FIGURE 3.1. **PRISMA flow-chart of included studies**.

3.4.2 Characteristics of included studies

Studies were conducted in all seven major geographical (World Bank) regions of the world; 28% of the studies were done in North America [155–177], 28% in sub-Saharan Africa [178–200], 20% in Europe and Central Asia [201–217], 8% in East Asia & Pacific [218–224],

5% in Latin America and the Caribbean [225–228], 2% in South Asia [229,230], and 1% in the Middle East and North Africa [231]. Studies were conducted in more than 34 countries. Of all included studies, 10 were conducted in multiple countries (5 or more) [206,207,212,217,232–237], six of which spanned multiple geographical regions [232–237]. Supplementary Table 3.1 (Appendix B) displays the characteristics of included studies.

There was a relatively even distribution of studies across the focus areas: 30 (36%) provided evidence on the impact of COVID-19 on access to or utilization of contraceptive services, 21 (25%) on abortion services, 20 (24%) on GBV/IPV services, and 33 (40%) on STI-related services. Studies were conducted in a variety of economic settings and among subgroups with specific SRH needs. Almost half (49%) of the included studies were conducted in high income countries, 16% in upper middle-income countries, 12% in lower middle-income countries, 12% in low-income countries, and 11% in multiple countries with a mix of economic classifications. While most studies (61%) did not specify setting, a quarter took place in urban or peri-urban regions, 8% in rural areas, and 7% directly compared outcomes in urban versus rural areas. Figure 3.2 illustrates the distribution of studies among each of the four SRH service focus area by region and by study type.

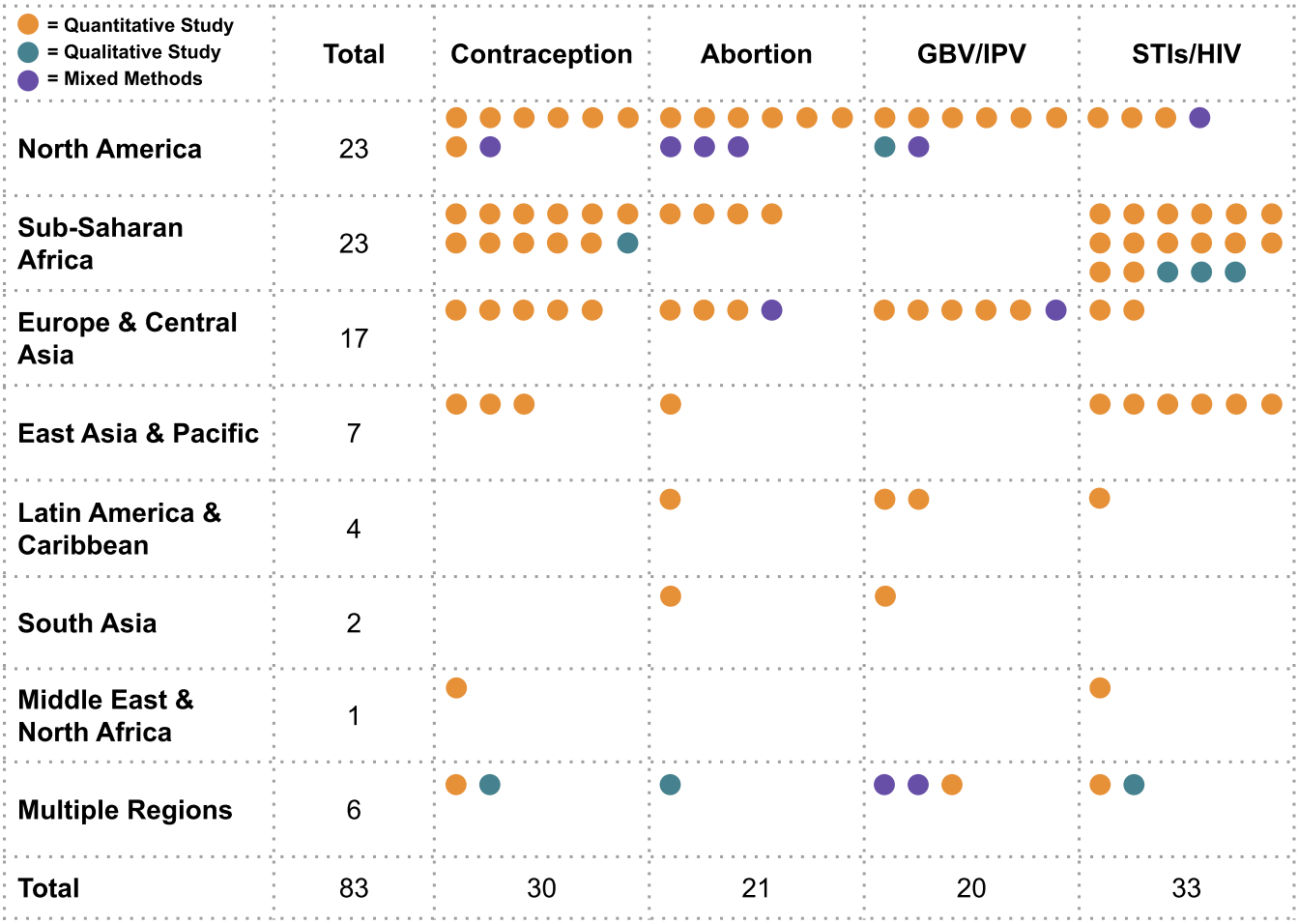

FIGURE 3.2. **Distribution of studies by region, SRH service area, and study design (n=83).**

3.4.3 Findings from included studies

Figure 3.3 illustrates the number of studies providing evidence within the respective SRH service areas, and the directionality of changes to access/utilization. Below, we present our findings per SRH service area.

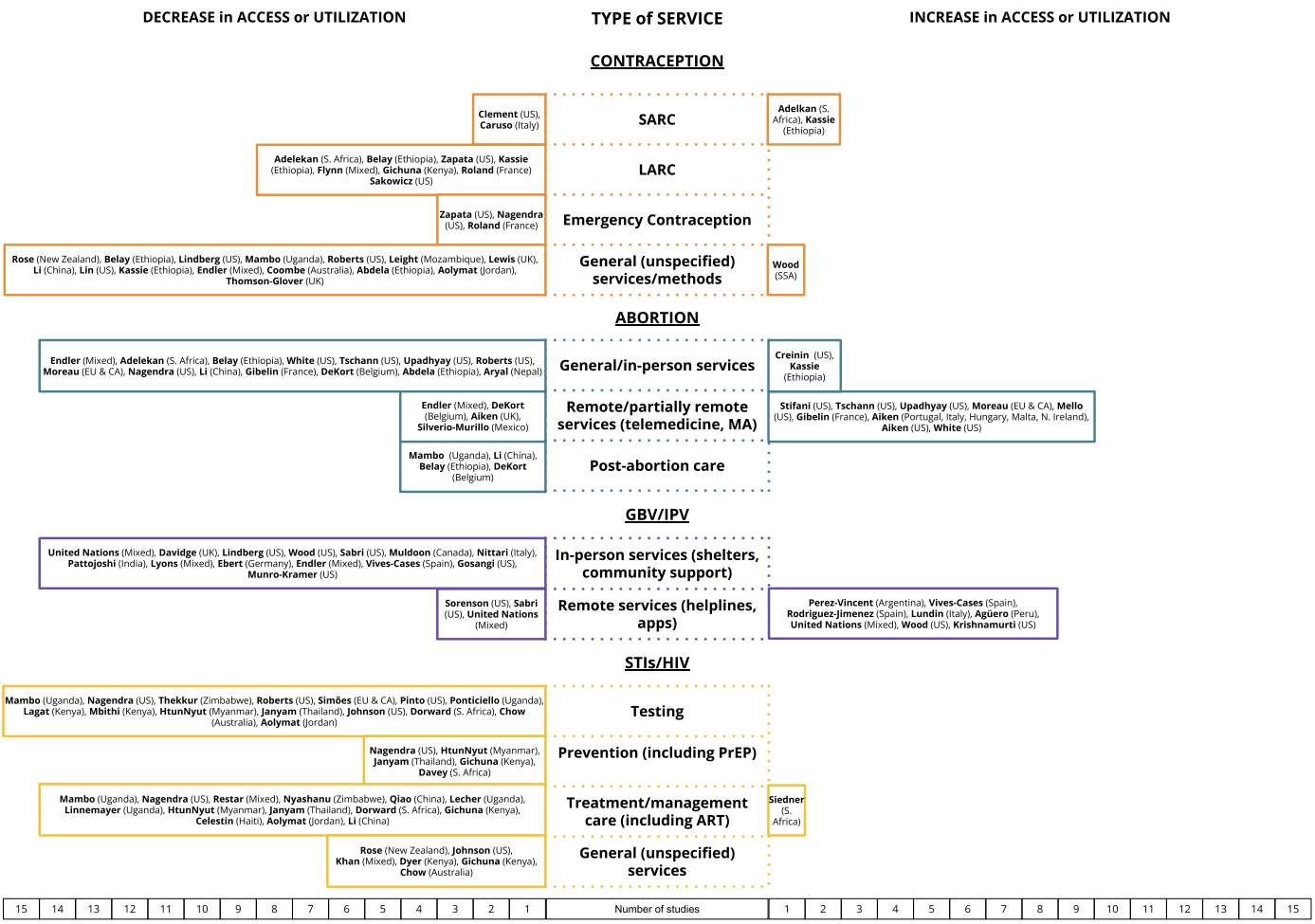

FIGURE 3.3. **Relative impact of COVID-19 on access and utilization of SRH services (n=83).**

3.4.3.1 Contraception services

Nearly one-third of studies (24, 30%) provided evidence of a decrease in access or utilization of contraceptive services, evenly distributed across various contexts and populations [155,156,162,164,167,169,174,178–180,190,195,198,200,202,205,210,215,218,220,224,231,236,237]. Utilization of short-acting reversible contraception (SARC) was analyzed by four studies in total [174,178,195,215], all of which provided evidence of reduced utilization. Of these studies, two conducted in sub-Saharan

Africa showed mixed results with an increase in SARC utilization in some clinical contexts [178,195]. Nonetheless, a large majority of included studies showed a decline in access to and utilization of long-acting reversible contraception (LARC). Included studies found substantial declines in the administration of injectables and placement of LARCs [156,164,178,179,195,198,205,237], a reduction in tubal ligation procedures [179], challenges with scheduling LARC removal [156], and reduced provision of emergency contraception [156,202,205].

Many studies referenced access to contraceptive services more broadly – not specified by LARC/SARC – and fifteen reported decreases in family planning attendance, appointment availability, and declines in unspecified contraceptive method utilization [155,162,169,179,180,190,195,200,202,210,218,220,224,231,236]. For instance, Belay et al. noted a 27% reduction in clinic visits for contraception and a 67% reduction in postpartum visits in one tertiary hospital in Ethiopia [179] while 55% of clinics surveyed in a study in the United States (US) had to cancel or postpone contraceptive visits due to the pandemic [162]. More generally, among a survey of SRH clinicians and stakeholders in 29 countries, 86% perceived that access to contraceptive services was less or much less because of the pandemic [236]. Only one study showed a slight increase in overall contraceptive utilization in sub-Saharan Africa [181].

3.4.3.2 Safe abortion services

In-person services for abortion were overwhelmingly curtailed during COVID-19 while remote services, such as online consultations for mailed medical abortion pills, saw an uptick in use. Fourteen studies documented a decrease in access to or utilization of abortion services,

including in-person services such as testing and consultations, medical abortion dispensation, and surgical abortion procedures [157,160–162,167,178,179,200,207,214,216,220,230,236]. These studies, which generally took place in areas with restrictive abortion policies, described precipitous drops in abortion clinic operations, evidenced by a 16% reduction in safe abortion services in Ethiopia [179], a 38% decrease in abortions performed in Texas [157], closure of 35% and 21% of SRH clinics providing abortion in the South and Midwest of the US, respectively [162], and a 26% decline in women accessing safe abortion services during lockdown in Nepal [230]. Several studies reported difficulty accessing in-person services, which led some abortion clinics to remove requirements for ultrasounds and Rh factor testing to reduce the need for in-person visits [160,161,214]. Access to postabortion care was negatively impacted as reported in China [220], Ethiopia [179], Uganda [180], and Belgium [216]. Two studies described an increase in abortion service utilization at tertiary care facilities in the US [176] and among teenagers in Ethiopia [195].

Decreases in access or utilization of remote or partially remote abortion services were described by three studies [88,89,108]. Endler et al. and DeKort et al. observed declines in at-home medical abortion utilization and Aiken et al. found that telemedicine abortion requests through Women on Web (WoW), an online telemedicine abortion service, increased significantly in Portugal, Italy, Hungary, Malta, and Northern Ireland, while they decreased significantly in the United Kingdom (UK). This decrease is speculated to be caused by a change in abortion legislation in the UK, whereby access to no-test abortions through the formal health sector significantly increased [217]. Several countries made policy changes during the pandemic to allow for medical abortion through telemedicine; these policy changes were more likely to be implemented in countries with liberal abortion laws, compared to countries with strict abortion

laws [217]. Nine studies found an increase in access and utilization of remote or partially remote abortion services in countries with relatively liberal abortion laws [157,159–161,170,177,207,214,238].

3.4.3.3 Gender-based and intimate partner violence services

Studies (14, 17%) on the impact of the COVID-19 pandemic on services for GBV/IPV described decreases in access or utilization of in-person services [155,158,163,165,166,172,173,175,201,203,204,208,211,213,225,228,229,232,234,236]. These studies described limited access to information and service availability [213,229,232,234,236], diversion of resources for GBV and sexual assault examinations to COVID-19 relief and limited medical resources to support survivors [158,165,166,208,232], a decrease in vacancies in shelters and operational capacity of safe-housing services [158,201], curtailed mutual aid, community support, advocacy, and intervention services [163,201,203,229], and challenges or delays in seeking support upon being quarantined with an abuser [155,173]. A multi-country survey found that financial instability and mobility restrictions robbed many women of the resources and mechanisms needed to leave the perpetrator of violence and seek refuge [234].

Generally, remote (not in-person) services for GBV and IPV saw higher rates of utilization during the COVID-19 pandemic compared to before the pandemic. Indeed, eight studies found increases in utilization of remote services for women experiencing GBV or IPV in HIC and UMIC [158,172,203,204,211,225,228,232]. Calls to domestic violence helplines and antiviolence centers increased in Argentina [225], Spain [203,204], Italy [211], Peru [228], Malaysia, China, Somalia, Tunisia, Uruguay, Saint Vincent and Grenadines, Kenya, India, and Zimbabwe [232]. Wood et al. described a 51% increase in video conferences to provide client

services at IPV and sexual assault-oriented agencies in the US [158], and Krishnamurti et al. found an increase in utilization of an app-based IPV assessment during the shelter-in-place order in the US [172]. Despite a general increase in remote service utilization, three studies documented decreases in utilization of mobile services; two of these took place in the US and found decreases in calls to "911" and a sexual assault crisis hotline [175] and reduced use of helplines by immigrant women experiencing IPV [163]. In a multinational survey led by the United Nations, decreases in calls to helplines, hotlines, police, and health centers in Ethiopia, Nepal, Trinidad and Tobago, and Rwanda were reported [232].

3.4.3.4 STIs/HIV services

Nearly half of included studies (40, 48%) found a decrease in access or utilization of STIs/HIV services [162,167,168,171,180,182–189,191–193,196–200,206,212,218–223,227,231,233,235]. STI testing reductions were reported in Uganda [180], the US [162], Jordan [231], Thailand [222] and Uganda [187]. Simões et al. found that 95% of community STI testing clinics in 53 countries in Europe and Central Asia experienced decreased testing for all STIs [206], while Nagendra et al. and Chow et al. noted significant reductions in asymptomatic STI screening in the US and Australia, respectively [167,223]. Two US studies also reported reductions in testing volumes for chlamydia and gonorrhea [168,171]. The negative impact of the pandemic on HIV testing was documented in two studies in Kenya [188,193], one in the US [167], and one in Myanmar [221]. Access to STI prevention services was also negatively impacted by the pandemic as documented by five studies. Among these findings were an 80% decrease in PrEP initiations and follow-up in the US [167], qualitative reports of reduced barrier prevention and PrEP outreach services for sex workers in Myanmar [221], Thailand [222], and

Kenya [198], and increased incidence of missed PrEP follow-up visits among vulnerable women in South Africa [199].

Evidence of the negative impact of the pandemic on access to services for treatment and management of STIs was reported by fourteen studies [167,180,186,189,191,196,198,219–222,227,231,233]. Difficulty accessing antiretroviral treatment (ART) was reported in several countries with a high incidence of HIV, including Zimbabwe [186], Uganda [180,191], South Africa [196], Kenya [198], and Haiti [227], as well as Myanmar [221], Thailand [222], China [219,220], and the US [167]. Lecher et al. found that viral load testing to monitor HIV status among PLWH decreased by 71% in all PEPFAR-supported countries in March 2020 [189]. Restar et al. reported that less than half of trans and nonbinary PLWH surveyed in a multi-country study perceived themselves to have unburdened access to HIV treatment [233]. Seven additional studies noted a decrease in access to unspecified STI-related services [171,197,198,218,223,231,235]. Only one study reported an increase in utilization of STI-related services immediately after lockdown in South Africa [184]. Three studies found that the COVID-19 pandemic did not significantly impact access to PrEP [192]. availability of clinic visits for ART [200]. or HIV clinic operations [212].

3.4.3.5 Reported barriers to access or utilization of services

Several studies (33, 40%) provided evidence regarding the challenges faced when attempting to access and utilize SRH services that were caused by COVID-19 (Table 3.1). Figure 3.4 illustrates how reported barriers were distributed within each SRH focus area. Transportation and mobility restrictions, such as shutdown of public transport, curfews and abuse by police/soldiers at roadblocks, limited access to contraceptive services and GBV/IPV services in

particular [162,180,186,187,191,192,198,210,218–220,224,230,232,234–236]. On the demand side, increased financial burdens due to the pandemic, including the ability to pay for face masks, transportation, and childcare, were reported equally within all SRH service areas except abortion [155,163,169,180,188,191,198,234,235]. In addition, lack of information [180,186,210,213,218,232], fear of contracting COVID-19 at a service location, and lack of privacy to schedule or attend appointments resulted in reduced SRH service access and utilization [162,163,187,188,191,198,210,218,224,232,235,236]. Self-censorship of needs also limited access to care for some individuals seeking contraception and STI/HIV services.[82,90]. On the supply side, limited availability of medical and social resources such as stockouts, shortages of staff, clinic closures and decrease in shelters, were reported to have prohibited utilization of services for all SRH services, HIV/STI, GBV/IPV and contraception especially [158,162,163,167,171,180,186,189,191,198,201,206,210,212,219,224,232,234,236]. Furthermore, although telehealth was put in place as a response to COVID-19 as a way of improving access, technological challenges were reported as a barrier to care for some seeking contraception, GBV/IPV, and abortion services [156,158,159,163,216,232]. Finally, certain legal restrictions related to IPV/GBV (1 study) and abortion (3 studies) imposed in response to COVID-10, including labelling safe abortion as a non-essential service, negatively affected SRH service availability [161,162,207,234]

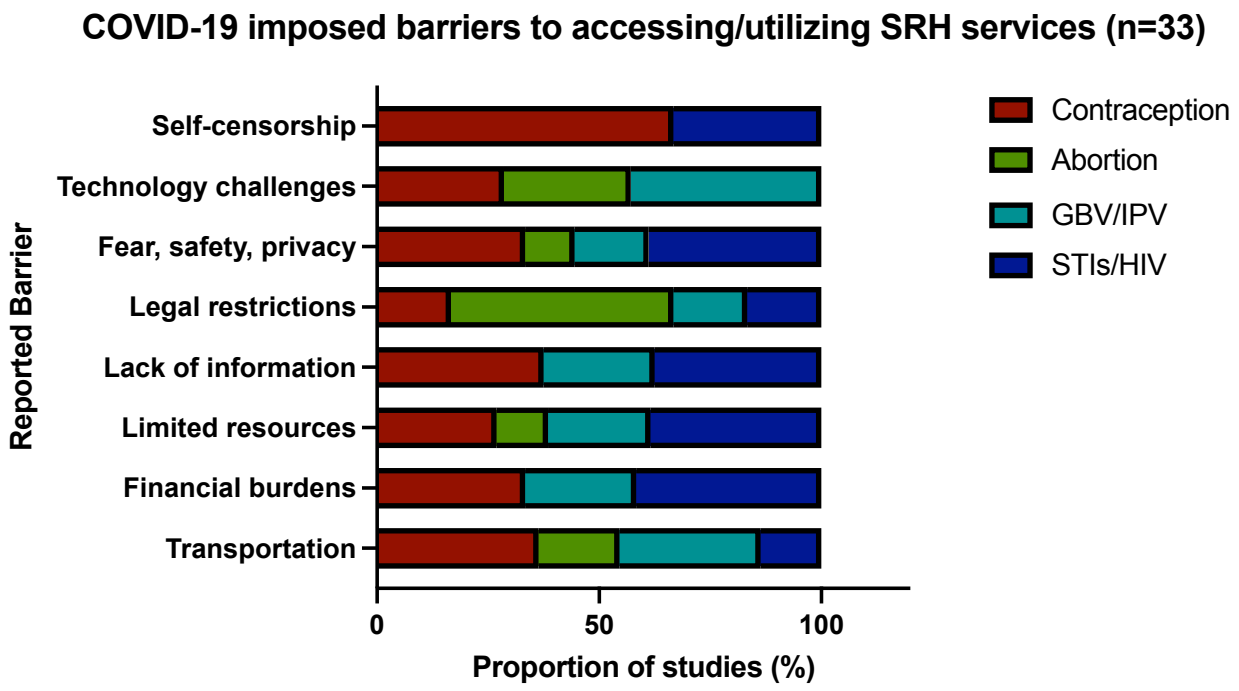

FIGURE 3.4. **Proportion of each COVID-19 related challenge to service access and utilization reported within each SRH focus area.**

3.4.3.6 Impact of COVID-19 on individuals with specific SRH needs

A minority of studies (16, 19%) included one or more subgroups with specific SRH needs in their analysis [155,163,169,180,192,195,197,198,202,210,218,220–222,232,233]. Overall, these studies point to a negative impact on both access and utilization of SRH services for these sub-populations who already experience disproportionately limited access to services (Table 3.2). Among this subset of studies, seven described the impact on adolescents [180,195,197,202,210,218,220] and three discussed the experiences of LGBTQIA+ individuals [155,218,233]; these groups more commonly experienced self-censorship of needs and lack of information about available SRH care. One study described the impact on displaced people and refugees [232] and four reported the impact on racial and ethnic minorities, immigrant groups, or Indigenous Peoples [155,163,169,218]; distinct hardships such as financial barriers to care were

exacerbated for women who faced multiple forms of discrimination. Significant loss of income as well as travel restrictions affected the ability of sex workers to access STI testing, prevention, and treatment services, as reported in four studies [192,198,221,222].

3.4 DISCUSSION

In this systematic scoping review, we found that women and girls faced reduced access to key SRH services globally due to the COVID-19 pandemic and related mitigation efforts, which resulted in decreased utilization of SRH services compared to previous years. We found that there were significant gaps in the geographical distribution of this body of research. The majority of included research has been conducted on populations in North America and sub-Saharan Africa, with a disproportionate focus on the United States at the national level (22 out of 83). Overall, studies were significantly less representative of countries in East Asia & the Pacific – where COVID-19 restrictions were very strict [239]– Latin America & the Caribbean, South Asia, and the Middle East & North Africa compared to North America, sub-Saharan Africa, and Europe & Central Asia. Differences in demand for SRH services cannot entirely explain the geographical unevenness of this research field. For example, as of 2019 the abortion rate per 1000 women of reproductive age was highest in West Asia and North Africa, a region in which no studies were conducted to assess the impact of the COVID-19 pandemic on abortion access, and second highest in South Asia, which only had one study on this topic [240].

We found that decreases in contraceptive access and utilization during to the COVID-19 pandemic were observed globally, which compromises progress towards the SDGs and may leave millions of women vulnerable to unwanted pregnancies [241,242]. We found that the same barriers that prevented women from accessing contraception also prevented access to abortion

consultations, procedures, and post-abortion care. It is known that when barriers to safe abortion exist, such as legal restrictions, women are more likely to turn to unsafe methods [243]. However, none of the included studies reported on utilization of unsafe abortion methods to compensate for reduced access to safe abortion. Consequently, it remains unclear whether efforts aimed at increasing the portion of abortions that are safely self-managed curbed a projected increase in unsafe abortion. Many studies reported that COVID-19 mitigation measures inadvertently reduced access to GBV/IPV related circumstances; this is particularly troubling as researchers have determined a correlation between pandemic stressors and IPV [244] with an increase in the incidence of IPV during stay-at-home orders [245]. The increase in IPV incidence may be the cause of the increase in utilization of remote GBV/IPV services; however, more research is necessary to identify the effectiveness of remote GBV prevention and intervention services, particularly in LMIC [246].

Specific challenges posed by the COVID-19 pandemic on SRH services are critical to understand in order to restore and ensure access to essential SRH care during future pandemics. We saw that some reported challenges were distributed unevenly across geographical regions and selected SRH services. For instance, challenges such as reliance on public transportation, living far from SRH service providers, relying on income from a job sector affected by the pandemic, and technology related issues were cited more often in studies from LMIC, thus reflecting a disproportionate burden of the COVID-19 pandemic in economically disadvantaged settings [180,186–188,191,192,198,230]. Concurrently, limited resources, such as clinic closures, stock outs, and financial burdens were reported less frequently in studies focusing on abortion services. In response to social distancing measures and limited in-person service capacity, many SRH service providers in HIC and UMIC adopted telemedicine as a service

delivery model, primarily for abortion, but also for contraceptive counseling and GBV/IPV. In many settings, telemedicine is a highly acceptable alternative to in person treatment as it can reduce risk of contracting COVID-19, minimize travel time, and increase patient ease and comfort [159,161,218,235]. Our review findings support the notion that the pandemic has accelerated a shift from in-person care to self-management through telemedicine, which may have maintained access to safe abortion services [89] and could partly explain why abortion services were less impacted by both supply and demand side challenges. Still, telehealth may have limitations in some circumstances such as lack of privacy [218], technological challenges [156,159,232], and reduced perceived comfort and safety related to GBV/IPV services [158,163]. Further research is warranted to inform where telemedicine in connection to SRH services is beneficial and where it may exacerbate healthcare inequities.

Although few studies included populations such as refugees, ethnic minorities, LGBTQI individuals and adolescents, our findings suggest that the COVID-19 pandemic has disproportionately impacted SRH access and utilization for groups with specific SRH needs. The SRH needs of these groups differ only slightly from women in general; however, distinct barriers to accessing care engender unique needs in order to achieve sexual and reproductive justice [123–126]. For instance, displaced people and refugees are at a heightened risk of sexual assault and gender-based violence in crisis settings [232] but face increased barriers to access to SRH services during humanitarian emergencies; this is characterized by discontinuation of contraceptive services, increased rates of unsafe abortion, and substandard STI and HIV care [247]. It can be assumed that these challenges were aggravated during the pandemic; however, more evidence is necessary to properly inform the extent of harm to refugee populations. LGBTQIA+ individuals have similar SRH needs to adults and adolescents; however, accessing

these needs is often prohibited by stigma, discrimination, and even violence [248]. Most lesbian, gay, and transgender youth have not disclosed their sexual orientation to healthcare providers [249]; this undermines care quality and poses difficulties in collecting accurate data on the specific needs of this group. This may be reflected in the dearth of studies characterizing their experiences during the pandemic.

Indigenous People are another population with distinct SRH needs who have and continue to face disempowerment, discrimination, and erasure and have consistently been insufficiently addressed in healthcare policies and programs, particularly during infectious disease outbreaks [250–253]. Indigenous women worldwide are at an increased risk of GBV including sexual and physical abuse [254]; as global rates of sexual assault and violence increase during pandemics, it is imperative to understand and address access to SRH care including GBV services for Indigenous women. Only a small number of studies looked at the impact of the COVID-19 pandemic on sex workers [192,198,221,222], who require consistent access to contraceptives and STI/HIV services. This may be because in-person sex work was difficult during social distancing making this population especially hard to reach. The fact that only one included study considered the perspectives of people with intersecting identities or who face multiple forms of discrimination highlights a significant research gap that must be bridged in order to fully appreciate the impact of the COVID-19 pandemic.

The findings of this review have implications for policy, research, and practice. We highlight the geographical unevenness of this research field and suggest the allocation of research to regions, particularly Latin America, the Caribbean, South Asia, the Middle East, and North Africa, in which the impacts of the COVID-19 pandemic on SRH are less understood. Moreover, research efforts should prioritize study populations with intersecting identities for

which barriers to SRH care are exacerbated and marginalized groups who faced a disproportionate burden of impact by the COVID-19 pandemic. Specific research questions have arisen from this review, such as the impact of the pandemic on the incidence and risk of unsafe abortion. Insofar as policy, supply side barriers to care may be alleviated by automatic allocation of funds and resources to maintain SRH services during public health emergencies. This review provides evidence for liberal policies with regard to reproductive choice, as countries with laws that protect abortion access tended to report an increase in utilization of safe, remote abortion services, while settings with more restrictive laws reported a decrease in abortion access. Banke-Thomas and Yaya highlighted service delivery adaptations that have been implemented to resolve demand-side barriers [246], such as free ride shares to clinics [255], family planning commodity delivery [133], and informational social media campaigns [256]. Given supply-side barriers such as transportation disruptions and fear of clinic attendance, clinical practices adaptations that minimize the frequency of or combine provider visits (e.g. contraception and STI testing/treatment) may increase accessibility. Further research on the efficacy, equity, and acceptability of these interventions is necessary to inform their continued use.

3.5 STRENGTHS AND LIMITATIONS

A key strength of this review is the breadth of systematic database screening and number of studies reviewed. The scoping review protocol allowed for consideration and inclusion of various study designs within multiple SRH subject areas. We included studies from a variety of settings, representing research from high income to low-income countries, which showcased the inherent disparities in SRH research volume among certain regions. This work is also strengthened by the inclusion of research that examined the unique impact of the COVID-19

pandemic on groups with distinct SRH needs. A limitation of this work is that it excluded studies not published in English, which may have incorporated bias in the geographical distribution of published research.

3.6 CONCLUSION

We found that the COVID-19 pandemic impacted access to and utilization of contraceptive services, safe abortion services, IPV/GBV and STI/HIV services negatively across the globe. The studies included in this review reported reduced utilization of contraception services, reduced use of LARCs, and diminished access to safe abortion services, which threaten progress towards the SDGs. Further, survivors of GBV and IPV faced reduced access to in-person services such as shelters and social support networks, despite increased demand. Access and utilization of HIV/STI testing, prevention, treatment/care, and counselling were also curtailed by the COVID-19 pandemic. Our work evidences the scarcity of SRH research in settings with high burden of disease and on marginalized groups with distinct SRH needs, underscoring a theme of widened health disparities caused by the pandemic. As the COVID-19 pandemic continues, findings from this review highlight the importance of maintaining access to SRH services to ensure that traction towards global development goals are not lost. There is a clear need for policy and practice adaptations that maintain and improve access to SRH services now and in future public health crises.

TABLE 3.1. Thematic summary of the reported challenges related to reduced access and utilization of SRH services (n=33).

Cause	Description	Study Settings (n)	References
Transportation restrictions and disruptions (n=16)	• Shutdown of public transportation made it difficult to access a clinic • Travel/mobility restrictions confined patients to certain regions and cut off access to distant clinics • Abuse by police and soldiers at road blocks made travel difficult • Quarantine orders and curfew made it impossible to leave the home, schedule or attend appointments	Australia (1), China (1), Kenya (1), Nepal (1), New Zealand (1), Uganda (3), UK (1), US (2), Zimbabwe (1), Mixed (4)	[34,41,52,58,59,63,64,70,82,90,91, 96,102,104,106-108]
Financial burdens (n=9)	• Income loss due to the pandemic made it more difficult to afford SRH services • Financial challenges made it difficult to afford resources to access services, such as cloth masks, public transportation, and child care	Kenya (2), Uganda (2), US (3), Mixed (2)	[27,35,41,52,60,63,70,106,107]
Limited medical or social resources (n=19)	• Medical resources (staff, PPE, viral testing, etc.) diverted from SRH services to COVID-19 effort • Stockouts: shortage of medications (particularly ARVs) and transport disruptions on essential supplies • Complete closure of SRH clinics or service provision facilities • Decrease in the number of available shelters for women seeking refuge services due to increased demand and social distancing • Lack of interpreters to support women who need them • Community mutual aid efforts curtailed (e.g. community babysitting for domestic violence survivors)	Australia (1), China (1), Kenya (1), Uganda (3), UK (2), US (5), Zimbabwe (1), EU&CA (2), Mixed (3)	[30,34,35,39,43, 52,58,61,63,70,73,78, 82,84,91,96, 104,106,108]
Lack of information (n=6)	• Lack information on available services or avenues of support • Misunderstandings about follow-up after telehealth • Confusing information on threat of COVID-19	Germany (1), New Zealand (1), Uganda (1), UK (1), Zimbabwe (1) Mixed (1)	[52,58,82,85,90, 104]
Legal restrictions and disruptions (n=4)	• Abortion not deemed an essential service • Laws limit procedural changes necessary to restore access to SRH services, primarily abortion • Disruptions to legal proceedings complicated care-seeking for IPV victims	US (2), EU&CA (1), Mixed (1)	[33,34,79,106][161, 162,207,234]

Fear, safety or privacy concerns (n=12)	• Lack of privacy to call provider or have telehealth appointment due to stay-at-home orders • Fear of exposure or contracting COVID-19 at a medical facility • Fear of being undocumented • Fear of receiving substandard medical care due to COVID-19	Australia (1), Kenya (2), New Zealand (1), Uganda (2), UK (1), US (2), Mixed (3)	[34,35,59,60,63, 70,82,90,96,104, 107,108]
Technological challenges (n=6)	• Shortage of technological facilities for virtual services • Patients or providers not as comfortable with telehealth services or perceive them as less effective or of lower quality • Increase in health disparities for patients who have less access to technology or language barriers	Belgium (1), US (4), SSA (1)	[28,30,31,35,88, 104][156,158,159, 163,216,232]
Self-censorship of needs (n=2)	• Patients did not think service was necessary in light of the pandemic and could wait to seek care	New Zealand (1), UK (1)	[82,90]

TABLE 3.2. Effect of the COVID-19 pandemic on subgroups with distinct SRH needs (n=16).

Subgroup	Study (Author, Setting)	Effect of COVID-19
Adolescents	Rose (New Zealand) [218]	Young people faced barriers for SRH care during lockdown including self-censorship of care-seeking, lack of privacy or transportation, lack of information about service availability, and COVID-19 related concerns.
	Mambo (Uganda) [180]	Access to SRH information and services diminished among youths during lockdown due to lack of transportation, distance to health facilities, and high cost of services.
	Thomson-Glover (UK) [202]	Adolescents in both rural and urban settings exhibited a substantial decrease in attendance at sexual health services and less frequently utilized emergency contraception.
	Lewis (UK) [210]	Young women and reported significant difficulties accessing contraception, including condoms, during the pandemic. Challenges were associated with a lack of in person appointments to start, stop, switch, or continue contraceptive methods, lack of information about available care, fear of contracting COVID-19, risking privacy to access contraception, and self-censorship of SRH needs.
	Li (China) [220]	About one-third of sexually active adolescents reported difficulties accessing abortion, post abortion care, STI advice and management, or contraceptives due to COVID-19.
	Kassie (Ethiopia) [195]	The proportion of teenage pregnancy increased during the pandemic as well as the proportion of teenagers using abortion services, possibly indicating reduced access or utilization of birth control among this group.
	Dyer (Kenya) [197]	COVID-19 impacted adolescents living with HIV's ability to access medical support and some had difficulty refilling ARVs, resulting a relatively high rate of missed ARV treatments.
LGBTQIA+ Identifying Individuals	Rose (New Zealand) [218]	Respondents who identified as LGBTQIA+ were as likely as non-identifying respondents to have received SRH care during lockdown
	Lindberg (US) [155]	COVID-19 caused women to delay or cancel accessing SRH providers for contraception, an effect which was more pronounced for sexual minority women

	Restar (Mixed) [233]	COVID-19 imposed burdens on accessing HIV treatment and prescription refills among trans and nonbinary people living with HIV; nearly one-third of respondents reported not having access to an HIV provider since pandemic control measures were implemented
Displaced People and Refugees	United Nations (Mixed) [232]	COVID-19 resulted in a decrease in reporting of violence against women and limited access to social and health services; the situation is exacerbated for women and girls who face multiple forms of discrimination, such as refugees and migrant workers.
Racial and Ethnic Minorities, Immigrant Groups, and Indigenous Peoples	Rose (New Zealand) [218]	Indigenous Māori women were less likely than NZ European, Pacific Islander, or Asian respondents to have been able to access SRH care during the pandemic.
	Lindberg (US) [155]	Hispanic and non-Hispanic black women were more likely to have experienced pandemic-related delays or cancellations of contraceptive care or other SRH services.
	Sabri (US) [163]	Immigrant survivors of IPV, particularly those who are undocumented, faced distinct hardships in accessing care due to greater financial hurdles and lack of public benefits such as unemployment and government assistance including medical insurance.
	Lin (US) [169]	Racial minority women disproportionately struggled to access contraceptive care, including being able to access a pharmacy, afford care, get a prescription, or get a LARC method replaced or removed; this was largely due to decreased financial assets.
Sex Workers	Mantell (Kenya) [192]	Though the pandemic did not significantly affect sex workers enrolled in an active RCT's access to provided PrEP; where access was affected it was primarily due to difficulties traveling to pick up medication.
	Htun Nyunt (Myanmar) [221]	COVID-19 affected HIV prevention services such as condom distribution and HIV testing for female sex workers. The pandemic caused a decrease in ART initiation immediately following stay-at-home order. Most HIV services were returned to pre-pandemic levels by June 2020.
	Janyam (Thailand) [222]	COVID-19 significantly impacted sex workers' ability to access STI testing a treatment as well as STI prevention services such as condoms, PrEP, and drug treatment services. Sex workers with HIV reported difficulties accessing ART. Loss of access may be explained in part by significant loss of income and travel restrictions.
	Gichuna (Kenya) [198]	COVID-19 restriction measures has had detrimental impacts on access to SRH services for sex workers living in informal settlements outside of Nairobi. Curfews, police mistreatment, fear of COVID-19, social distancing measures, contraceptive shortages, and financial losses contribute to reduced access/utilization of contraception and HIV treatment.

Chapter 4. DRUG-ELUTING EMBOLIZATION PARTICLES FOR PERMANENT CONTRACEPTION

Adapted from: Drug Eluting Embolization Particles for Permanent Contraception. **VanBenschoten H**, Yao S, Jensen J, Woodrow KA. ACS Biomaterials and Engineering (2022).

4.1 ABSTRACT

Medical technology that blocks the fallopian tubes nonsurgically could increase access to permanent contraception and address current unmet needs in family planning. In order to achieve total occlusion of the fallopian tube via scar tissue formation, acute trauma to the tubal epithelium must first occur followed by a sustained and ultimately fibrotic inflammatory response. Here, we developed drug-eluting fiber-based microparticles that provide tunable dose and release of potent sclerosing agents. This fabrication strategy demonstrates high encapsulation of physicochemically diverse agents and the potential for scalable manufacturing by utilizing free-surface electrospinning to generate material for particle micronization. Manipulation of nanofiber formulation characteristics, including drug loading, drug hydrophobicity, polymer hydrophobicity and crystallinity allowed for modulation of the sustained release properties of our microparticles. We assessed various fibrous microparticle formulations *in vivo* using a newly developed and validated guinea pig model for contraception. We found that fiber microparticles with bolus release doxycycline effectively elicited acute trauma and those formulated with highly loaded phenyl benzoate caused sustained inflammation in the target organs. The demonstrated potency of these electrospun microparticles, as well as their embolic size and shape, suggest

potential for proximal agglomeration and inflammatory activity in the fallopian tubes following transcervical delivery.

4.2 INTRODUCTION

Female permanent contraception is currently the most common form of birth control used worldwide, as it is the method of choice for almost a quarter of reproductive age women [257]. This high demand for permanent birth control is met entirely by surgical intervention. Surgical approaches involve removing a segment or the entirety of both fallopian tubes or placing mechanically occlusive devices such as clips or bands. Both laparotomic and laparoscopic approaches require intraabdominal access which exposes women to the myriad risks and drawbacks of any invasive surgery – including adverse reactions to anesthesia, possible injury to local organs, bleeding, pain, and increased time and financial commitment [258,259]. While surgical permanent contraception is highly effective and safe when quality medical facilities and trained clinicians are available, approximately 5 billion people worldwide lack access to safe and affordable surgical care. A safe and effective nonsurgical method of permanent contraception could help address the unmet need for contraception in women who have completed desired family size.

The fallopian tubes have a unique immunological and anatomical makeup that is intrinsically pro-healing in order to maintain tubal and reproductive function. Flow cytometric analysis of $CD45^+$ leukocyte populations in the female reproductive tract show that fallopian tube tissue is the most populated site of immune cells, the majority of which are $CD3^+$ T cells and $CD66b^+$ granulocytes [260]. Fallopian tube physiology is characterized by extensive vascularization, high levels of mucosal secretions, and minimal luminal space surrounded by a muscular myometrium to restrict the entrance of contaminants – traits which collectively promote strong innate

immunity. To overcome these barriers and elicit complete tubal occlusion, initial trauma to the fallopian tubes must be sufficient to provoke extensive epithelial damage followed by chronic inflammation that resolves in pathological scarring in lieu of re-epithelialization. This effect is mediated by the dose and duration of exposure to an antagonistic agent. The natural tubal occlusion that occurs following infection with sexually transmitted pathogens such as *N. gonorhoeae* and *C. trachomatis* illustrates this principle. Upon infection, the body's innate immune system employs a mechanism of epithelial exfoliation to prevent colonization of harmful pathogens in the genital mucosa [261]. Fallopian sequelae due to epithelial shedding and inflammation developed as survival mechanisms to combat systemic infection. Tubal occlusion prevents ascension of harmful pathogens into the peritoneal cavity, which is accessed by fimbriae at the distal end of the fallopian tubes. Interestingly, *N. gonorrhoeae* is capable of causing tubal occlusion after a single infection due to the potency of the lipoologosaccharide toxin released by the pathogen which causes total epithelial desquamation [262]. In contrast, *C. trachomatis* induces tissue damage but not total desquamation, therefore multiple infections are required for occlusive tubal scarring to occur. Pursuant to the pathology of these infections, we hypothesize that the potency of an antagonistic agent can compensate for the duration of exposure, and vice-versa. This paradigm potentiates the design strategy for novel nonsurgical permanent contraception.

Several current and prior methods of permanent contraception demonstrate this principle [263–265]. While many surgical methods that use ligation or clipping function independently of time, other methods, such as thermally induced trauma via cautery or cryosurgery, require prolonged exposure to induce sufficient and irreversible tissue damage. Indeed, such injury is dampened by thermal buffering from extensive blood flow [263]. Essure, a dynamically

expanding nitinol and stainless-steel micro-coil that is placed transcervically into both fallopian tubes, was highly effective at eliciting fibrotic tissue encapsulation. This response was similarly time-dependent; clinical reports show that the rate of successful closure of the tubal lumen increased by over 50% when wear-time extended from a 4-week interval to an 8-week interval [264]. Chemical sterilization approaches, which employ inflammatory agents that directly cause epithelial detachment or apoptosis leading to pathological scarring, show strong dose-and-time-dependent occlusive effects. For instance, in a study evaluating the fibrotic effect of quinacrine pellet insertion in the fallopian tubes, the successful occlusion rate increased from 56% to 92% for pellet residency of 0-6 weeks to 7 or more weeks, respectively. The same study showed a distinct dose-dependent response, with the success rate increasing from 43% to 100% for a 100 versus 252 mg dose of the sclerosant [265]. The Essure permanent implant and use of quinacrine pellets, though effective, serve only as lessons regarding features of successful occlusive techniques; both therapies lack full FDA approval due to severe side-effects. Though perhaps safer, instillation of liquid sclerosing agents, such as tetracycline and polidocanol, is limited by insufficient delivery to target tissue. Indeed, intrauterine administration often results in the target organ being exposed to less than 5% of the administered dose due to significant leakage [265]. Thus, there remains a challenge to develop FDA-approved nonsurgical sterilization that targets the fallopian tubes and elicits fibrosis according to principles that govern successful occlusion.

While we know, from naturally occurring infections and prior clinical attempts, that successful nonsurgical tubal occlusion is a dose-and-time dependent process, a technique that integrates both features into an effective and clinically acceptable technology has yet to be developed. Additionally, there is currently no well-established or consistent platform to systematically investigate the optimal dose and time of exposure for a given antagonistic agent

that could mediate effective tubal occlusion. In order to address these gaps, we aimed to develop a scalable platform to generate drug-eluting microparticles that can efficiently deliver sclerosing agents of diverse physicochemical properties to the fallopian tubes. We hypothesized that free surface electrospinning could be used as a scalable method for generating microparticles composed of polyester nanofibers that encapsulate highly loaded active agents and provide drug release at various timescales. We investigated polyesters, including poly(lactic-co-glycolic) acid (PLGA), polycaprolactone (PCL), and poly(L-lactic) acid (PLLA), to generate fibrous microparticles that could offer tunable release of encapsulated agents. These polymers biodegrade into readily metabolized products, which allows for transient residency in the fallopian isthmus and reduces potential migratory effects seen with other permanent contraceptive implants [266]. Furthermore, evidence suggests that the release of acidic byproducts at the site of polyester degradation could enhance inflammation [267,268]. We further hypothesized that polyester microparticles of inhomogeneous shape and size within a 100 – 300 μm diameter range may target and agglomerate in the fallopian isthmus into which they are perfused; this solid dosage modality can therefore deliver active agent while minimizing leakage associated with liquid-based treatments. Thus, our aims were to develop microparticles that (1) achieve high encapsulation efficiency of physicochemically diverse sclerosing agents, (2) can be processed into microparticles of target size and shape, and (3) can release encapsulated agents on a variety of timescales, from bolus release to investigate acute tissue responses to sustained release (>30 days) to assess long-term treatment outcomes. To test our hypothesis that these particles could elicit precursors to tubal occlusion, we validated a guinea pig model for permanent contraception and found that polyester fibers enhance acute inflammation, hemorrhage, and long-term fibrous capsule formation at the utero-tubal junction. These *in vivo*

findings, along with the design space established by our versatile and scalable biomaterial fabrication approach, potentiates this method as a suitable alternative to nonsurgical permanent contraception methods previously under investigation.

4.3 MATERIALS AND METHODS

4.3.1 Materials

Poly (D,L-lactic-co-glycolic) acid (PLGA) with a 50:50 LA:GA ratio, acid termination, and an inherent viscosity of 0.55-0.75 dL/g, and poly (L-lactic) acid (PLLA) with ester termination and an inherent viscosity of 0.90-1.20 dL/g in $CHCl_3$ were purchased from Lactel Absorbable Polymers (Birmingham, AL, USA). Polycaprolactone (PCL) with an average molecular number (M_n) of 80,000 Da, poly (DL-lactide) (PDLLA) with an average molecular weight (M_w) of 21,000 Da and an acid termination, and poly (vinyl alcohol) (PVA) with an average M_w of 105,000 Da were purchased from Sigma-Aldrich (St. Louis, MO, USA). Doxycycline hyclate was purchased from MP Biomedicals, LLC (Santa Ana, CA), and doxycycline hydrochloride (HCL) was purchased from Research Products International (Mount Prospect, IL, USA). Phenol and nonaethylene glycol monodecyl ether (Polidocanol) were purchased from Sigma-Aldrich. Phenyl Benzoate was purchased from Alfa Aesar (Tewksbury, MA, USA). The solvents hexafluoroisopropanol (HFIP), 2,2,2-trifluoroethanol, chloroform, and dimethyl sulfoxide (DMSO) were purchased from Oakwood Laboratories (Wayne County, MI, USA), Sigma-Aldrich, Avantor Performance Materials (Bridgewater, NJ, USA), and VWR (Randor, PA, USA), respectively. Veterinary gelatin capsules (size 9, batch #VC191168) were purchased from Torpac Inc (Fairfield, NJ, USA). Cremophor A25 was purchased from Sigma-Aldrich. High-performance liquid chromatography (HPLC) grade acetonitrile, trifluoroacetic

acid, and water were obtained from Fisher Scientific (Pittsburgh, PA, USA). Dulbecco's phosphate buffered saline (DPBS) was purchased from Mediatech Inc. (Central Valley, PA, USA).

4.3.2 Drug treatment of tissue explants

Two fallopian tubes were obtained from an adult female *M. Mulatta* (hybrid, 12.5 y/o) rhesus macaque via the Washington National Primate Research Center Tissue Distribution Program. IACUC approval was not needed for *ex vivo* experimentation. Fresh fallopian tubes were collected in chilled Dulbecco's Modified Eagle Medium with Nutrient Mixture F12 (DMEM:F12, Thermo-Fisher Scientific, Waltham, MA, USA), supplemented with 10% fetal bovine serum (FBS) (Gemini Bio-Products, Sacramento, CA, USA). Fallopian tubes were dissected to remove adventitial tissue and 12, 3 mm cross-sectional biopsy punches were taken from the ampulla of each tube, totaling 24 biopsy punches. Biopsies were placed in a 24 well plate and 500 µL of warmed DMEM:F12-FBS media supplemented with no drug, 1 µg/mL lipopolysaccharide (LPS), doxycycline hyclate in a 1%, 5%, or 10% (mg/mL) dose, or phenol in a 1%, 5%, or 10% (mg/mL) dose was added to each biopsy in triplicate. Samples were incubated at 37°C for 24 hours. After 24 hours, media was removed from each sample and centrifuged at 10000 rpm for 5 minutes to remove cellular debris. Tissues were washed twice with PBS; two biopsies for each condition were placed a fresh 24 well plate with 400 µL of warmed DMEM:F12-FBS. 80 µL of CellTiter Blue (Promega, Madison, WI, USA) was added to each biopsy and to three wells containing only media and incubated at 37°C. After 4 hours, 100 µL samples of media were taken in triplicate from each biopsy incubated with CellTiter Blue and fluorescence was recorded at $560_{Ex}590_{Em}$. The remaining biopsy from each condition was fixed

in 20 mL of formalin for 24 hours at 4°C before being sent to the University of Washington Histology and Imaging Core for sectioning and hematoxylin and eosin (H&E) staining. The extent of cell infiltration and percent of epithelial detachment were quantified using ImageJ (NIH) by tracing and measuring the pathlength of in-tact epithelium divided by the total epithelial length. This percentage was defined as the percent of attached epithelium; the opposite of which was the percent of detached epithelium.

4.3.3 Preparation of electrospun fibers

Polyester blends loaded with doxycycline and phenyl benzoate were generated via uniaxial needle electrospinning and selected formulations were fabricated on a Production Line 1S500U Elmarco Nanospider. 80:20 PLGA/PCL was made by dissolving PLGA and PCL in an 80:20 (wt/wt) ratio at 15% (wt/vol) in HFIP. PLLA/PDLLA blends were made by dissolving PLLA and PDLLA at 100:0, 75:25, and 50:50 (wt/wt) ratios at 15% (wt/vol) in a 1:1 (vol/vol) mixture of chloroform and 2,2,2-trifluoroethanol. PLLA/PLGA blends were made by dissolving PLLA and PLGA in 100:0, 80:20, 50:50, and 20:80 (wt/wt) ratios at 15% (wt/vol) in a 1:1 (vol/vol) mixture of chloroform and 2,2,2-trifluoroethanol. 80:20 PLLA/PCL was made by dissolving PLLA and PCL in an 80:20 (wt/wt) ratio at 15% (wt/vol) in a 1:1 (vol/vol) mixture of chloroform and 2,2,2-trifluoroethanol. PVA was made by dissolving PVA at 15% (wt/vol) in water and heating slowly. Polymers were allowed to dissolve in solvent overnight and drugs were added a minimum of 1 hour prior to electrospinning. All polymer formulations were also electrospun in the absence of drug (blank fibers). For 80:20 PLGA/PCL, doxycycline was added at 20%, 40%, 60%, and 80% (wt/wt); for PLLA, doxycycline was added at 20%, 40%, and 60% (wt/wt); for PLLA/PDLLA blends and PLLA/PLGA blends (excluding 20:80 PLLA/PLGA),

doxycycline was added at 20% (wt/wt). For 80:20 PLGA/PCL blends, phenyl benzoate was added at 20%, 40%, 60%, and 80% (wt/wt). For needle electrospinning, approximately 500 µl of polymer solutions were loaded into a 1 mL glass gastight syringe equipped with a 21 gauge stainless steel dispensing needle and set into a NE1000 precision syringe pump (New Era Pump Systems Inc., Farmingdale, NY, USA). Unless otherwise noted, solutions were pumped at a rate of 30-50 µl/min through a 13 kV electric field applied by a high voltage generator (Gamma High Voltage Research) between the needle and a grounded metal plate covered by a sheet of wax paper set 13-15 cm from the needle tip. PVA was electrospun at 18 kV and pumped at a rate of 5 µl/min. For electrospinning on the Production Line NS 1S500U Nanospider (Elmarco, Czech Republic), fiber mats were generated in static conditions using 20 mL of polymer/drug solution. A 0.6 mm orifice was used to coat 350 mm of a rotating wire set 200 cm from a metal collector covered by a sheet of wax paper. A 100 kV charge was applied between the coated wire and the collector for a total run time of 15 minutes. Collected fiber mats were dried in a fume hood overnight and stored in vacuum sealed bags until use or analysis.

4.3.4 Drug loading and in-vitro drug release from electrospun fibers

Effective drug loading, termed "encapsulation efficiency," was defined as the total amount of drug associated with the fibers relative to theoretical loading. To determine encapsulation efficiency of doxycycline and phenyl benzoate in electrospun fibers, each fiber type was cut into approximately 4 mg samples (n=3); exact mass was recorded for each sample. Fibers were placed in 7 mL of DMSO and attached to a rotisserie shaker for 3 days or until fibers were completely dissolved. 200 µL of supernatant was collected for HPLC analysis. Drug content was quantified with a Shimadzu Prominence LC20AD UV-HPLC system equipped with

a Phenomenex Luna C18 column (250 x 4.6 mm, 5 µm) and LC Solutions software. Doxycycline was detected with a mobile phase of HPLC grade water and acetonitrile (75:25) supplemented with 0.1% trifluoroacetic acid, eluted at an isocratic flow rate of 1 µL/min for 15 minutes and an injection volume of 20 µL. Column oven temperature was 30°C. Doxycycline standards were prepared in DMSO with a linear range from 0.001 to 1 mg/mL, detection at 265 nm, and a retention time of 7.2 minutes. Phenyl benzoate was detected with a mobile phase of HPLC grade water and acetonitrile (70:30) supplemented with 0.1% trifluoroacetic acid eluted at an isocratic flow rate of 1 µL/min for 15 minutes and an injection volume of 40 µL. Column oven temperature was 30°C. Phenyl benzoate standards were prepared in acetonitrile with a linear range from 0.05 to 0.5 mg/mL, detection at 265 nm, and a retention time of 5.93 minutes. Encapsulation efficiency was determined by calculating the drug concentration in the supernatant of dissolved fibers using standard curves and dividing by theoretical drug content according to the following equation:

$$\%EE = \frac{Measured\ drug\ concentration}{Initial\ fiber\ mass\ \times\ theoretical\ loading} \times 7\ mL\ x\ 100$$

In vitro release of doxycycline and phenyl benzoate from electrospun fibers was carried out in 1X DPBS and in 1X DPBS supplemented with 1% Cremophor, respectively, in sink conditions. Sink conditions for doxycycline were determined using the published solubility of doxycycline in PBS (50 mg/mL). We determined the solubility of phenyl benzoate in 1% Cremophor by saturating an aliquot of PBS-1% Cremophor, centrifuging the supernatant upon equilibrium informed by visible precipitation of drug, and analyzing the saturation concentration on HPLC (2.4 mg/mL). Fibers were cut into 5 mg samples (n = 3), placed in 10 mL of release medium, and incubated in a 37°C shaker. Spiked samples were prepared containing the theoretical amount of

drug retained in each sample type dissolved directly in release medium with an equivalent mass of drug-free (blank) fiber (C_{spiked}). Blank fibers in drug-free release medium were also prepared for each release study (C_{blank}). At predetermined time points, 400 µL of solution was removed from each sample for analysis by HPLC and replaced with fresh media to maintain sink conditions. For *in vitro* release, the HPLC detection method for doxycycline was the same as that described above; doxycycline standard curves were prepared in 1X DPBS with a linear range from 0.1 to 2 mg/mL, detection at 265 nm, and a retention time of 8.3 - 8.5 minutes. The HPLC detection method for phenyl benzoate release was the same as described above, with the same standard curve for analysis prepared in acetonitrile. Because phenyl benzoate hydrolyzes to phenol and benzoic acid *in vivo* and in simulated *in vitro* release medium, standard curves were also prepared for pure phenol in acetonitrile following the same HPLC method as described for phenyl benzoate, with linearity established between 0.001 and 0.5 mg/mL, detection at 265 nm, and a retention time of 5.7 minutes. For quantification of drug release from fibers, the concentration of drug in solution at each time point was calculated from standard curves. For phenyl benzoate-loaded fibers, phenyl benzoate and phenol content were calculated independently from respective standard curves in acetonitrile and summed *post hoc* to capture the total hydrolysable and hydrolyzed sclerosing agent content released. Therefore, "released phenol" refers to the total concentration of phenol and phenyl benzoate detected in release medium. Cumulative percent and cumulative dose of drug released from fibers was calculated according to the following equations:

$$\% \, Released = \left(1 - \frac{C_{spiked} - C_{sample}}{C_{spiked} - C_{blank}}\right) \times \, 100$$

4.3.5 Micronization of electrospun fibers

Micronization was performed on nanofiber mats electrospun on the Elmarco Nanospider. Mats were cut into 1 inch by 1 inch squares and massed. Approximately 2 grams of fibers were placed into a BlendTec MiniTwister Jar fashioned with a custom polystyrene lid that reduced jar volume to 8 oz. Rasping cycles of increasing intensity were used to generate microparticles, which were filtered through a 150 μm pore-size sieve (VWR), massed, and collected in a glass scintillation vial. Micronized particles were placed in a sterile tissue culture hood under UV light for 24 hours. To confirm sterility, a 10 mg sample of drug-free particles were submerged in 40 mL of LB Broth (Sigma) and incubated at 37°C. After 24 hours, the sample was centrifuged to remove suspended particles and absorbance measured at 600 nm. The OD600 was compared to a sample incubated with no particles to verify the absence of bacterial growth. Sterile particles were then stored at 4°C until use.

4.3.6 Polyester blend puncture and adhesion testing

Uniaxial puncture testing was performed with an Instron 5943 Mechanical Testing System (Instron) equipped with Bluehill 3 software. For puncture force analysis, polyester blends of 80:20 PLGA/PCL, PLLA, 80:20 PLLA/PLGA, 50:50 PLLA/PLGA, 20:80 PLLA/PLGA, and 80:20 PLLA/PCL prepared via uniaxial electrospinning were cut into ⅞" discs, massed and measured for thickness using digital calipers calibrated to 0.01 mm. A ¼" probe was attached to the load cell and fibers were fixed onto the sampling platform above a ½" beveled hole. A 100N load was applied at a rate of 3 mm/s to the center of the sample until failure. The elongation to puncture was calculated by:

$$Elongation\ fraction = \frac{([R]^2 + [D]^2)^{1/2} - R}{R}$$

Where R is the radius of fiber exposed to the beveled hole (½") and D is displacement of the probe from the point of contact to the point of fiber puncture. The puncture strength was calculated by:

$$Puncture\ strength\ \left(\frac{N}{mm^2}\right) = \frac{F}{A_{cs}}$$

Where F is the burst load required to puncture the fiber and A_{cs} is the cross-sectional area of the fiber at the edge of the beveled hole (thickness times circumference). This calculation normalizes for differences in sample thickness. The ratio of puncture strength to elongation fraction, herein called the relative puncture strength, was calculated from these equations. For mucoadhesion testing, PVA, 80:20 PLGA/PCL + 20 wt% doxycycline, 50:50 PLLA/PLGA + 20 wt% doxycycline, and 80:20 PLGA/PCL + 80 wt% phenyl benzoate fibers were cut into ⅞" discs, massed and measured for thickness. Approximately 1g of Type II mucin from porcine stomach (Sigma-Aldrich) was rehydrated in a petri dish with 2 mL of deionized water to form a sticky paste. Fibers were fixed flat to the upper load cell and lowered to contact the mucus; upon contact, a 10N load was applied vertically to separate the specimen from the mucus until load returned to baseline.

4.3.7 Scanning Electron Microscopy

Representative micronized fibers composed of 80:20 PLGA/PCL loaded with 20 wt% doxycycline were spread in a monolayer on an SEM stub using conductive carbon tape. Samples were sputter coated with gold and palladium. Imaging was performed with a JSM-7000F SEM (JEOL Ltd.) at the Materials Science and Engineering Department at the University of Washington. An acceleration voltage of 10 kV and working distance 6 mm were used with

magnifications of 50x, 250x, and 5,000x. Fiber diameter was measured from the 5,000x micrograph with ImageJ (NIH) software for a total of n = 30 fibers.

4.3.8 Laser Diffraction particle sizing

Microparticles generated with a 150 μm sieve were suspended at 5-10 mg/mL concentrations in a 5% surfactant (polidocanol) solution. Particle sizing was performed with a Horiba LA-960 Particle Size Analyzer (Kyoto, Japan) at the Materials Science and Engineering Department at the University of Washington. Deionized water with a real refractive index of 1.33 was used as the dispersion medium; electrospun fibers loaded with 20 wt% doxycycline and 80 wt% phenyl benzoate were sized with real refractive indices of 1.54 and 1.58, respectively. Circulation and agitation modes were set to 1, the system was de-bubbled, aligned, and blanked. Sample suspensions were added until transmittance was reduced by approximately 5%, then measurements were taken in n = 5 replicates. Particle diameter was calculated based on a Mie Theory scattering algorithm and reported as the volumetric mean, D[4,3], and span is calculated according to the following equation:

$$Span = \frac{D_{v,0.9} - D_{v,0.1}}{D_{v,0.5}}$$

Where $D_{v,0.9}$ represents the diameter where 90% of the volumetric distribution lies below, the $D_{v,0.1}$ where 10% of the volumetric distribution lies below, and the $D_{v,0.5}$ represents the median diameter which half of the distribution lies above and half lies below.

4.3.9 In vivo Guinea Pig procedures

Female guinea pigs housed at the Oregon National Primate Research Center were anesthetized prior to bilateral incision and flank laparotomy to expose the distal uterine horn on each side. We then injected 5% polidocanol foam (PF) or saline (1 mL) into the lumen of the distal uterine horns using a 23 gauge needle. Immediately following this, we made a small incision in the uterine wall to insert the gelatin capsules containing treatment into the distal horn. We secured in place with a small loop of suture proximal to the capsule to close the space. Prior to the procedure, gelatin capsules were sterilized under a UV sterilizer (Dermologic-209) for 1 hour. In a cell culture hood, sterile active materials were massed and packed into individual capsules using a capsule filling applicator. Uterine horn treatment groups included phenol (20 mg), phenyl benzoate (20 mg), silver nitrate (16 mg), empty capsules with 5% PF, doxycycline hyclate powder (10 mg) with 5% PF, 80:20 PLGA/PCL drug-free fibers (10 mg), 80:20 PLGA/PCL fibers + 70 wt% doxycycline hyclate (20 mg) with and without 5% PF, 80:20 PLGA/PCL fibers + 30 wt% doxycycline monohydrate (20 mg), and 80:20 PLGA/PCL fibers + 80 wt% phenyl benzoate (20 mg). Animals were allowed to recover and monitored daily for their post-operative behavior, ability to eat and maintain weight, and stool quality. Guinea pigs were euthanized and dissected 7 days and 30 days post-surgery. Immediately after necropsy, reproductive tracts were obtained and separated into upper ovary/horn and lower horn. Specimen were fixed in 4% paraformaldehyde, dehydrated in alcohol and embedded with paraffin. Continuous 5 μm cross sectional samples were taken and processed for H&E staining. Histological features were scored based on predetermined criteria.

4.3.10 Ethics statement

In vivo animal studies were approved by the Institutional Animal Care and Use Committee (IACUC) at the Oregon National Primate Research Center (Protocol #IP00003599). All animals were obtained and cared for in accordance with the IACUC guidelines.

4.3.11 Statistical methods

Graphical results were expressed as the mean of each replicate ± standard deviation. One-way analysis of variance (ANOVA) using Tukey's multiple comparison post-test was performed when comparing outcomes between groups, with statistical significance defined as $p < 0.05$ (*). Statistical analysis was performed on GraphPad Prism 8 software.

4.4 RESULTS AND DISCUSSION

4.4.1 Sclerosing agents induce cell death, epithelial delamination, and leukocyte infiltration of macaque fallopian tubes

Doxycycline and phenol have been used extensively as sclerosing agents for endovascular sclerotherapy and lymphatic cyst ablation [269,270], but exhibit unique tissue responses that may be explained by their distinct mechanisms of action. The molecular mechanism of doxycycline as a tissue antagonist is speculated to involve inhibition of matrix metalloproteinases and suppression of vascular endothelial growth factor-induced angiogenesis, thereby preventing tissue repair and endothelial maintenance [271]. The effect of doxycycline on epithelial layers has been studied using human bronchial epithelial cells, where it was shown to induce apoptotic pathways, necrosis, and cell detachment in a time and concentration dependent manner [272]. Ultimately, this is correlated with in an inflammatory response that causes fibrosis

and involution of endothelial-lined luminal structures. Phenol is a mildly acidic organic compound that has been used to treat hemorrhoids and varicose veins by causing hemorrhage of the endothelial submucosa resulting in obliteration of tissue [270,273]. It has a direct toxic effect on human colonic epithelial cells cultured *in vitro*, consistent with the well-known ability of phenol to damage plasma membranes and inhibit cell growth [274]. Here, we demonstrated the ability of both doxycycline and phenol to induce cell death and enhance leukocyte infiltration with unique effects on fallopian epithelial integrity.

We treated explant fallopian tubes obtained from a mature female *Rhesus Macaque* with varying concentrations of doxycycline and phenol to investigate the potential of these two active agents in initiating acute tissue trauma to fallopian epithelium. Phenyl benzoate is utilized in biomaterial formulations because it is a solid at room temperature and therefore able to form a solid dispersion while functioning as a sclerosant after dissolution and hydrolysis. Phenol and phenyl benzoate are considered analogous pharmaceutical compounds since the latter is an ester of phenol, which hydrolyzes in physiological conditions at a pH dependent rate to form phenol and benzoic acid. In weak basic conditions, such as the fallopian tube, complete hydrolysis is expected to occur in under 30 minutes [275,276]. Doxycycline was used in concentrations of 0.01 to 0.1% on monolayer epithelial cell cultures [272] and is typically employed as a sclerosing agent in concentrations of 0.5 to 10% [271]. Phenol has been assayed at concentrations of 0.1 to 0.5% in epithelial cell cultures [274] and is injected in a 5% concentration in almond oil [270]. As such, we chose to assay the inflammatory potential of 1%, 5%, and 10% solutions of each drug, concentrations that are 10-fold greater than those used to assay monolayer epithelial cell cultures. We chose to increase the concentration to account for the thickness of biopsy samples in comparison to single cell layer cultures and to recapitulate

clinical doses. Lipopolysaccharide is a bacterial endotoxin commonly used to elicit a strong inflammatory response; at 1 μg/mL, it does not cause cell death but does stimulate the recruitment of leukocytes and release of inflammatory cytokines [277]. As such, LPS was a positive control for assessing nontoxic inflammatory effects of the candidate sclerosants, whereas cell death, an important mechanism for inflicting acute trauma, was treated as a binary measurement in comparison to the media-treated control.

After 24 hours, biopsies treated with LPS, 1% phenol, and 1% doxycycline conditions showed no significant decrease in cell viability compared to media-treated controls (Figure 4.1A). Higher drug doses of 5 and 10% resulted in significantly reduced cell viability, indicating cytotoxicity of these treatments on explant biopsies after 24 hours. We found that doxycycline results in a near dose-dependent decrease in epithelial integrity, visible in representative histological images (Figure 4.1I,J,K). This exfoliation was significantly greater than the untreated control (Figure 4.1B). In particular, the 5% doxycycline treatment condition resulted in severe destruction of the epithelium, causing approximately 80% of the columnar cell layer to detach from the lamina propria. Surprisingly, phenol results in a dose-dependent increase in the integrity of the epithelium and we observed marked preservation of the mucosal layer on the apical surface of the epithelium (Figure 4.1E,F,G). However, this observation may be an artifact of phenol acting as a fixative in conjunction with formalin. Indeed, the addition of 2% phenol to a 4% formaldehyde (formalin) solution has been shown to accelerate fixation processes and result in reduced tissue shrinkage and distortion [278]. Despite differences in tissue morphology among the treatment groups, both drugs resulted in a significant increase in leukocyte infiltration consistent with that caused by LPS (Figure 4.1C). Based on the observed tissue effects of the sclerosants on fallopian biopsies, we conclude that doxycycline has an antagonistic effect on

fallopian epithelial structures that results in cell apoptosis, detachment, and inflammation. Although phenol did not enhance epithelial delamination, it caused cytotoxicity and immune-cell infiltration. We therefore posit that phenol has interesting sclerosing potential based on its immune activation that warrants further investigation. Thus, both drugs represent promising candidates for evaluation of physiologically distinct chemical induction of time- and dose-dependent fallopian fibrosis.

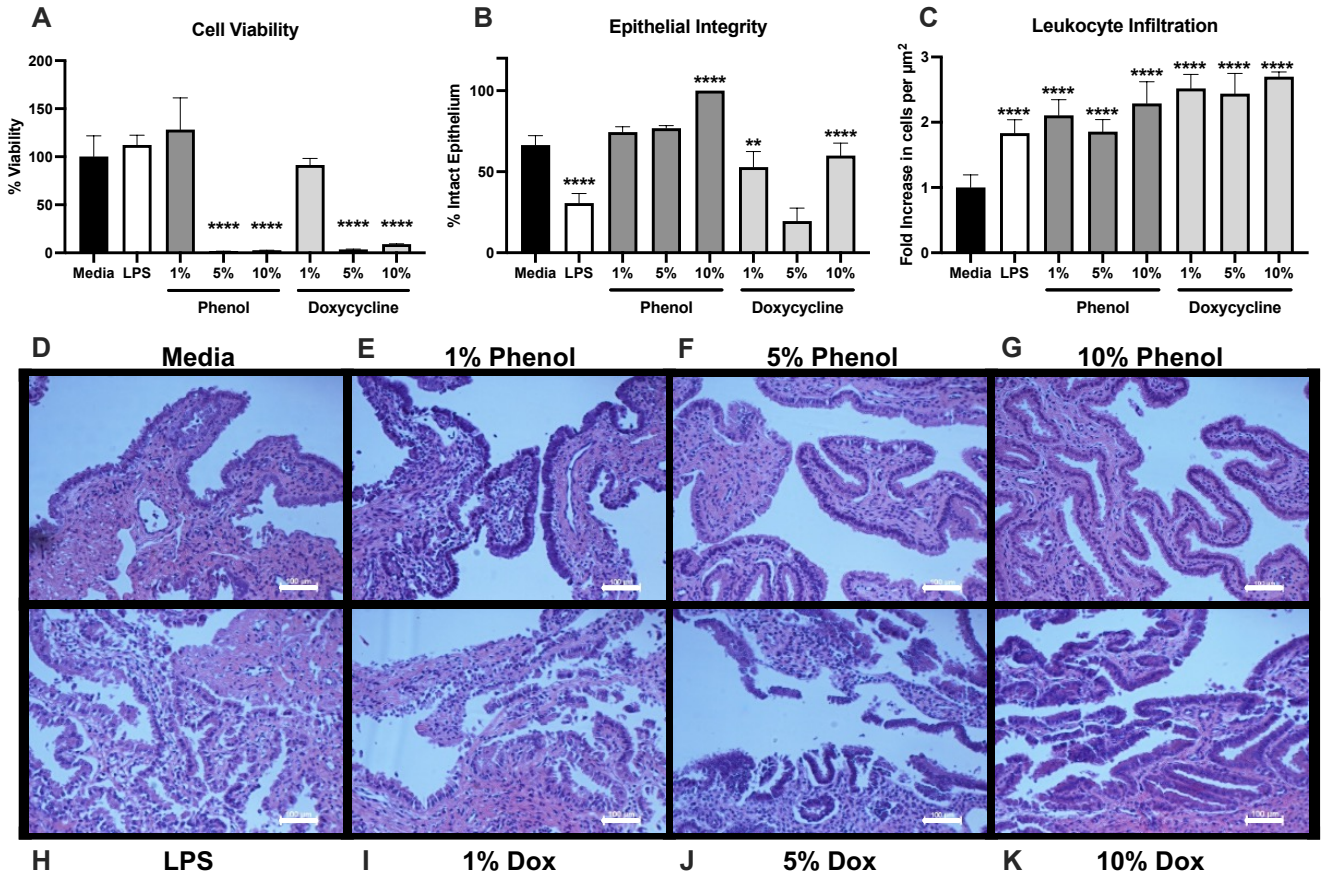

FIGURE 4.1. **Treatment with sclerosing agents causes tissue damage and leukocyte infiltration.** (A) Cell viability fraction of treated samples normalized to media treated samples. Percent expressed as the relative mean fluorescence ± standard deviation of n=2 biopsies assayed with CellTiter Blue. (B) Percent of intact epithelium is expressed as the fraction of attached epithelium over the entire epithelial distance; results represent the mean ± standard deviation of n=5 histological images taken at 10X magnification with widefield microscopy, capturing approximately 5000 µm of epithelial length per image. (C) Leukocyte increase expressed as fold-increase in cells per μm^2 of lamina propria over the media-treated sample; results represent the mean ± standard deviation of n=5 histological images taken at 20X magnification with widefield

microscopy, capturing approximately 11,000 μm^2 of tissue per image. (D-K) Fallopian tube biopsies cross sectioned and stained with H&E; images collected with 10X widefield microscopy. Scale bars represent 100 μm. (****) represents $p < 0.0001$. (**) represents $p < 0.01$.

4.4.2 Electrospun polyester blends show high encapsulation efficiency and processability for micronization

Electrospun polyester blends were loaded with doxycycline and phenyl benzoate ranging from 20 wt% to 80 wt% drug loading. PLGA/PCL (80:20) and PLLA fibers loaded with doxycycline and phenyl benzoate show high encapsulation efficiency at all drug loadings (Table 4.1), with up to 77% and 73% encapsulation efficiency measured for the 80 wt% drug loading, respectively. Doxycycline could not be spun at 80 wt% in PLLA as it was insoluble in the electrospinning solvent at a concentration above the critical micelle concentration of the polymer. A general trend of decreasing encapsulation efficiency with increasing drug loading is observed for both active agents. This result is consistent with previous data showing that higher drug loading is typically associated with a greater fraction of drug being surface associated which results in a relative reduction of encapsulated drug within the fiber matrix [279]. Variations in polyester blend formulation had little impact on encapsulation efficiency (Table 4.2). Doxycycline loading at 20 wt% in PDLLA/PLLA and PLLA/PLGA blends achieved 83% to 93% encapsulation efficiency, despite differences in polymer crystallinity and hydrophobicity. Phenyl benzoate loaded at 20 wt% in 50:50 PLLA/PLGA achieved 72% encapsulation efficiency (not shown). We did not measure a significant difference in efficiency between the 20 wt% and 80 wt% loading conditions. The high loading efficiency of electrospun material demonstrates the utility of this approach in formulating scalable biomaterials with minimal active agent loss compared to other particle fabrication approaches. Indeed, single and double emulsion particle formulation methods often fail to achieve higher than 10% efficiency in drug loading [280,281].

TABLE 4.1. Drug encapsulation in formulations with incremental theoretical loading.

Theoretical loading (wt%)		**20%**	**40%**	**60%**	**80%**
Doxycycline	**80:20 PLGA/PCL**	18.93% (94.64 ± 2.91)	34.96% (87.40 ± 1.79)	48.12% (80.20 ± 1.05)	61.58% (76.98 ± 1.24)
	PLLA	18.79% (93.79 ± 12.31)	39.42% (98.55 ± 5.54)	52.61% (87.69 ± 6.79)	
Phenyl Benzoate	**80:20 PLGA/PCL**	18.07% (90.34 ± 2.21)	34.48% (86.19 ± 2.03)	46.38% (77.30 ± 4.36)	58.62% (73.27 ± 1.60)

NOTE: Actual loading expressed as wt% and (mean encapsulation efficiency (%) ± standard deviation of 3 samples per condition)

TABLE 4.2. Drug encapsulation (20 wt% theoretical loading) in polyester blends.

Fiber Blend	**50:50 PLGA/PLLA**	**80:20 PLGA/PLLA**	**75:25 PLLA/PDLLA**	**50:50 PLLA/PDLLA**
Doxycycline	16.70% (83.50 ± 0.17)	17.00% (84.99 ± 10.84)	18.29% (91.45 ± 8.60)	18.00% (89.98 ± 14.99)

NOTE: Actual loading expressed as wt% and (mean encapsulation efficiency (%) ± standard deviation of 3 samples per condition)

We micronized drug-loaded electrospun fibers to efficiently generate microparticles for transcatheter instillation and anatomical targeting. We first produced large nanofiber mats on a commercial-scale Elmarco NanoSpider and micronized the mats via a process similar in principle to traditional milling techniques, in which fiber comminution is the product of attrition and impact against steel blades and vessel walls [282]. As this process is relatively low energy, mechanical properties of the electrospun fibers play a role in the success of micronization. High brittleness and minimal elongation before fractionation is desirable when impact is responsible for granulation. The combination of these properties can be described by material toughness. Radenbaugh et al. presented methods for characterizing material toughness via puncture test, which was shown to better resolve differences in the elongation property between materials than the tensile test [283]. Prior experiments demonstrate that 80:20 PLGA/PCL electrospun fibers

can be micronized with greater than 50% yield (data not shown), indicating promising processability characteristics of that blend. We measured the puncture strength divided by the elongation prior to puncture, herein called relative puncture strength, of candidate materials as a metric to identify polyester blends that could be successfully micronized. The burst load (maximum load before puncture), puncture strength, elongation fraction, and relative puncture strength of each blend is presented in Supplementary Table 4.1 (Appendix C). Using the average of at least n=3 puncture loads (N) versus probe extention (mm) (Figure 4.2A), we found that 80:20 and 50:50 PLLA/PLGA blends have relative puncture strengths that are not significantly different from 80:20 PLGA/PCL fibers (Figure 4.2B). PLLA alone showed a more than two-fold reduction in relative puncture strength; the dynamic behavior upon extension showed a protracted necking period followed by relaxation, rather than fractionation, which indicates highly ductile behavior (Figure 4.2A). Indeed, micronization of PLLA was unsuccessful and resulted in compression of fiber segments rather than comminution. Though 80:20 PLLA/PLGA exhibited a comparable relative puncture strength to that of 80:20 PLGA/PCL, its micronization was unsuccessful as well, perhaps due to elongation prior to fractionation. The 50:50 blend of PLLA/PLGA, which exhibited the highest relative puncture strength, was amenable to successful micronization with a yield of 8.5%, which was similar to the positive control.

Differences in micronization success were likely dictated in part by the glass transition temperature (T_g) and melting temperature (T_m) of electropsun fibers. The T_g of PLGA and PLLA (Supplementary Table 4.2, Appendix C) and their blends are in the range of 40°C to 60°C, while the T_m of PCL is around 60°C with a very low T_g. Due to friction during the micronization process, it is possible that electrospun fibers experiences an increase in temperature nearing the T_g of PLGA and PLLA and near the T_m of PCL. This would have caused the material to change

from its glassy, brittle state to an elastic and more ductile state, which would have impeded micronization. Informed by mechanical properties of each nanofiber formulation, we rationally selected blends that could be successfully micronized.

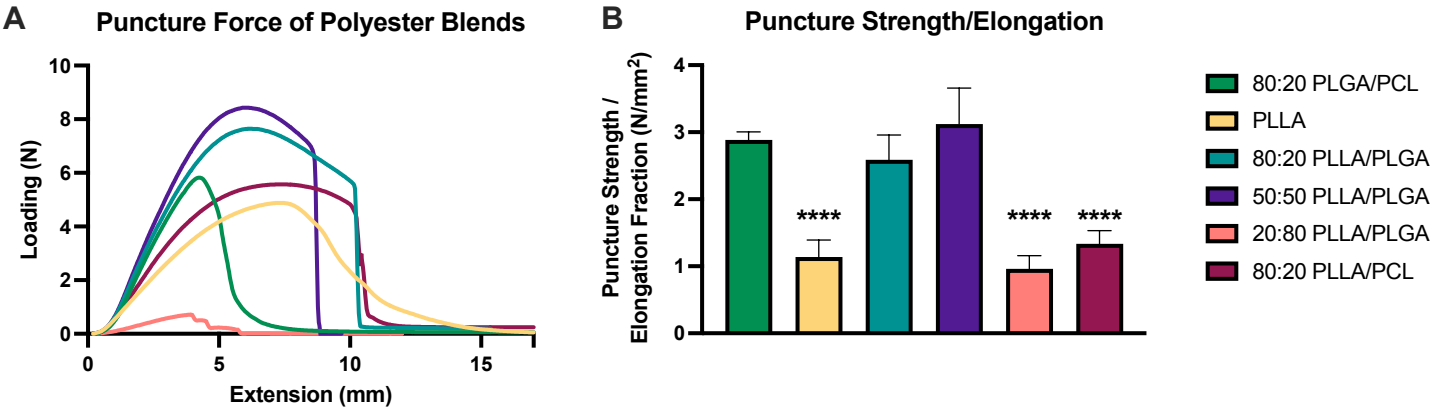

FIGURE 4.2. **Puncture force of polyester blends informs micronizable formulations.** (A) Puncture force of drug-free polyester blends generated via uniaxial electrospinning performed by a puncture test. (B) Calculated puncture strength per elongation fraction of polyester blends. Results presented as the mean ± standard deviation of tensile tests performed on at least n=3 individual fiber samples per condition.

We used scanning electron microscopy and laser diffraction particle sizing to verify the success of fiber micronization. SEM images of sub-150 µm micronized particles achieved the desired heterogeneous size and shape (Figure 4.3A,B,C). According to prior studies evaluating the occlusive propensity of commercially available embolization particles, shape heterogeneity is generally considered to enhance macroparticle aggregation [284]. Mesh fibers maintained a dense matrix with an average fiber diameter of 0.802 ± 0.133 µm (Figure 4.3A). In comparison, Carson et al. reported an average fiber diameter of 1.0 – 1.6 µm for PLGA/PCL blends that were not micronized but prepared with the same electrospinning parameters [285]; therefore, we assume that micronization does not significantly effect fiber microarchitecture. Microparticles of PLGA/PCL (80:20) loaded with 20 wt% doxycycline had an average diameter of 141.47 µm; 50:50 PLLA/PLGA + 20 wt% doxycycline particles had an average diameter of 107.40 µm; and

microparticles of PLGA/PCL (80:20) loaded with 80 wt% phenyl benzoate had an average diameter of 111.17 µm (Figure 4.3D-F). Alternate methods of particle synthesis are limited to generating particles of nanometers to several micrometers in diameter. These approaches fail to reach the 100 – 300 µm size specification for fallopian tube embolization [267]. Using our micronization approach, all three particles exhibited favorable size distributions where the average diameter was below that of the guinea pig fallopian isthmus, allowing for entry and penetration.

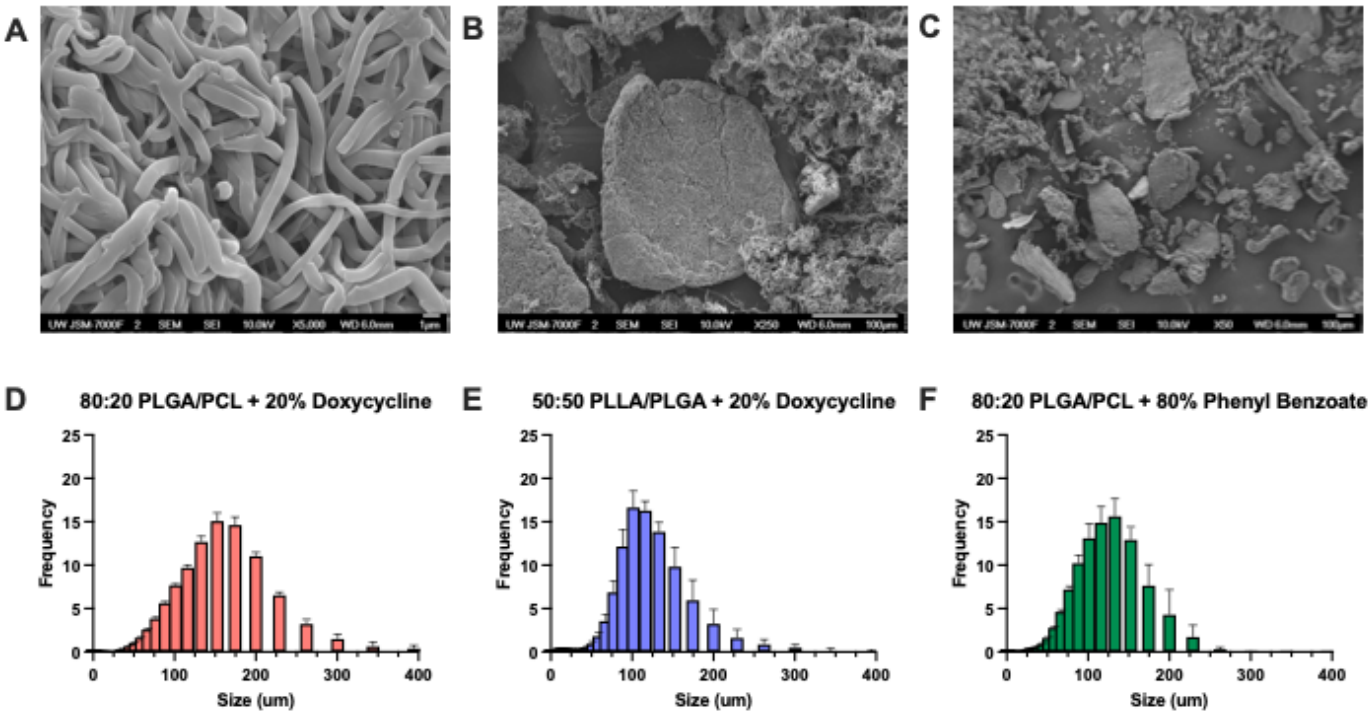

FIGURE 4.3. **Fiber micronization generates particles of inhomogeneous shape with a gaussian size distribution.** Scanning electron microscopy of micronized 80:20 PLGA/PCL fibers loaded with 20% (wt/wt) doxycycline taken at (A) 5,000X, (B) 250X, and (C) 50X. Volumetric particle size distribution of (D) 80:20 PLGA/PCL with 20% (wt/wt) doxycycline particles, (E) 50:50 PLLA/PLGA with 20% (wt/wt) doxycycline particles, and (F) 80:20 PLGA/PCL with 80% phenyl benzoate particles. Amplitude is represented as the mean ± standard deviation of 5 repeated measurements for each particle type on the laser diffraction particle sizer.

Particulate formulation at this scale has many therapeutic advantages. The industry standard for commercial embolization particles describes particle size ranges that span 200 μm, which has been proven to allow for site-specific accumulation [286]. The targeted portion of the human oviduct, called the isthmus, has a 1 mm to 0.1 mm diameter lumen with numerous longitudinal mucosal folds and extensive secondary folds that collectively fill the lumen [263]. We propose that particles calibrated to match this luminal diameter, such as the 100-300 μm size range of our microparticles, may effectively aggregate within mucosal folds. Furthermore, the isthmus is the primary site of mucin production in the fallopian tubes [287]. Therefore, the mucoadhesive property of these polyester blends provides further evidence for the potential of anatomically-targeted particle aggregation. Indeed, PLGA/PCL and PLLA/PLGA fibers loaded with doxycycline and phenyl benzoate showed equivalent or significantly increased tensile adhesion to rehydrated porcine mucin compared to nanofibers composed of polyvinyl alcohol (PVA), a highly mucoadhesive polymer (Supplementary Figure 4.2, Appendix C). Therefore, our electrospun microparticles have potential for proximal aggregation in the human fallopian isthmus via intrauterine transcervical catheter delivery due to their gaussian granulometric distribution that matches anatomical specifications of target tissue, inhomogeneity in shape, and mucoadhesive surface properties.

4.4.3 Microparticles demonstrate tunable drug release in vitro

We formulated polyester blends to achieve release of encapsulated sclerosing agents ranging from burst release within 24 hours to sustained release out to several weeks. These release kinetics were selected in order to recapitulate both the acute and chronic wound healing that has been observed to precipitate occlusion of the fallopian tubes. Thus, one burst release and

one sustained release formulation were sought for this purpose. Previous work has shown that the addition of PCL to PLGA fibers affords greater tunability of drug release of tenofovir (TVF), a water soluble antiretroviral [285]. Therefore, we selected an 80:20 PLGA/PCL blend, which demonstrated sustained release of TVF, for electrospinning doxycycline hydrochloride (HCl, herein referred to as doxycycline), which is similarly water-soluble in its salt form. We investigated the effect of high drug loading on release kinetics from 80:20 PLGA/PCL fibers loaded with 20 wt% to 80 wt% doxycycline (Table 4.1, Figure 4.4A). For fibers loaded with 20 wt% drug, an initial burst release of 60% of encapsulated drug was followed by sustained release for 24 hours. However, for each fiber formulation containing 40 wt% doxycycline or higher, approximately 90% to 100% of doxycycline burst released within the first hour. Doxycycline HCl is hydrophilic with a partition coefficient of -1.9 and may become more surface associated during the electrospinning process, resulting in rapid drug partitioning (release) into the aqueous medium. The relative ratio of polymer matrix to doxycycline appears to affect the partitioning kinetics, wherein a formulation of 80 wt% polymer matrix dampens diffusion for 24 hours while formulations composed of 60 wt% or less in polymer mass fail to offer any sustained release. Thus, highly hydrophilic doxycycline is ideally formulated into burst release particles to elicit initial acute inflammation.

In addition to burst release particles formulated with PLGA/PCL, we sought to investigate the more crystalline PLLA to achieve sustained release of doxycycline. To directly investigate the effect of polymer crystallinity, we electrospun fibers containing 20 wt% doxycycline in blends of PLLA with its amorphous isomer poly-D-L-lactic acid (PDLLA) (Table 4.2). There was no difference in doxycycline release between the three PLLA blends, thus the higher capacity for water penetration into racemic PDLLA chains did not increase drug

release as expected (Figure 4.4B). However, PLLA achieved sustained release of doxycycline loaded at 20 wt% for 7 days. We next sought to investigate the effect of higher loading on the release of doxycycline from PLLA. We observed that PLLA fibers loaded with over 20 wt% doxycycline exhibited burst release of approximately 100% of encapsulated drug (Figure 4.4C), which may be due to higher amounts of surface associated drug. To confirm the relative effect of PLLA to PLGA fiber content on drug release kinetics, we electrospun blends of PLLA/PLGA (100:0, 80:20, and 50:50) fibers loaded with 20 wt% doxycycline (Table 4.2). As expected, we found that increasing PLLA content increased sustained release that could be tuned incrementally from 4-14 days (Figure 4.4D). Thus, the increased hydrophobicity of PLLA compared to PLGA permitted effective tuning of the release of water-soluble doxycycline with fine temporal resolution. These doxycycline formulations sustained release up to two-weeks which may be sufficient to elicit a chronic response *in vivo*.

To generate material that could offer sustained release with a higher dose of encapsulated agent, we formulated particles with phenyl benzoate which is highly hydrophobic compared to doxycycline and has a logP partition coefficient of 3.59. Interestingly, 20 wt% phenyl benzoate exhibited slower release from 80:20 PLGA/PCL fibers than from a PLLA-based fiber blend (Figure 4.4E). After 7 days, approximately 22% more phenol was detected from 50:50 PLLA/PLGA fibers than 80:20 PLGA/PCL fibers. Accordingly, 80:20 PLGA/PCL fibers were assayed for *in vitro* release of 20 wt% to 80 wt% phenyl benzoate until 100% release was observed. This fiber formulation showed sustained release of all drug loading conditions for up to 4 weeks, representing a promising candidate for release of a high drug dose from electrospun fibers over an extended period (Figure 4.4F). Previous research demonstrates that the degradation of PLGA/PCL blends is insignificant at timescales relevant to these release rates;

therefore, we expect that water penetration and drug diffusion are primarily responsible for drug release [285,288]. The release kinetics demonstrated by polyester microparticles may be advantageous in contributing to a persistent inflammatory state that recapitulate the timeline of physiological events necessary for tubal occlusion. This platform is therefore useful to probe dose- and time-response to pro-inflammatory and pro-fibrotic agents.

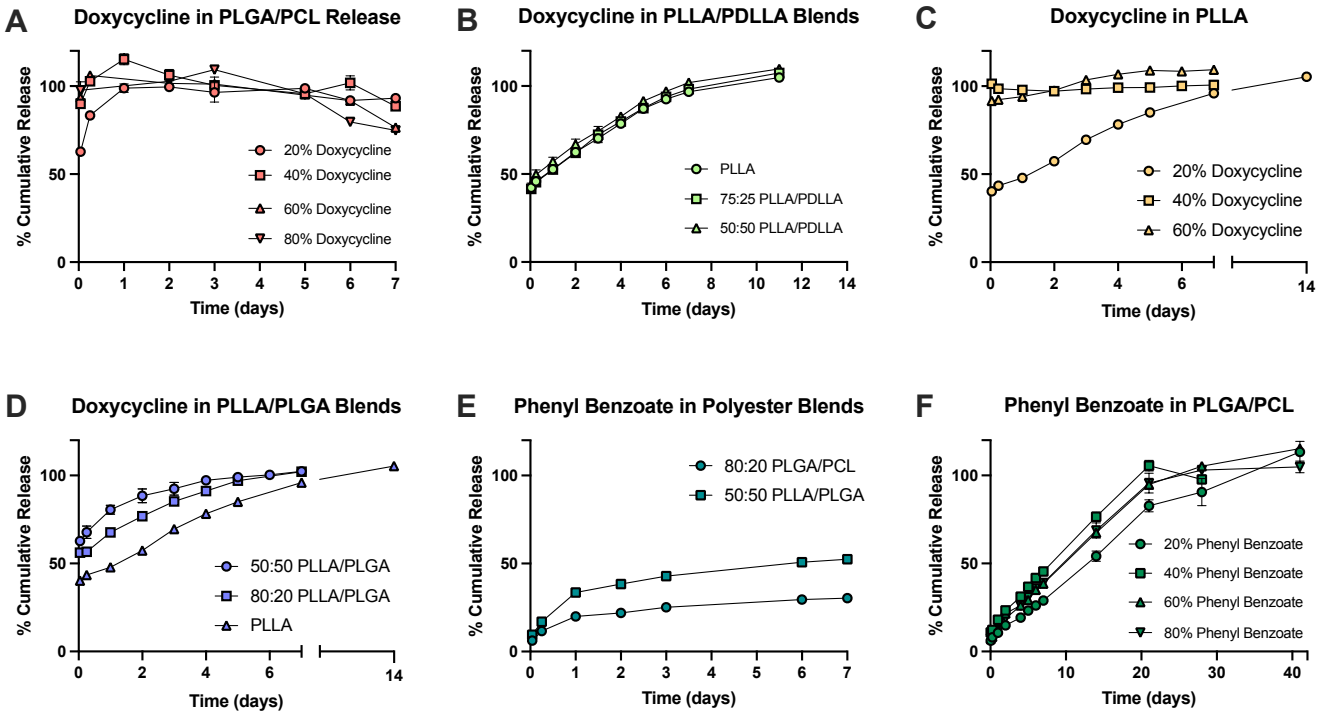

FIGURE 4.4. **Fiber blends containing varied drug type and loading show tunable release profiles.** *In vitro* drug release profile of (A) doxycycline from 80:20 PLGA/PCL fibers, (B) 20 wt% doxycycline from PLLA/PDLLA fiber blends, (C) doxycycline from PLLA fibers, (D) 20 wt% doxycycline from PLLA/PLGA blends, (E) 20 wt% phenyl benzoate from 80:20 PLGA/PCL and 50:50 PLLA/PLGA fibers, and (F) phenyl benzoate from 80:20 PLGA/PCL fibers. Results presented as the mean ± standard deviation of n=3 fiber samples per condition, taken over a one-to-six-week time course.

4.4.4 Validation and sensitivity assessment of guinea pigs as a model for permanent contraception

Both acute inflammation and long-term antagonistic activity are critical to eliciting permanent fibrotic tissue formation for tubal occlusion [289]. Here, we used a guinea pig model to investigate the activity of sclerosing agents and the impact of polyester fibers as both a delivery vehicle for burst and sustained release of drug as well as the antagonistic materials themselves. Significant research emphasis in contraception, including permanent contraception, has been placed on nonhuman primate (NHP) models due to similarities with human reproductive anatomy and physiology [290]. Rodent models, including guinea pigs, have been used in contraceptive studies to identify molecular contraceptive targets, however, their use has not been reported for studying fallopian occlusion. We selected guinea pigs for these procedures as their uterine horns are 3 to 4-times larger in diameter than mice and rats (6-8 mm versus 2 mm), allowing for easier instillation of treatments [291,292]. Here, we sought to identify if guinea pigs could be used as a model to assess tubal occlusion and then applied this model to assess our treatment regimens for this purpose.

Guinea pigs have anatomically distinct uterine horns that allow administration of different treatment conditions to the left and right horns in the same animal. We took histological samples in the proximal region of the uterine horn directly below the suture location as well as the distal region above the suture location where the uterine horn meets the oviduct. These anatomical locations are referred to as the uterine horn and oviduct, respectively. We qualitatively assessed the acute tissue response 7-days after various treatments according to epithelial detachment, inflammation, subepithelial thickening, and the presence of residual material in the uterine horn lumen. Long term affects were characterized 30-days after treatment

based on inflammation remaining near capsule placement, fibrous encapsulation of lumenal contents, and occlusive scarring (Table 4.3). No adverse side effects of this treatment were observed during the 7- or 30-day study periods. All animals had normal post-procedure behavior, ate, and maintained weight with an average change in weight between surgery and necropsy among all treatment groups of 1.68 ± 11.7%. No other parameters of well-being were collected in this study; future iterations of evaluating this treatment must involve characterizing its long-term side effects.

To understand the utility and constraints of the guinea pig model for evaluating sclerosant agents for tubal occlusion, we treated uterine horns with active agents alone including treatments comparable to published trials in higher order animals. We assessed the long-term effects of silver nitrate, a highly potent sclerosant, in the guinea pig model as a positive control. Silver nitrate was the first chemical agent tested for nonsurgical sterilization and subsequent studies have shown that silver nitrate at low doses is superior to phenol at inducing long-lasting tubal occlusion in primates [293]. Despite its potential, silver nitrate is considered highly toxic to skin and mucosal surfaces and thus is not FDA approved for use in humans and used here only as a positive control [294]. Indeed, we observed extensive fibrotic tissue and near complete reduction of patency caused by occlusive scarring in the uterine horn and oviduct after treatment with 16 mg of silver nitrate (Figure 4.5B&C). Therefore, the guinea pig model recapitulates the phenotype of tubal occlusion when exposed to highly potent sclerosants such as silver nitrate and is valid for assessing permanent contraception at this potency threshold.

We next evaluated the sensitivity of this model relative to the tissue response in NHPs treated with less potent sclerosing agents than the positive control. We selected polidocanol foam as it requires repeated dosing in rhesus macaques to elicit tubal damage and blockade; therefore

it is known to cause occlusion but is less potent than silver nitrate [295]. Indeed, varied results have been seen in single treatment trials in rodents which has motivated addition of more potent agents with longer residency to elicit more consistent occlusion [296]. Here, we instilled a single dose of 5% polidocanol foam in empty gelatin capsules to improve residency time in the uterine horns. We minor epithelial detachment in one of three treated horns but no acute tissue trauma as seen with the silver nitrate (Figure 4.5A). In guinea pigs, polidocanol foam at this dose alone does not cause a robust tissue response and gelatin capsules do not sufficiently enhance residence time and increase the local effect of polidocanol. The guinea pig horns are more recalcitrant than NHP fallopian tubes to the effects of polidocanol foam, which makes the model appropriate for identifying highly potent sclerosants.

As experimental controls for our materials, we characterized the response of guinea pig uterine horns to the active agents used in our formulations (neat phenol, phenyl benzoate and doxycycline). Phenol resulted in extensive epithelial damage and inflammation in addition to appearance of unknown lumenal contents that may suggest early collagen deposition or hemorrhage (Figure 4.5D). Tissue surrounding the affected lumen shows vascular hyperemia, further evidence of acute damage and inflammation (Figure 4.5E). *In vivo*, phenyl benzoate resulted in extensive purulent discharge into the fallopian lumen containing a mass of inflammatory cells (Figure 4.5F). As phenyl benzoate was instilled in its crystalline form, we anticipated slower degradation and thus examined its long-term effect on the oviduct. In contrast to its acute effects, phenyl benzoate resulted in minimal long term tissue responses that would indicate persistent irritation (Figure 4.5G&H). The final drug-only treatment we tested was the effect of adding doxycycline powder to 5% polidocanol foam. Previous trials in baboons have shown that 5% PF supplemented with a 100 mg bolus dose of doxycycline causes a significant

reduction in tubal patency marked by complete obliteration of the tubal epithelium and replacement with collagen-III [297]. However, we observed in the guinea pig uterine horn model that this treatment resulted in minimal epithelial damage and inflammatory exudate in only one uterine horn (Figure 4.5I). Observing little tissue change or inflammation in guinea pig uterine horns due to this treatment also supports that a higher threshold of acute trauma is needed for an observable effect, thereby demonstrating the rigor of this model. Differences in the effect of treatment with polidocanol, phenol/phenol benzoate, and polidocanol with doxycycline show that this model displays a dynamic range of tissue responses that allow us to draw comparisons between treatment modalities based on their relative effects. These studies further validate our use of sclerosing agents in biomaterial formulations and the results allow us to interpret the additive therapeutic effect of encapsulating these agents in electrospun microparticles with bolus and sustained release properties.

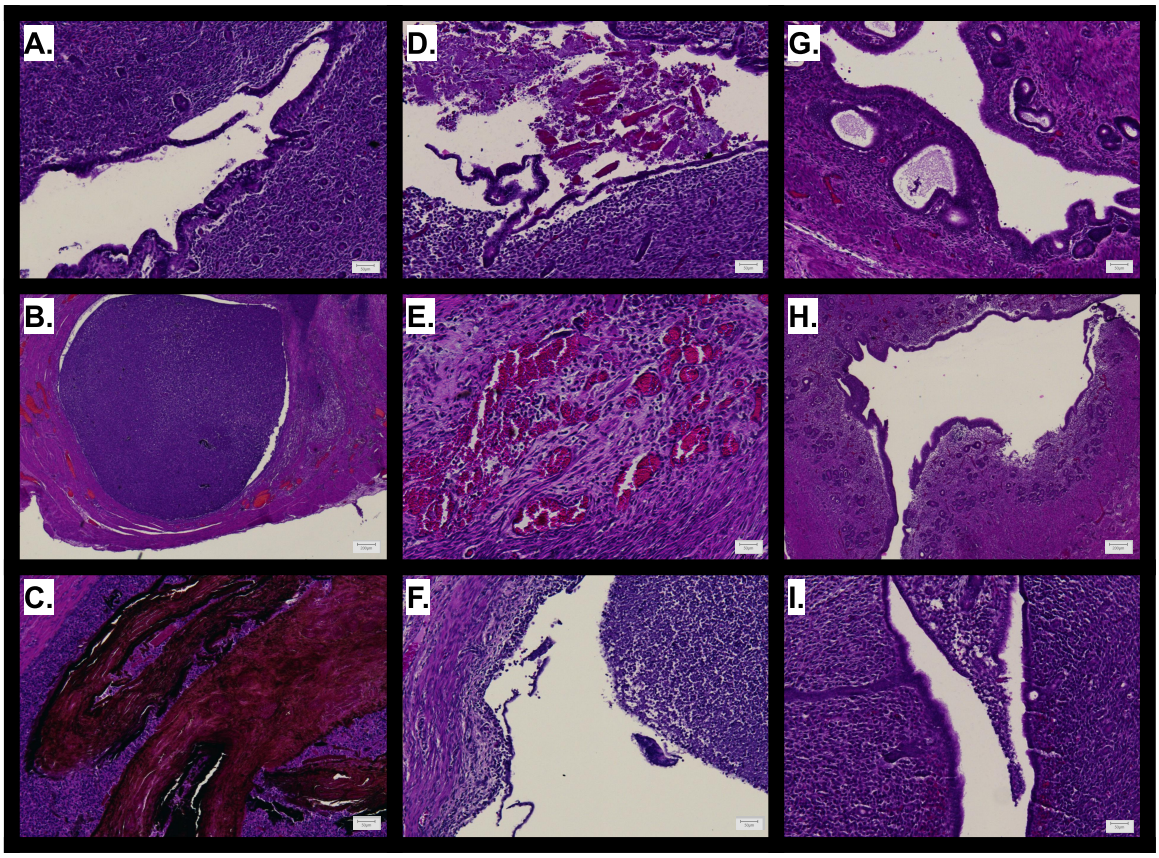

FIGURE 4.5. **Histological features of guinea pig oviducts and uterine horns after treatment with active agents.** Representative images from uterine horns treated with: (A) empty gelatin capsule instilled with 0.5 mL of 5% PF for 7 days; (B&C) 16 mg of silver nitrate instilled with saline for 30 days; (D&E) 20 mg of phenol for 7 days; (F) 20 mg of phenyl benzoate instilled with saline for 7 days; (G&H) 20 mg of phenyl benzoate instilled with saline for 30 days; and (I) 10 mg of doxycycline powder instilled with 0.5 mL of 5% PF for 7 days.

4.4.5 Sustained release polyester embolization particles enhance tubal damage in vivo

We assessed the therapeutic potential of delivering active sclerosing agents encapsulated in polyester microparticles in order to probe the effects of material potency and acute versus sustained treatment residency. We first investigated the role of polymer materials (vehicle only) in eliciting tissue trauma by instilling drug-free microparticles alone in gelatin capsules. We anticipated that in the low-fluid environment of the uterine horn, degradation of PLGA nanofibers would be slow and acute tissue responses would dampen the sclerosant effect. At 30

days, we observed extensive epithelial detachment and encapsulation of implanted materials (Figure 4.6A&B). There also appears to be inflammatory cells surrounding the implant, which indicates that polyester fibers alone have active antagonistic properties capable of instigating a cellular response and inflicting long term damage on the fallopian tubes. Their contribution to acute tissue responses was assessed by testing microparticles containing doxycycline instilled in 5% PF foam and saline. Polyester blend particles loaded with 70 wt% doxycycline were considered bolus release particles as we saw that drug loading above 40 wt% drove rapid drug release from all fiber formulations. Treatment with bolus release doxycycline microparticles and 5% PF resulted in distention of the distal uterine horns accompanied by extensive lumenal residue and a solid yellow discharge containing significant inflammatory cell infiltrate (Figure 4.6C). Bolus release doxycycline particles inserted with saline, instead of PF, caused slightly less consistent epithelial detachment in all three treated horns, but similar inflammatory cell infiltrate and lumenal residue and an overall very similar acute response (Figure 4.6D). Compared to the treatment group with free doxycycline powder and PF foam control (Figure 4.5I), the treatment groups with bolus release doxycycline particles (with and without PF) resulted in significantly more inflammation and epithelial damage at 7 days. While the formulated sclerosant is more active than the neat sclerosant, it is unclear whether this is due to release effects of the sclerosant from the polyester fibers or an additive/synergistic effect of the vehicle and sclerosant. Given either mechanism, it is clear that polyester fibers play a necessary role in bolstering the acute tissue response to delivered sclerosing agent.

Finally, we assessed sustained release formulations to examine long term effects of drug-releasing microparticles. Sustained release microparticles were formulated with 30 wt% doxycycline monohydrate, which is slightly less hydrophilic than the hyclate salt form. While

bolus release microparticles showed inflammation but no encapsulation of particle debris at 30 days (Figure 4.6E), sustained release particles caused fibrous encapsulation of the particle-containing gelatin capsule (Figure 4.6F) and more extensive inflammation and epithelial distension (Figure 4.6G). Ultimately, occlusive scarring did not occur in any doxycycline macroparticle treatments groups. However, the emergence of red blood cell infiltrate potentiates a foreign body response (FBR), as contact to blood is the first step of fibrous capsule formation [297]; therefore the FBR is a potential downstream response to this treatment group. While sustained release particles elicited more extensive fibrous encapsulation, perhaps due to prolonged residency of polyester fibers, epithelial damage was comparable to that of drug-free particles, suggesting the low dose of doxycycline was insufficient to cause significant epithelial trauma.

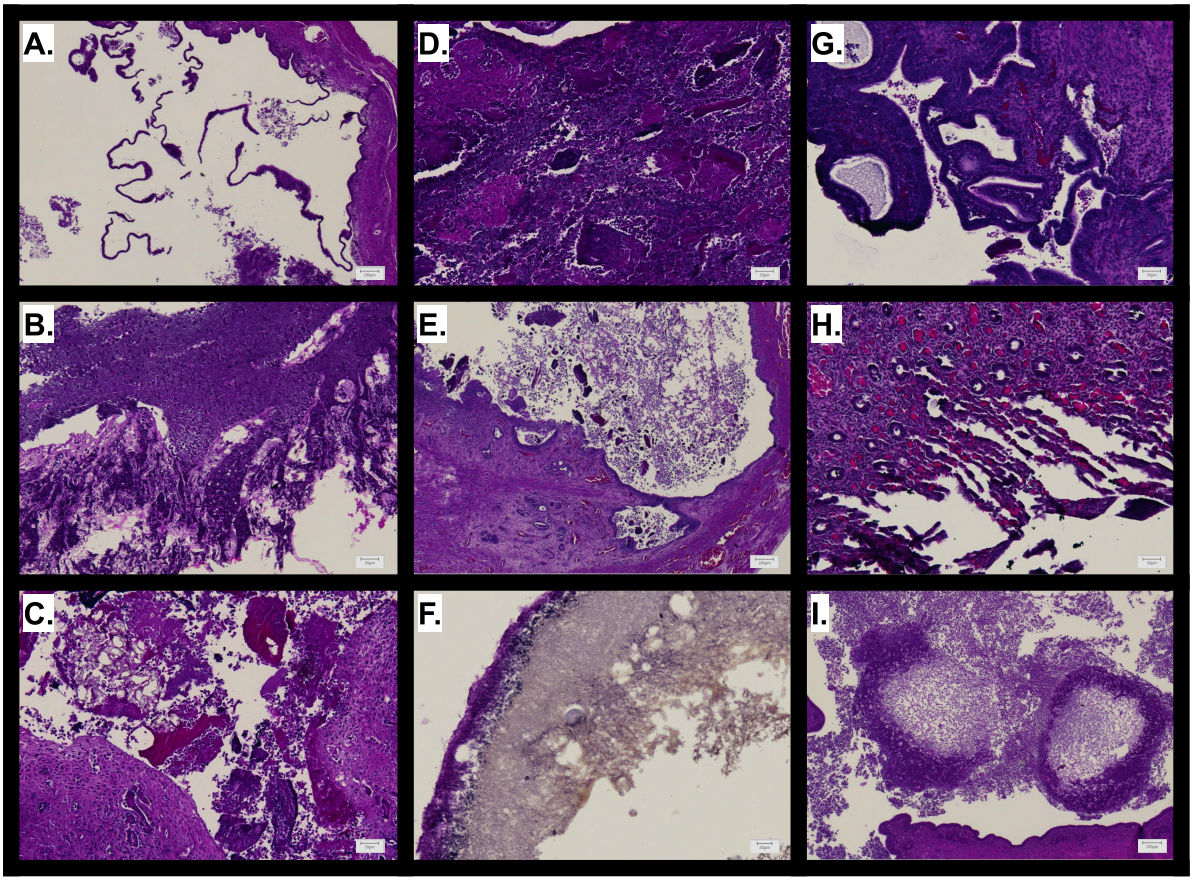

FIGURE 4.6. **Histological features of guinea pig oviducts and uterine horns after treatment with encapsulated microparticles**. Representative images from uterine horns treated with: (A&B) 10 mg of drug-free fiber microparticles for 30 days; (C) 20 mg of fiber microparticles loaded with 70 wt% doxycycline instilled with 0.5 mL of 5% PF for 7 days; (D) 20 mg of fiber microparticles loaded with 70 wt% doxycycline instilled with saline for 7 days; (E) 20 mg of fiber microparticles loaded with 70 wt% doxycycline instilled with saline for 30 days; (F&G) 20 mg of fiber microparticles loaded with 30 wt% doxycycline monohydrate instilled with saline for 30 days; (H) 20 mg of fiber microparticles loaded with 80 wt% phenyl benzoate instilled with saline for 7 days; and (I) 20 mg of fiber microparticles loaded with 80 wt% phenyl benzoate instilled with saline for 30 days.

The balance between treatment residency and potency was addressed by testing highly loaded phenyl benzoate microparticles. Microparticles containing 80 wt% phenyl benzoate showed first-order sustained release for approximately 25 days *in vitro*, likely due to the high hydrophobicity and crystalline drug form. Treatment with this formulation elicited acute hemorrhage of surrounding tissue at 7 days (Figure 4.6H) followed by long-term inflammation

and fibrous encapsulation of remaining lumenal content, ultimately causing modest occlusive scar tissue formation at 30 days (Figure 4.6I). These results potentiate polyester phenyl benzoate embolization particles as a viable treatment which may cause tubal blockade at later timepoints. It is evident that phenyl benzoate is a potent sclerosant, however, it only exerted long term effects when formulated into electrospun fibers. This is particularly interesting considering the composition of the solid dispersion, which is only 20 wt% polyester blend and 80 wt% drug crystal. One might expect only a modest contribution of the polymer matrix based on this ratio. The mechanism by which fiber encapsulation causes sustained release and durable action of phenyl benzoate remains to be elucidated and may relate to the crystalline state of the drug as it is influenced by electrospinning processing parameters. It is also likely that electrospinning with such a low polymer concentration relative to drug resulted in electrospraying, which would have bound phenyl benzoate crystals into nanocapsules that were compressed together and milled in the micronization process [298]. In this case, the polymer matrix would contribute to surface area-mediated diffusion of drug into the low-fluid environment. Further investigation into the morphology and dissolution characteristics of supersaturated solid dispersions of hydrophobic drugs is warranted. This sustained release behavior was used to our advantage in this study, wherein phenyl benzoate loaded microparticles were the most promising experimental group.

This is the first study to use guinea pigs as a model for permanent contraception. In contrast to prior studies using polidocanol foam and bolus doxycycline in nonhuman primates, our results show a consistently higher threshold of antagonistic action required to elicit chronic inflammation and fibrotic tissue formation in guinea pigs [295]. Thus, achieving moderate to successful occlusion of a guinea pig uterine horn may imply more robust occlusion in a higher order model. Testing this strategy in the more sensitive macaque fallopian tubes may better

represent its potential for permanent contraception in humans compared to these trials. Our findings that polyester material persists in the oviduct for 30 days, and that fibers themselves elicit an inflammatory response and cause fibrous capsule formation, implicates the foreign body response in addition to anticipated wound healing mechanisms. As such, this treatment can be considered a hybrid method of occlusion that is, in theory, capable of generating collagen deposition and scar tissue caused by chemical trauma and fibrotic encapsulation of implanted polyester microparticles. Moreover, the foreign body response has been shown to depend significantly on the size and shape of macroparticle (> 100 μm) implants [299]. We propose that delivery of micronized fiber particles of heterogenous size and shape is an opportune method of optimizing a FBR, as it is likely that some population of particles within a delivered dose elicits maximum fibrosis with respect to dimensionality. To confirm this conclusion, further research must be done to characterize the nature of the immune response to polyester material and candidate sclerosing agents in the fallopian tubes. Hernandez et al. recently showed that the uterus is a tolerogenic environment that dampens a foreign body response; however, the existence of such immune privilege in the immediate utero-tubal junction and the further distal fallopian isthmus warrants investigation [300]. Optimization of drug loading and release characteristics may better take advantage of the postulated hybrid immune response by instigating stronger acute trauma to initiate wound healing and longer chronic inflammation to facilitate fibrous capsule formation.

A limit of this *in vivo* model is the use of gelatin capsules to isolate particles into the target anatomical location, thus eliminating the variable of particle delivery due to species anatomy. Though the use of capsules is appropriate to test efficacy in theory, it is not directly translatable to a procedure that can be performed in women without a practiced physician, as is

the ultimate goal. As such, we conclude that this treatment has significant potential as a nonsurgical permanent contraceptive and warrants further investigation to address delivery and proximal fallopian tube targeting via transcervical catheterization. In future studies, the safety and efficacy of this approach must be rigorously investigated in higher order animals and humans. This work potentiates electrospun microparticles as an effective alternative to repeated administration of drug in bolus form.

4.5 CONCLUSION

In this work, we investigated drug-eluting polyester microparticles as a biomaterial agent for nonsurgical permanent contraception. We examined the potential of two candidate FDA-approved sclerosing agents, doxycycline and phenyl benzoate, to elicit tissue damage and acute inflammation in explant *rhesus macaque* fallopian epithelial tissue. We saw that both drugs caused extensive cell infiltration and epithelial trauma which warranted their formulation into a biomaterial drug delivery system. Electrospinning proved an effective method of loading both physiochemically diverse agents with high encapsulation efficiency into polyester nanofibers, thus overcoming limitations of low drug loading seen with other particle formulation strategies. The versatility of blending polymers allowed us to design materials with mechanical characteristics amenable to processing into micronizable nanofiber mats, thereby permitting scalable microparticle production via free-surface electrospinning. Further, we evaluated the release profile of candidate sclerosing agents from nanofibers contingent on several tunable factors, including drug loading, encapsulated agent hydrophobicity, polymer hydrophobicity and crystallinity, ultimately generating bolus and sustained release particles with potential to elicit acute and prolonged tissue responses. Finally, we validated a guinea pig uterine horn model for

tubal occlusion and evaluated the potential of this approach, observing significant acute tissue trauma and sustained inflammation in treatment groups containing nanofibers. We ultimately determined that these materials represent an innovative formulation strategy for generating tunable polymer microparticles that hold significant potential to elicit fibrotic tissue formation and tubal occlusion.

TABLE 4.3. Guinea pig oviduct/uterine horn acute and long-term treatment outcomes.

	Acute responses: 7 days (horn/oviduct)				Long term responses: 30 days (oviduct)		
Treatment	**Epithelial damage**	**Inflammation**	**Subepithelial thickening**	**Lumen residue**	**Capsule Inflammation**	**Fibrous encapsulation**	**Occlusive scarring**
Empty capsule + 5% PF foam	-/-	-/-	-/-	-/-			
Silver Nitrate					++	++	++
Phenol	+/+	+/++	+/-	-/-			
Phenyl Benzoate	+/+	+/++	-/-	-/-	-	-	-
Doxycycline powder + 5% PF foam	+/-	-/-	-/-	-/-			
Drug-free fibers only					++	+	-
Bolus release doxycycline fibers + 5% PF foam	+/++	++/+++	-/-	+/+			
Bolus release doxycycline fibers + saline	+/++	++/+++	-/-	+/+	+	-	-
Sustained release doxycycline fibers + saline					+	+	-
Phenyl benzoate fibers					++	+	+

NOTE: Scoring represents the median qualitative score of three animals per treatment group
Epithelial Damage: Broad area of epithelium stripped off (++); local/acute epithelial detachment (+); no epithelial detachment (-)
Inflammation: Massive inflammatory cells and exudate in lumen or treated area (++); few inflammatory cells or exudate near treated area (+); no inflammatory cell infiltration or exudate (-)
Subepithelial Thickening: Significant distention of the subepithelial stroma (++); minor distention of stroma (+); no stromal thickening (-)
Lumen Residue: Presence of non-biologic material in uterine horn lumen (+); no remaining material in uterine horn lumen (-)
Capsule Inflammation: Significant inflammatory infiltrate surrounding capsule (++); minor to moderate inflammatory infiltrate surrounding capsule (+); no inflammatory infiltrate (-)
Fibrous Encapsulation: Total encapsulation of capsule/microparticles (++); partial or minor encapsulation of capsule/microparticles (+); no fibrous encapsulation (-)
Occlusive Scarring: Total tubal occlusion (++); partial tubal occlusion or some reduction in patency (+); no reduction in patency (-)

Chapter 5. DESIGN AND DEVELOPMENT OF AN ARV-RELEASING COPPER IUD FOR LONG-ACTING MULTIPURPOSE PREVENTION

For the proposed manuscript: Development and Pharmacokinetics of an Antiretroviral Releasing Intrauterine Device for Long-Acting Multipurpose Prevention Technology. **VanBenschoten H**, Doan MA, Roberts M, Suydam I, Yao, S, Jensen JT, Woodrow KA. *In preparation*.

5.1 ABSTRACT

Next generation multipurpose prevention technology (MPT) has the potential to address unmet needs in family planning and HIV prevention; however, there remains a need for MPT that is coitally- and adherence-independent, long-acting, reversible, discreet, and female-controlled. Here, we design and develop an antiretroviral-releasing copper intrauterine device (ARV-IUD) that combines long-term pre-exposure prophylaxis (PrEP) and nonhormonal contraception. We demonstrate the effect of thermoplastic polyurethane (TPU) hydrophobicity, water uptake, and crystallinity on drug release from monolithic matrix drug delivery systems (DDS), as well as the influence of sheath polymer chemistry and thickness on core-sheath reservoir DDS. Using iterative *in vitro* release testing and fitting to first-order, Higuchi, and Korsmeyer-Peppas models, we selected optimal matrix and reservoir DDS polymers and formulations to achieve tunable durations of sustained release. Combining experimental release data with predictive *in silico* modelling, we designed highly-loaded DDS capable of delivering one topical ARV – dapivirine – and three physicochemically distinct ARVs – raltegravir, maraviroc, and etravirine – for at least one year at a relevant release rate. Ultimately, this work strongly premises investigation of the safety and pharmacokinetics of matrix and reservoir DDS

for the ARV-IUD system in a primate uterine model with significant potential for clinical translation.

5.2 INTRODUCTION

Human immunodeficiency virus (HIV) is a major health burden among people with female reproductive anatomy as AIDS remains the leading cause of death among women aged 15-49 [21]. In regions with the highest incidence of HIV, such as sub-Saharan Africa, women are twice as likely as men to be living with HIV and accounted for 63% of new infections in 2020 [20]. HIV acquisition by people with female genital tracts (FGT) predominately occurs by viral transmission in the vaginal mucosa [22]; thus, prevention methods that interfere with vaginal HIV transmission are key to alleviating the burden of HIV among this demographic. Currently, pre-exposure prophylaxis (PrEP), the administration of antiretroviral (ARV) medication prior to a person's exposure to HIV, is approved as a daily oral pill [4,33]. Daily oral PrEP offers systemic protection against HIV if adhered to rigorously; however, even with perfect adherence, orally administered ARVs exhibit poor partitioning to tissues in the lower female reproductive tract (FRT) [1,2,52]. In addition to challenges of poor adherence due to daily or coitally-dependent PrEP, barriers such as low acceptance, side effects, cost, access to providers, and awareness have prevented widespread PrEP use among the most vulnerable populations [35]. As such, there remains a significant need for adherence-independent, long-acting PrEP that can reach highly protective levels in the FRT.

Long-acting reversible contraceptives (LARC), such as intrauterine devices (IUDs) and subcutaneous implants, have demonstrated the ability to deliver various active pharmaceutical agents (APIs) to the FRT for durations ranging from three to ten years [110,111,301]. IUDs in

particular, such as the hormonal levonorgestrel (LNG) releasing IUD, are able to deliver drug to target FRT tissue at high levels while minimizing systemic drug concentrations [127]. As such, LARC technologies provide a strong premise for long-acting delivery of API locally to the FRT. This presents an opportunity to integrate PrEP with contraception in the form of next generation multipurpose prevention technology (MPT). MPTs are highly sought-after biomedical interventions with potential to revolutionize the global sexual and reproductive health landscape by addressing the syndemics of unintended pregnancy and HIV among people who can become pregnant. Female and male condoms are currently the only approved and widely used MPT; however, end-user studies indicate a preference for female controlled, discrete, and long-acting products to prevent HIV and pregnancy [18]. At present, there are 14 MPTs at various stages of research and development designed to prevent HIV and pregnancy, including several vaginal rings [78–81,83–87,302], vaginal inserts and gels [83,88,89], an oral pill [92], and a microarray patch [91]. Two modalities, a long-acting injectable combination of LNG and integrase inhibitors [90], and an in-situ forming implant [82], are under investigation and propose to achieve 6-months of protection. No MPT has been investigated or developed with a duration of use longer than 6 months, nor have long-acting, hormone-free MPTs been proposed.

In order to fill this gap, we aimed to develop an ARV-releasing copper intrauterine device that retains its ability to prevent pregnancy via the spermicidal activity of copper ions while releasing single or combination ARVs locally to the FRT. We designed the ARV-IUD around a novel shape-memory copper IUD (VeraCept) that boasts a 20% smaller wire frame and 50% less copper surface area than the T380A (ParaGard) [301]. This low-profile frame can accommodate the addition of width from an integrated ARV DDS while maintaining the contraceptive copper delivery component. We prioritized the formulation of dapivirine (DPV), a

non-nucleoside reverse transcriptase inhibitor (NNRTI) with a preponderance of clinical data supporting its use as a topical ARV with protective efficacy in the FGT. Indeed, the ASPIRE and RING-004 clinical trials showed that DPV delivered via intravaginal ring at a 50 μg/day dose resulted in cervicovaginal fluid concentrations nearly 4000-fold above the IC_{99} [15,63]. It is known that administering multiclass ARVs in combination can offer synergistic anti-HIV activity and minimize the potential for drug-resistant HIV infection [43]. Therefore, we also developed a DDS capable of delivering multiclass ARVs – the integrase inhibitor raltegravir (RAL), CCR5 agonist maraviroc (MVC), and NNRTI etravirine (ETR) – drugs that in synergy could increase the protective efficacy of this MPT strategy many-fold.

Here, we investigate two types of long-acting drug delivery systems (DDS) – the monolithic matrix and the core-sheath reservoir – to assess their potential to deliver physicochemically distinct ARVs. Monolithic matrix DDS consist of drug homogenously dispersed or dissolved within a polymer matrix. In these systems, drug release can be modulated by the geometry of the device, particularly the surface area to volume ratio [98], polymer swelling, porosity, water uptake, and API diffusivity through the matrix [303]. Matrix-based delivery systems have been used extensively in controlled release applications, predominately in oral formulations, but with a growing role in drug delivery for sexual and reproductive health in the form of vaginal films [11,304,305], patches [306–308], microbicidal nanoparticles [309–311], and intravaginal rings [85,312,313]. Core-sheath reservoir DDS have also been used extensively in long-acting drug delivery systems, including vaginal rings [85,86,314], hormonal intrauterine devices [111], and hormonal subcutaneous implants [110]. Reservoir DDSs are capable of achieving zero-order release for several years given that a drug is loaded in excess – above the saturation solubility – within the core polymer [315]. In this case, release is modulated

by the diffusion coefficient of drug in the sheath polymer, thickness of the rate-controlling membrane, partitioning coefficient of drug between the core and sheath, and dimensions of the device [93].

For long-acting polymeric DDS, thermoplastic polyurethanes (TPU) have emerged as leading candidates due to their versatility, material flexibility, and biocompatibility [316]. TPUs are synthetic polymers that consist of linear segmented block copolymers containing carbamate (urethane) bonds in their main chains and composed of soft and hard segments [317]. Polyurethanes are produced by reacting an isocyanate with a polyol; due to the wide range of starting material, the material properties of PUs can be tuned to meet a range of specifications and applications. Bio-inert and biodegradable PUs have been used in a variety of medical applications including artificial organs [318,319], implants for tissue repair [320], and drug delivery [321–323]. In the context of drug delivery using nondegradable PUs, drug release can be modulated by controlling the swelling of the polymer matrix, hydrophobicity, and crystallinity [324–326]. Johnson et al. demonstrated the use of a water swellable and non-swellable PU to deliver dapivirine from a segmented intravaginal ring (IVR); they reported a 50% difference in cumulative release of DPV at 30 days between swellable and nonswellable PU [327].

Physicochemical characteristics of a drug also play a significant role in drug release. The drug-polymer interaction, described by the diffusion coefficient and solubility of an API within a polymer matrix, as well as drug loading and partitioning can modulate the rate and kinetics of drug dissolution [328]. In the segmented IVR, the initial loading of hydrophilic Tenofovir in a hydrophilic PU matrix correlated linearly with cumulative drug release over time [327]. Verstraete et al. developed a TPU-based IVR for prophylaxis and treatment of bacterial vaginosis by simultaneously delivering lactic acid and metronidazole [329]. They found that highly

crystalline hydrophobic TPUs were required to offer sustained release of water-soluble lactic acid, while hydrophilic TPUs were required to achieve release of metronidazole over the desired release period. Due to the variety of tunable properties granted by TPUs, iteration and selection of an appropriate polymer characteristic profile for a given API is necessary in the development of long-acting drug release systems.

In this study, we demonstrate the development an integrated ARV-IUD designed to offer protection against HIV in the FGT for at least one and up to three years. We performed rapid prototyping of matrix and reservoir DDS loaded with physicochemically distinct ARVs and used *in vitro* characterization methods to probe material and drug release properties of our prototypes. We supplemented experimental methods with *in silico* mechanistic modelling of drug dissolution to rationally design optimal devices for long-term use.

5.3 MATERIALS AND METHODS

5.3.1 Preparation of TPU matrix device prototypes

Thermoplastic polyurethanes (PY-PT42DE35, PY-PT83AE35, PY-PT72AE, and PY-PT87AE, gifted by Lubrizol Life Science) were dissolved overnight at 10% wt/vol in chloroform. Micronized Dapivirine (DPV) (International Partnership for Microbicides) dissolved in polymer solution at 1% wt. drug/wt. polymer (wt/wt) or 16.6% wt/wt for ≥ 6 hours. Etravirine (ETR), Maraviroc (MVC) and Raltegravir (RAL) (NIH AIDS Reagent Program) were isolated and purified form their pharmaceutical formulations as previously described [330] prior to being dissolved in polymer solution at 1% wt. drug/wt. polymer (wt/wt) or 16.6% wt/wt for ≥ 6 hours. Polymer-drug solutions (40 mL) were poured into a 100 mm x 15 mm glass petri dish and placed uncovered in a fume hood for 24 hours. Solvent cast films were placed in a high-vacuum

desiccator for ≥ 4 hours on each side to remove residual solvent. Films were cut into disks with a 1-inch diameter die punch; disks were stacked and placed between two pieces of aluminum foil and compressed under a metal weight on a 120°C dry bath. Thickness was monitored frequently until it measured 3.5 mm with digital calipers calibrated to 0.01 mm. Devices were cut from thick films using a custom rectangular 3.5 mm x 13.3 mm die punch.

5.3.2 Preparation of TPU reservoir device prototypes

Reservoir DDS prototypes were prepared by Lubrizol Life Sciences using a heated coextrusion process. Briefly, core polymer (PY-PT43DE20) was melted and homogenized with the appropriate mass of dapivirine to achieve 1 wt% and 30 wt% core polymer loading. Core polymer and sheath polymer (PY-PT72AE or PY-PN73AE) were simultaneously extruded at 170-190°C through a custom crosshead to meet target tube dimensions with a 1.5 mm inner diameter (lumen), 3.56 mm outer diameter, a 1.0 mm wall (core + sheath) thickness, and 100 to 200 μm sheath thickness. The inner crosshead diameter was varied mid-extrusion to generate devices with sheath thicknesses ranging from 100 – 200 μm while retaining a constant outer diameter. Material was cut to the desired length per device (13.33 mm) and in-spec devices were identified based on sheath thickness using brightfield microscopy. Devices were incubated for two weeks at 40°C to equilibrate drug in the core and sheath compartments. Reservoirs used for *in vitro* release studies were end-capped with 2 mm thick discs of drug-free sheath polymer generated via solvent cast and heated compression methods described in section 6.3.1.

5.3.3 Dimensional analysis of IUD frames and prototypes

The dimensional specification of the LevoCept™ and VeraCept® IUD frames (Figure 5.1) (generous gift from Sebela Pharmaceuticals Inc.) were analyzed using digital calipers calibrated to 0.01 mm. Matrix device prototype dimensions were measured using digital calipers. Reservoir device prototype height and outer diameter dimensions were measured using digital calipers; sheath thickness was measured using brightfield microscopy couples with image analysis.

5.3.4 HPLC Analytical Methods

High-performance liquid chromatography (HPLC, Shimadzu Prominence) was used to measure DPV independently and RAL, MVC, and ETR in tandem using a diode array detector (Shimadzu Prominence SPD-20A) and a C18 column (5 μm, 100 Å, 250 x 4.6 mm, Phenomenex Kinetex). For DPV, samples were analyzed at 30°C at a 1 mL/min isocratic flow rate, 10-minute run time and 10 μL injection volume. The mobile phase was composed of a 65:35 ratio of acetonitrile (ACN) and 10 mM ammonium acetate in water. DPV was detected at approximately 6.2 minutes with 310 nm detection wavelength with a linear range of 0.1 – 500 μg/mL. RAL, MVC, and ETR samples were analyzed at 35°C at a 1 mL/min flow rate, 20-minute run time and 10 μL injection volume. The mobile phase was a gradient of 38 – 73% ACN and 25 mM monopotassium phosphate in water (KH_2PO_4); the mobile phases began at a ratio of 38:62 ACN/ KH_2PO_4, increased to 73% ACN over 8 minutes, and returned to 38% ACN by the end of the 20 minute run. RAL was detected at 7.2 minutes and 300 nm with a linear range of 0.5 – 500 μg/mL; MVC was detected at 4.5 minutes and 193 nm with a linear range of 1 – 100 μg/mL; ETR was detected at 15.2 minutes and 234 nm with a linear range of 0.5 – 500 μg/mL. All

HPLC samples were filtered with a 0.22 μm syringe tip filter (Millex Durapore, Millipore) prior to sample analysis.

5.3.5 Drug loading in matrix and reservoir devices

For matrix and reservoir prototypes, drug content was extracted from 3 devices of each formulation. Devices were cut into three equal segments (4.43 mm long), massed, and submerged in 10 mL tetrahydrofuran (THF) in a 20 mL glass scintillation vial. Vials were sealed and placed on a rotisserie shaker at room temperature for at least 24 hours. THF solutions were vortexed and diluted 10X in dimethyl sulfoxide (DMSO) prior to drug content analysis by HPLC.

5.3.6 Saturation solubility of water-insoluble drugs in release media

The solubility of DPV, MVC, and ETR in candidate *in vitro* release media was determined at physiological temperature (37°C). Release media (2% Cremophor) was prepared consisting of phosphate buffered saline (DPBS, no calcium, no magnesium, pH 7.4, 9.55 g/L in Millipore Milli-Q water) and 2% wt/vol Cremophor® A25/Emulgin® B25. 10 mL aliquots of 2% Cremophor were prepared in triplicate for each drug in 20 mL glass scintillation vials. 10 mg of each drug was added to individual aliquots which were sealed and heated to 70°C on a ChemX hot plate under constant stirring to accelerate dissolution. After 4 hours, the temperature was reduced to 37°C and samples stirred for 24 hours. Saturated solutions were centrifuged for 5 minutes at 2300 RPM and filtered through a 0.22 μm syringe tip filter prior to analysis on HPLC. If drug appeared fully soluble at the original concentration (1 mg/mL), no additional drug was

added and samples were diluted 10X with DMSO to bring the sample concentration below the upper limit of quantification.

5.3.7 Saturation solubility of DPV in reservoir core polymer

Flat solvent cast films of reservoir device core polymer (PY-PT43DE20) were prepared according to methods presented in section 6.3.1. 10 thin film disks were cut with a ½ inch diameter die punch, massed, and placed in a 24-well plate. Propylene glycol (Sigma Aldrich) was selected for its compatibility with PY-PT43DE20 (no solvent uptake, swelling, or dissolution) and high saturation solubility of DPV, which was determined according to methods presented in section 6.3.6 [331]. Core polymer thin film disks were immersed in 3 mL of a solution of propylene glycol saturated with DPV. Films were incubated at 37°C for 5, 10, and 20 days. After incubation, films were removed from the solution, rinsed briefly in Milli-Q water, dried lightly with a Kimwipe, and dried for ≥ 6 hours. Dry films were then immersed in 5 mL of THF, sealed, and placed on a rotisserie shaker for 24 hours to extract drug. THF solutions were diluted 10X in DMSO prior to sample injection and drug content analysis by HPLC.

5.3.8 Swelling and equilibrium water content of matrix device TPUs

Drug-free matrix devices of each TPU type in triplicate were used to assess swelling and equilibrium water content. Initial device length (L_0) was measured using digital calipers and initial mass (M_0) was recorded. Devices were immersed in PBS for 96 hours, then dried lightly to remove surface-associated liquid. Device length at equilibrium (L_{eq}) and mass at equilibrium (M_{eq}) were recorded. Swelling (%) was calculated according to the change in device length:

$$Swelling\ (\%) = \frac{L_{eq} - L_0}{L_0} \times 100 \qquad \text{(Eq. 1)}$$

Equilibrium water content was calculated according to the change in device mass:

$$Eq. Water\ Content\ (\%) = \frac{M_{eq} - M_0}{M_0} \times 100 \qquad \text{(Eq. 2)}$$

5.3.9 In vitro release testing

In vitro drug release from matrix and reservoir DDS prototypes was performed in a rotating shaker set to 60 RMP and 37°C. All release tests were performed in sink conditions in PBS supplemented with 2% w/v Cremophor® A25/Emulgin® B25. For the first 7-days of drug release testing, 1 mL samples were taken daily; following 7 days, samples were taken every 3-4 days. At all timepoints, bottles were drained and replaced with fresh media following sampling. For reservoir DDS prototypes, three replicates of each formulation were end capped and one device was tested with no end cap to confirm the integrity of the end cap in preventing uncontrolled diffusion form the exposed core.

5.3.10 Statistical analysis

All data were presented as mean ± standard deviation. Linear regressions and determinations of statistical significance were made using GraphPad Prism (San Diego, CA, USA, Version 9). Ordinary one-way ANOVAs multiple comparisons were used to calculate significant differences in drug loading, encapsulation efficiency, TPU swelling and equilibrium water content. Ordinary two-way ANOVA was used to calculate significant differences in prototype surface area to volume ratios with Dunnett's multiple comparisons test to compare matrix devices with reservoir devices. Significant differences were accepted when p value < 0.05.

5.4 RESULTS AND DISCUSSION

5.4.1 Design of an ARV-releasing polymer sheath for IUD integration

We analyzed the dimensions of the LevoCept hormonal IUD nitinol wire frame (Figure 5.1A) and the VeraCept copper (Cu) IUD (Figure 5.1B) to design an API-releasing sheath (herein called ARV sheath) amenable to integration onto a modified VeraCept device. Table 5.1 presents the dimensions of both devices. The LevoCept frame is designed specifically for integration of a drug releasing sheath, thus we based several specifications on its dimensions with the intention to combine the attributes of the VeraCept and LevoCept into a single IUD. The dimensions of the ARV sheath were originally developed for the reservoir DDS and subsequently adopted for the matrix DDS. The reservoir DDS cross-sectional diameter dimensions were constrained by the following specifications: the inner diameter (lumen) must be wide enough for the device to slip over the loop of the LevoCept (Figure 5.1A, dimension B) for permanent placement on narrow wire segment (Figure 5.1A, dimension A). The outer diameter was constrained by the diameter of the VeraCept inserter, which is 3.65 mm. We therefore arrived at 1.4668 mm and 3.556 mm as the inner and outer cross-sectional diameters, respectively (Figure 5.1C), to allow for tolerance and assuming some flexibility of the device. We designed the reservoir DDS prototypes to have a 100 to 200 μm thick sheath membrane, which is reflected in the cross-sectional core diameter (3.156 mm).

The length of the device must permit integration of copper ferrules at the bottom of the Cu-IUD frame, where they are required to maintain contraceptive action. We assumed that one-third of the total surface area of copper (175 mm^3) is maintained by the bottom ferrules. By combining the ferrules into a single ferrule that is twice the diameter of the existing ferrules

(Figure 5.1B, dimension I), one single long ferrule (5.626 mm) can be incorporated onto the bottom of the Cu-IUD frame to maintain the requisite surface area of copper. We assumed that the height of the reservoir DDS could occupy the narrow wire segment (Figure 5.1A, dimension D) minus the extended copper ferrule height. We therefore calculated 13.33 mm as the ideal length of the DDS (Figure 5.1C). As such, the composite design of the ARV-IUD consists of a nitinol wire frame with two existing copper ferule segments on the arms and a modified segment on the base. Assembly thus involves slipping the reservoir or molding the matrix DDS around a straight wire segment (Figure 5.1E).

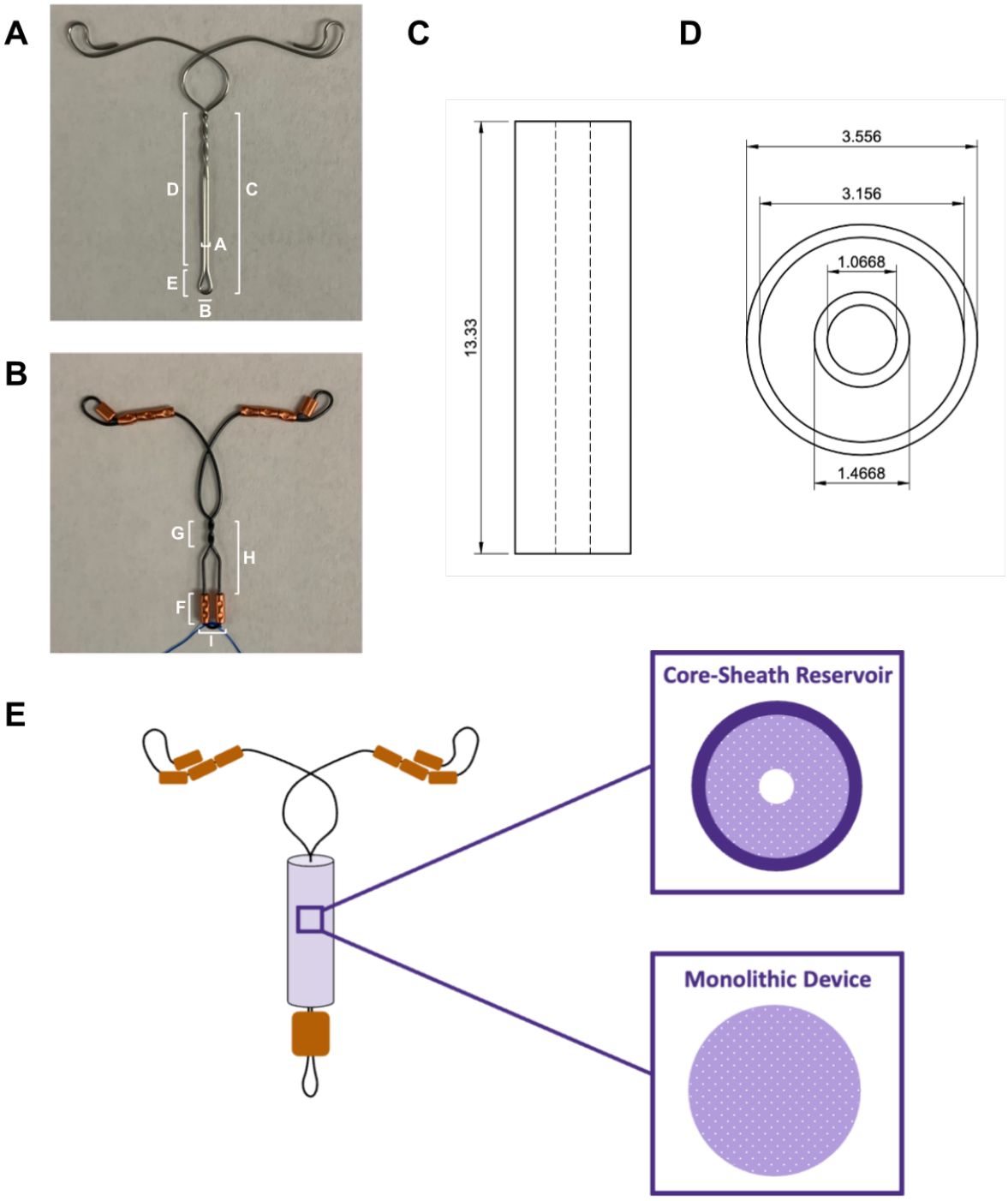

FIGURE 5.1. **Design specifications of a combined ARV-IUD.** (A) LevoCept IUD nitinol wire frame and (B) VeraCept IUD; all labelled dimensions detailed in Table 5.1. Computer aided design drawing of the (C) side profile and (D) cross-sectional profile of the reservoir DDS. (E) Schematic of the integrated ARV-IUD design with a core-sheath reservoir DDS or a monolithic (matrix) DDS.

TABLE 5.1. Dimensions of the LevoCept and VeraCept IUD.

IUD	***Label***	***Component name***	***Dimension***
LevoCept	A	Width of double wire	0.80 mm
	B	Width of loop	1.74 mm
	C	Length of entire straight segment	21.71 mm
	D	Length of straight segment minus loop	18.96 mm
	E	Length of loop	2.78 mm
VeraCept	F	Copper ferrule height	3.78 mm
	G	Length of twisted segment	3.72 mm
	H	Length of straight segment minus ferrules	9.72 mm
	I	Width of bottom ferrules	3.30 mm

5.4.2 Matrix and reservoir DDS fabrication, dimensional analysis, and drug loading validation

Matrix DDS prototypes were fabricated by heated compression of solvent cast films. Four Lubrizol Pathway TPUs with distinct attributes were selected for matrix DDS investigation as described in Table 5.2. We confirmed that matrix DDS prototype fabrication maintained the relative water uptake and predicted swelling behavior of the four TPU candidates by measuring the equilibrium mass and dimensional change of drug-free matrix devices soaked in PBS (Figure 5.2). As expected, TPU1 and TPU2 exhibited significantly greater swelling (Figure 5.2A) and equilibrium water content (Figure 5.2B) than hydrophobic TPU3 and TPU4. TPU2 exhibited significantly greater swelling and water uptake than TPU1; no differences were observed between TPU3 and TPU4. All matrix DDS TPUs were aliphatic polyethers due to their superior resistance to hydrolysis and microbial growth compared to polyester-based TPUs. Hardness, water uptake and hydrophobicity can modulate the release rate of encapsulated API. Hardness of a polyurethane as determined by a shore durometer reflects the ratio of hard to soft segments in

the copolymer. Long, low polarity segments are called “soft” while short, high polarity segments are characterized as “hard.” The high polarity of hard segments results in greater aggregation and crystallization, which can reduce the permeability, water uptake, and/or the diffusion coefficient of API within the polymer matrix [316]. Various studies have shown that a decrease in the soft to hard segment ratio results in a decrease in the release rate of encapsulated drug [329,332]. Water uptake and hydrophobicity are closely related and generally result in an increase in swelling of the polymer matrix, which accelerates drug release by increasing the porosity and free volume for diffusion [327].

TABLE 5.2. Summary of matrix DDS prototype attributes.

Matrix ID	***Lubrizol TPU***	***PU Classification***	***Durometer Hardness***	***Water Uptake***	***Hydrophobicity***
TPU1	PY-PT42DE35	Aliphatic Polyether	43D	35%	Hydrophilic
TPU2	PY-PT83AE35	Aliphatic Polyether	83A	100%	Hydrophilic
TPU3	PY-PT72AE	Aliphatic Polyether	72D	<2%	Hydrophobic
TPU4	PY-PT87AE	Aliphatic Polyether	87A	<2%	Hydrophobic

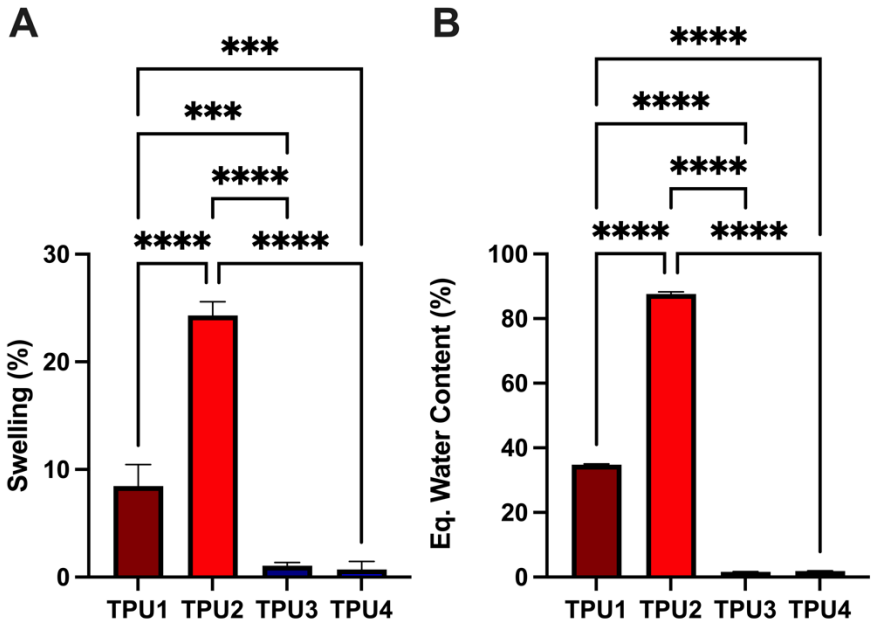

FIGURE 5.2. **Water uptake properties of TPU matrix DDS prototypes.** (A) Swelling measured length-wise and (B) water content at equilibrium measured mass-wise of drug-free TPU matrix DDS prototypes. Results expressed as the mean ± standard deviation of n=3 devices per TPU type. (***) represents $p < 0.001$. (****) represents $p < 0.0001$.

Four comparator groups of reservoir DDS devices were designed to assess the effect of sheath polymer chemistry and sheath thickness on drug release (Table 5.3). The significance of these two properties on drug release from a core-sheath reservoir device is mathematically described by Baker and Lonsdale's derivation of the radial flux of drug from a cylindrical reservoir, given by Equation 3 [107]:

$$\frac{dM}{dt} = \frac{2\pi HDKC_s}{ln\frac{r_o}{r_i}} \qquad \text{(Eq. 3)}$$

Where M is the mass of drug that diffuses out of the device, H is the device height, D is the diffusion coefficient of drug through the membrane polymer, K is the partition coefficient of drug between the core and membrane polymer, c_s is the saturation solubility of drug on the core polymer, r_o is the outer radius (core plus sheath) and r_i is the inner radius (core) of the device. Evidently, the choice of sheath polymer chemistry affects drug release based on its relationship

to drug diffusion (D) and drug partitioning kinetics at the core-sheath interface (K). Because radial flux is directly proportional to these parameters, a sheath that is more permeable to API and offers more favorable partitioning for a given core polymer will release drug faster. Conversely, given a constant outer radius (r_o), a thicker sheath membrane implies a smaller core radius (r_i) and results in in slower drug release due to the inverse relationship of flux with the natural log of the ratio of outer to inner radius. This is intuited by the understanding that a sheath acts as a rate-controlling membrane (RCM); a thicker or less permeable RCM will slow the release rate of a drug to a greater extent than a thinner or more permeable RCM.

TABLE 5.3. Summary of reservoir DDS prototype attributes.

Reservoir ID	***Sheath Thickness***	***Sheath Polymer***	***Sheath PU Description***	***Core Polymer***	***Core PU Description***
R1	100 μm	PY-PT72AE	Hydrophobic, mid HS/SS, polyether	PY-PT43DE20	Hydrophilic, high HS/SS*, polyether
R2	200 μm				
R3	100 μm	PY-PN73AE	Hydrophobic, mid HS/SS, polycarbonate		
R4	200 μm				

* HS/SS refers to the ratio of hard to soft segments, characterized relatively based on shore hardness

We prepared TPU matrix DDS prototypes loaded with 1 wt% (low loading) and 16.6 wt% (high loading) dapivirine (DPV), raltegravir (RAL), maraviroc (MVC) and etravirine (ETR) (Figure 5.3A-H). Only TPU4 was used for high drug loading prototypes. Matrix DDS prototypes loaded with 1 wt% drug were translucent and showed no apparent drug crystallization. Those loaded with 16.6 wt% DPV, RAL, MVC, and ETR showed visible crystal formation and an opaque appearance; this is likely the result of drug being above the saturation solubility of the

polymer. The observation of large crystal formation implicates Ostwald ripening, the process by which small drug crystals dissolve and disperse into a matrix and then redeposit into larger crystals, driven by a decrease in total surface free energy [333]. Four comparator reservoir DDS prototypes loaded with 1 wt% DPV show consistent translucence and hollow cylindrical structure (Figure 5.3I-J). Both matrix DDS and reservoir DDS prototypes were successfully integrated onto a nitinol wire IUD frame (Figure 5.3M-N), demonstrating feasibility of both fabrication techniques at generating devices amenable to system integration.

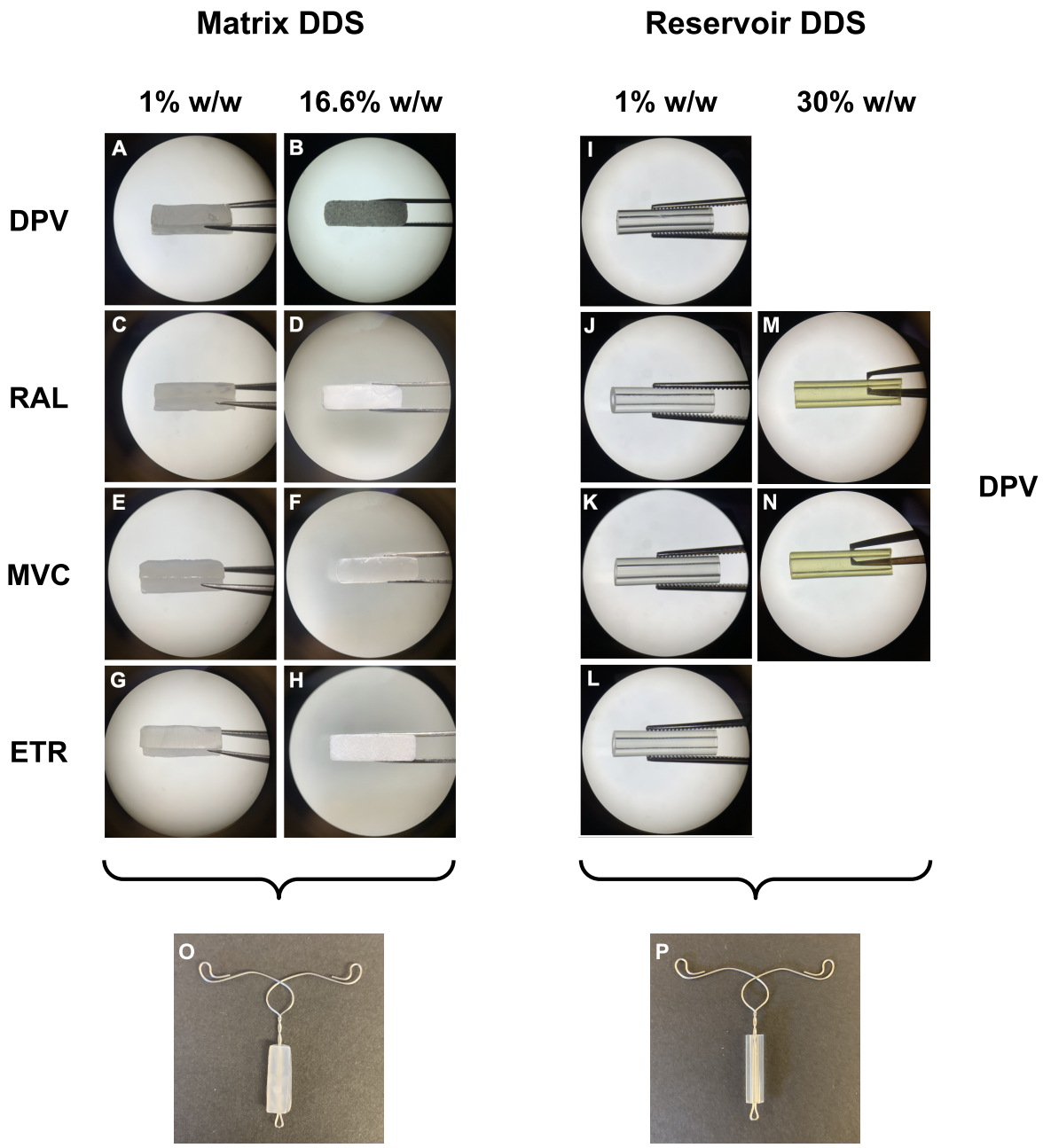

FIGURE 5.3. **Representative images of TPU matrix and reservoir DDS prototypes.** Images of TPU4 matrix DDS loaded with (A) 1% DPV, (B) 16.6% DPV, (C) 1% RAL, (D) 16.6% RAL, (E) 1% MVC, (F) 16.6% MVC, (G) 1% ETR, and (H) 16.6% ETR. Images of TPU reservoir DDS consisting of 1% DPV loaded at the core of (I) R1, (J) R2, (K) R3, and (L) R4 device configurations; TPU reservoir DDS consisting of 30% DPV loaded at the core of (M) R3, and (N) R4 device configurations. (O) Matrix DDS prototype and (P) reservoir DDS prototype integrated onto a bare LevoCept nitinol wire frame.

We confirmed the dimensions and specifications of the matrix and reservoir DDS (Supplementary Table 5.1, Appendix D). We found no significant differences in the surface area to volume ratios of any TPU-type matrix device loaded with any ARV, nor did we find any significant differences between matrix DDS and reservoir DDS prototypes SA/V loaded with DPV (Supplementary Figure 5.1, Appendix D). The addition of drug had little to no impact on device dimensions, thus we expect devices with higher drug loading to maintain the same SA/V ratio as low loading devices. The relative standard deviation of SA/V for all devices was below 2.2, reflecting good uniformity within formulations. It was necessary to ensure that the surface area to volume ratio (SA/V) of all devices was consistent to allow for comparison of drug release between groups. Indeed, Reynolds et al. showed that increasing the surface area to volume ratio of hydroxypropyl methylcellulose (HPMC) matrix tablets of the same geometry resulted in accelerated release of encapsulated promethazine HCL [98]. Moreover, they showed that tablets of the same shape with different diameters and tablets of different shapes released drug at the same rate given that the surface area to volume ratio was held constant. Because we controlled for dimensional consistency, we concluded that it was possible to compare the release rate of these devices without dimensional confounding.

We verified the effective drug loading in each DDS prototype and calculated the encapsulation efficiency based on the theoretical drug loading (Supplementary Figure 5.2, Appendix D). For all low loading matrix DDS prototypes, the average effective loading is 0.91 ± 0.14 wt% with an average encapsulation efficiency of 91.13 ± 13.38%. Low loading TPU3-MVC, TPU4-MVC, and TPU4-ETR devices had significantly lower encapsulation efficiency than other TPU-ARV formulations. However, this difference is not reflected significantly in the effective loading and therefore should not significantly affect drug release. High loading TPU4

matrix prototypes had an average effective loading of 16.46 ± 1.12 w% with an encapsulation efficiency of 99.12 ± 6.28% and no statistically significant differences among each ARV. Reservoir DDS prototypes were effectively loaded with 1.08 ± 0.19% drug in the core which translates to an average encapsulation efficiency of 107.85 ± 19.44%. No significant differences in effective drug loading or encapsulation efficiency were found between the four reservoir DDS groups.

5.4.3 In vitro release testing of single-ARV matrix DDS prototypes

We investigated the *in vitro* release kinetics of DPV from four TPU-based matrix DDS prototypes (Table 5.2). We used phosphate buffered saline with 2% w/v Cremophor, a nonionic surfactant, as dissolution media in order to enhance the solubility of DPV such that it could be detected in sink conditions above the lower limit of quantification via HPLC. The saturation solubility of DPV in 2% Cremophor was 163.76 ± 9.40 μg/mL; compared to 0018 ± 0.001 μg/mL in water, this represents a significant enhancement in solubility allowing for reasonable release media volumes to be used while maintaining aqueous conditions for physiologically relevant swelling behavior of the TPU matrix [337]. Several studies have described the use of hydro-organic media, such as isopropanol:water solutions, to facilitate the dissolution of DPV from vaginal rings during in vitro dissolution studies [334–336]. However, in a monolithic system where drug release is influenced by water penetration into and swelling of the polymer matrix, aqueous-based media is a more appropriate selection to recapitulate *in vivo* release kinetics. Indeed, Bao et al. demonstrated artificial acceleration of LNG dissolution from a PDMS reservoir device *in vitro* using various hydro-organic release media solutions; in their study, release rates correlated linearly with increased swelling induced by organic media [108].

In vitro release of 1% DPV from TPU matrix devices demonstrated dependence on crystalline and water-uptake properties of each polymer (Figure 5.4). The cumulative release rates for TPU1 and TPU2, two hydrophilic, water swelling polymers, were not statistically different over the 30-day release period (Figure 5.4A). Surprisingly, TPU3, a hydrophobic TPU with a higher soft-to-hard segment ratio than the other three TPUs, resulted in the most rapid dissolution of DPV, releasing approximately 95% of encapsulated DPV by 30-days. This evidences the significance of polymer crystallinity in mediating drug release despite relatively limited water uptake and swelling. Having fewer polar, hard segments, TPU3 is less crystalline and therefore more flexible allowing for an increase in the free volume available for diffusion of permeant molecules [338]. It can be inferred from this data that the diffusion coefficient of DPV through a wetted TPU3 matrix is significantly greater than that of the other TPUs assayed here.

All four TPUs released DPV within a target 10-50 μg/day dose range (Figure 5.4B). The release rate per day plot displays a sharp peak at early time points indicating burst release followed by a steady decline to near zero-order release by 30-days. A key qualification for selecting an optimal TPU for DPV delivery in this application is the time to achieve 50% cumulative release of drug. This is based on the standard use time of hormonal IUDs, which in practice are removed when about half of the initial load of drug is depleted from the device [111]. This is a clinical practice to maintain the integrity of the daily drug dose provided by a reservoir-based IUD – once a certain amount of drug is depleted from the core of the device, its release is no longer zero-order an begins to decrease over time. Here, we use this standard as a benchmark to evaluate the sustained release duration of candidate DDS designs.

Though the time to release 50% DPV ($T_{50\%}$) is resolved within 30 days of *in vitro* release for three of the four TPUs assessed here, we fit cumulative release data to empirical models of

drug release in order to establish methods to predict $T_{50\%}$ mathematically. We assessed the fit of first-order release kinetics to our data (Figure 5.4C); this equation describes drug release from a system where dissolution is dependent on a concentration gradient; it is given by Equation 4A&B:

$$\frac{dC}{dt} = -kt \qquad \text{(Eq. 4A)}$$

or

$$Log(C_t) = Log(C_0) - \frac{kt}{2.303} \qquad \text{(Eq. 4B)}$$

Where k is the first order rate constant, C_t is the concentration of drug in solution at time t and C_0 is the initial concentration of drug [101]. We also fit cumulative release data to the Higuchi model (Figure 5.4D), which describes the release of drugs from an insoluble matrix based on Fickian diffusion and a square-root of time relation given by the simplified expression:

$$Q = k_h t^{1/2} \qquad \text{(Eq. 5)}$$

Where Q is the amount of drug release in time t and k_h is the Higuchi release constant [99,101]. Here, the square-root of time relation fits the *in vitro* release data better than first-order release kinetics for all TPU types (Table 5.4). Based on the best-fit square-root of time relation, $T_{50\%}$ was calculated for each TPU. Predicted values for $T_{50\%}$ closely matched experimentally observed data, indicating that this approach is suitable for predicting device use duration. This is a useful method for determining the sustained release duration of devices for which the $T_{50\%}$ cannot be captured reasonably in *in vitro* dissolution experiments, such as devices designed for up to 3 years of use.

Korsmeyer and Peppas provided a method for understanding drug release mechanisms of swelling and non-swelling polymeric systems, given by Equation 6 [105]:

$$\frac{M_t}{M_\infty} = Kt^n \qquad \text{(Eq. 6)}$$

Where M_t/M_∞ is the fraction of drug released at time *t*, *K* is the rate constant, and *n* is the release exponent. For a cylindrical polymeric DDS, which we use as an approximation of these rectangular prism DDS, the Korsmeyer-Peppas model defines $0.45 < n < 0.89$ as anomalous transport characterized by both diffusion and matrix relaxation (Table 2.5) [106]. The TPU matrices here have release exponents ranging from 0.525 to 0.614. Anomalous release seems an appropriate description of the drug release mechanism of these TPUs based on their variable, nonzero water uptake and non-erosion properties. Accordingly, in these TPU matrices, the diffusion rate and polymer relaxation rate are of the same order of magnitude [339].

This *in vitro* release data allowed us to screen for the TPU matrix that is most likely to achieve sustained release of more highly loaded DPV, ideally reaching $T_{50\%}$ at one year or later. Here, we observed that TPU4 released drug the slowest, releasing approximately 43% of loaded DPV at 16.5 μg/day by 30 days. Though this is not an ideal $T_{50\%}$, cumulative release is relative to the initial loading of drug in the matrix; thus, increasing the loading given a constant release rate decreases cumulative release and extends $T_{50\%}$. As such, we determined that TPU4 would be the most likely matrix to achieve sustained release at the desired timescale and therefore investigated its release behavior at higher DPV loading.

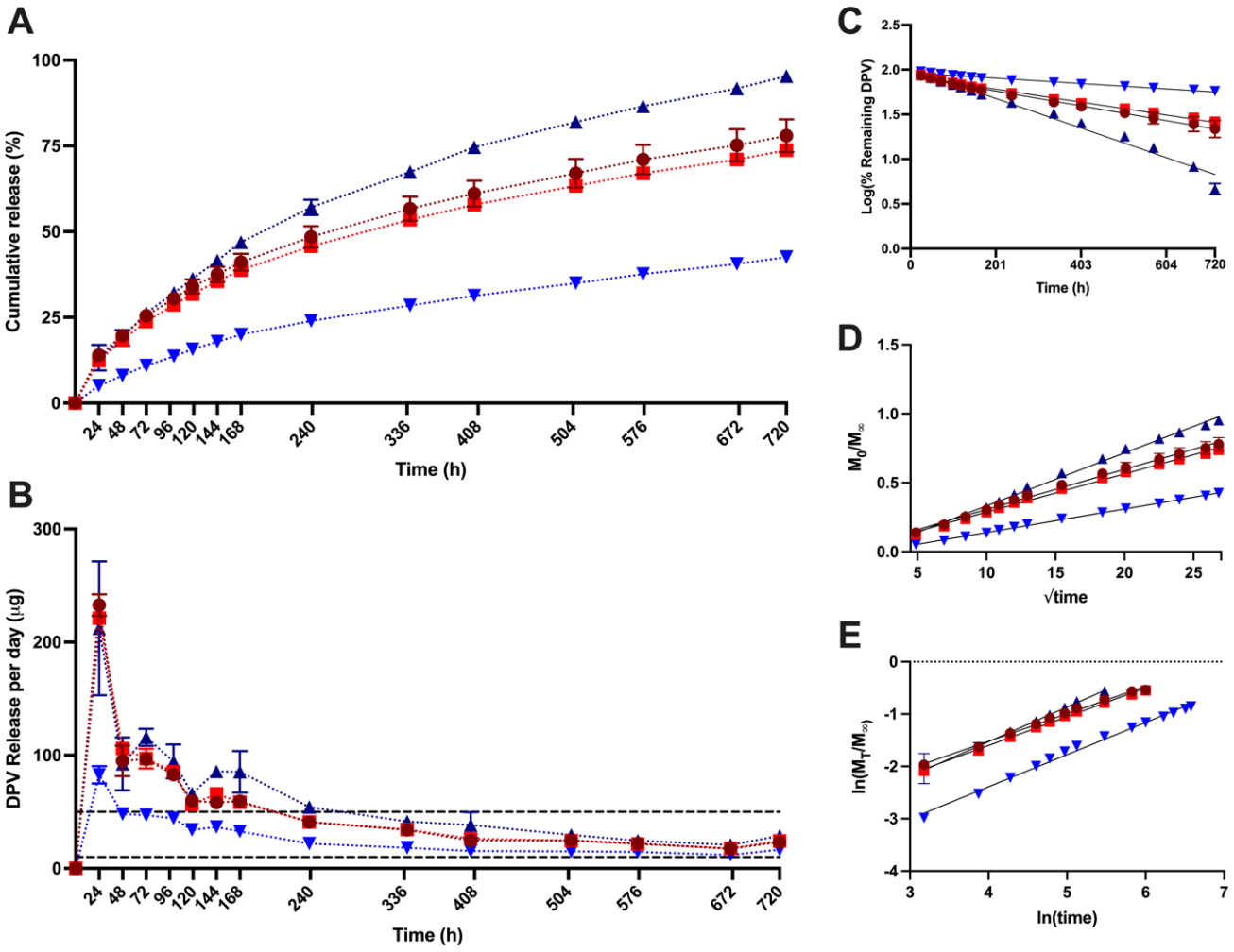

FIGURE 5.4. **DPV Release from TPU matrix DDS prototypes.** (A) Cumulative release (%) and (B) amount of DPV release per day from four TPUs loaded at 1 wt% drug over 30 days. Dashed lines at 10 and 50 µg represent target daily *in vivo* release. (C) First-order release kinetics fit to cumulative release data by plotting the percent of drug remaining in each device versus time. (D) Higuchi release kinetics fit to cumulative release data by plotting the fraction of drug released (M_0 = mass of drug released, M_∞ = total mass of drug in each device) versus the square root of time. (E) Korsmeyer-Peppas plot of the natural log of the fraction of drug released versus the natural log of time, fitted to the first 60% of drug released. Values represent the mean of n=3 devices; error bars represent standard deviation. Dark red circles represent TPU1, light red squares represent TPU2, dark blue upright triangles represent TPU3, and light blue upside-down triangles represent TPU4.

TABLE 5.4. DPV matrix DDS release parameters and $T_{50\%}$ estimation.

Loading (wt%)	*TPU*	*Release Exponent*		*Korsmeyer-Peppas Constant: n, R^2*	*Predicted $T_{50\%}$ (d)*	*Actual $T_{50\%}$ (d)*
		Higuchi: k_H (%/$h^{1/2}$), R^2	*First-Order: k (h^{-1}), R^2*			
1%	TPU1	0.029, 0.996	0.002, 0.995	0.525, 0.994	12	12
	TPU2	0.027, 0.996	0.002, 0.992	0.549, 0.996	13.5	12
	TPU3	0.038, 0.996	0.004, 0.978	0.662, 0.997	7	7
	TPU4	0.017, 0.999	0.0007, 0.981	0.614, 0.993	36	-
16.6%	TPU4	0.014, 0.995	0.0005 0.964	0.674, 0.976	53.5	-

After screening for the optimal TPU matrix DDS for DPV release, we loaded TPU4 with 16.6 wt% DPV. This loading was selected as it would allow a device to release at least 10 μg of DPV per day for at least one year while retaining at least 50% of its initial drug loading. We found that at high loading in TPU4, DPV release *in vitro* was similar to that of the low loading condition (Figure 5.5). Indeed, the TPU4 matrix DDS released approximately 33.5% of loaded DPV after 30 days (Figure 5.5A) at a final release rate of approximately 62.56 μg/day (per each 1/3 segment of the device) (Figure 5.5B). Despite an increase in the daily release rate, a smaller percentage of DPV was released over the *in vitro* dissolution period than the 1 wt% DPV-TPU4 device. This demonstrates the trade-off between high loading and cumulative release. It is often held that higher drug loading in a matrix system results in more rapid drug release due to the more amorphous and potentially porous architecture of a polymer matrix with a higher relative drug content and due to the higher chemical gradient at the diffusion front [101]. Here, we observed that daily flux did increase, but this did not account for an increase in the cumulative release rate due to the daily flux being a smaller fraction of drug relative to the total drug loading.

The significance of this trade-off for DDS development is emphasized in the predicted $T_{50\%}$. First-order and Higuchi release models were fit and, once again, the square-root of time dependence was most closely correlated with *in vitro* release data (Figure 5.5C&D, Table 5.4). The Higuchi model predicted that $T_{50\%}$ would be reached at 53.5 days; this is significantly less than the one-year target, but greater than $T_{50\%}$ for 1 wt% DPV in TPU4. The exponent of the Korsmeyer-Peppas model confirms that anomalous release remains the driving drug release mechanism in this device (n = 0.674) (Figure 5.5E, Table 5.4). Because the release mechanism was the same as the 1 wt% DPV-TPU4 device, we propose that the crystallinity of DPV in the 16.6 wt% DPV-TPU4 device drove its relatively slower release. Because only soluble drug is available for diffusion in a monolithic polymer matrix, DPV must first dissolve and partition out of its crystalline form before it can diffuse through the matrix device [93]. Therefore, this rate-limiting step likely slowed release from the TPU4 matrix DDS. Despite slower release, it is evident that a highly load TPU4 matrix DDS does not sufficiently sustain the release of DPV to achieve one-year of dissolution.

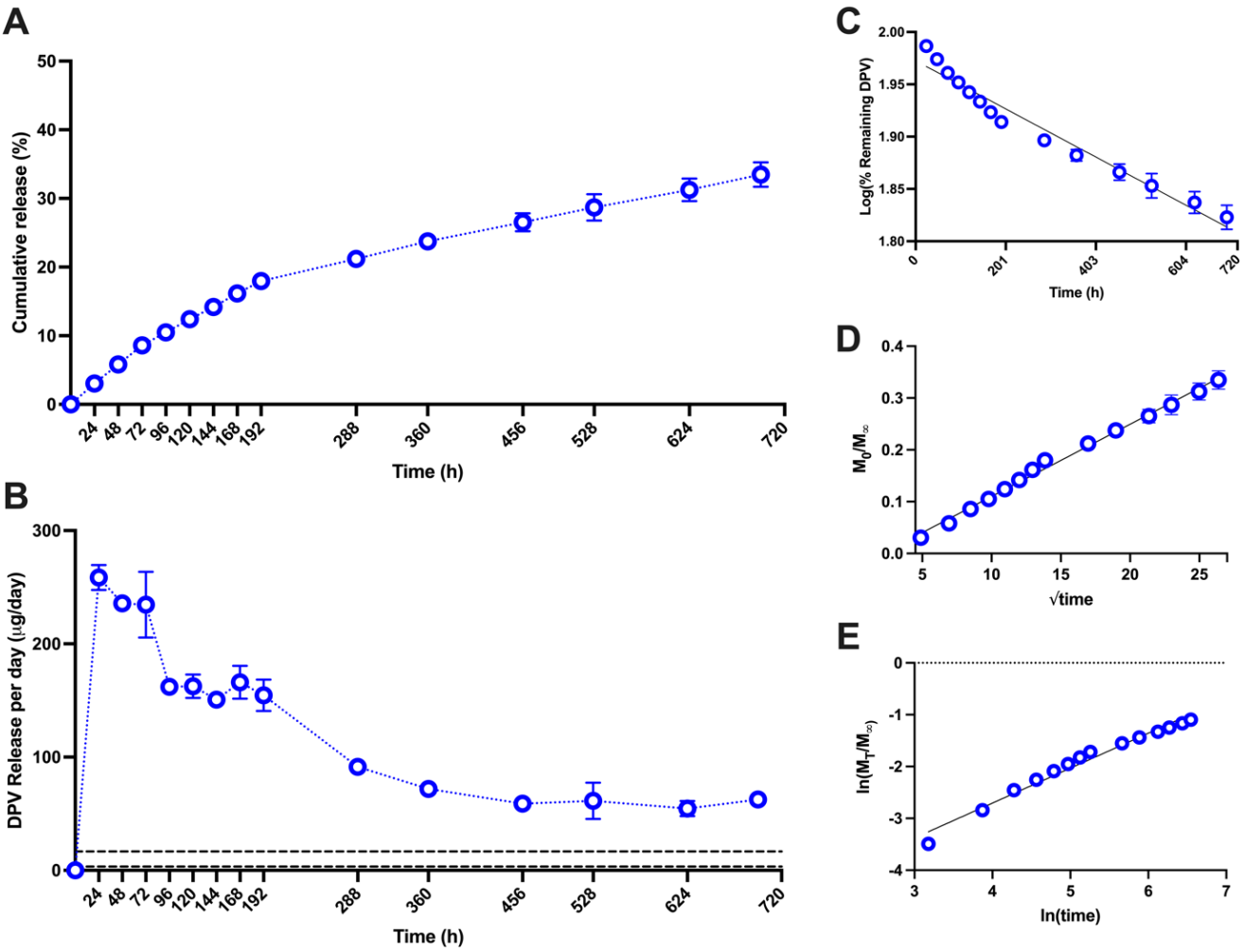

FIGURE 5.5. **High loading DPV release from TPU4 matrix DDS.** (A) Cumulative release (%) and (B) amount of DPV release per day from TPU4 loaded with 16.6 wt% DPV over 30 days. Dashed lines at 3.3 and16.6 µg represent target daily *in vivo* release, adjusted for analyzing a one-third segment of a DDS prototype. (C) First-order release kinetics fit to cumulative release data by plotting the percent of drug remaining in each device versus time. (D) Higuchi release kinetics fit to cumulative release data by plotting the fraction of drug released (M_0 = mass of drug released, M_∞ = total mass of drug in each device) versus the square root of time. (E) Korsmeyer-Peppas plot of the natural log of the fraction of drug released versus the natural log of time, fitted to the first 60% of drug released. Values represent the mean of n=3 device segments; error bars represent standard deviation.

5.4.4 In vitro release testing of triple-ARV matrix DDS prototypes

We investigated the potential of TPU matrix DDSs to deliver multiple physicochemically distinct drugs in order to probe the sensitivity of matrix release kinetics to API properties. We

selected three antiretrovirals – raltegravir (RAL), maraviroc (MVC), and etravirine (ETR) – that represent a synergistic anti-HIV combination. The physicochemical and antiviral properties of these agents are described in Table 5.5.

TABLE 5.5. Physicochemical characteristics of combination ARVs [340].

ARV	***Drug Class***	***IC_{50} (ng/mL)***	***LogP***	***Molecular Weight (g/mol)***	***Water Solubility (mg/mL)***
Raltegravir (RAL)	Integrase Inhibitor	8.94	1	444.4	53.9
Maraviroc (MVC)	CCR5 Agonist	3.07	4.3	513.68	0.011
Etravirine (ETR)	NNRTI	0.61	>5	435.3	0.00397

Screening the release of 1 wt% RAL, MVC and ETR from TPU2, TPU3 and TPU4 matrices showed significantly distinct release rates (Figure 5.6A). We excluded TPU1 in this iteration as we did not believe it was necessary to test two similar hydrophilic, water-swellable polymers. TPU2 released approximately 50% of encapsulated RAL and MVC within the first 24 hours of dissolution and reached 100% release by day 7 and 13, respectively. TPU3 also released approximately 50% of encapsulated RAL in the first 24 hours but then showed more sustained, first order release behavior with cumulative release reaching 100% at one month. TPU4 offered sustained and consistent dissolution of all ARVs; it released 31.71% RAL, 33.83 % MVC, and 27.70% ETR by 30-days. Release of all ARVs within the target dose per day window was only achieved by TPU3 at 30 days (Figure 5.6B).

Release data fit to first order release kinetics (Figure 5.6C), Higuchi release kinetics (Figure 5.6D) and the Korsmeyer-Peppas Model (Figure 5.6E) are summarized in Table 5.6.

First order release was a superior fit to Higuchi release for RAL in TPU2 and TPU3 and MVC in TPU3. First-order and Higuchi models are generally less able to predict $T_{50\%}$ when it occurs upon burst release or at very early timepoints, such as the case of RAL in TPU2 and TPU3 (first-order) and MVC in TPU2 (Higuchi). TPU4 offered the most favorable sustained release profiles for all ARVs as $T_{50\%}$ was 109 days, 68 days, and 90 days for RAL, MVC, and ETR, respectively. Interestingly, RAL, the most hydrophilic ARV, was released the slowest from the hydrophobic TPU4 matrix. Korsmeyer-Peppas modelling for RAL in TPU3 and 4 indicates Quasi-Fickian drug transport wherein drug release is mediated by non-swellable matrix diffusion. Thus, the diffusion coefficient of RAL in each polymer is a significant mediator of dissolution. It is likely that RAL, being highly hydrophilic, is less compatible with hydrophobic TPU4 than the other hydrophobic ARVs and therefore exbibits slower diffusion through the matrix.

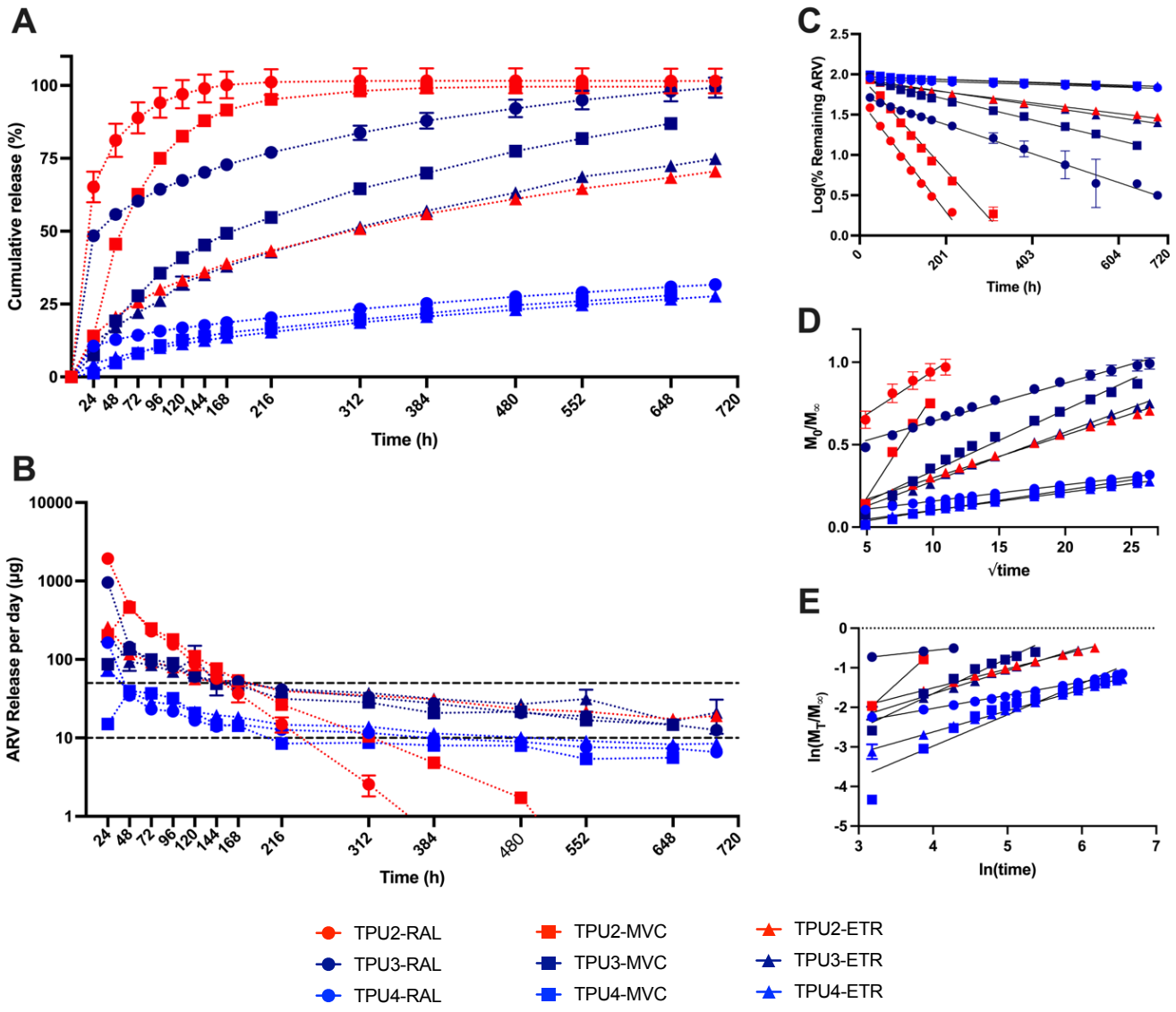

FIGURE 5.6. **RAL, MVC, and ETR release from TPU2, TPU3, and TPU4 matrix DDS.** (A) Cumulative release (%) and (B) amount of RAL, MVC, and ETR release per day from TPU2, TPU3, and TPU4 loaded with 1 wt% drug over 30 days. Dashed lines at 10 and 50 µg represent target daily *in vivo* release. (C) First-order release kinetics fit to cumulative release data by plotting the percent of drug remaining in each device versus time. (D) Higuchi release kinetics fit to cumulative release data by plotting the fraction of drug released (M_0 = mass of drug released, M_∞ = total mass of drug in each device) versus the square root of time. (E) Korsmeyer-Peppas plot of the natural log of the fraction of drug released versus the natural log of time, fitted to the first 60% of drug released. Values represent the mean of n=3 device segments; error bars represent standard deviation. Circles represent RAL, squares represent MVC, and triangles represent ETR. Red markers represent TPU2, dark blue markers TPU3, and light blue markers represent TPU4.

TABLE 5.6. 3-ARV matrix DDS release parameters and $T_{50\%}$ estimation.

ARV	*Loading (wt%)*	*TPU*	*Release Exponent*		*Korsmeyer-Peppas Constant: n, R^2*	*Predicted $T_{50\%}$ (d)*	*Actual $T_{50\%}$ (d)*
			Higuchi: k_H (%/$h^{1/2}$), R^2	*First-Order: k (h^{-1}), R^2*			
RAL	1%	TPU2	0.052, 0.959	0.016, 0.982	-	2	< 1
		TPU3	0.023, 0.987	0.004, 0.992	0.201, 0.999	7	1
		TPU4	0.010, 0.999	0.0004, 0.979	0.333, 0.995	109	-
	16.6%	TPU4	0.006, 0.998	0.0002, 0.970	0.455, 0.999	251	-
	30%	TPU4	0.005, 0.998	0.0002, 0.98		363	-
MVC	1%	TPU2	0.125, 0.986	0.013, 0.984	-	1	2.5
		TPU3	0.037, 0.978	0.003, 0.992	0.890, 0.960	7.5	7
		TPU4	0.012, 0.973	0.0005, 0.928	0.793, 0.886	68	-
	16.6%	TPU4	0.007, 0.995	0.0002, 0.976	0.529, 0.993	221	-
	30%	TPU4	0.003, 0.942	0.0001, 0.985		737	-
ETR	1%	TPU2	0.026, 0.995	0.002, 0.989	0.484, 0.997	15.5	13
		TPU3	0.030, 0.997	0.002, 0.995	0.585, 0.995	12	13
		TPU4	0.011, 0.999	0.0004, 0.975	0.535, 0.998	90	-
	16.6%	TPU4	0.003, 0.998	0.0001, 0.985	0.599, 0.999	857	-

Due to its durable release of all three ARVs at low loading, TPU4 was selected to investigate dissolution at high drug loading. RAL, MVC, and ETR were independently loaded at 16.6 wt% into TPU4 matrix DDSs. We observed significant sustained release behavior of all ARVs from TPU4 matrix DDS (Figure 5.7). After 30-days of *in vitro* dissolution, approximately 18% of RAL and MVC were released while only 8.5% of total ETR was released (Figure 5.7A). The release rate of all three ARVs remained at or above the target dose per day for 30-days (Figure 5.7B), leveling off around 22, 16, and 14 μg/day (per each 1/3 segment of the device) of RAL, MVC, and ETR, respectively. The Higuchi model most closely fit *in vitro* release data

from all ARVs (Figure 5.7D) in comparison to first order release kinetics (Figure 5.7C, Table 5.7). The Korsmeyer-Peppas model indicates that anomalous, non-Fickian drug transport characterizes the matrix relaxation and diffusion-driven drug release mechanism present in these matrix DDSs (Figure 5.7E). Using the best-fit *in vitro* release model, we predicted that $T_{50\%}$ would be reached at 251, 221, and 857 days for RAL, MVC, and ETR, respectively (Table 5.6). This represents a range from 0.60 to 2.34 years of sustained release with ETR exceeding our target of a one-year duration of action.

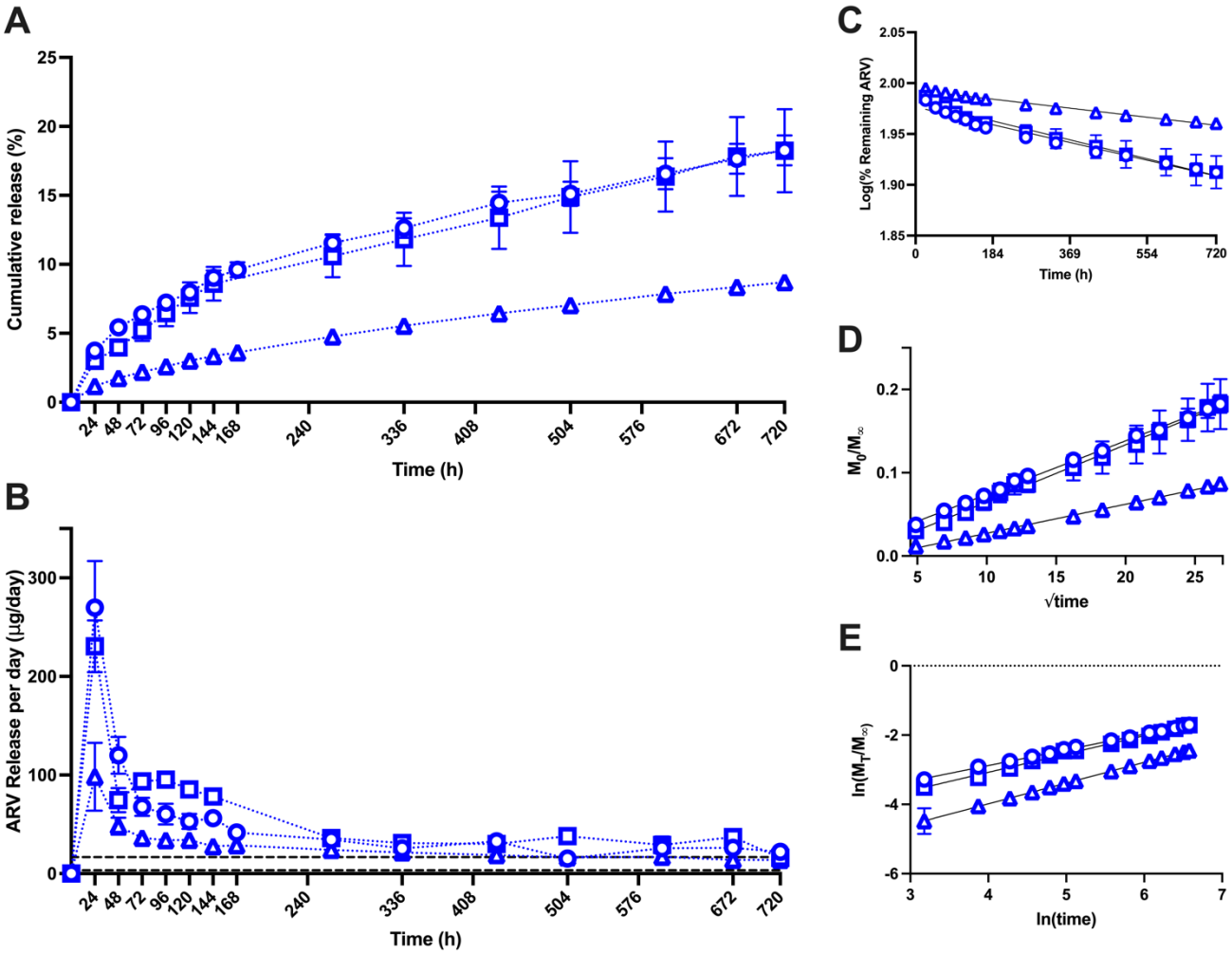

FIGURE 5.7. **High loading RAL, MVC, and ETR release from TPU4 matrix DDS.** (A) Cumulative release (%) and (B) amount of RAL, MVC, and ETR release per day from TPU4 loaded with 16.6 wt% drug over 30 days. Dashed lines at 3.3 and16.6 µg represent target daily *in vivo* release, adjusted for analyzing a one-third segment of a DDS prototype. (C) First-order

release kinetics fit to cumulative release data by plotting the percent of drug remaining in each device versus time. (D) Higuchi release kinetics fit to cumulative release data by plotting the fraction of drug released (M_0 = mass of drug released, M_∞ = total mass of drug in each device) versus the square root of time. (E) Korsmeyer-Peppas plot of the natural log of the fraction of drug released versus the natural log of time, fitted to the first 60% of drug released. Values represent the mean of n=3 device segments; error bars represent standard deviation. Circles represent RAL, squares represent MVC, and triangles represent ETR.

5.4.5 In silico modelling and rational design of matrix DDS prototypes

In order to understand and more efficiently select drug loading targets for ARV release from matrix DDS prototypes, we fit *in vitro* release data to theoretical models of drug dissolution from monolithic solutions and monolithic dispersions. Drug release at early timepoints ($M_t/M_\infty < 0.4$) from a cylindrical matrix in which drug exists as a monolithic solution, meaning it is molecularly soluble and below the saturation solubility, can be described by Equation 7:

$$\frac{M_t}{M_\infty} = 4\left(\frac{Dt}{\pi R^2}\right)^{1/2} - \frac{Dt}{R^2} \qquad \text{(Eq. 7)}$$

Where M_t/M_∞ is the fraction of drug released at time *t,* D is the diffusion coefficient of drug in the polymer matrix, and R is the radius of the matrix. Drug release from a cylindrical monolithic dispersion at late timepoints ($M_t/M_\infty > 0.6$) can be described by Equation 8:

$$\frac{M_t}{M_\infty} = 1 - \frac{4}{2.405^2}\exp\left(-\frac{2.405^2 Dt}{R^2}\right) \qquad \text{(Eq. 8)}$$

Where M_t/M_∞, D, and R are as described above. Our matrix DDS prototypes can be approximated to a cylindrical device using the width as the dimensional equivalent of the diameter of a cylinder. We fit the first seven consecutive timepoints of *in vitro* release data from TPU matrix DDS loaded with 1 wt% ARVs to the appropriate dissolution equation (Equation 7 or 8) in order to determine the diffusion coefficient parameter for each ARV-TPU combination (Figure 5.8, A-D). Subsequently, we used the diffusion coefficient for each ARV-TPU

combination to fit and predict dissolution from a saturated matrix DDS. Dissolution from a cylindrical monolithic dispersion is given by the implicit Equation 9:

$$\frac{M_t}{M_\infty} + \left(1 - \frac{M_t}{M_\infty}\right) ln\left[1 - \frac{M_t}{M_\infty}\right] = \frac{4D}{R^2} \cdot \frac{c_s}{c_{ini}} \cdot t \qquad \text{(Eq. 9)}$$

Where M_t/M_∞, D, and R are as defined above, c_s is the saturation solubility of drug in the matrix polymer, and c_{ini} is the initial concentration (loading) of drug in the matrix. This equation is valid for all time. Using the diffusion coefficient for each ARV in TPU4 determined by their corresponding dissolution from a monolithic solution (Equation 7 or 8), we fit 30-days of *in vitro* release data for TPU4 loaded with 16.6 wt% of each ARV to Equation 9 for monolithic dispersions (Figure 5.8 E&F). This allowed us to determine c_s for each drug in TPU4, thereby fully parametrizing the dissolution equation for a monolithic dispersion.

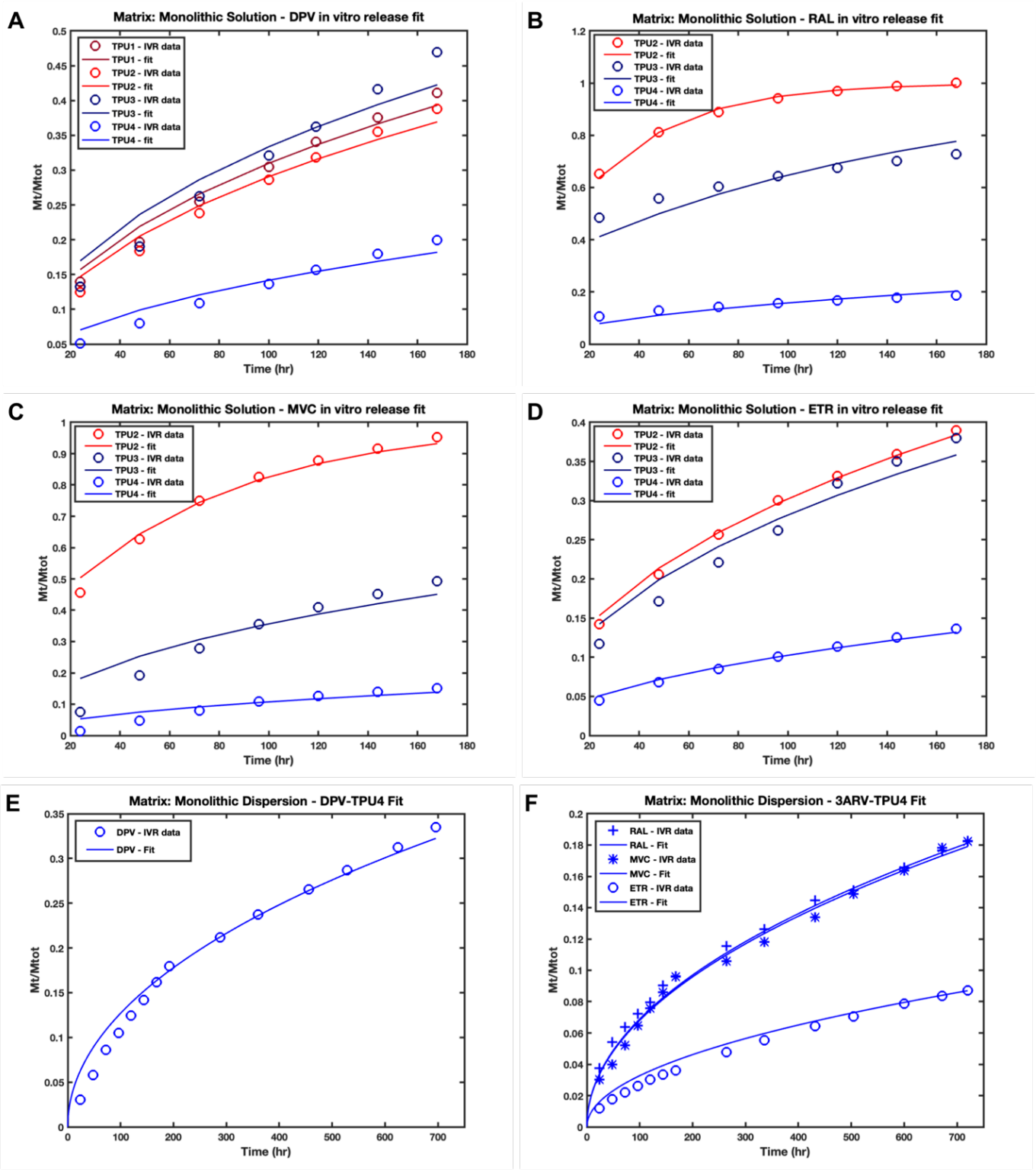

FIGURE 5.8. ***In vitro*** **release of ARVs from matrix DDS prototypes fit to drug dissolution equations.** (A) DPV, (B) RAL, (C) MVC, and (D) ETR dissolution from unsaturated TPU matrix DDS prototypes composed of TPU1 (dark red, DPV only), TPU2 (light red), TPU3 (dark blue), and TPU 4 (light blue). Circles represent the mean of n=3 data points taken from *in vitro*

release studies. (E) DPV and (F) 3-ARV dissolution from saturated TPU matrix DDS prototypes composed of TPU4 (light blue). Circles represent the mean of n=3 data points taken from *in vitro* release studies of DPV (E) and ETR (F); crosses represent RAL (F); and stars represent MVC (F). Solid lines represent optimized early- or late-time monolithic solution and monolithic dispersion equations fit to experimental data.

We used the saturation solubility of each ARV in TPU4 derived from Equation 9 as an approximation for the saturation solubility in the remaining TPUs tested for each ARV in order to assess the ability of any drug-polymer dispersion to achieve at least one year of sustained drug release. The diffusion coefficient was derived from Equation 7 or 8 for each TPU-ARV combination. We plotted the fraction of drug released at a constant time, one year, as a function of drug loading; this allowed us to determine which TPUs could release 50% or less of encapsulated drug in the target time period (Figure 5.9). These curves represent drug dissolution from a monolithic dispersion; therefore, we plotted a range from 5 to 50 wt%, the lower bound representing an approximation of the saturation solubility of the ARVs and the upper bound indicating the highest loading that we assume would be practically feasible to manufacture. Here, the intersection of each curve with the dashed line at $M_t/M_{total} = 0.5$ indicates the requisite drug loading at which $T_{50\%}$ equals one year for that device. We found that no TPU is capable of releasing DPV for one year at any loading (Figure 5.9A). Only TPU4 can offer sustained release of RAL and MVC for one year, requiring 25.21 wt% and 24.28 wt% of each ARV, respectively (Figure 5.9B&C). All TPUs tested for ETR are able to deliver the drug for at least one year with loading within the target window – TPU2 at 49.40 wt% ETR, TPU3 at 42.47 wt% and TPU4 at 5.22 wt% (Figure 5.9D). This data validates the selection of TPU4 as the leading candidate for delivery of all ARVs and offers insight into necessary loading targets to achieve the target drug release duration for the 3-ARV combination. We also see that a matrix DDS within this design

space of polymer type and geometry are not capable of delivering DPV for a sustained period. This strongly motivates the development of a reservoir-based delivery system for DPV.

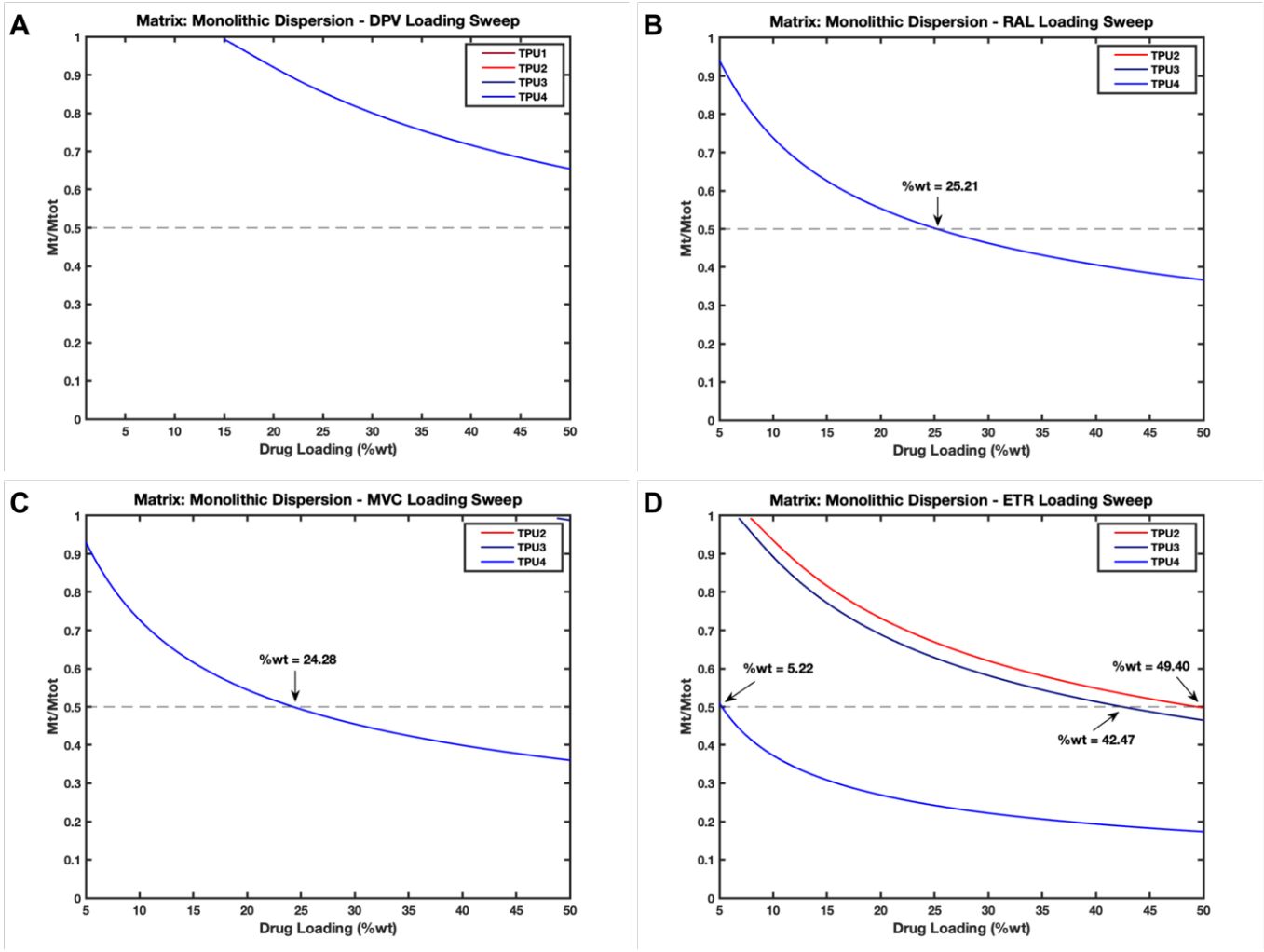

FIGURE 5.9. **Predicted drug dissolution at one year from TPU monolithic dispersions as a function of drug loading.** Predicted release of (A) DPV, (B) RAL, (C) MVC, and (D) ETR from TPU1 (DPV only, dark red line), TPU2 (light red line), TPU3 (dark blue line), and TPU4 (light blue line) monolithic dispersions. Curves plotted for t = 8760 hours (1 year), D (diffusion coefficients) derived from the fit of each ARV released from each TPU as a monolithic solution, R = 1.75 mm, representing the radius of cylinders with a diameter equivalent to the matrix DDS prototypes tested, and c_s (saturation solubilities) derived from each ARV released from TPU4 as a monolithic dispersion.

As it was clear that for all ARVs, TPU4 was the leading candidate for offering sustained release for at least one year, we modelled the release of each ARV from TPU4 for one, two, and three years to determine the required drug loading to achieve an extended duration of use (Figure 5.10). This model confirms that no drug loading up to the theoretical 50 wt% maximum is capable of offering one year of release of DPV (Figure 5.10A). The requisite loading for one year of sustained release of RAL, MVC, and ETR agree with those demonstrated in the previous model (Figure 5.9). RAL and MVC can achieve two years of sustained release if loaded at 50.34 wt% and 48.62 wt%, respectively, with RAL slightly exceeding the maximum theoretical loading of 50 wt% (Figure 5.10B&C). Neither RAL nor MVC can reach three years of sustained release within the loading maximum defined here. ETR loaded at approximately 10.46 wt% and 15.70 wt% can achieve two and three years of release, respectively (Figure 5.10D). We know that these are only estimations, as *in vitro* release data showed that a TPU4 matrix DDS with a theoretical 16.6 wt% ETR loading – which equated to a 15.32 wt% actual loading – resulted in approximately 2.35 years of sustained release. Rather than extracting a precise relationship between drug loading and duration of release, it may be more appropriate to consider these predictions estimates of loading thresholds. For instance, in order to achieve greater than one year of release of RAL and MVC, this modelling tells us to load greater than approximately 25 wt% for each drug.

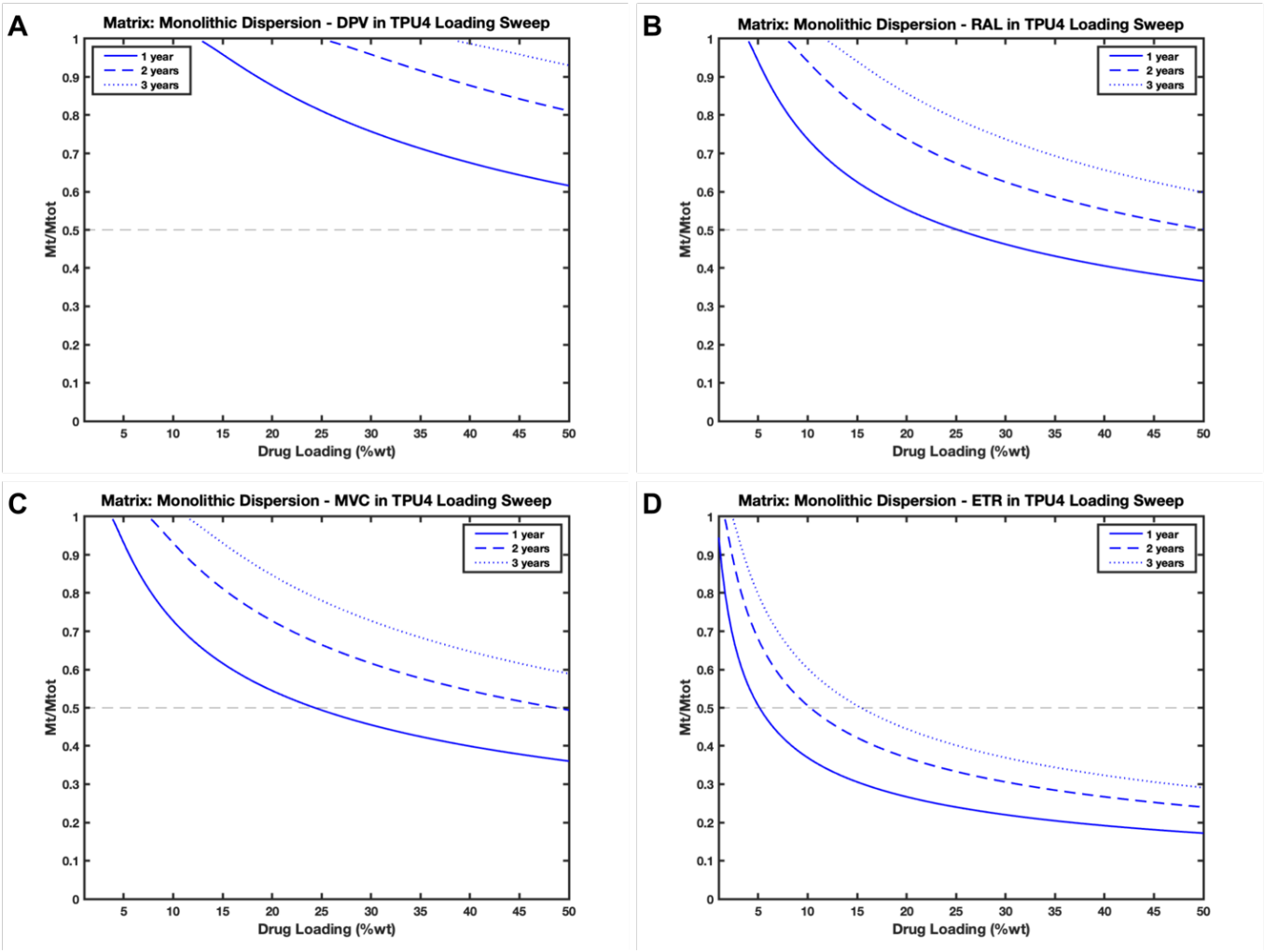

FIGURE 5.10. **Predicted drug dissolution at one, two, and three years from TPU4 monolithic dispersions as a function of drug loading.** Predicted release of (A) DPV, (B) RAL, (C) MVC, and (D) ETR from TPU4 monolithic dispersions for t = 8760 hours (one-year, solid line), t = 17520 hours (two years, dashed line), and t = 26280 hours (three years, dotted line). Curves plotted with D (diffusion coefficients) derived from the fit of each ARV released from TPU4 as a monolithic solution, R = 1.75 mm, and c_s (saturation solubilities) derived from each ARV released from TPU4 as a monolithic dispersion.

5.4.6 In vitro release testing of matrix DDS with model-informed ARV loading

As determined by *in silico* modelling of ARV release from cylindrical monolithic dispersions, RAL and MVC must be loaded above approximately 25 wt% in TPU4 in order to achieve at least one-year of sustained release (Figure 5.9). As such, we fabricated very highly loaded TPU4 matrix DDS containing 30 wt% RAL and MVC to optimize the probability of

predicting $T_{50\%}$ > 1 year. We conducted *in vitro* dissolution testing for 30 days and observed slower cumulative release than 16.6 wt% loaded RAL and MVC in TPU4 DDS (Figure 5.7A). Indeed, 30 wt% TPU4-RAL release approximately 15.7% of encapsulated drug at 30 days, while 30 wt% TPU4-MVC released even less, approximately 7.1% of encapsulated drug (Figure 5.11A). The release rate of RAL and MVC remained above the target dose per day by study terminus at 41.1 ug/day and 27.7 ug/day, respectively (per each 1/3 segment of the device) (Figure 5.11B). The release of very highly loaded RAL was described best mathematically by the Higuchi, square-root of time relation (Figure 5.11C), whereas MVC dissolution was described best by the first-order equation (Figure 5.11D), as presented in Table 5.6. The best-fit release exponents were used to predict $T_{50\%}$ for RAL and MVC, which was 363 days and 737 days, respectively.

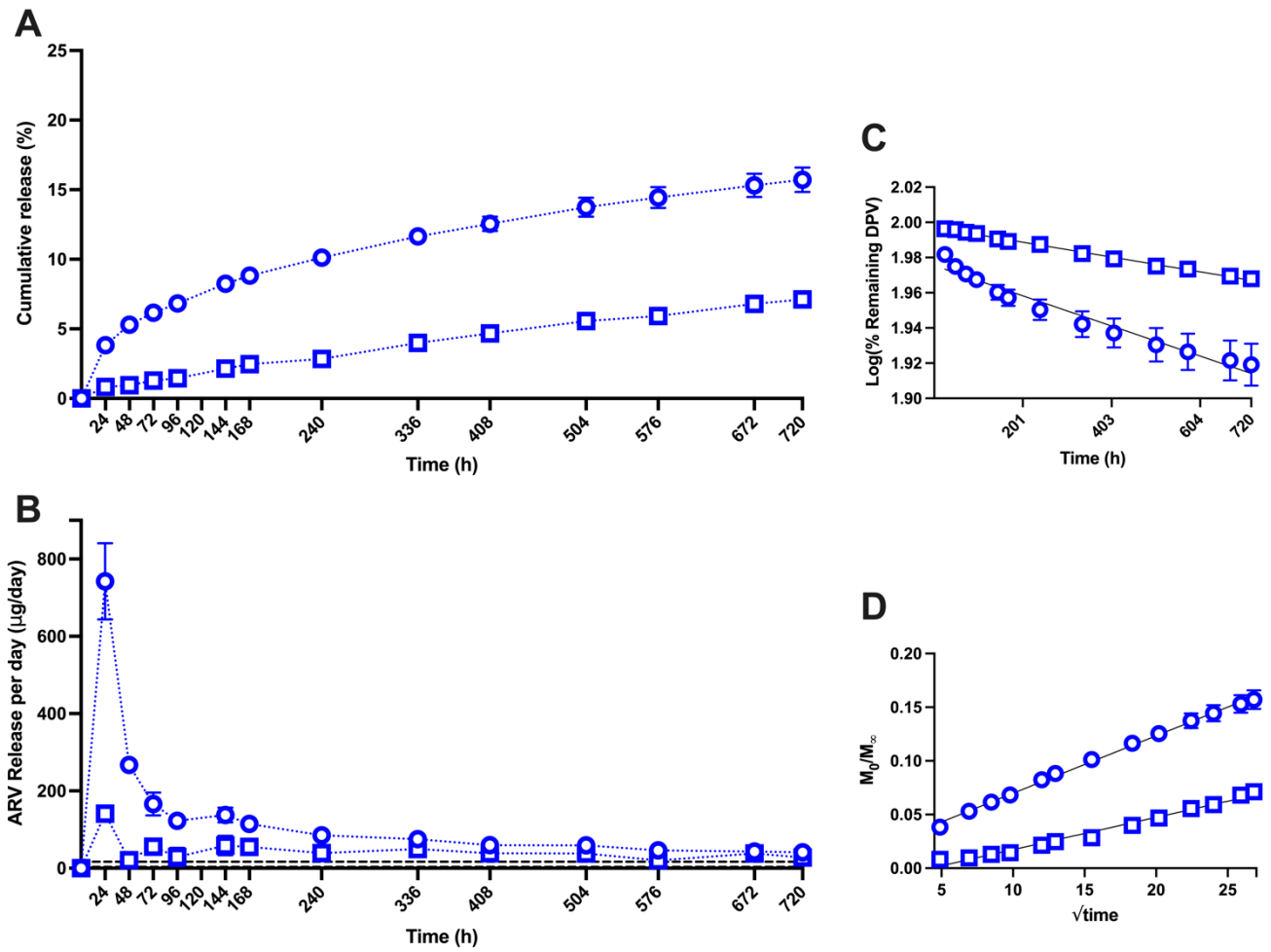

FIGURE 5.11. **RAL and MVC release from TPU4 with model informed loading.** (A) Cumulative release (%) and (B) amount of RAL and MVC release per day from TPU4 loaded with 30 wt% drug over 30 days. Dashed lines at 3.3 and 16.6 µg represent target daily *in vivo* release, adjusted for analyzing a one-third segment of a DDS prototype. (C) First-order release kinetics fit to cumulative release data by plotting the percent of drug remaining in each device versus time. (D) Higuchi release kinetics fit to cumulative release data by plotting the fraction of drug released (M_0 = mass of drug released, M_∞ = total mass of drug in each device) versus the square root of time. Values represent the mean of n=3 device segments; error bars represent standard deviation. Circles represent RAL and squares represent MVC.

This analysis suggests that RAL loaded at 30 wt% in a TPU4 matrix DDS can offer durable release for approximately one year and MVC loaded at 30 wt% in TPU4 can achieve approximately two years of release, similar to ETR loaded at 16.6 wt%. As such, we have demonstrated the ability to fabricate monolithic dispersions of three physicochemically distinct

ARVs in the same TPU that can release each drug for at least one year and up to nearly 2.5 years. Given a modular device in which each drug is incorporated into an independent matrix DDS segments, this device would be duration-limited by the dissolution of RAL. This is unsurprising given that RAL is much more water soluble than MVC and ETR. However, this work remains significant as it demonstrates the potential to deliver multiclass ARVs for the targeted window of protection using a simple matrix DDS fabrication process and modular device integration approach.

5.4.7 In vitro release testing of single-ARV reservoir DDS with a nonconstant activity source

We investigated four designs of core-sheath reservoir DDSs for sustained release of DPV (Table 5.3); groups included two sheath polymer chemistries combined with two sheath membrane thicknesses. The *in vitro* release profile of DPV loaded at 1 wt% from the reservoir formulations corresponded with predicted relative release rates based on sheath thickness – reservoirs with 100 μm sheaths (R1 & R3) released drug faster than 200 μm reservoir devices with the same respective sheath polymers (Figure 5.12A). Both polyether sheath reservoirs (R1 & R2) released DPV faster than polycarbonate sheath reservoirs (R3 & R4). It can be concluded from this data that DPV exhibits slower diffusion through a TPU with polycarbonate chemistry than a polyether. All reservoir formulations released DPV within the target dose of 10-50 μg/day, ranging from 11.7 μg/day to 15.7 μg/day at 30 days (Figure 5.12B). In order to understand the drug release kinetics of these low-loading reservoir devices, we determined the saturation solubility of DPV in the core polymer to determine if these reservoirs contained a constant or a non-constant activity source. We found that the saturation solubility of DPV in a PY-PT43DE20 core is 5.46 ± 0.93 wt%. Thus, with DPV loaded at 1 wt% which is below the

saturation solubility, these reservoirs contain a nonconstant activity source. Pursuant to the behavior of reservoirs with a nonconstant activity source, these reservoirs released drug following first-order release kinetics (Figure 5.12C) [93]. Despite this expectation, drug release from all four reservoir devices was described slightly better by a square-root of time dependence (Figure 5.12D). Similar to the matrix DDS, the best-fit release profile, here the square-root of time dependence, was used to calculate the predicted $T_{50\%}$ of each reservoir (Table 5.7). These predictions were generally less accurate than those made for the matrix DDS, with an average error relative to experimental data of 19.7%.

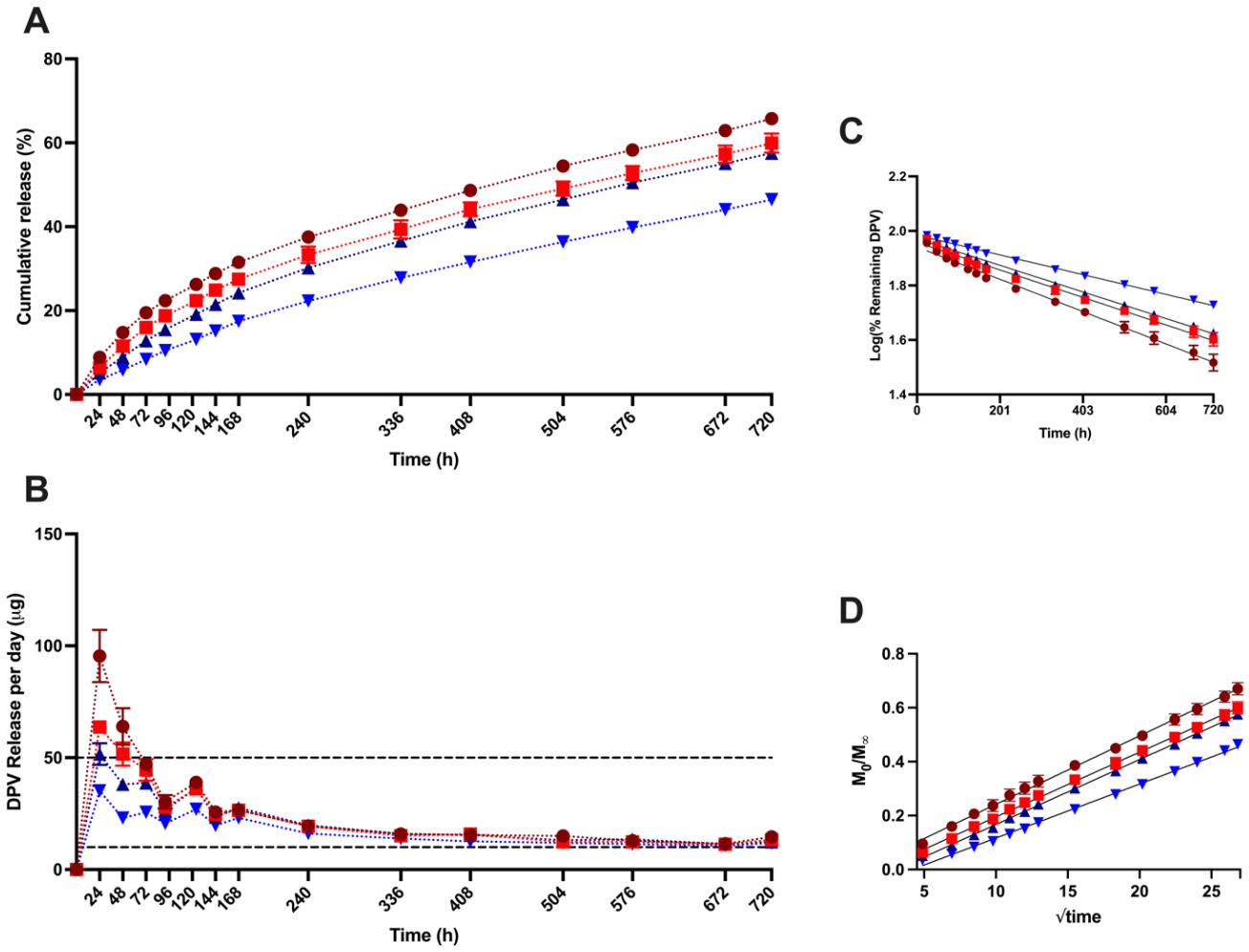

FIGURE 5.12. **DPV Release from low loading TPU reservoir DDS prototypes**. (A) Cumulative release (%) and (B) amount of DPV release per day from four TPU reservoirs loaded

at 1 wt% drug over 30 days. Dashed lines at 10 and 50 μg represent target daily *in vivo* release. (C) First-order release kinetics fit to cumulative release data by plotting the percent of drug remaining in each device versus time. (D) Higuchi release kinetics fit to cumulative release data by plotting the fraction of drug released (M_0 = mass of drug released, M_∞ = total mass of drug in each device) versus the square root of time. Values represent the mean of n=3 devices; error bars represent standard deviation. Dark red circles represent R1, light red squares represent R2, dark blue upright triangles represent R3, and light blue upside-down triangles represent R4.

TABLE 5.7. DPV reservoir DDS release parameters and $T_{50\%}$ estimation.

Loading (% w/w)	***Reservoir***	***Release Exponent***		***Predicted $T_{50\%}$ (d)***	***Actual $T_{50\%}$ (d)***
		Higuchi: k_H (%/$h^{1/2}$), R^2	***First-Order: k (h^{-1}), R^2***		
1%	R1	0.025, 0.998	0.001, 0.993	16	19
	R2	0.024, 0.999	0.001, 0.992	18	22
	R3	0.024, 0.999	0.001, 0.996	18	24
	R4	0.020, 0.997	0.0008, 0.997	26	>30

5.4.8 In silico modelling and rational design of reservoir DDS prototypes

In order to obtain more accurate predictions of reservoir DDS behavior and design high-loading reservoirs capable of releasing drug for at least one year, we fit *in vitro* release data to mechanistic equations for drug dissolution from reservoirs with constant and non-constant activity sources (Figure 5.12). The equation for drug dissolution from a core-sheath reservoir with a nonconstant activity source, meaning that drug exists in the core polymer below its saturation solubility, is given by Equation 10:

$$\frac{M_t}{M_\infty} = 1 - \exp\left[-\frac{(R_i H + R_o H + 2R_i R_o)DKt}{R_i^2 H(R_o - R_i)}\right] \qquad \text{(Eq. 10)}$$

Where M_t/M_∞ is the fraction of drug released at time *t*, R_i is the inner radius (radius of the core), R_o is the outer radius (radius of the core + sheath), H is the height, *D* is the diffusion coefficient

of drug through the sheath, and *K* is the partition coefficient of drug between the core and sheath. Equation 9 was fit to the first 30 days in *in vitro* release of DPV from each of the four reservoir DDS prototypes (Figure 5.13A) in order to determine the product of the diffusion and partitioning coefficient, given by the parameter *DK*.

With *DK* known for each formulation and the experimentally determined value for the saturation solubility of DPV in the core polymer, we were able to parameterize the expression for drug release from a reservoir with a constant activity source, given by Equation 11:

$$M_t = \frac{2\pi HDKc_s}{\ln\left(\frac{R_o}{R_i}\right)} \cdot t \qquad \text{(Eq. 11)}$$

Where M_t represents the amount of drug released at time *t*, c_s represents the saturation solubility of drug in the core polymer, and R_i, R_o, H, D, and K are as defined above. Using Equation 11, we simulated the release of DPV from each reservoir DDS prototype to determine the final mass of drug released at one year (Figure 5.13B). As expected, a reservoir with a constant activity source, in which drug is loaded above the saturation solubility of the core polymer, gives drug release with zero-order release behavior. From these predictions we determined the mass and loading of DPV required to make $T_{50\%}$ equal to one year for each reservoir, given by double the total amount of drug released in one year (Table 5.8). We also calculated the dose of drug released per day by each reservoir, given by the slope of each release prediction.

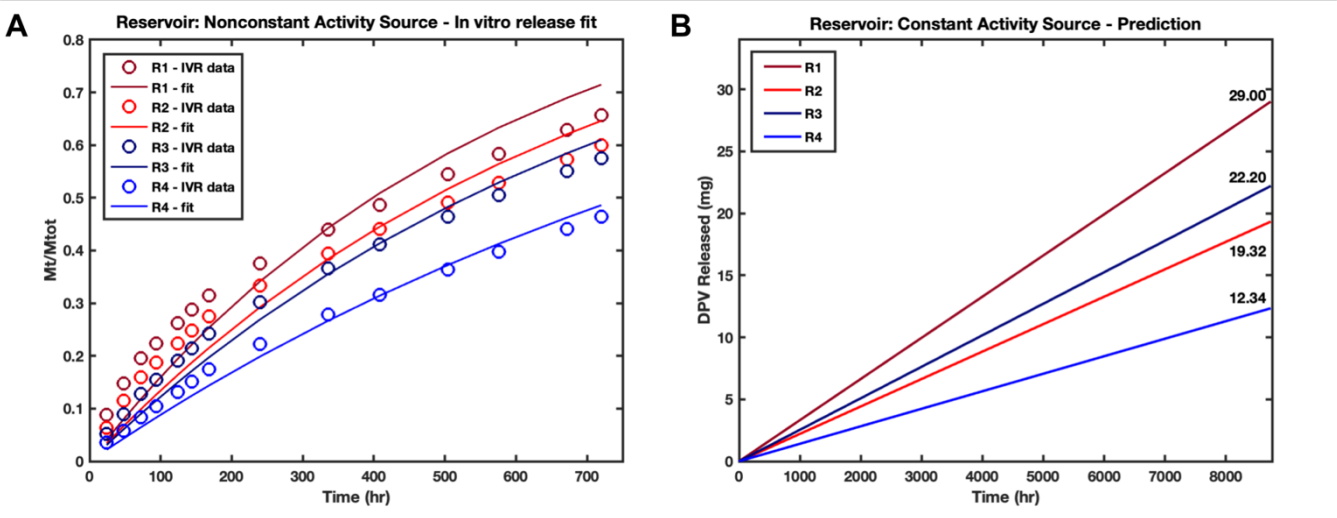

FIGURE 5.13. **DPV dissolution models from reservoirs with nonconstant and constant activity sources.** (A) DPV dissolution from reservoir DDS prototypes with nonconstant activity sources (loaded with 1 wt% DPV). Circles represent the mean of n=3 data points taken from *in vitro* release studies. Solid lines represent Equation 9 fit to experimental data. (B) Predictions of DPV dissolution over one year from reservoir DDS prototypes with constant activity sources (loaded above c_s). R1 is represented by dark red, R2 by light red, R3 by dark blue, and R4 by light blue.

TABLE 5.8. Predicted loading and release rate for highly loaded reservoir DDS prototypes.

Reservoir DDS	***Total DPV release in one year (mg)***	***Target DPV loading (mg) ****	***Core loading (%wt) *****	***Daily release rate (μg/day)***
R1	29.00	58.00	52.76%	79.2
R2	19.32	38.64	35.15%	52.8
R3	22.2	44.40	47.41%	60.0
R4	12.34	24.68	26.35%	33.6

* To retain 50% of loaded drug after 1 year of release
** Calculated using the core volume for each sheath thickness and average TPU density (1.215 g/cm^3)

In accordance with experimental observations, R1 was expected to release the most drug over one year and R4 the least. Interestingly, R3 surpassed R2 in its cumulative release from a saturated reservoir despite its slightly slower release from the unsaturated reservoir (Figure 5.13A). This suggests that in reservoirs with nonconstant activity sources, sheath polymer

chemistry plays a more significant role in mediating drug release than in reservoirs with constant activity sources. In the latter condition, sheath polymer thickness played a dominant role as the two reservoir DDS prototypes with 100 μm thick sheaths (R1 & R3) released drug the fastest. Here, we show that ultimately all reservoir devices are theoretically capable of releasing drug for one year with characteristics that match or are relatively similar to our initial design specifications. All reservoirs except R1 can be loaded below a theoretical 50 wt% loading target. However, the relevance of this cutoff is perhaps less significant for a reservoir DDS than a matrix DDS, as total device loading is lower than the core polymer loading and the sheath polymer can provide mechanical stability that a highly loaded core may lack. Indeed, based on mass of drug loaded, 58 mg of DPV loaded in R1 is similar to the 52 mg of LNG loaded into a Mirena IUD [111]. All of the highly loaded reservoir DDS prototypes would release drug above the 10 μg/day minimum, with R1, R2, and R3 exceeding the 50 μg/day target. As this specification is only a rough estimation of the drug release required to provide protection in the lower FRT based on the DPV ring ASPIRE clinical trial, we believe it would be suitable to test DDS that release drug at a slightly higher rate [15].

5.4.9 In vitro release testing of highly loaded reservoir DDS prototypes

Informed by our predictions of DPV release from TPU reservoirs loaded above the core polymer saturation solubility (section 5.4.10), we loaded the leading candidate reservoir formulation, R4, with 30 wt% DPV in the core polymer. We selected this loading as it approximates that of the predicted 26.35 wt% to achieve one year of DPV release at 33.6 μg/day (Table 5.8). We also included a comparator reservoir formulation, R3, loaded with the same wt% DPV in the core. We conducted *in vitro* release for 30 days in sink conditions and observed

minimal difference in cumulative release between the two formulations. DPV exhibited a more rapid release rate during the first week of *in vitro* release (Figure 5.14A) compared to the average release for the duration of the 30-day period (Figure 5.14B). This is likely due to burst effects caused by equilibration of DPV across the core and membrane polymer that results in the reservoir initially behaving as a matrix device, as described by van Laarhoven et al. [109] and demonstrated computationally by Clark et al. [86]. Indeed, devices were incubated post-fabrication for 2 weeks at 40°C in order to achieve DPV equilibration as described and prevent the opposite early-time phenomena called "lag-time" effects. Lag-time effects occur right after dosage form preparation when the sheath membrane is devoid of drug, requiring time for drug diffusion and resulting in a slower initial drug release rate [93].

Despite a decrease in the release rate after the initial burst period, the equilibrium dosage fell well within the target dose per day with R3 (full device) releasing an average of 24.23 (±3.79) μg/day for and R4 (full device) releasing 22.08 (±3.75) μg/day at day 30 (Figure 5.14C). Averaged over the entire 30-day period, R3 released an average dose of 51.76 μg/day and R4 an average dose of 41.66 μg/day; these dosages are similar to those estimated by our predictions indicated in Table 5.9, where R3 was expected to release 60.0 μg/day and R4 33.6 μg/day given a core loaded with a constant activity source. We further validated our modelling predictions by fitting a zero-order line through the full 30-day IVR dataset for each reservoir and predicting the time it would take for each device to reach $T_{50\%}$ (Table 5.9). We found that R3 would take approximately 424 days to reach $T_{50\%}$ and would release 43.07% of its initial cargo in one year, while R4 would take 436 days to reach $T_{50\%}$ and would release only 41.90% of its cargo in one year. These results are largely consistent with our initial predictions, especially given the slight variance in the actual amount of DPV loaded into the core of R3 and R4 (30 wt%) compared to

the model-informed loadings generated by our initial $T_{50\%}$ predictions (47.41% and 26.35%, respectively). Ultimately, this data shows that highly loaded TPU reservoirs of various sheath thicknesses (100-200 μm) are capable of releasing DPV *in vitro* on durable timescales greater than one year while providing consistent drug release per day. This data also validates our approach of screening low loading reservoir formulations to inform DDS formulation parameters using a semi-empirical model for drug release from reservoir devices.

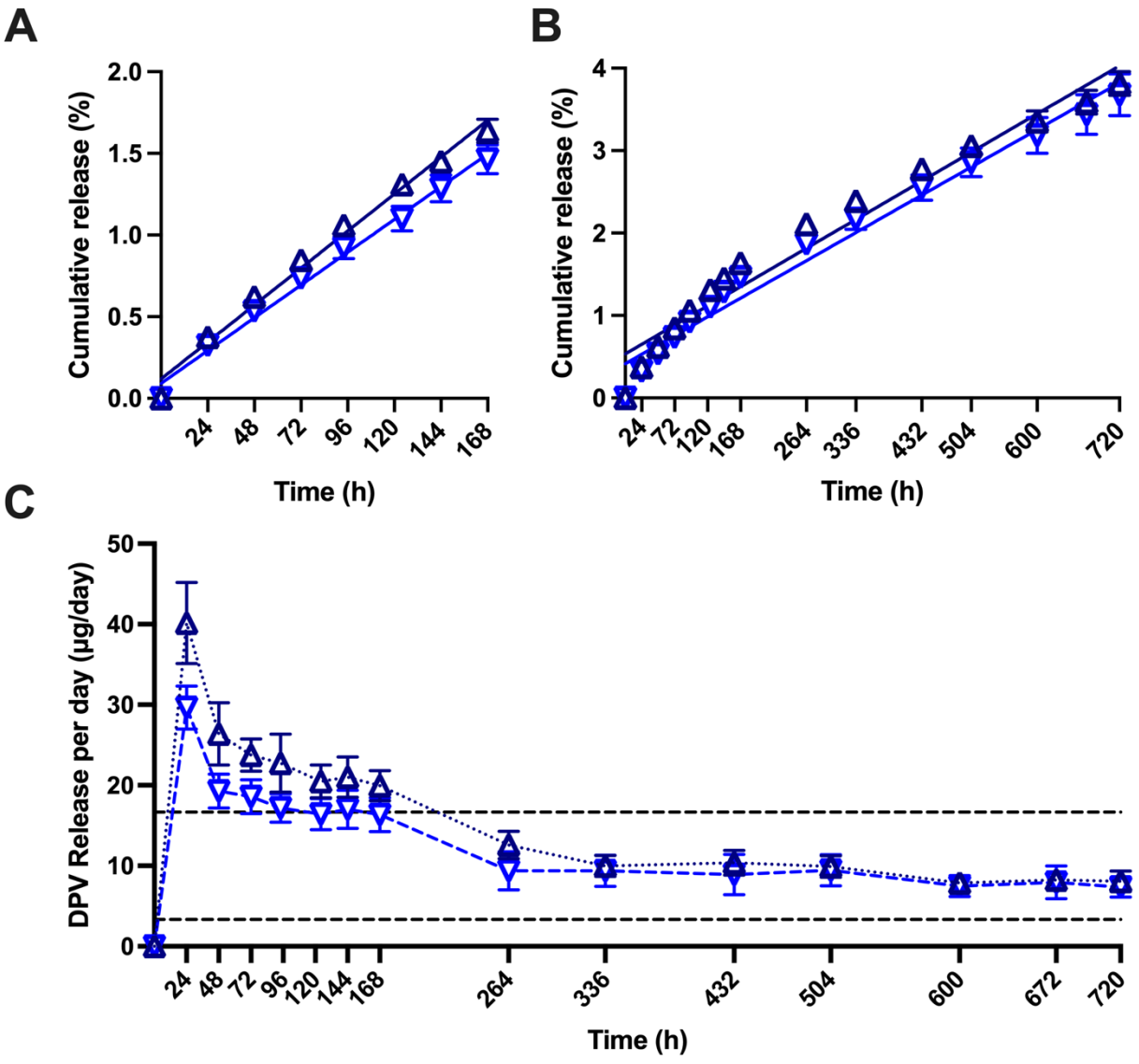

FIGURE 5.14. **DPV release from high loading TPU reservoirs**. Cumulative release (%) of DPV from two TPU reservoirs loaded at 30 wt% drug in the core over (A) 7 days and (B) 30

days. Dark and light blue solid lines represent linear regressions through IVR data from R3 and R4, respectively. (B) Amount of DPV release per day from highly loaded TPU reservoirs over 30 days. Dashed lines at 3.3 and 16.6 μg represent target daily *in vivo* release, adjusted for analyzing a one-third segment of a DDS prototype. Plotted values represent the mean of n=3 devices; error bars represent standard deviation. Dark blue triangles represent R3 and light blue triangles represent R4.

TABLE 5.9. Estimated duration of use of highly loaded DPV reservoirs.

Reservoir DDS	***Zero-Order Slope***	***R^2***	***Cumulative release (%) at 1 year***	***$T_{50\%}$ (days)***
R3	0.0049 (0.0094)	0.961 (0.987)	43.07 (88.16)	424.45 (218.52)
R4	0.0047 (0.0084)	0.987 (0.990)	41.90 (73.66)	436.25 (247.10)

In vitro dissolution testing is useful for understanding drug release mechanisms and comparatively evaluating DDS formulations; however, it is limited in its ability to recapitulate *in vivo* release kinetics. Conditions of *in vitro* release simulate the *in vivo* environment by controlling parameters such as temperature, pH, sink conditions, and aqueous conditions. Simulated conditions do not account for the low-flow environment *in vivo*, dynamics of protein binding, or metabolic effects. We used a non-ionic surfactant to increase the solubility of DPV, MVC, and ETR in release media to ensure sink conditions. Drug solubility in dissolution media is directly proportional to particle dissolution; as such, *in vitro* dissolution testing conditions here may have accelerated drug release [341]. Indeed, Baoa et al. observed a two-fold acceleration in levonorgestrel (LNG) dissolution from a PDMS reservoir when dissolution media was supplemented with 0.25% SDS compared to “real time” dissolution in pure aqueous media [108]. However, the two-fold acceleration in release determined by Baoa et al., which equates to approximately 20 μg/day, matches the 20 μg/day *in vivo* release rate of the Mirena IUD, as determined by clinical studies [111]. In a clinical pharmacology review by the Center for Drug

Evaluation and Research, an *in vitro-in vivo* correlation (IVIVC) was described for the Mirena IUD in which the dissolution profiles of LNG tested *in vitro* and *in vivo (ex vivo)* correlated with a slope of 1.165, indicating a nearly directly proportional relationship [342]. The *in vitro* dissolution conditions were not described. Based on these reports, it appears possible that "accelerated" *in vitro* dissolution due to increased solubility does not necessarily preclude interpretation of data with regard to *in vivo* performance. This *in vitro* release data and consideration for previously reported *in utero* release kinetics allows us to conclude that we have developed matrix and reservoir DDS that are promising for delivery of physicochemically distinct ARVs for several months to years. It remains necessary to evaluate the dissolution of leading matrix and reservoir DDS candidates *in utero* for a more exact understanding of the duration and kinetics of drug release.

5.5 CONCLUSION

We successfully developed both matrix and reservoir drug delivery systems for sustained release of multiclass, physicochemically distinct antiretrovirals in an integrated ARV-IUD design. We showed that a hydrophobic, highly crystalline TPU matrix can release RAL, MVC, and ETR for over one year while retaining 50% of its original drug, thus offering a consistent, theoretically protective dose of the triple drug combination. Moreover, we demonstrated a method for evaluating reservoir devices with low drug loading and showed that sheath thickness and sheath polymer chemistry play significant roles in mediating drug release. Ultimately, we selected a candidate reservoir formulation for high DPV loading and found that it exceeded our target duration of release and achieved and optimal daily release rate to meet our clinical specification. Our *in vitro* and *in silico* data strongly premise further evaluation of both matrix

and reservoir ARV-IUDs in an *in vivo* nonhuman primate reproductive tract model. Once fully realized, this work has tremendous potential to motivate clinical translation of a novel long-acting MPT device which could alleviate the incidence unintended pregnancy and HIV among people with FRTs in regions where both public health challenges are endemic.

Chapter 6. SAFETY AND PHARMACOKINETICS OF ANTIRETROVIRAL DRUG DELIVERY TO THE UPPER FEMALE REPRODUCTIVE TRACT

For the proposed manuscript: Development and Pharmacokinetics of an Antiretroviral Releasing Intrauterine Device for Long-Acting Multipurpose Prevention Technology. **VanBenschoten H**, Doan MA, Roberts M, Suydam I, Yao, S, Jensen JT, Woodrow KA. *In preparation*.

6.1 ABSTRACT

Human immunodeficiency virus (HIV) resulting in acquired immunodeficiency syndrome (AIDS) is the leading cause of death among women of reproductive age, a burden that is exacerbated in settings where the virus is endemic. Daily oral pre-exposure prophylaxis (PrEP) with antiretroviral (ARV) medication is an effective HIV prevention modality if adhered to rigorously. However, achieving perfect adherence is a significant challenge that, coupled with other barriers to use, makes oral PrEP insufficient to meet the demands of at-risk women globally. Integrating ARV delivery with existing long-acting drug delivery modalities, such as long-acting reversible contraception (LARC), has the potential to ameliorate challenges with adherence and bolster the acceptability and prevalence of both contraception and PrEP. The intrauterine device (IUD) has a long history of safe and effective delivery of active agents to the female reproductive tract (FRT); incorporating an ARV delivery component onto an IUD frame could offer local delivery of microbicides to the female reproductive tract (FRT). However, it is not known if and how transport of intrauterinely delivered drug to the lower FRT occurs. As such, we assessed the safety and pharmacokinetics of intrauterine ARV delivery in a nonhuman primate model by assaying drug concentrations in systemic circulation, upper- and lower-FRT tissue, and vaginal secretions. This work serves as a foundation for further research on uterine-

to-vaginal drug transport and evidences the potential of an ARV-releasing IUD to protect against HIV for long-acting multipurpose prevention.

6.2 INTRODUCTION

HIV/AIDS is the leading cause of death globally among women of reproductive age and exerts a disproportionate burden on marginalized populations and women in regions with endemic disease such as sub-Saharan Africa [21]. The WHO estimated that 19.3 million women were living with HIV in 2020 [19]; in sub-Saharan Africa, women account for 63% of new infections and are twice as likely as men to become infected with HIV [20]. The situation is more dire for individuals who face multiple forms of discrimination; indeed, the incidence of HIV among female sex workers is 10-times higher than the general population. Widespread adaptation of strategies to prevent HIV transmission is critical to alleviating this global burden of disease. One such approach is pre-exposure prophylaxis (PrEP), which is the administration of antiretroviral (ARV) medication to an individual prior to exposure to HIV. Two PrEP medications are currently approved and have seen widespread adoption as over 70 countries have expanded normative recommendations for their use since 2019 [4,33,34]. Despite its potential for stemming the spread of HIV, PrEP use is limited by significant barriers including dosing frequency and adherence, cost, inefficient service delivery modalities, and lack of awareness [35]. Less than 500,000 people globally were estimated to have initiated PrEP as of 2019, representing a significant deficit in prevalence [36].

PrEP is conventionally formulated as a once daily oral tablet; this dosing modality must be adhered to near-perfectly to achieve sufficient partitioning to female genital tissue, the site of HIV infection in women and people with FRTs [1–3]. This adherence requirement has been

identified as the most prohibitive challenge preventing widespread use of PrEP and clinical studies show that women have as low as 40% adherence to daily oral PrEP [50]. A Phase 4 clinical study of oral PrEP among young African women found adherence as low as 9% at 12 months [343]. Decreasing the dosing frequency of PrEP has been the object of alternative delivery systems such as vaginal gels and films that offer on-demand, peri-coital protection against vaginal HIV transmission, vaginal rings that can be worn for 4-13 weeks, and long-acting injectables that require injections every 8 weeks. Issues of adherence and acceptance remain with all existing modalities and no ultra-long-acting ARV delivery system has thus far been developed.

Long-acting reversible contraception (LARC) is a promising example of technology that offers sustained, user-independent, and discreet drug delivery that targets the FRT. Local delivery of contraceptive agents via intrauterine device (IUD) result in high local tissue concentrations without the need for partitioning to the FRT [127] and protection against unwanted pregnancy for three to twelve years [111,301]. The possibility to integrate an ARV delivery component onto an existing IUD design potentiates a promising long-acting multipurpose prevention technology (MPT) that could prevent unwanted pregnancy and HIV simultaneously. This design would rely on ARV delivery into the intrauterine space and transport to the lower FRT where it must reach effective levels in genital tissue to prevent HIV infection. The feasibility of local, directional transport from the upper to the lower FRT is not known nor does any pharmacokinetic data on the concentration of intrauterinely delivered drugs in vaginal tissue or secretions exist. These gaps in knowledge pose a barrier to developing long-acting MPT using existing LARC technology.

Though the existence and mechanics of uterine-to-vaginal drug transport remains unstudied, the anatomy and physiology of the FRT suggests the possibility of a local transport system. Indeed, the human uterus is connected to the vagina by the cervical canal, an elliptical cavity that is fused circumferentially to the vaginal exocervix and uterine endocervix [344]. When properly placed, the body of an IUD sits directly superior to the endocervix at the uterine isthmus; thus, any pharmaceutical agent released from the body of an IUD is directly exposed to tissue and fluid adjacent to the cervical canal. In addition to transport through the cervical canal, direct absorption of IUD-delivered drugs by uterine tissue and redistribution through systemic circulation could contribute to uterine-to-vaginal drug transport. Other mechanisms of transport, such as direct diffusion through tissue and counter current exchange between the uterine venous plexus and vaginal artery, are also substantiated by basic anatomical parameters [122]. Despite the theoretical possibility of uterine-to-vaginal transport of active pharmaceutical agents, the therapeutic potential of intrauterine drug delivery systems for vaginal targeting is constrained by a dearth of pharmacokinetic evidence.

To address this gap in knowledge as well as a clinical demand for long-acting MPT, we used a nonhuman primate model to investigate the local and systemic pharmacokinetics of intrauterine delivery of the antiretroviral drug dapivrine. Dapivirine (DPV) is a nonnucleoside reverse transcriptase inhibitor (NNRTI) that displays improved activity against wild-type HIV-1 and strains with NNRTI-resistant mutations compared to other ARVs of the same class [345]. It has shown promise as a candidate for vaginal PrEP in safety and pharmacokinetic trials of intravaginal rings, wherein it is formulated to provide one-month of protection against HIV [15,63]. Here, we compared two candidate drug delivery systems for long-acting PrEP, the monolithic matrix and core-sheath reservoir, using a novel intrauterine device frame. Evidence of

local drug transport in the FRT is supported by assaying drug concentrations in several FRT compartments, including endometrial, cervical, and vaginal tissue as well as vaginal secretions. We show that dapivirine partitions favourably into the lower FRT at concentrations that potentiate viral inhibition while resulting in minimal systemic drug levels. Moreover, we measured residual drug content in devices placed in baboons for one month to validate the design of matrix and reservoir drug delivery systems (DDS) for long-acting *in vivo* release of ARV for up to one year. This study supports the development of long-acting MPT that leverages intrauterine drug delivery to target lower FRT tissue for durable, discreet, and user-independent protection against unwanted pregnancy and HIV.

6.3 MATERIALS AND METHODS

6.3.1 Materials and reagents

Micronized dapivirine was acquired from the International Partnership for Microbicides. Dapivirine internal standard ($^{2}H_4$-dapivirine, d4) was purchased from Aurora Fine Chemicals LLC (San Diego, CA, USA). Chloroform was purchased from Cambridge Isotope Laboratories (Andover, MA, USA), tetrahydrofuran (THF) was purchased from Sigma Aldrich (St. Louis, MO, USA), and Optima-LC/MA grade acetonitrile (ACN) and methanol (MeOH) were purchased from Thermo Fisher Scientific (Waltham, MA, USA). Ultrapure water was obtained using a Milli-Q UF Plus Apparatus (Millipore, Burlington, MA, USA). Thermoplastic polyurethane (PY-PT87AE) was a generous gift from Lubrizol Corporation (Wickliffe, OH, USA).

6.3.2 Preparation of integrated ARV-IUDs

Solvent cast matrix and co-extruded core-sheath reservoir DDS loaded with DPV were prepared as previously described in section 5.3.2. In brief, matrix DDS were prepared by dissolving PY-PT87AE (TPU4) at 10% wt/vol in chloroform. Micronized DPV was added at 16.6% wt/wt (drug/polymer) to the polymer solution and stirred for at least 6 hours until fully dissolved. Polymer-drug solution (40 mL) was poured into a glass petri dish and placed in a fume hood to evaporate overnight and subsequently in a desiccator to remove residual solvent. Films were cut into 1-inch diameter disks, disks were stacked and compressed under a metal weight in a 120°C dry bath until desired thickness, 3.5 mm, was reached. Matrix devices were cut from thickened disks using a 3.5 mm x 13.3 mm die punch. A 21-gauge stainless steel needle was inserted longitudinally through the rectangular device which was then rolled on a ceramic hot plate to form a hollowed, cylindrical monolithic matrix. Matrix devices were pushed onto the sheath of mini-Cu-IUD frames and situated above the retrieval thread loop. Polypropylene sutures were tied to the retrieval thread loop and frame arms were cut to measure approximately 14 mm across. All integrated ARV-IUDs underwent ethylene oxide sterilization prior to *in vivo* insertion.

Core-sheath reservoirs were prepared by melting PY-PT43DE20 and homogenizing with dapivirine to achieve 30 wt% core loading. Core polymer-drug solutions and sheath polymer, PY-PN73AE, were coextruded at 170-190°C through a custom crosshead. Target dimensions were set to 1.5 mm inner diameter (lumen), 3.56 mm outer diameter, a 1.0 mm wall (core + sheath) thickness, and 100 to 200 μm sheath thickness. Devices were cut to 13.33 mm in length and subsequently incubated for two weeks at 40°C to equilibrate drug in the core and sheath polymer. Reservoirs were pushed onto the mini-Cu-IUD frames, situated above the retrieval loops, and ends sealed with Loctite cyanoacrylate glue. Several studies have demonstrated the

use of acrylate glue (Loctite® 4011, Henkel, Düsseldorf, Germany) to prevent longitudinal diffusion from exposed reservoir cores in in vitro release studies [22,23]. To both integrated matrix and reservoir IUDs, polypropylene sutures were tied to the retrieval thread loop and frame arms were cut to measure approximately 14 mm across. All integrated ARV-IUDs underwent ethylene oxide sterilization prior to in vivo insertion.

6.3.3 Insertion and removal of ARV-IUDs in baboon uteri

Sterilized ARV-IUDs were loaded into a 12 Fr polypropylene insertion tube or medical grade stainless steel insertion tube measuring 4.4 mm to 5.15 mm outer diameter. Six reproductive aged (9-18 years old) female, parous Anubis baboons were used in a crossover study design. Prior to insertion, Misoprostol (400 μg) was administered to each animal to soften the cervix. Animals were sedated with ketamine, intubated endotracheally, and anesthetized with isoflurane. A speculum was inserted into the vaginal canal for visualization of the cervix and ARV-IUDs were implanted transcervically with ultrasound guidance. Devices were placed for 28 days and then removed with animals under the same sedation, intubation and atheization protocol as described for insertion. Following removal, females underwent a "wash-out" period of 5 weeks prior to placement of a second device constituting the second study arm.

6.3.4 Biological sample collection

Plasma samples were collected prior to ARV-IUD insertion, at hours 24, 48 and 72 after insertion, and weekly thereafter until removal. K2 EDTA-treaded tubes were used to collect 5 mL of plasma drawn from the medial saphenous vein at each timepoint. Tubes were centrifuged for 5 minutes at 2500 RCF, plasma was aspirated and deposited into a microcentrifuge tube.

Secretion samples were collected prior to insertion and weekly thereafter until removal; vaginal secretions were obtained by insertion of Weck-Cel cellulose sponges (Beaver Visitec International, Waltham, MA) for 5 minutes into the vaginal tract. Vaginal biopsies were taken prior to insertion, at 7 days post-insertion, and upon device removal. Cervical biopsies were taken prior to insertion and upon device removal. Vaginal and cervical pinch biopsies were taken with a Kevorkian Biopsy device (Monarch Medical Supply, Cumming, GA). Endometrial tissue was retrieved prior to insertion and immediately after IUD removal using a vacuum aspirator. All samples were stored at -80°C until analysis.

6.3.5 Safety assessment and histology

Animals were monitored for signs of discomfort including decreased appetite, lethargy, and hunched posture. Tissue biopsies for histological analysis were fixed in 4% paraformaldehyde, dehydrated in alcohol, and embedded in paraffin. Cross sectional samples (5 μm) were taken and stained with hematoxylin and eosin (H&E) stain.

6.3.6 LC-MS/MS instrumentation and acquisition parameters

A liquid chromatography system was equipped with an I-Class Acquity UPLC (Waters Corporation, Milford, MA, USA); separation was achieved using a Waters Acquity BEH c18, 50 x 2.1 mm UHPLC column with a 1.7 mm particle size maintained at ambient temperature. Mobile phase A was composed of water with 0.1% formic acid and mobile phase B was composed of 50:50 ACN:MeOH with 0.1% formic acid. The mobile phase gradient was as follows: holding at initial conditions of 98% A:2% B for 1 min, ramping to 100% B by 6 min, holding for 2 min, and then transitioning back to initial conditions over 1.5 min. The flow rate

was 0.5 mL/min with an injection volume of 10 mL. Detection of dapivirine (DPV) was performed by a Waters Xevo TQ-S tandem quadrupole mass spectrometer with a Micromass Zspray™ Atmospheric Pressure Ionization Source. Data was acquired and analyzed using MassLynx® software (version 4.2). The mass spectrometer was operated in positive ion mode with the following ionization parameters: capillary voltage of 3.0 kV, source temperature of 150°C, cone gas flow of 150 L/h, desolvation gas flow of 1000 L/h, and collision gas flow of 0.15 mL/min. The selected *m/z* transitions were 330.4>158.3 and 334.5>159.1 for DPV and its isotopically labeled internal standard ($^2H_4$-dapivirine, d_4-DPV), respectively. All species were analyzed at a cone voltage of 96 V (DPV) or 86 V (d_4-DPV) and collision energy of 34 V (DPV) or 36 V (d_4-DPV). Typical retention time for both analytes was 4.21 minutes.

Stock solutions of dapivirine and its isotopically labeled internal standard (d_4-DPV) were prepared at 1 mg/mL in LC-MS-grade acetonitrile. We prepared working stocks containing unlabeled DPV in ACN at concentrations ranging from 30 to 22500 ng/mL. Calibration standards contained 10 ng/mL of internal standard and 0.1, 0.25, 0.5, 1, 2.5, 5, 10, and 50 ng/mL concentrations of unlabeled DPV. Quality control samples were prepared fresh for each sampling batch by spiking < 1 μL of 22500 ng/mL DPV in ACN into neat or baseline biological samples before or after extraction to achieve final concentrations within the linear range of the standard curve.

6.3.7 Preparation of plasma, vaginal secretions, and tissue biopsy samples for LC-MS/MS

Thawed plasma samples were precipitated with cold ACN, vortexed thoroughly, and centrifuged for 10 minutes at 10,000 RPM. Supernatant was filtered using a 0.22 μm PVDF syringe tip filter into a 200 μL glass autosampler vial. Solvent was removed by placing uncapped

samples in a desiccator overnight. After solvent was completely evaporated, analytes were resuspended in an equal volume of ultrapure water and ACN containing internal standard (d_4-DPV). Tissue samples were screened for quality; samples with excess blood or negligible mass (<1 mg) were not included in analysis. Thawed tissue samples were precipitated with cold ACN containing internal standard (d_4-DPV) and homogenized in an Eppendorf tube containing 640 mg of 1.4 mm and six 2.8 mm zirconium oxide ceramic beads on a Precellys® 24 tissue homogenizer (Precellys, Bertin Corporation, Rockville, MD, USA) at 6,500 RPM for three cycles of 20 seconds. Samples were then centrifuged for 10 minutes at 10,000 RPM and supernatant filtered using a 0.22 μm PVDF syringe tip filter into a 200 μL glass autosampler vial containing an equal volume of ultrapure water. Vaginal secretion samples were thawed, diluted in 300 μL of phosphate buffered saline (PBS), and incubated for 1 hour at 4°C. Sponge and buffer were placed in Spin-X centrifuge tubes containing 0.45 μm cellulose acetate filters (Corning Inc., Corning, NY, USA) and precipitated with cold ACN containing internal standard (d_4-DPV), vortexed thoroughly, and centrifuged for 10 minutes at 10,000 RPM. Supernatant was filtered using a 0.22 μm PVDF syringe tip filter into a 200 μL glass autosampler vial containing an equal volume of ultrapure water. For quantification, the volume of vaginal secretion collected per samples was presumed to be 17.3 μL according to published data on vaginal mucosal volume collected by the Weck-Cel method [346].

6.3.8 Residual drug analysis and quantification by HPLC

Drug delivery systems were removed from previously implanted ARV-IUDs and cut into three equal segments. Segments were massed and submerged in 10 mL of tetrahydrofuran (THF) in glass scintillation vials. Vials were sealed and incubated at 37°C for at least 24 hours until

devices were fully dissolved. THF solutions were vortexed, diluted in acetonitrile (ACN), and filtered with a 0.22 μm syringe tip filter (Millex Durapore, Millipore) prior to drug content analysis by high-performance liquid chromatography (HPLC). HPLC methods for detecting DPV were used as previously described in section 5.3.4. Briefly, samples were analyzed using a C18 column (5 μm, 100 Å, 250 x 4.6 mm, Phenomenex Kinetex) with 30°C column temperature at a 1 mL/min isocratic flow rate, 10-minute run rime and 10 μL injection volume. A 65:35 ratio of ACN and ultrapure water with 10 mM ammonium acetate was used as the mobile phase. The linear range of DPV was 0.1 – 500 μg/mL and the retention time was approximately 6.2 minutes.

6.3.9 Animal care and ethics statement

Female baboons were treated with oral contraceptives (0.15 mg levonorgestrel and 0.03 mg ethinyl estradiol) daily throughout the study and beginning at least two weeks prior to initial IUD insertion to suppress cyclicity and maintain tissue homogeneity. Prior to all sampling timepoints, animals were sedated with ketamine; for tissue biopsy samples, biopsy areas were treated with silver nitrate to stop bleeding. The following medications were administered as needed for pain management throughout the study: Meloxicam (1.5 mg/mL), Buprenorphine (0.3 mg/mL), topical lidocaine (4%), Carprofen (50 mg/mL), and Ondansetron (2 mg/ml) for anti-nausea. Animal procedures were approved by the Institutional Animal Care and Use Committee (IACUC) at the Oregon National Primate Research Center (ONPRC). Animal husbandry was provided by ONPRC in accordance with the National Institutes of Health Guidelines for Care and Use of Laboratory Animals.

6.3.10 Statistical methods

All statistical analyses were conducted using GraphPad Prism (Version 9.5.0). Comparison between drug concentrations were performed using Mann-Whitney rank comparison tests. Differences in residual drug analyses were assessed using a parametric, unpaired t-tests. Graphical results were expressed as the mean of each replicate ± standard deviation.

6.4 RESULTS AND DISCUSSION

6.4.1 Integrated ARV-IUDs can be placed non-surgically in the baboon uterus

In order to investigate the pharmacokinetics of ARV delivered to the intrauterine space, we integrated matrix and reservoir DDS onto a miniature copper IUD frame (without copper wire) (Figure 6.1A&D). The delivery systems were situated on the vertical body of the IUD frame such that insertion into baboon uteri with standard polypropylene or custom stainless steel 12-14 French insertion tubes was feasible. The baboon model was selected for PK evaluation of the DDS because baboons have reproductive anatomy that is similar to humans with short rectilinear cervical canals that allow for nonsurgical, transcervical IUD implantation [347]. Compared to macaques, baboons have a larger uterus that accommodates a human-sized IUD with minimal modification, permitting us to recapitulate the biomechanics and positioning of human IUD placement [348]. We confirmed placement of the ARV-IUDs via fluoroscopy (Figure 6.1B&E) and ultrasonography (Figure 6.1C&F). Indeed, ARV-IUDs situated evenly within the uterine cavity with the body containing DDS positioned superior to the cervical canal.

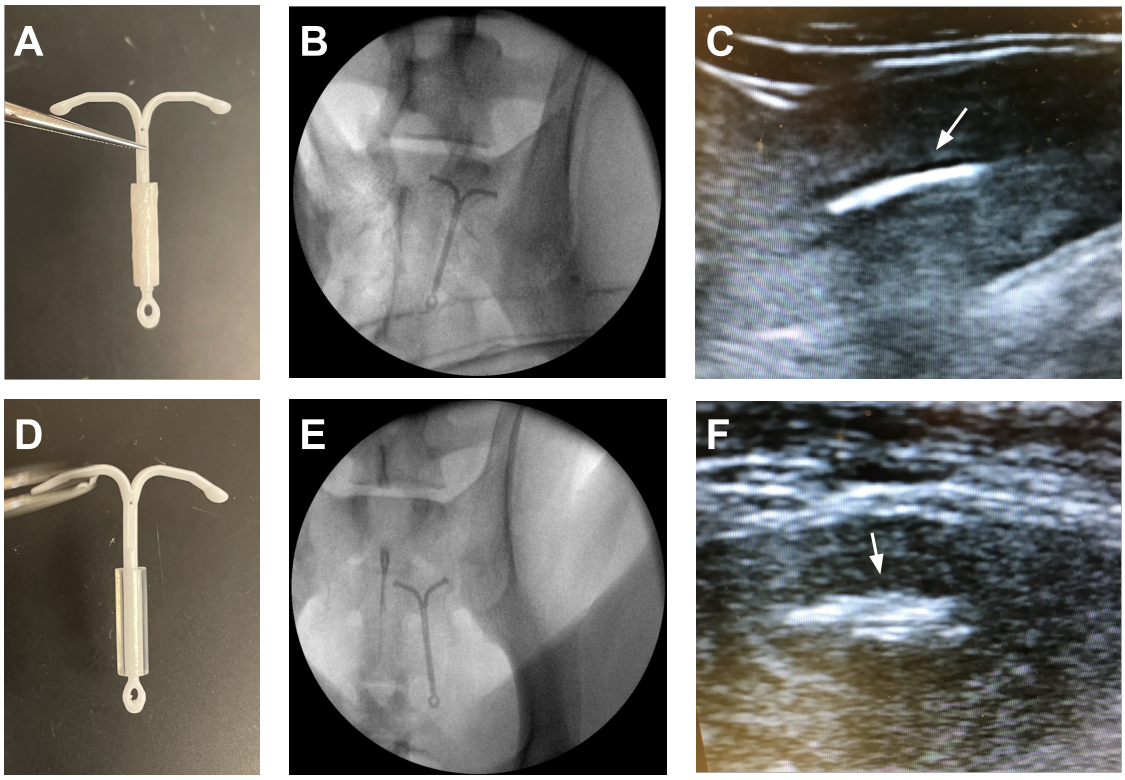

FIGURE 6.1. **Integration and placement of matrix and reservoir ARV-IUDs in Anubis baboon uteri.** Monolithic matrix DDS (A) integration with mini-Cu-IUD frame, (B) fluoroscopic image of placement in a baboon uterus, and (C) transverse ultrasound image of a baboon uterus with IUD position indicated by white arrow. Core-sheath reservoir DDS (D) integration with mini-Cu-IUD frame, (E) fluoroscopic image of placement in a baboon uterus, and (F) transverse ultrasound image of a baboon uterus with IUD position indicated by white arrow. Fluoroscopic and sonographic images taken immediately after placement of ARV-IUDs.

6.4.2 ARV-releasing IUDs are well tolerated in upper FRT of Anubis baboons

Histological assessment of vaginal, cervical, and endometrial tissue after one month of ARV-IUD instillation indicated minimal impact of this device on tissue microenvironment. Vaginal tissue biopsies taken pre-insertion and 28-days post-insertion show characteristic features of healthy a vaginal epithelium, including a multilayered stratified squamous epithelium consisting of enucleated cells, a densely nucleated basal cell layer, and an inconspicuous lamina propria (Figure 6.2A&B, white arrows) [349]. Importantly, vaginal tissue biopsied 28-days post

insertion has an intact stratified squamous epithelium that measures approximately 200 μm thick. This non-keratinized, multilayered structure is a key feature of innate mucosal immunity; indeed, a weakened vaginal epithelium is a characteristic pathway by which HIV and other STI virions can invade the genital mucosa [350]. Cervical biopsies were expected to contain tissue from the endocervix and the exocervix. The former is characteristically lined by a single columnar epithelium while the latter is lined by a stratified squamous epithelium consistent with that of the vaginal mucosa. Both pre-insertion and 28-days post-insertion cervical biopsies contain regions of a single columnar epithelium (Figure 6.2C&D, white arrows), while the underlying cervical stroma is composed of densely vascularized, fibromuscular tissue. The 28-day post-insertion cervical biopsy contains a thick stratus corneum of the exocervix (Figure 6.2D, white arrow); the epithelium overlays a prominent lymphoid aggregate (Figure 6.2D, white circle), a feature of mucosa-associated lymphoid tissue (MALT) in the type I mucosa of the endocervix and uterus [351]. The adjacency of the stratus corneum with lymphoid aggregates in the lamina propria suggest this biopsy is taken near the transformational zone. Some cellular atypia is notable as a few epithelial cells display irregular nuclear membranes and perinuclear halos. The pre-insertion endometrium consists of a columnar epithelium that forms tubular glands (Figure 6.2E, white arrow) overlaying a thick vascular stroma. An increase in mononuclear cells is notable throughout the stroma of the 28-day post-insertion endometrial biopsy along with some epithelial erosion (Figure 6.2F, white arrow); this is indicative of an inflammatory response and contact with a foreign body.

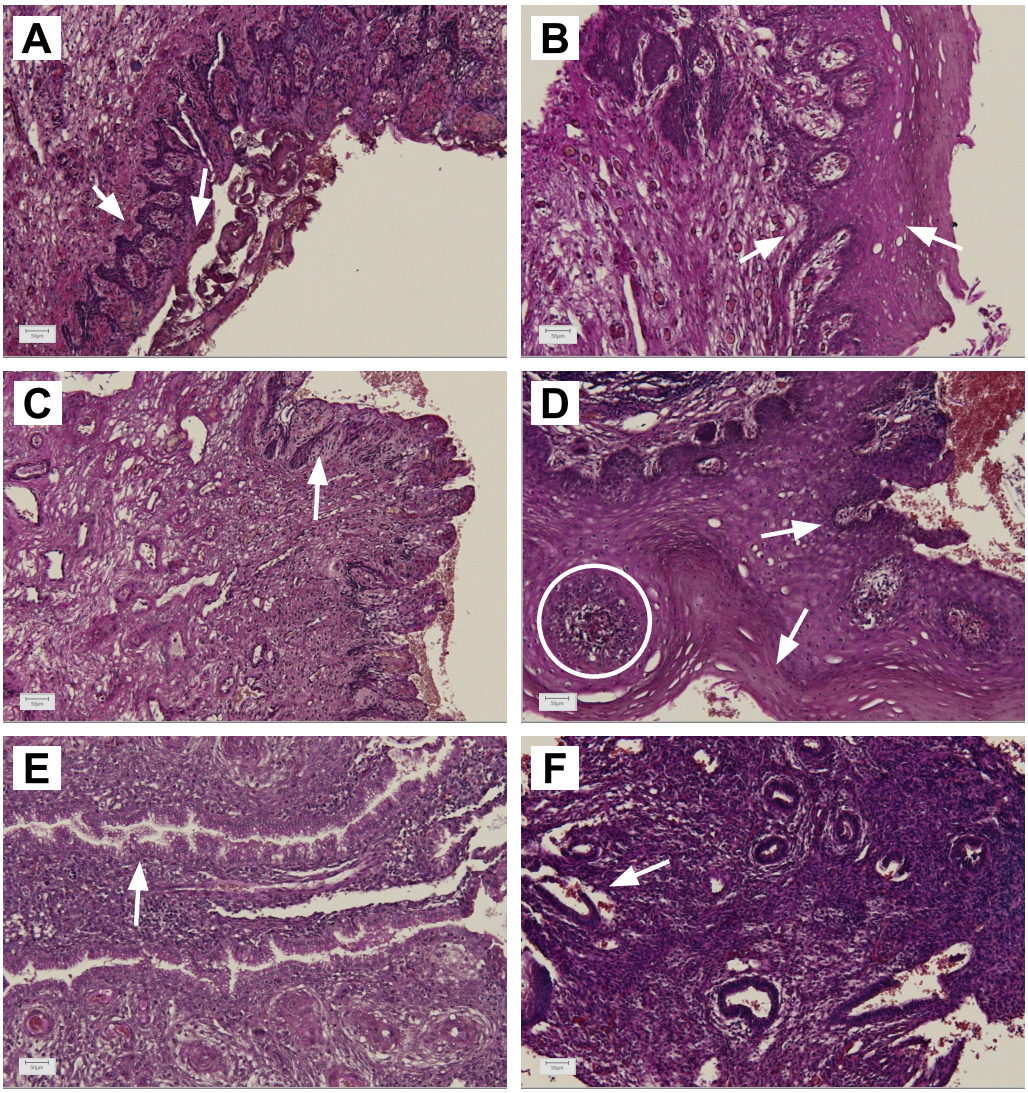

FIGURE 6.2. **Histological images of endometrial, cervical, and vaginal tissue prior to and after ARV-IUD insertion.** Representative hematoxylin and eosin (H&E) stained histology images of: vaginal tissue biopsied (A) prior to ARV-IUD placement and (B) 28 days after ARV-IUD placement; cervical tissue biopsied (C) prior to ARV-IUD placement and (D) 28 days after ARV-IUD placement; and endometrial tissue biopsied (E) prior to ARV-IUD placement, (F) 28 days after ARV-IUD placement.

The results of this histological assessment are in accordance with our expectations regarding insertion and use of a standard IUD. IUD placement involves necessary infliction of trauma on the cervical canal due to dilation and transcervical passage of an insertion tube. Moreover, IUD placement in the uterine cavity invariably results in morphological and cellular

changes to the uterine mucosa and endometrium. The IUD is a foreign body; when in contact with the endometrium, the mucosa becomes flattened, atrophic, and eroded and a nonspecific inflammatory response is elicited that consists of focal inflammatory infiltrate and increased local vascularization, as noted in our histological analysis [352]. Typically, vaginal tissue morphology is unaffected by the presence of an IUD, whereas cervical tissue often contains inflammatory cells and squamous abnormalities, consistent with our findings [352]. These anti-implantation effects, particularly in the endometrium, are essential to the contraceptive function of the IUD, and are therefore not considered safety concerns of IUD use. The histological responses noted in this study agree with expected changes to tissue morphology upon foreign body implantation.

The IUD frame used in this study, the Mona Lisa NT Cu380 Mini, is composed of bioinert polyethylene polymer and has a long history of safety and use in non-US markets [353]. The primary safety concern associated with Cu380 Mini is perforation of the uterine corpus or cervix; this most often occurs during insertion; however, the incidence of occurrence is low (1 per 1000 insertions) and similar to that of other IUD types [354]. Therefore, in the context of this study, the IUD frame itself is not expected to contribute to aberrant safety concerns. Similarly, in a safety and pharmacokinetic trial of dapivirine delivery to the vaginal tract by way of an intravaginal ring, no treatment-emergent adverse events were observed in women exposed intravaginal dapivirine for one month [355], nor does dapivirine exert any toxicity on ex vivo polarized cervical tissue at concentrations up to 1 mM (0.33 mg/mL) [356]. Direct administration of antiretroviral agents to the uterine cavity is the only unique intervention implicated in this delivery system that has not yet been investigated insofar as safety. The toxicity of DPV on endometrial tissue explants should be evaluated directly in future study. However, there is cause

to assume DPV would be tolerated in the endometrium at similar concentrations to the tolerance of cervicovaginal tissue. Given that histological examination of endometrial, cervical, and vaginal tissue did not deviate from anticipated effects of IUD placement, we conclude that intrauterine delivery of dapivirine is likely safe and well-tolerated in baboons.

6.4.3 Intrauterine DPV results in high drug partitioning to local tissue and vaginal secretions

We quantified DPV concentrations in tissue biopsies taken from multiple locations in the upper and lower female reproductive tracts. Vaginal tissue biopsies were taken at day 7 and 28 during the study period while cervical and endometrial biopsies were taken at day 28 only (in addition to baseline samples). No quantifiable drug was measured in baseline tissue samples taken 1 hour to 1 week prior to IUD insertion. One-week post-insertion of ARV-IUDs, vaginal tissue samples measured an average DPV concentration of 78.1 (±80.5) ng/mL; this value declined slightly but not statistically significantly to 61.1 (±25.6) ng/mL at device removal (Figure 6.3B, Table 6.1). By comparison, reservoir ARV-IUDs resulted in vaginal tissue samples with an average DPV concentration of 54.5 (±39.0) ng/mL at one week. In the cervix, matrix ARV-IUDs resulted in an average DPV concentration of 65.6 (±31.5) ng/mL at device removal, while reservoir ARV-IUDs resulted in 124.6 (±72.5) ng/mL of DPV in the cervix (Figure 6.3C, Table 6.1). Endometrial DPV concentrations were high for both matrix and reservoir ARV-IUDs at device removal, measuring 759.7 (±443.2) ng/mL and 2380.0 (±1028) ng/mL, respectively (Figure 6.3D, Table 6.1). The highest measured endometrial DPV concentration remains nearly 100-fold below the maximum tolerable DPV concentration tested on cervicovaginal tissue (0.33 mg/mL). The differences in tissue DPV concentrations for all biopsy locations were not statistically significant between matrix and reservoir DDS. For all biopsy locations, we

confirmed that tissue concentrations returned to baseline prior to reinsertion of devices in the second study arm (data not shown).

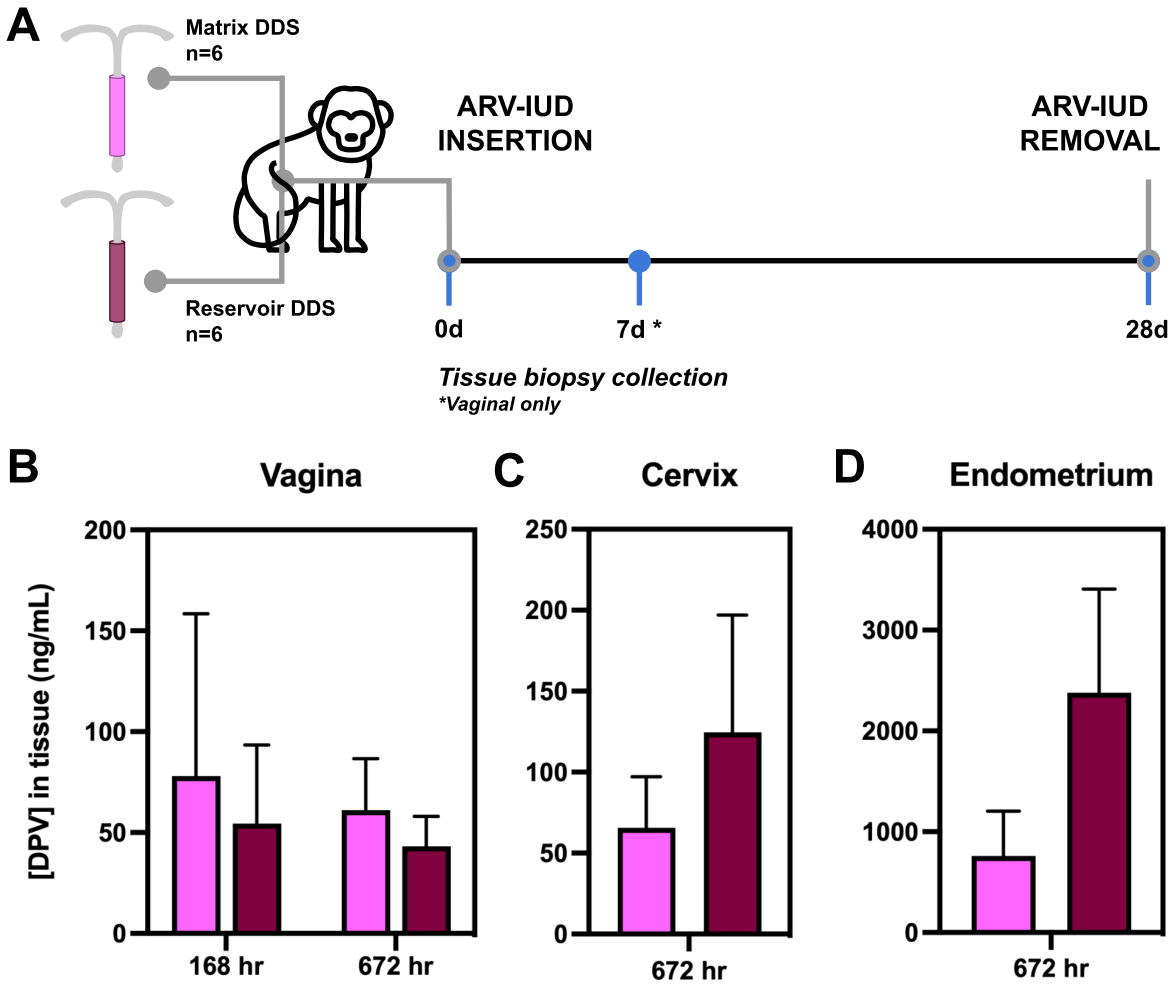

FIGURE 6.3. **Female reproductive tract tissue DPV concentrations in baboons with ARV-IUDs.** (A) Tissue biopsy sampling timeline for matrix and reservoir DDS ARV-IUD study arms. DPV concentrations in (A) vaginal, (B) cervical, and (D) endometrial tissue at 7-days (vaginal only) and 28-days (all tissue types). Values represent the mean ± standard deviation of biopsies from n=2-6 animals per DDS.

TABLE 6.1. DPV concentrations in baboon FRT tissue.

Tissue Type	Time (hr)	[DPV] (ng/mL) (SD)		Significance (p-value)
		Matrix	Reservoir	
Vaginal	168	78.06 (80.5)	54.5 (39.0)	NS (0.841)
	672	61.1 (25.6)	43.16 (14.94)	NS (0.343)
Cervical	672	65.6 (31.5)	124.56 (72.48)	NS (0.132)
Endometrial	672	759.7 (443.2)	2380.0 (1028)	** (0.004)

Values represent the mean ± standard deviation of n=6 animals for matrix devices and n=2 animals for reservoir devices. Statistical significance is determined as any p-value < 0.05.

The vaginal and cervical tissue concentrations measured here are the most relevant with respect to the prophylactic potential of this drug delivery modality. In an *ex vivo* viral inhibition model, dapivirine inhibited productive infection of ectocervical tissue at concentrations as low as 0.1 nM (0.033 ng/mL), while 99% of provirus formation was inhibited at 1 nM (0.33 ng/mL) [356]. At 10 nM (3.3 ng/mL), dapivirine prevented 90% of infection caused by dissemination of HIV-1 by $CD4^+$ dendritic cells, a necessary inhibition mechanism to prevent HIV infection. This inhibitory potency was retained in the presence of biological fluids such as cervicovaginal mucus and whole semen; thus, the IC_{90} of DPV in cervicovaginal tissue is taken to be 3.3 ng/mL. It is worth noting that this IC_{90} value reflects the concentration of DPV with which tissue explants were treated, not the measured intracellular concentration of DPV; thus, the intracellular IC_{90} in tissue may be even less. Here, matrix and reservoir DDS ARV-IUDs resulted in cervical tissue DPV concentrations that were, on average, nearly 20 and 40 -times this IC_{90}, respectively. Similarly, vaginal tissue measured up to 19-times the cervicovaginal IC_{90}, thus suggesting protective potential of this MPT. Given variation in anatomical length scales and mucosal physiology between female baboons and humans, we cannot expect the concentration of drug in

cervicovaginal tissue measured here to perfectly recapitulate human pharmacokinetics. However, the general anatomical and physiological similarities in FRT's permits speculation that similar partitioning will likely occur in humans and will result in comparable, high levels of DPV in human cervicovaginal tissue upon ARV-IUD instillation.

We measured DPV concentrations in vaginal secretions weekly after insertion of matrix and reservoir ARV-IUDs (Figure 6.4A). Matrix ARV-IUDs resulted high vaginal secretion concentrations 7-days post-insertion, averaging 1073.24 (± 1376.87) ng/mL. This concentration was durable out to 28-days, where DPV measured 933.68 (± 799.76) ng/mL. Similarly, reservoir DDS ARV-IUDs resulted in DPV concentrations of 1037.44 (±46.41) ng/mL and 3536.51 ng/mL in vaginal secretions at day 7 and day 28, respectively. At IUD removal, matrix and reservoir DDS ARV-IUDs resulted in vaginal secretion concentrations were approximately 283 times and 1072 times the IC_{90} determined in *ex vivo* cervicovaginal tissue culture (3.3 ng/mL) [356].

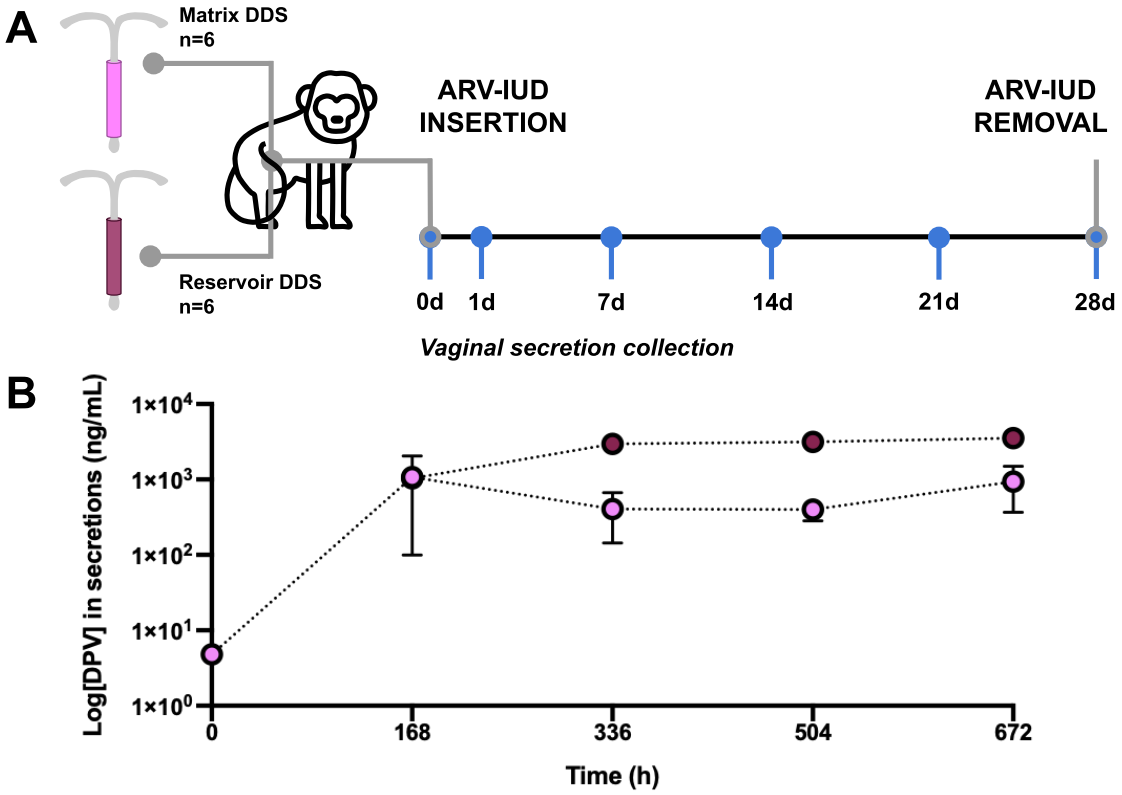

FIGURE 6.4. **Vaginal secretion DPV concentrations in baboons with matrix and reservoir ARV-IUDs**. (A) Vaginal secretion sampling timeline for matrix and reservoir DDS ARV-IUD study arms. (B) Concentration of DPV in vaginal secretions over time in baboons treated with matrix and reservoir DDS ARV-IUDs. Plotted values represent the mean ± standard deviation of measured vaginal secretion DPV concentration in n=3 animals.

In a pharmacokinetic study of a DPV intravaginal ring (IVR), Nel et al. reported that after 28 days of use in humans, the IVR resulted in DPV vaginal fluid concentrations that exceeded the IC_{90} 3900-fold. The discrepancy between the vaginal secretion concentrations measured in our study and that of the IVR trial likely relates to interspecies variability, but could also be explained by the distance between DDS placement and fluid sampling location. Nel et al. sampled vaginal fluid at three locations – near the ring, at the cervix, and at the introitus – and found that vaginal fluid concentrations correlated with distance from the DDS, with the highest concentration of DPV measured at the site of the ring and the lowest at introitus. Given that our

ARV-IUDs were placed in the uterus and vaginal secretion samples were collected between the cervix and the introitus, DPV would have had to travel through the internal OS, endocervical canal, and external OS to reach the nearest possible sampling location. The cervix is the most active site of mucus production in the female reproductive tract; as such, dilution of DPV-containing luminal fluids upon passage through the cervix may explain relatively lower secretion concentrations measured in this study compared to the IVR [357].

Not only was the concentration of DPV measured in vaginal secretions significantly higher than the minimum concentration for protection against HIV for matrix and reservoir DDS, it was higher than the concentrations measured in vaginal, cervical, and endometrial tissue biopsies at day 28 for respective study arms, the latter of which were taken directly adjacent to the DDS implantation site. This could indicate a greater propensity for transport of small molecules from the upper to lower FRT via the cervical lumen, rather than by direct diffusion through tissue or by direct or countercurrent venous or lymphatic circulation, as suggested by Cicinelli and De Ziegler [122]. The dominance of this transport pathway is supported in theory by anatomy and physiology of the female reproductive tract. Indeed, it is known that, by way of myometrial contractions and cervical peristalsis, uterine contents can travel inferiorly through the cervical lumen. This is demonstrated by the processes of menstruation and childbirth [125]. These pharmacokinetic findings could inform DDS design for other small molecules or biologics for which transport from the uterus to the vaginal tract may have prophylactic or therapeutic potential. Uterine to vaginal drug delivery warrants further investigation, for example by organ explant open perfusion studies such as those which elucidated the reverse vaginal-to-uterine first pass effect, to identify precise biophysical mechanisms responsible for pharmacokinetic outcomes.

6.4.4 Intrauterine delivery of ARV results in low systemic drug concentrations

We measured the concentration of DPV in plasma for the first three days after IUD insertion and once a week thereafter until study terminus (Figure 6.5A). For matrix DDS ARV-IUDs, a quantifiable plasma DPV concentration was measured at the first sampled timepoint, 24 hours after IUD insertion, in only one of six baboons (658.71 pg/mL) (Figure 6.5B). The remaining five animals had individual plasma DPV concentrations near or below the lower limit of quantification (LLOQ) for this assay (250 pg/mL), collectively averaging a plasma DPV concentration of 137.53 pg/mL. Thereafter throughout the 28-day study period, each baboon exhibited two to three DPV plasma concentrations that were above the LLOQ, ranging from 304.14 – 749.11 ng/mL with an average C_{max} of 539.4 (±221.1) pg/mL. Within this range of values, the individual t_{max} per animal occurred at hours 48, 72, 336, 504 and 672 equating to a median t_{max} of 420 hours (17 days). While all plasma samples measured a DPV concentration were above the lower limit of detection (LLOD), suggesting that they do contain some concentration of DPV, the arithmetic and geometric means of aggregated plasma DPV concentrations for the duration of the study are consistently below or very close to the LLOQ (Figure 6.5B). This pharmacokinetic pattern suggests that matrix ARV-IUDs largely do not contribute to meaningful systemic concentrations.

Reservoir DDS ARV-IUDs resulted in more significant, quantifiable plasma concentrations of DPV (Figure 6.5C). Plasma DPV concentrations increased from insertion to day 3, reaching a peak of 744.75 (±698.89) pg/mL three-days post-insertion (t_{max}). A trough at 14 days post-insertion, which measured 295.37.78 (±147.16) pg/mL, was followed by another peak in concentration at 21 days post-insertion of 768.36 (±389.98) pg/mL. Upon device removal, the

average DPV concentration in plasma measured 192.30 (±88.43) pg/mL. Reservoir ARV-IUDs resulted in a more consistent pattern of DPV distribution in systemic circulation compared to matrix ARV-IUDs; however, neither delivery system resulted in plasma DPV concentrations that were comparable in magnitude to those measured in FRT tissue or secretions.

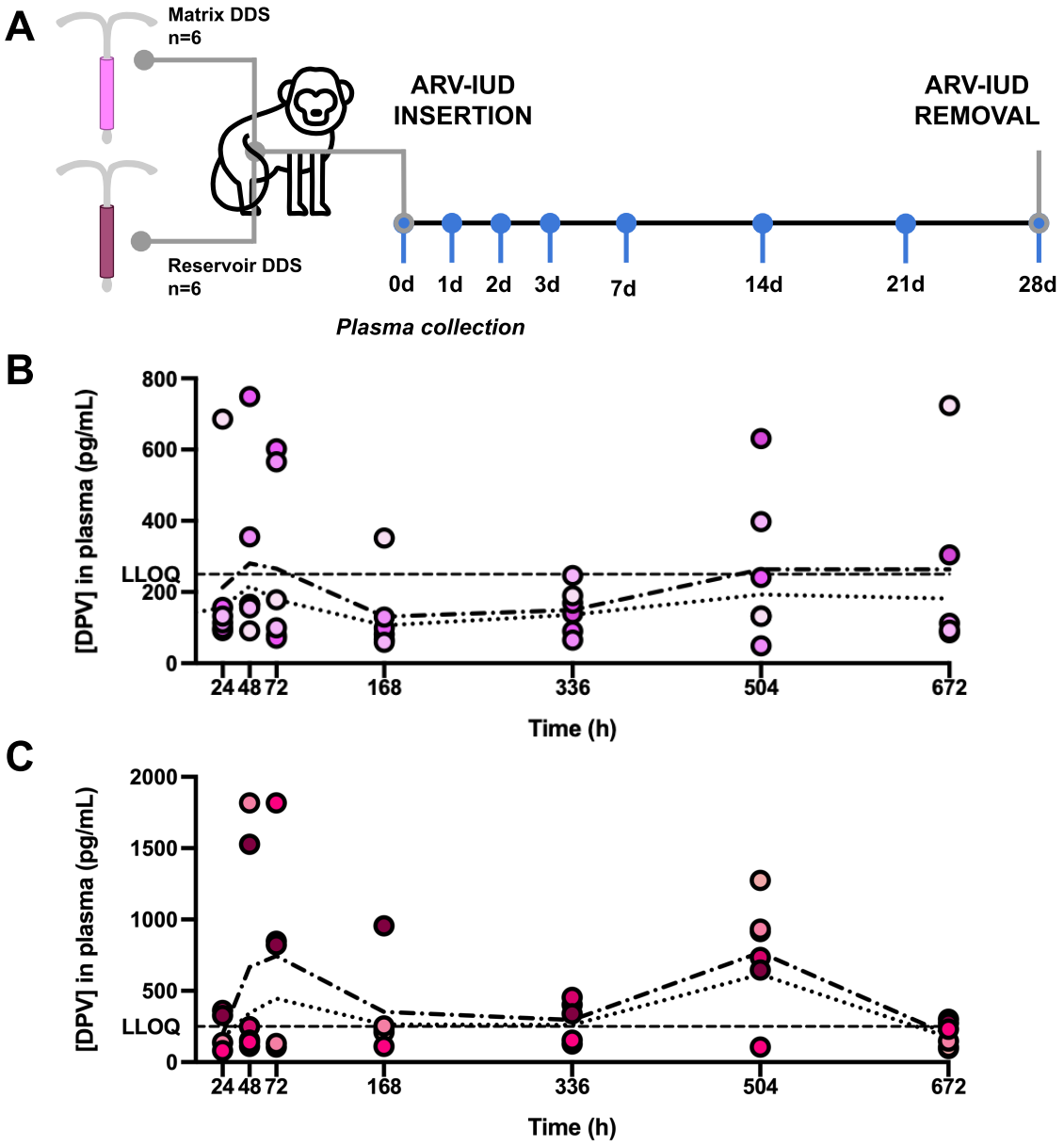

FIGURE 6.5. **Plasma DPV concentrations in baboons with matrix and reservoir ARV-IUDs.** (A) Plasma sampling timeline. (B) Concentration of DPV in plasma over time in baboons treated with ARV-IUDs. Pink circles represent the measured plasma DPV concentration for individual

animals at each timepoint (n=6); each shade of pink corresponds to one animal. (C) Concentration of DPV in plasma over time in baboons treated with reservoir DDS ARV-IUDs. Maroon circles represent the measured plasma DPV concentration for individual animals at each timepoint (n=2); each shade of maroon corresponds to one animal. The dotted line represents the geometric mean, and the dashed-dotted line represents the arithmetic mean of all animals at each the given sampling timepoint. The dashed vertical line represents the lower limit of quantification (LLOQ) for the DPV detection assay for the given sample batch; here, 250 pg/mL.

The plasma DPV concentrations measured after instillation of matrix and reservoir ARV-IUDs were consistent in order of magnitude with reported values of ARV and hormone in human plasma upon intravaginal ring and hormonal IUD use, respectively. In a clinical trial of DPV vaginal rings in women, authors Nel et al. found that plasma concentrations upon vaginal DPV delivery had a C_{max} of 355 pg/mL. They noted that this is well below the concentration required to reduce viral load by oral DPV administration, which is on the order of 100-200 ng/mL, and is a concentration that is unlikely to cause viral DPV-specific resistant mutations [63]. This is not unlike findings reported by Nilsson et al. upon measuring plasma levonorgestrel (LNG) concentrations after administering LNG-IUDs to women [127]. Nilsson found that IUD delivery resulted in plasma LNG concentrations of 202 ± 102 pg/mL, whereas oral LNG dosing with the drug Cyclabil resulted in plasma LNG concentrations of 559 ± 209 pg/mL. While we did not include an oral control in this nonhuman primate study, we would expect oral DPV to have resulted in comparatively higher plasma drug levels than the ARV-IUD study arms. Given high tissue and vaginal secretion concentrations of DPV, our data suggests that ARV delivered into the uterine space preferentially partitions to local mucosal and tissue compartments while resulting in low systemic exposure. We therefore conclude that DPV delivered in the uterus follows non-systemic routes of transport to distribute in lower FRT tissue, thereby further substantiating the theory of direct uterine-to-vaginal drug transport.

6.4.5 Residual drug analysis suggests long-acting potential

We quantified the amount of residual DPV in each DDS upon 28 days of *in utero* instillation order to predict the duration of action of matrix and reservoir delivery systems. Matrix ARV-IUDs retained an average of 81.78% (±5.44%) of their initially loaded DPV; thus, matrix DDS released approximately 18% of their DPV after 28 days *in utero* (Figure 6.6A, Table 6.2). By comparison, reservoir ARV-IUDs retained on average 95.84% (±2.93%) of initial DPV and released approximately 4.2% of their initial drug load after 28 days. The difference in percent of drug released between matrix and reservoir DDS was statistically significant ($p = 0.0002$). Assuming a constant release rate, matrix DDS had a daily release rate of 80.97 (±29.28) µg/day, while reservoir DDS released approximately 101.75 (±60.23) µg/day of DPV (Figure 6.6B. Table 6.2); this difference in daily dose was not significant ($p = 0.4648$). Upon extrapolation, matrix DDS would release 50% of their total drug loading after 76.85 days of use ($T_{50\%}$); reservoir DDS would reach $T_{50\%}$ after 303.58 days (Figure 6.6C, Table 6.2).

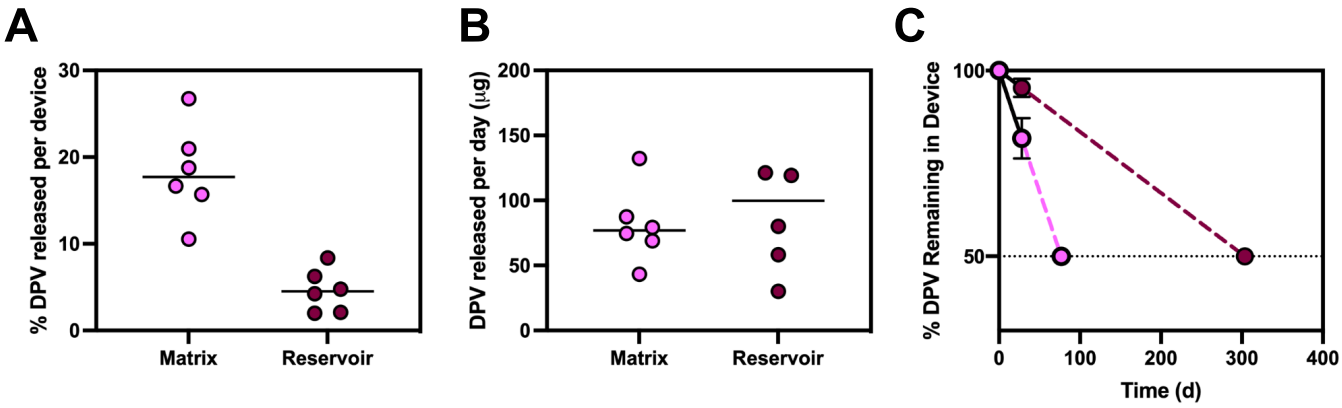

FIGURE 6.6. **Residual drug in matrix and reservoir DDS upon removal from baboon uteri at 28 days post-insertion**. (A) Amount of DPV (µg) released per day based on total mass of dapivirine released from devices over 28-day time period. (B) Percent of initially loaded DPV released per device. Plotted points represent individual devices from n=2-6 animals in each study arm; horizontal bars represent the mean. (C) Linear extrapolation of the time until 50% of initially loaded DPV is released from each device type. Plotted points represent the mean ± standard deviation of devices from n=2-6 animals; dashed line represents linear extrapolation

between 100% drug remaining (i.e., initial loading), to the percent of drug remaining at 28 days. Pink points represent matrix DDS, maroon points represent reservoir DDS.

TABLE 6.2. Residual drug analysis from removed ARV-IUD DDS.

DDS	Initial DPV loading (mg) (wt%)	Total DPV released (mg)	Average dose (μg/day)	$T_{50\%}$ (days)
Matrix	12.3 (16.0)	2.67	80.97	76.85
Reservoir	25.4 (18.8)	2.94	101.75	303.58

As expected, reservoir DDS are poised to offer DPV release on a more sustained timescale compared to matrix DDS and our predictions nearly meet the one-year target proposed in the design of this MPT. Moreover, these devices achieved sustained release at a target that exceeds the anticipated daily dose (50 μg/day) required for protection against HIV, as benchmarked by the DPV intravaginal ring trial [15]. The higher daily dose of DPV released by reservoir DDS likely explains pharmacokinetic differences between matrix and reservoir ARV-IUDs; indeed, reservoir devices resulted in higher endometrial, vaginal secretion, and plasma concentrations of DPV. In order to extend the duration of release, a higher initial drug loading is a promising approach. The quantity of DPV loaded into these reservoirs (25.40 mg) was less than half of the initial API loaded into the Mirena IUD, for example, which contains 52 mg of levonorgestrel [111]. Given that the drug loading assessed here already exceeded the saturation solubility of the core TPU, there is no reason to assume a higher mass fraction of drug would inhibit device fabrication or alter release kinetics. Other strategies, such as altering sheath polymer chemistry or thickness, could be explored to extend device duration; however, these would likely lower the daily DPV release rate. Ultimately, while this estimation of T50%

potentiates device viability for up to a year, the actual duration of use must be rigorously evaluated in subsequent clinical trials.

6.5 CONCLUSION

We tested the *in vivo* performance two drug delivery systems, monolithic matrix and core-sheath reservoir, as candidates for long-acting delivery of a clinically relevant dose of the NNRTI dapivirine upon intrauterine instillation via an intrauterine device. We showed that matrix and reservoir DDS can be effectively integrated with an IUD system, termed ARV-IUDs, and safely inserted trancervically into adult female baboons. ARV-IUDs were well tolerated with limited histological evidence of drug or DDS-mediated adverse effects on local tissue. Intrauterine DPV delivery resulted in high concentrations of drug in the endometrium, cervix, and vagina, and both delivery systems resulted in high vaginal secretion DPV concentrations that measured approximately 300 to 1000-fold the IC_{90} of DPV in cervicovaginal fluid. Low systemic DPV concentrations were detected, suggesting that systemic circulation plays a small role in the transport of drug from the upper to lower FRT upon uterine delivery; this is the first evidence of a uterine to vaginal "first-pass" effect. Lastly, both matrix and reservoir DDS offered durable release of DPV *in vivo* suggestive of up to a year of drug release and protection against HIV in the vaginal tract.

This work is the first to exploit the IUD as a drug delivery modality for purposes beyond contraception. Our findings represent a promising development towards long-acting multipurpose prevention technology and elucidates the potential of the uterus as an implantation site for drug delivery systems targeting both the upper and lower FRT. Given the tunable and modular design of our matrix and reservoir DDS ARV-IUDs, this work potentiates formulation

of various prophylactic and therapeutic small molecules, alone and in combination, for long-acting delivery to the FRT.

APPENDIX A: PUBLICATIONS AND PRESENTATIONS

A.1 PUBLICATIONS

[1] Development and Pharmacokinetics of an Antiretroviral Releasing Intrauterine Device for Long-Acting Multipurpose Prevention Technology. VanBenschoten H, Doan MA, Roberts M, Suydam I, Yao, S, Jensen JT, Woodrow KA. *In preparation*.

[2] Impact of the COVID-19 Pandemic on Access to and Utilization of Services for Sexual and Reproductive Health: A Systematic Scoping Review. VanBenschoten H, Kuganantham H, Larsson EC, Endler M, Thorson A, Gemzell-Danielsson K, Hanson C, Ganatra B, Ali M, Cleeve A. BMJ Global Health. (2022).

[3] Drug Eluting Embolization Particles for Permanent Contraception. VanBenschoten H, Yao S, Jensen JT, Woodrow KA. ACS Biomaterials Science & Engineering. 8(7) 2995-3009 (2022).

[4] Vaginal Delivery of Vaccines. VanBenschoten H, Woodrow KA. Advanced Drug Delivery Reviews. 178 (2021).

[5] Telemedicine as an alternative way to access abortion in Italy and characteristics of requests during the COVID-19 pandemic. Brandell K, VanBenschoten H, Parachini M, Gomperts R, Gemzell-Danielsson K. BMJ Sexual and Reproductive Health. (2021).

[6] Scalable electrospinning methods to produce high basis weight and uniform drug eluting fibrous materials. Hernandez JL, Doan MA, Stoddard R, VanBenschoten H, Chien ST, Suydam IT, Woodrow KA. Frontiers in Biomaterials Science. (2022).

[7] A Viral Toolbox of Genetically Encoded Fluorescent Synaptic Tags. Bensussen B, Shankar S, Ching KH, Zemel D, Ta TL, Mount RA, Shroff SN, Gritton HJ, Fabris P, VanBenschoten H, Beck C, Man HY, Han X. iScience. 23(7) (2020).

A.2 PRESENTATIONS AND CONFERENCE PRECEEDINGS

[1] Biomedical Engineering Society Annual Meeting (BMES); San Antonio, TX. “Drug Eluting Embolization Particles for Permanent Contraception.” 13 October 2022 (upcoming). *Oral Presentation*.

[2] 16th Congress of the European Society of Contraception and Reproductive Health; Abstract Book. “Drug Eluting Embolization Particles for Permanent Contraception.” 13 May 2020. *Poster Presentation (cancelled).*

APPENDIX B: SUPPLEMENTARY MATERIAL FOR CHAPTER 3

Search Strategy: PubMed/MEDLINE

#	Concept	Searches	Results
1	SRHR focus areas: • Abortion • Contraception • IPV/GBV • STIs/HIV	**Abortion, Induced [Mesh]** OR **Abortion, Spontaneous [Mesh]** OR miscarriage* [TW] OR abort* [TW] OR "termination of preg*" [TW] OR "pregnancy termination*" [TW] OR **Pregnancy, unplanned [Mesh]** OR **Pregnancy, unwanted [Mesh**] OR "Unplanned preg*" [TW] OR "Unwanted preg*" [TW] OR "Unintended preg*" [TW] OR contracept* [TW] OR **Contraception [Mesh]** OR **family planning services [Mesh]** OR "family planning" [TW] OR **Gender-based violence [Mesh]** OR **Intimate partner violence [Mesh]** OR "Gender-based violence" [TW] OR "Intimate partner violence" [TW] OR "violence against women" [TW] OR "dating violence" [TW] OR **Sexually Transmitted Diseases [Mesh]** OR "Sexually transmi*" [TW] OR **HIV Testing [Mesh]** OR "HIV test*" [TW] OR "HIV Diagnos*" [TW] OR "HIV prevent*" [TW] OR "prevention of HIV" [TW] OR **Pre-Exposure Prophylaxis [Mesh]** OR **Post-Exposure Prophylaxis [Mesh]** OR "Pre-Exposure Prophylaxis" [TW] OR "Post-Exposure Prophylaxis" [TW] OR **Antiretroviral therapy, Highly active [Mesh]** OR "Antiretroviral therapy" [TW] OR "HIV therapy" [TW] OR "HIV treat*" [TW] OR "HIV care" [TW] OR "HIV Services" [TW]	619,001
2	COVID-19	**COVID-19 [Mesh]** OR "2019 novel coronavirus" [TW] OR "2019-nCoV" [TW] OR "COVID" [TW] OR "COVID-19" [TW] OR "COVID19" [TW] OR "SARS coronavirus 2 infection" [TW] OR "SARS-CoV-2" [TW] OR "SARS-CoV2" [TW] OR "SARSCoV2" [TW] OR "Wuhan coronavirus" [TW] OR "coronavirus disease 2019" [TW] OR "nCoV 2019" [TW] OR "novel coronavirus 2019" [TW] OR "novel coronavirus disease 2019" [TW] OR "novel coronavirus infection 2019" [TW]	144,286

APPENDIX C: SUPPLEMENTARY MATERIAL FOR CHAPTER 4

SUPPLEMENTARY TABLE 4.1. Puncture Testing of Polyester Blends.

Fiber Blend	Burst Load (N)	Puncture Strength (N/mm^2)	Elongation Fraction	Relative puncture strength (N/mm^2)
80:20 PLGA/PCL	5.856 (0.562)	0.5871 (0.056)	.2032 (1.313)	2.886 (0.119)
PLLA	4.969 (0.103)	0.6228 (0.129)	.5595 (10.73)	1.138 (0.254)
80:20 PLLA/PLGA	7.810 (1.258)	0.9788 (0.158)	.3785 (2.725)	2.587 (0.373)
50:50 PLLA/PLGA	9.172 (1.270)	1.149 (0.159)	.3699 (1.703)	3.122 (0.535)
20:80 PLLA/PLGA	0.7938 (0.097)	0.1990 (0.025)	.2126 (4.020)	0.962 (0.195)
80:20 PLLA/PCL	5.577 (0.701)	0.6989 (0.088)	.5255 (3.208)	1.335 (0.195)
Note: Data represents the mean of n=5 samples (± standard deviation)				

SUPPLEMENTARY TABLE 4.2. Glass and Melting Transition Temperature of Polyesters.

Polyester	T_g (°C)	T_m (°C)	References
PLGA	40	260	[47]
PLLA	59	190	[48, 49]
PCL	– 60	60	[31, 40]

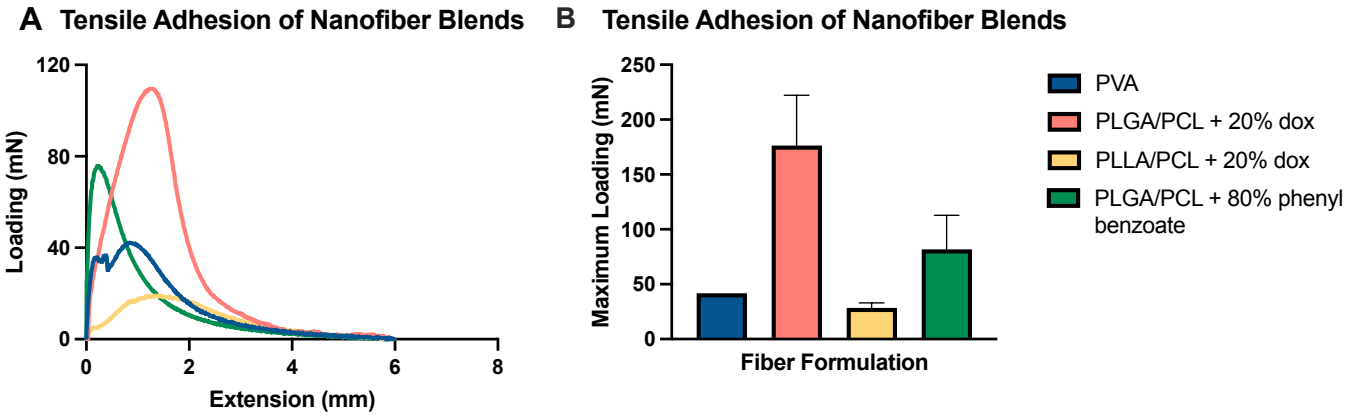

SUPPLEMENTARY FIGURE 4.2. **Tensile adhesion of polyester blends shows mucoadhesive potential.** (A) Loading force (mN) plotted against extension and (B) maximum adhesive force of drug-loaded polyester fiber blends to rehydrated porcine mucin. Results presented as a the mean ± standard deviation of at least n=3 individual fiber samples per condition. One-way ANOVA performed for maximum loading of nanofibers determined that no formulation was significantly less adhesive than PVA (significance defined as $p < 0.05$).

APPENDIX D: SUPPLEMENTARY MATERIAL FOR CHAPTER 5

SUPPLEMENTARY TABLE 5.1. Dimensional analysis of matrix and reservoir DDS prototypes.

Matrix DDS

Drug	***Matrix ID***	***Mass (mg)****	***Surface Area (mm^2)****	***Volume (mm^3)****	***SA/V (mm^{-1})****
DPV	TPU1	177.14 ± 1.87	206.42 ± 4.86	155.53 ± 6.75	1.22 ± 0.05
	TPU2	180.07 ± 1.72	165.38 ± 2.99	213.5 ± 2.15	1.14 ± 0.02
	TPU3	163.08 ± 1.28	163.01 ± 0.00	211.8 ± 0.00	1.16 ± 0.00
	TPU4	166.42 ± 2.92	161.04 ± 7.07	210.38 ± 5.09	1.18 ± 0.05
RAL	TPU2	182.20 ± 0.52	166.56 ± 1.36	214.35 ± 0.98	1.13 ± 0.01
	TPU3	174.26 ± 3.26	165.38 ± 2.89	213.50 ± 2.08	1.14 ± 0.02
	TPU4	180.82 ± 1.21	167.15 ± 3.54	214.78 ± 2.55	1.13 ± 0.02
MVC	TPU2	181.52 ± 2.98	170.89 ± 2.73	217.47 ± 1.96	1.11 ± 0.02
	TPU3	169.43 ± 2.36	164.78 ± 1.18	213.08 ± 0.85	1.15 ± 0.01
	TPU4	171.42 ± 3.34	165.38 ± 8.18	213.50 ± 5.89	1.14 ± 0.06
ETR	TPU2	191.71 ± 1.99	164.19 ± 2.36	212.65 ± 1.70	1.15 ± 0.02
	TPU3	172.95 ± 1.53	164.98 ± 1.78	213.21 ± 1.28	1.15 ± 0.01
	TPU4	183.27 ± 0.90	163.80 ± 2.73	212.37 ± 1.96	1.15 ± 0.02

Reservoir DDS

Drug	***Reservoir ID***	***Sheath thickness (μm)****	***Mass (mg)****	***Surface Area (mm^2)****	***Volume (mm^3)****	***SA/V (mm^{-1})****

DPV	R1	119 ± 15	128.26 ± 2.72	147.61 ± 0.00	130.26 ± 0.00	1.13 ± 0.00
	R2	219 ± 22	127.31 ± 4.48	148.86 ± 0.00	132.49 ± 0.00	1.12 ± 0.00
	R3	86 ± 6	129.69 ± 5.15	149.92 ± 0.00	134.18 ± 0.00	1.12 ± 0.00
	R4	175 ± 9	129.55 ± 2.52	148.44 ± 0.01	131.74 ± 0.00	1.13 ± 0.00

All values reported as the mean ± standard deviation of *n=3 devices and **n=20 devices

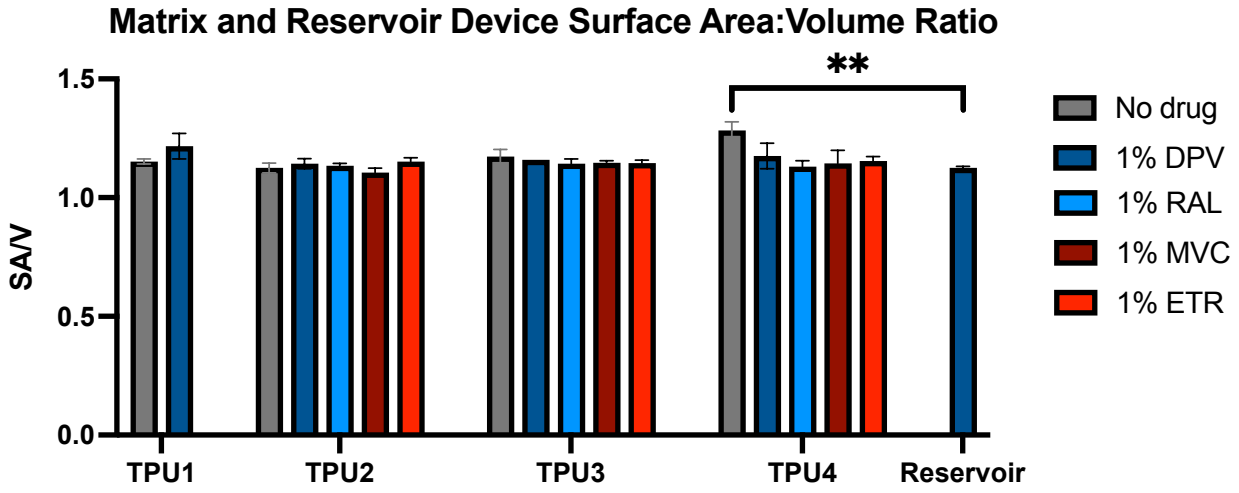

SUPPLEMENTARY FIGURE 5.1. **Surface area to volume ratio of matrix and reservoir DDS prototypes**. Plotted values represent the mean ± standard deviation of n=3 matrix devices and n=80 reservoir devices. (**) represents $p < 0.01$.

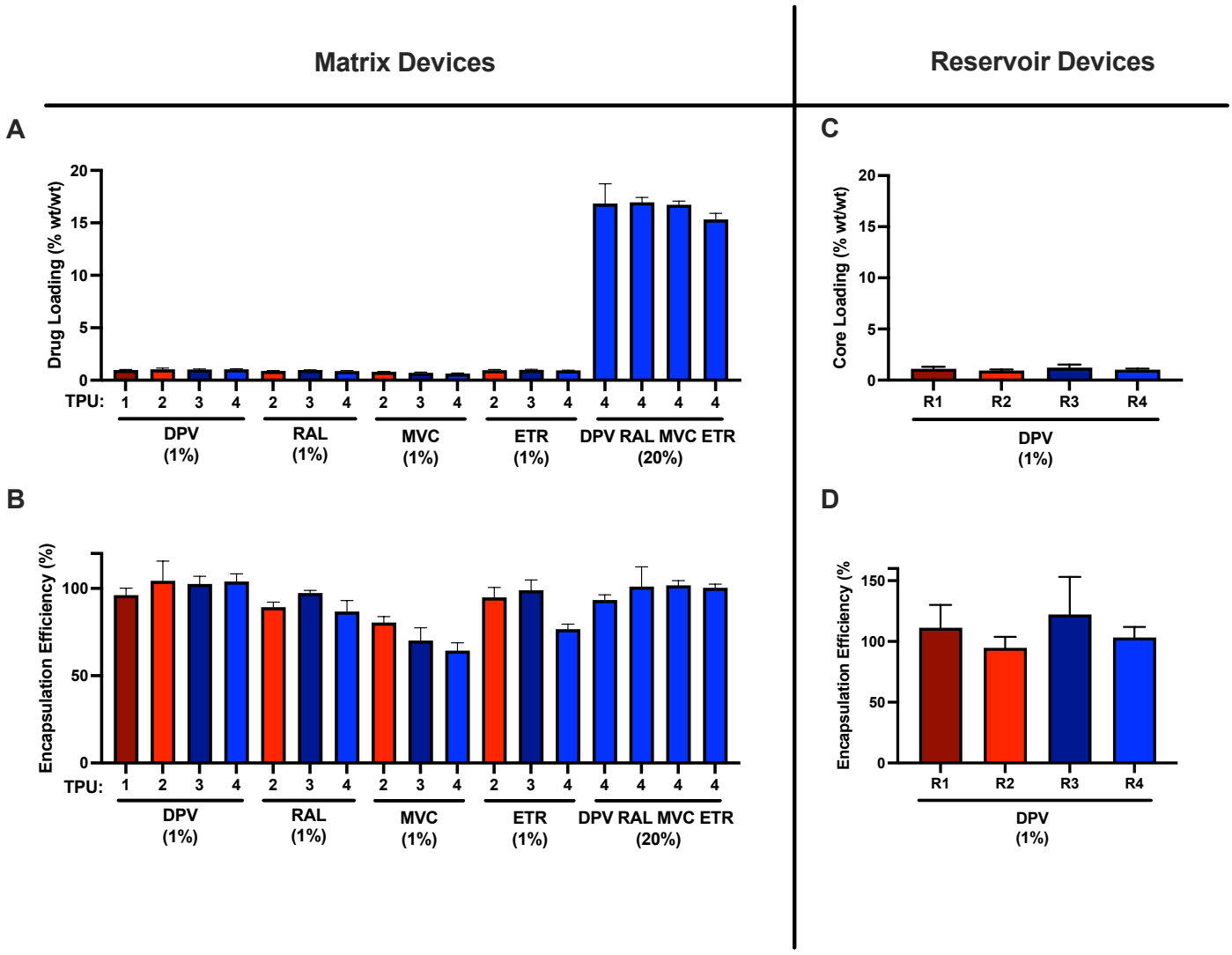

SUPPLEMENTARY FIGURE 5.2. **Loading and encapsulation efficiency of ARVs in matrix and reservoir DDS.** (A) Effective loading (% wt/wt) and (B) encapsulation efficiency (%) of ARVs in matrix DDS prototypes composed of different TPUs. Values represent the mean ± standard deviation of n=3 segments of matrix material taken from three different devices per formulation. (C) Effective loading (%wt/wt) and (D) encapsulation efficiency (%) of DPV in the core polymer of reservoir DDS prototypes.

Bibliography

[1] C.R. Trezza, A.D.M. Kashuba, Pharmacokinetics of antiretrovirals in genital secretions and anatomic sites of HIV transmission: Implications for HIV prevention, Clin Pharmacokinet. 53 (2014) 611–624. https://doi.org/10.1007/s40262-014-0148-z.

[2] M.S. Cohen, M.K. Smith, K.E. Muessig, T.B. Hallett, K.A. Powers, A.D. Kashuba, Antiretroviral treatment of HIV-1 prevents transmission of HIV-1: Where do we go from here?, The Lancet. 382 (2013) 1515–1524. https://doi.org/10.1016/S0140-6736(13)61998-4.

[3] Q.A. Karim, S.S.A. Karim, J.A. Frohlich, A.C. Grobler, C. Baxter, L.E. Mansoor, A.B.M. Kharsany, S. Sibeko, K.P. Mlisana, Z. Omar, T.N. Gengiah, S. Maarschalk, N. Arulappan, M. Mlotshwa, L. Morris, D. Taylor, Effectiveness and safety of tenofovir gel, an antiretroviral microbicide, for the prevention of HIV infection in women, Science (1979). 329 (2010) 1168–1174. https://doi.org/10.1126/science.1193748.

[4] S. McCormack, D.T. Dunn, M. Desai, D.I. Dolling, M. Gafos, R. Gilson, A.K. Sullivan, A. Clarke, I. Reeves, G. Schembri, N. Mackie, C. Bowman, C.J. Lacey, V. Apea, M. Brady, J. Fox, S. Taylor, S. Antonucci, S.H. Khoo, J. Rooney, A. Nardone, M. Fisher, A. McOwan, A.N. Phillips, A.M. Johnson, B. Gazzard, O.N. Gill, Pre-exposure prophylaxis to prevent the acquisition of HIV-1 infection (PROUD): Effectiveness results from the pilot phase of a pragmatic open-label randomised trial, The Lancet. 387 (2016) 53–60. https://doi.org/10.1016/S0140-6736(15)00056-2.

[5] K.A. Thomson, J.M. Baeten, N.R. Mugo, L.G. Bekker, C.L. Celum, R. Heffron, Tenofovir-based oral preexposure prophylaxis prevents HIV infection among women, Curr Opin HIV AIDS. 11 (2016) 18–26. https://doi.org/10.1097/COH.0000000000000207.

[6] AVAC Global PrEP Tracker, Q1 2022, 2022.

[7] J.A. Robinson, M.A. Marzinke, E.J. Fuchs, R.P. Bakshi, H.M.L. Spiegel, J.S. Coleman, L.C. Rohan, C.W. Hendrix, Comparison of the Pharmacokinetics and Pharmacodynamics of Single-Dose Tenofovir Vaginal Film and Gel Formulation (FAME 05), J Acquir Immune Defic Syndr (1988). 77 (2018) 175–182. https://doi.org/10.1097/QAI.0000000000001587.

[8] M.R. Beymer, I.W. Holloway, C. Pulsipher, R.J. Landovitz, Current and Future PrEP Medications and Modalities: On-demand, Injectables, and Topicals, Curr HIV/AIDS Rep. 16 (2019) 349–358. https://doi.org/10.1007/s11904-019-00450-9.

[9] K.E. Bunge, C.S. Dezzutti, L.C. Rohan, C.W. Hendrix, M.A. Marzinke, N. Richardson-Harman, B.J. Moncla, B. Devlin, L.A. Meyn, H.M.L. Spiegel, S.L. Hillier, A Phase 1 trial to assess the safety, acceptability, pharmacokinetics, and pharmacodynamics of a novel dapivirine vaginal film, in: J Acquir Immune Defic Syndr (1988), Lippincott Williams and Wilkins, 2016: pp. 498–505. https://doi.org/10.1097/QAI.0000000000000897.

[10] K.E. Bunge, C.S. Dezzutti, C.W. Hendrix, M.A. Marzinke, H.M.L. Spiegel, B.J. Moncla, J.L. Schwartz, L.A. Meyn, N. Richardson-Harman, L.C. Rohan, S.L. Hillier, K. Bunge, FAME-04: A Phase 1 trial to assess the safety, acceptability, pharmacokinetics and pharmacodynamics of film and gel formulations of tenofovir, (2018). https://doi.org/10.1002/jia2.25156/full.

[11] A. Akil, M.A. Parniak, C.S. Dezzutti, B.J. Moncla, M.R. Cost, M. Li, L.C. Rohan, Development and characterization of a vaginal film containing dapivirine, a non-nucleoside reverse transcriptase inhibitor (NNRTI), for prevention of HIV-1 sexual transmission, Drug Deliv Transl Res. 1 (2011) 209–222. https://doi.org/10.1007/s13346-011-0022-6.

[12] W. Spreen, S.L. Ford, S. Chen, D. Wilfret, D. Margolis, E. Gould, S. Piscitelli, GSK1265744 Pharmacokinetics in Plasma and Tissue After Single-Dose Long-Acting Injectable Administration in Healthy Subjects, 2014. www.jaids.com.

[13] W. Spreen, P. Williams, D. Margolis, S.L. Ford, H. Crauwels, Y. Lou, E. Gould, M. Stevens, S. Piscitelli, Pharmacokinetics, Safety, and Tolerability With Repeat Doses of GSK1265744 and Rilpivirine (TMC278) Long-Acting Nanosuspensions in Healthy Adults, 2014. www.jaids.com.

[14] D.A. Margolis, J. Gonzalez-Garcia, H.J. Stellbrink, J.J. Eron, Y. Yazdanpanah, D. Podzamczer, T. Lutz, J.B. Angel, G.J. Richmond, B. Clotet, F. Gutierrez, L. Sloan, M.S. Clair, M. Murray, S.L. Ford, J. Mrus, P. Patel, H. Crauwels, S.K. Griffith, K.C. Sutton, D. Dorey, K.Y. Smith, P.E. Williams, W.R. Spreen, Long-acting intramuscular cabotegravir and rilpivirine in adults with HIV-1 infection (LATTE-2): 96-week results of a randomised, open-label, phase 2b, non-inferiority trial, The Lancet. 390 (2017) 1499–1510. https://doi.org/10.1016/S0140-6736(17)31917-7.

[15] J.M. Baeten, T. Palanee-Phillips, E.R. Brown, K. Schwartz, L.E. Soto-Torres, V. Govender, N.M. Mgodi, F. Matovu Kiweewa, G. Nair, F. Mhlanga, S. Siva, L.-G. Bekker, N. Jeenarain, Z. Gaffoor, F. Martinson, B. Makanani, A. Pather, L. Naidoo, M. Husnik, B.A. Richardson, U.M. Parikh, J.W. Mellors, M.A. Marzinke, C.W. Hendrix, A. van der Straten, G. Ramjee, Z.M. Chirenje, C. Nakabiito, T.E. Taha, J. Jones, A. Mayo, R. Scheckter, J. Berthiaume, E. Livant, C. Jacobson, P. Ndase, R. White, K. Patterson, D. Germuga, B. Galaska, K. Bunge, D. Singh, D.W. Szydlo, E.T. Montgomery, B.S. Mensch, K. Torjesen, C.I. Grossman, N. Chakhtoura, A. Nel, Z. Rosenberg, I. McGowan, S. Hillier, Use of a Vaginal Ring Containing Dapivirine for HIV-1 Prevention in Women, New England Journal of Medicine. 375 (2016) 2121–2132. https://doi.org/10.1056/nejmoa1506110.

[16] A.Y. Liu, C. Dominguez Islas, H. Gundacker, B. Neradilek, C. Hoesley, A. van der Straten, C.W. Hendrix, M. Beamer, C.E. Jacobson, T. Mcclure, T. Harrell, K. Bunge, B. Devlin, J. Nuttall, P. Spence, J. Steytler, J.M. Piper, Phase 1 pharmacokinetics and safety study of extended duration dapivirine vaginal rings in the United States Mark A Marzinke

8 and the MTN-036/IPM 047 Protocol Team for the Microbicide Trials Network §, (2021). https://doi.org/10.1002/jia2.25747/full.
[17] B.A. Chen, L. Panther, M.A. Marzinke, C.W. Hendrix, C.J. Hoesley, A. van der Straten, M.J. Husnik, L. Soto-Torres, A. Nel, S. Johnson, N. Richardson-Harman, L.K. Rabe, C.S. Dezzutti, Phase 1 Safety, Pharmacokinetics, and Pharmacodynamics of Dapivirine and Maraviroc Vaginal Rings: a Double-Blind Randomized Trial, J Acquir Immune Defic Syndr (1988). 70 (2015) 242–249. https://doi.org/10.1097/QAI.0000000000000702.Phase.
[18] J.S. Hynes, J.M. Sales, A.N. Sheth, E. Lathrop, L.B. Haddad, Interest in multipurpose prevention technologies to prevent HIV/STIs and unintended pregnancy among young women in the United States, Contraception. 97 (2018) 277–284. https://doi.org/10.1016/j.contraception.2017.10.006.
[19] World Health Statistics 2021: monitoring health for the SDGs, sustainable development goals, Geneva, 2021.
[20] UNAIDS Data 2021, Geneva, 2021.
[21] Unaids, Women and HIV — A spotlight on adolescent girls and young women, n.d.
[22] F. Hladik, M.J. McElrath, Setting the stage: Host invasion by HIV, Nat Rev Immunol. 8 (2008) 447–457. https://doi.org/10.1038/nri2302.
[23] D.J. Anderson, J. Marathe, J. Pudney, The Structure of the Human Vaginal Stratum Corneum and its Role in Immune Defense, American Journal of Reproductive Immunology. 71 (2014) 618–623. https://doi.org/10.1111/aji.12230.
[24] H.M. VanBenschoten, K.A. Woodrow, Vaginal delivery of vaccines, Adv Drug Deliv Rev. 178 (2021). https://doi.org/10.1016/j.addr.2021.113956.
[25] H. Xu, X. Wang, R.S. Veazey, Mucosal immunology of HIV infection, Immunol Rev. 254 (2013) 10–33. https://doi.org/10.1111/imr.12072.
[26] J.P. Hughes, J.M. Baeten, J.R. Lingappa, A.S. Magaret, A. Wald, G. De Bruyn, J. Kiarie, M. Inambao, W. Kilembe, C. Farquhar, C. Celum, Determinants of per-coital-act HIV-1 infectivity among African HIV-1-serodiscordant couples, Journal of Infectious Diseases. 205 (2012) 358–365. https://doi.org/10.1093/infdis/jir747.
[27] C.K. Mauck, M.M. Callahan, J. Baker, K. Arbogast, R. Veazey, R. Stock, Z. Pan, C.S. Morrison, M. Chen-Mok, D.F. Archer, H.L. Gabelnick, The effect of one injection of Depo-Provera® on the human vaginal epithelium and cervical ectopy, Contraception. 60 (1999) 15–24. https://doi.org/10.1016/S0010-7824(99)00058-X.
[28] B. Poonia, L. Walter, J. Dufour, R. Harrison, P.A. Marx, R.S. Veazey, Cyclic changes in the vaginal epithelium of normal rhesus macaques, Journal of Endocrinology. 190 (2006) 829–835. https://doi.org/10.1677/joe.1.06873.
[29] M.R. Anderson, S.M. Baig, C.J. Gioia, E.J. Spongberg, M. Sarah, Human cervicovaginal mucus contains an activity that hinders HIV-1 movement, 6 (2013) 427–434. https://doi.org/10.1038/mi.2012.87.Human.

[30] J. Hu, M. Pope, C. Brown, U. O'Doherty, C.J. Miller, Immunophenotypic characterization of simian immunodeficiency virus-infected dendritic cells in cervix, vagina, and draining lymph nodes of rhesus monkeys, Laboratory Investigation. 78 (1998) 435–451.
[31] S.G. Turville, J.J. Santos, I. Frank, P.U. Cameron, J. Wilkinson, M. Miranda-Saksena, J. Dable, H. Stõssel, N. Romani, M. Piatak, J.D. Lifson, M. Pope, A.L. Cunningham, Immunodeficiency virus uptake, turnover, and 2-phase transfer in human dendritic cells, Blood. 103 (2004) 2170–2179. https://doi.org/10.1182/blood-2003-09-3129.
[32] M. Zeng, A.J. Smith, S.W. Wietgrefe, P.J. Southern, T.W. Schacker, C.S. Reilly, J.D. Estes, G.F. Burton, G. Silvestri, J.D. Lifson, J. V. Carlis, A.T. Haase, Cumulative mechanisms of lymphoid tissue fibrosis and T cell depletion in HIV-1 and SIV infections, Journal of Clinical Investigation. 121 (2011) 998–1008. https://doi.org/10.1172/JCI45157.
[33] M. Martin, S. Vanichseni, P. Suntharasamai, U. Sangkum, P.A. Mock, M. Leethochawalit, S. Chiamwongpaet, M.E. Curlin, S. Na-Pompet, A. Warapronmongkholkul, S. Kittimunkong, R.J. Gvetadze, J.M. McNicholl, L.A. Paxton, K. Choopanya, S.S. Na Ayudhya, K. Kaewnil, P. Kitisin, M. Kukavejworakit, P. Natrujirote, S. Simakajorn, W. Subhachaturas, The impact of adherence to preexposure prophylaxis on the risk of HIV infection among people who inject drugs, AIDS. 29 (2015) 819–824. https://doi.org/10.1097/QAD.0000000000000613.
[34] C. Celum, J. Baeten, PrEP for HIV Prevention: Evidence, Global Scale-up, and Emerging Options, Cell Host Microbe. 27 (2020) 502–506. https://doi.org/10.1016/j.chom.2020.03.020.
[35] K. Mayer, A. Agwu, D. Malebranche, Barriers to the Wider Use of Pre-exposure Prophylaxis in the United States: A Narrative Review, Adv Ther. 37 (n.d.). https://doi.org/10.6084/m9.figshare.11961357.
[36] S. Johnson Lyons, Z. Gant, A. Satcher Johnson, X. Hu, C. Yu, C. Jin, J. Scott Cope, A.F. Dailey, B. Wu, J. Li, M. Chong, S. Wang, N. Harris, Y. Huang, D. McCree, K. Kota, A. Peruski, Monitoring Selected National HIV Prevention and Care Objectives by Using HIV Surveillance Data—United States and 6 Dependent Areas, 2019, n.d. http://www.cdc.gov/hiv/library/reports/hiv-surveillance.html.http://www.cdc.gov/hiv/library/reports/hiv-surveillance.htmlhttp://wwwn.cdc.gov/dcs/ContactUs/Form.
[37] E. de Clercq, The role of non-nucleoside reverse transcriptase inhibitors (NNRTIs) in the therapy of HIV-1 infection 1, 1998.
[38] P.K. Yap, G.L. Loo Xin, Y.Y. Tan, J. Chellian, G. Gupta, Y.K. Liew, T. Collet, K. Dua, D.K. Chellappan, Antiretroviral agents in pre-exposure prophylaxis: emerging and advanced trends in HIV prevention, Journal of Pharmacy and Pharmacology. 71 (2019) 1339–1352. https://doi.org/10.1111/jphp.13107.
[39] T.J. Henrich, D.R. Kuritzkes, HIV-1 entry inhibitors: Recent development and clinical use, Curr Opin Virol. 3 (2013) 51–57. https://doi.org/10.1016/j.coviro.2012.12.002.

[40] T. Kelesidis, R.J. Landovitz, Preexposure prophylaxis for HIV prevention, Curr HIV/AIDS Rep. 8 (2011) 94–103. https://doi.org/10.1007/s11904-011-0078-4.

[41] S. Chang, D. Zhuang, W. Guo, L. Li, W. Zhang, S. Liu, H. Li, Y. Liu, Z. Bao, J. Han, H. Song, J. Li, The antiviral activity of approved and novel drugs against HIV-1 mutations evaluated under the consideration of dose-response curve slope, PLoS One. 11 (2016). https://doi.org/10.1371/journal.pone.0149467.

[42] M.M. Baum, C.M. Ramirez, J.A. Moss, M. Gunawardana, M. Bobardt, P.A. Gallay, Highly synergistic drug combination prevents vaginal HIV infection in humanized mice, Sci Rep. 10 (2020). https://doi.org/10.1038/s41598-020-69937-5.

[43] R.W. King, R.M. Klabe, C.D. Reid, S.K. Erickson-Viitanen, Potency of nonnucleoside reverse transcriptase inhibitors (NNRTIs) used in combination with other human immunodeficiency virus NNRTIs, NRTIs, or protease inhibitors, Antimicrob Agents Chemother. 46 (2002) 1640–1646. https://doi.org/10.1128/AAC.46.6.1640-1646.2002.

[44] M.W. Tang, R.W. Shafer, HIV-1 Antiretroviral Resistance: Scientific Principles and Clinical Applications, 2012.

[45] A. Basavapathruni, J. Vingerhoets, M.P. de Béthune, R. Chung, C.M. Bailey, J. Kim, K.S. Anderson, Modulation of human immunodeficiency virus type 1 synergistic inhibition by reverse transcriptase mutations, Biochemistry. 45 (2006) 7334–7340. https://doi.org/10.1021/bi052362v.

[46] J.M. Whitcomb, W. Huang, K. Limoli, E. Paxinos, T. Wrin, G. Skowron, S.G. Deeks, M. Bates, N.S. Hellmann, C.J. Petropoulos, S. Francisco General Hospital, S. Francisco, the Roger, Hypersusceptibility to non-nucleoside reverse transcriptase inhibitors in HIV-1: clinical, phenotypic and genotypic correlates, Lippincott Williams & Wilkins AIDS. 16 (2002) 41–47. http://journals.lww.com/aidsonline.

[47] J.M. Baeten, D. Donnell, P. Ndase, N.R. Mugo, J.D. Campbell, J. Wangisi, J.W. Tappero, E.A. Bukusi, C.R. Cohen, E. Katabira, A. Ronald, E. Tumwesigye, E. Were, K.H. Fife, J. Kiarie, C. Farquhar, G. John-Stewart, A. Kakia, J. Odoyo, A. Mucunguzi, E. Nakku-Joloba, R. Twesigye, K. Ngure, C. Apaka, H. Tamooh, F. Gabona, A. Mujugira, D. Panteleeff, K.K. Thomas, L. Kidoguchi, M. Krows, J. Revall, S. Morrison, H. Haugen, M. Emmanuel-Ogier, L. Ondrejcek, R.W. Coombs, L. Frenkel, C. Hendrix, N.N. Bumpus, D. Bangsberg, J.E. Haberer, W.S. Stevens, J.R. Lingappa, C. Celum, Antiretroviral Prophylaxis for HIV Prevention in Heterosexual Men and Women, New England Journal of Medicine. 367 (2012) 399–410. https://doi.org/10.1056/nejmoa1108524.

[48] M.C. Thigpen, P.M. Kebaabetswe, L.A. Paxton, D.K. Smith, C.E. Rose, T.M. Segolodi, F.L. Henderson, S.R. Pathak, F.A. Soud, K.L. Chillag, R. Mutanhaurwa, L.I. Chirwa, M. Kasonde, D. Abebe, E. Buliva, R.J. Gvetadze, S. Johnson, T. Sukalac, V.T. Thomas, C. Hart, J.A. Johnson, C.K. Malotte, C.W. Hendrix, J.T. Brooks, Antiretroviral Preexposure Prophylaxis for Heterosexual HIV Transmission in Botswana, New England Journal of Medicine. 367 (2012) 423–434. https://doi.org/10.1056/nejmoa1110711.

[49] L. van Damme, A. Corneli, K. Ahmed, K. Agot, J. Lombaard, S. Kapiga, M. Malahleha, F. Owino, R. Manongi, J. Onyango, L. Temu, M.C. Monedi, P. Mak'Oketch, M. Makanda, I. Reblin, S.E. Makatu, L. Saylor, H. Kiernan, S. Kirkendale, C. Wong, R. Grant, A. Kashuba, K. Nanda, J. Mandala, K. Fransen, J. Deese, T. Crucitti, T.D. Mastro, D. Taylor, Preexposure Prophylaxis for HIV Infection among African Women, New England Journal of Medicine. 367 (2012) 411–422. https://doi.org/10.1056/nejmoa1202614.

[50] J.M. Marrazzo, G. Ramjee, B.A. Richardson, K. Gomez, N. Mgodi, G. Nair, T. Palanee, C. Nakabiito, A. van der Straten, L. Noguchi, C.W. Hendrix, J.Y. Dai, S. Ganesh, B. Mkhize, M. Taljaard, U.M. Parikh, J. Piper, B. Mâsse, C. Grossman, J. Rooney, J.L. Schwartz, H. Watts, M.A. Marzinke, S.L. Hillier, I.M. McGowan, Z.M. Chirenje, Tenofovir-Based Preexposure Prophylaxis for HIV Infection among African Women, New England Journal of Medicine. 372 (2015) 509–518. https://doi.org/10.1056/nejmoa1402269.

[51] M. Desai, N. Field, R. Grant, S. Mccormack, State of the art review: Recent advances in PrEP for HIV, n.d.

[52] J.B. Dumond, R.F. Yeh, K.B. Patterson, A.H. Corbett, B.H. Jung, N.L. Rezk, A.S. Bridges, P.W. Stewart, M.S. Cohen, A.D.M. Kashuba, Antiretroviral drug exposure in the female genital tract: Implications for oral pre- and post-exposure prophylaxis, AIDS. 21 (2007) 1899–1907. https://doi.org/10.1097/QAD.0b013e328270385a.

[53] S.S.A. Karim, A.D. Kashuba, L. Werner, Q.A. Karim, Drug concentrations after topical and oral antiretroviral pre-exposure prophylaxis: Implications for HIV prevention in women, The Lancet. 378 (2011) 279–281. https://doi.org/10.1016/S0140-6736(11)60878-7.

[54] C.W. Hendrix, B.A. Chen, V. Guddera, C. Hoesley, J. Justman, C. Nakabiito, R. Salata, L. Soto-Torres, K. Patterson, A.M. Minnis, S. Gandham, K. Gomez, B.A. Richardson, N.N. Bumpus, MTN-001: Randomized Pharmacokinetic Cross-Over Study Comparing Tenofovir Vaginal Gel and Oral Tablets in Vaginal Tissue and Other Compartments, PLoS One. 8 (2013). https://doi.org/10.1371/journal.pone.0055013.

[55] M.R. Beymer, I.W. Holloway, C. Pulsipher, R.J. Landovitz, Current and Future PrEP Medications and Modalities: On-demand, Injectables, and Topicals, Curr HIV/AIDS Rep. 16 (2019) 349–358. https://doi.org/10.1007/s11904-019-00450-9.

[56] J.A. Robinson, M.A. Marzinke, R.P. Bakshi, E.J. Fuchs, C.L. Radebaugh, W. Aung, H.M.L. Spiegel, J.S. Coleman, L.C. Rohan, C.W. Hendrix, Comparison of Dapivirine Vaginal Gel and Film Formulation Pharmacokinetics and Pharmacodynamics (FAME 02B), AIDS Res Hum Retroviruses. 33 (2017) 339–346. https://doi.org/10.1089/AID.2016.0040.

[57] A.G.A. Jackson, L.J. Else, P.M.M. Mesquita, D. Egan, D.J. Back, Z. Karolia, L. Ringner-Nackter, C.J. Higgs, B.C. Herold, B.G. Gazzard, M. Boffito, A compartmental pharmacokinetic evaluation of long-acting rilpivirine in HIV-negative volunteers for pre-

exposure prophylaxis, Clin Pharmacol Ther. 96 (2014) 314–323. https://doi.org/10.1038/clpt.2014.118.

[58] I. McGowan, C.S. Dezzutti, A. Siegel, J. Engstrom, A. Nikiforov, K. Duffill, C. Shetler, N. Richardson-Harman, K. Abebe, D. Back, L. Else, D. Egan, S. Khoo, J.E. Egan, R. Stall, P.E. Williams, K.K. Rehman, A. Adler, R.M. Brand, B. Chen, S. Achilles, R.D. Cranston, Long-acting rilpivirine as potential pre-exposure prophylaxis for HIV-1 prevention (the MWRI-01 study): an open-label, phase 1, compartmental, pharmacokinetic and pharmacodynamic assessment, Lancet HIV. 3 (2016) e569–e578. https://doi.org/10.1016/S2352-3018(16)30113-8.

[59] R.J. Landovitz, S. Li, B. Grinsztejn, H. Dawood, A.Y. Liu, M. Magnus, M.C. Hosseinipour, R. Panchia, L. Cottle, G. Chau, P. Richardson, M.A. Marzinke, C.W. Hendrix, S.H. Eshleman, Y. Zhang, E. Tolley, J. Sugarman, R. Kofron, A. Adeyeye, D. Burns, A.R. Rinehart, D. Margolis, W.R. Spreen, M.S. Cohen, M. McCauley, J.J. Eron, Safety, tolerability, and pharmacokinetics of long-acting injectable cabotegravir in low-risk HIV-uninfected individuals: HPTN 077, a phase 2a randomized controlled trial, PLoS Med. 15 (2018). https://doi.org/10.1371/journal.pmed.1002690.

[60] R.J. Landovitz, D. Donnell, M.E. Clement, B. Hanscom, L. Cottle, L. Coelho, R. Cabello, S. Chariyalertsak, E.F. Dunne, I. Frank, J.A. Gallardo-Cartagena, A.H. Gaur, P. Gonzales, H. v. Tran, J.C. Hinojosa, E.G. Kallas, C.F. Kelley, M.H. Losso, J.V. Madruga, K. Middelkoop, N. Phanuphak, B. Santos, O. Sued, J. Valencia Huamaní, E.T. Overton, S. Swaminathan, C. del Rio, R.M. Gulick, P. Richardson, P. Sullivan, E. Piwowar-Manning, M. Marzinke, C. Hendrix, M. Li, Z. Wang, J. Marrazzo, E. Daar, A. Asmelash, T.T. Brown, P. Anderson, S.H. Eshleman, M. Bryan, C. Blanchette, J. Lucas, C. Psaros, S. Safren, J. Sugarman, H. Scott, J.J. Eron, S.D. Fields, N.D. Sista, K. Gomez-Feliciano, A. Jennings, R.M. Kofron, T.H. Holtz, K. Shin, J.F. Rooney, K.Y. Smith, W. Spreen, D. Margolis, A. Rinehart, A. Adeyeye, M.S. Cohen, M. McCauley, B. Grinsztejn, Cabotegravir for HIV Prevention in Cisgender Men and Transgender Women, New England Journal of Medicine. 385 (2021) 595–608. https://doi.org/10.1056/nejmoa2101016.

[61] L.-G. Bekker, S. Li, E. Tolley, M. Marzinke, N. Mgodi, J. Justman, S. Swaminathan, A. Adeyeye, J. Farrior, N. Sista, HPTN 076: TMC278 LA Safe, Tolerable and Acceptable for HIV Pre-Exposure Prophylaxis, n.d.

[62] J. Romano, B. Variano, P. Coplan, J. van Roey, K. Douville, Z. Rosenberg, M. Temmerman, H. Verstraelen, L. van Bortel, S. Weyers, M. Mitchnick, Safety and Availability of Dapivirine (TMC120) Delivered from an Intravaginal Ring, n.d. www.liebertpub.com.

[63] A. Nel, W. Haazen, J. Nuttall, J. Romano, Z. Rosenberg, N. Van Niekerk, A safety and pharmacokinetic trial assessing delivery of dapivirine from a vaginal ring in healthy women, Aids. 28 (2014) 1479–1487. https://doi.org/10.1097/QAD.0000000000000280.

[64] J. Bearak, A. Popinchalk, B. Ganatra, A.B. Moller, Ö. Tunçalp, C. Beavin, L. Kwok, L. Alkema, Unintended pregnancy and abortion by income, region, and the legal status of abortion: estimates from a comprehensive model for 1990–2019, Lancet Glob Health. 8 (2020) e1152–e1161. https://doi.org/10.1016/S2214-109X(20)30315-6.
[65] L.B. Finer, M.R. Zolna, Declines in Unintended Pregnancy in the United States, 2008–2011, New England Journal of Medicine. 374 (2016) 843–852. https://doi.org/10.1056/nejmsa1506575.
[66] Guttmacher Institute, Unintended Pregnancy and Abortion Worldwide, 2022.
[67] M. Yazdkhasti, A. Pourreza, A. Pirak, F. Abdi, Unintended Pregnancy and Its Adverse Social and Economic Consequences on Health System: A Narrative Review Article, 2015. http://ijph.tums.ac.ir.
[68] J. Gipson, M. Koenig, M. Hindin, The Effects of Unintended Pregnancy on Infant, Child, and Parental Health: A Review of the Literature, (n.d.).
[69] L. Say, D. Chou, A. Gemmill, Ö. Tunçalp, A.B. Moller, J. Daniels, A.M. Gülmezoglu, M. Temmerman, L. Alkema, Global causes of maternal death: A WHO systematic analysis, Lancet Glob Health. 2 (2014). https://doi.org/10.1016/S2214-109X(14)70227-X.
[70] V. Kantorová, M.C. Wheldon, P. Ueffing, A.N.Z. Dasgupta, Estimating progress towards meeting women's contraceptive needs in 185 countries: A Bayesian hierarchical modelling study, PLoS Med. 17 (2020). https://doi.org/10.1371/JOURNAL.PMED.1003026.
[71] S. Singh, G. Sedgh, R. Hussain, Susheela Singh is Vice President for Research, Gilda Sedgh is Senior Research Associate, and Rubina Hussain is Research Associate, Guttmacher Institute, 2010.
[72] United Nations. Department of Economic and Social Affairs. Population Division, World family planning 2020 highlights : accelerating action to ensure universal access to family planning, 2020.
[73] World Health Organization, Johns Hopkins Bloomberg School of Public Health, Family Planning: A Global Handbook for Providers, 2018.
[74] United Nations. Department of Economic and Social Affairs. Population Division, Contraceptive use by method 2019 : data booklet, n.d.
[75] P.D. Blumenthal, A. Voedisch, K. Gemzell-Danielsson, Strategies to prevent unintended pregnancy: Increasing use of longacting reversible contraception, Hum Reprod Update. 17 (2011) 121–137. https://doi.org/10.1093/humupd/dmq026.
[76] S. Staveteig, L. Mallick, R. Winter, DHS Analytical Studies No. 54 Uptake and Discontinuation of Long-Acting Reversible Contraceptives (LARCs) in Low-Income Countries, 2015. www.dhsprogram.com.
[77] A. van der Straten, K. Agot, K. Ahmed, R. Weinrib, E.N. Browne, K. Manenzhe, F. Owino, J. Schwartz, A. Minnis, The Tablets, Ring, Injections as Options (TRIO) study: what young African women chose and used for future HIV and pregnancy prevention, (2018). https://doi.org/10.1002/jia2.25094/full.

[78] Initiative for Multipurpose Prevention Technologies, Copper Intravaginal Ring (Cu-IVR), MPT Product Development Database. (2021).
[79] Initiative for Multipurpose Prevention Technology, Dapivirine + Printelivir + Levonorgestrel 3D Printed IVR, MPT Product Development Database. (2022).
[80] Initiative for Multipurpose Prevention Technologies, Islatravir (EFdA) + Etonogestrel/Ethinyl Estradiol 3D Printed IVR, MPT Product Development Database. (n.d.).
[81] G. Günaydın, G. Edfeldt, D.A. Garber, M. Asghar, L. Noël-Romas, A. Burgener, C. Wählby, L. Wang, L.C. Rohan, P. Guenthner, J. Mitchell, N. Matoba, J.M. McNicholl, K.E. Palmer, A. Tjernlund, K. Broliden, Impact of Q-Griffithsin anti-HIV microbicide gel in non-human primates: In situ analyses of epithelial and immune cell markers in rectal mucosa, Sci Rep. 9 (2019). https://doi.org/10.1038/s41598-019-54493-4.
[82] B. Holt, S. Moore, 2 Multipurpose Prevention Technologies (MPTs): Technology Landscape and Potential for Low-and Middle-Income Countries, 2021.
[83] J.A. Moss, A.M. Malone, T.J. Smith, S. Kennedy, C. Nguyen, K.L. Vincent, M. Motamedi, M.M. Baum, Pharmacokinetics of a multipurpose pod-intravaginal ring simultaneously delivering five drugs in an ovine model, Antimicrob Agents Chemother. 57 (2013) 3994–3997. https://doi.org/10.1128/AAC.00547-13.
[84] A.S. Samuel, R.K. Naz, Isolation of human single chain variable fragment antibodies against specific sperm antigens for immunocontraceptive development, Human Reproduction. 23 (2008) 1324–1337. https://doi.org/10.1093/humrep/den088.
[85] P. Boyd, S.M. Fetherston, C.F. McCoy, I. Major, D.J. Murphy, S. Kumar, J. Holt, A. Brimer, W. Blanda, B. Devlin, R.K. Malcolm, Matrix and reservoir-type multipurpose vaginal rings for controlled release of dapivirine and levonorgestrel, Int J Pharm. 511 (2016) 619–629. https://doi.org/10.1016/j.ijpharm.2016.07.051.
[86] J.T. Clark, M.R. Clark, N.B. Shelke, T.J. Johnson, E.M. Smith, A.K. Andreasen, J.S. Nebeker, J. Fabian, D.R. Friend, P.F. Kiser, Engineering a segmented dual-reservoir polyurethane intravaginal ring for simultaneous prevention of HIV transmission and unwanted pregnancy, PLoS One. 9 (2014). https://doi.org/10.1371/journal.pone.0088509.
[87] M. Weitzel, B.B. North, D. Waller, Development of multipurpose technologies products for pregnancy and STI prevention: Update on polyphenylene carboxymethylene MPT gel development, in: Biol Reprod, Oxford University Press, 2020: pp. 299–309. https://doi.org/10.1093/biolre/ioaa087.
[88] National Institutes of Health, Long Acting Film Technology for Contraception and HIV Prevention (LATCH), RePORtER. (2021).
[89] L.A., K.S.A., N.C., L.E., D.Z., J.P., A.C., J.G., van der S.A., & J.L.M. Li, S.A. Krovi, C. Norton, E. Luecke, Z. Demkovich, P. Johnson, C. Areson, G. Jimenez, A. van der Straten, L.M. Johnson, Biodegradable Implant for Delivery of Antiretroviral (ARV) and Hormonal Contraceptive. CROI Conference. CROI Conference, in: CROI Conference, 2020.

[90] M.T.C. McCrudden, A.Z. Alkilani, C.M. McCrudden, E. McAlister, H.O. McCarthy, A.D. Woolfson, R.F. Donnelly, Design and physicochemical characterisation of novel dissolving polymeric microneedle arrays for transdermal delivery of high dose, low molecular weight drugs, Journal of Controlled Release. 180 (2014) 71–80. https://doi.org/10.1016/j.jconrel.2014.02.007.

[91] PrEP Watch, Developing and Introducing a Dual Prevention Pill Oral PrEP & oral contraceptive for HIV and pregnancy prevention, 2021. https://www.unaids.org/sites/default/files/media_asset/the-youth-.

[92] H. Abdelkader, Z. Fathalla, A. Seyfoddin, M. Farahani, T. Thrimawithana, A. Allahham, A.W.G. Alani, A.A. Al-Kinani, R.G. Alany, Polymeric long-acting drug delivery systems (LADDS) for treatment of chronic diseases: Inserts, patches, wafers, and implants, Adv Drug Deliv Rev. 177 (2021). https://doi.org/10.1016/j.addr.2021.113957.

[93] J. Siepmann, F. Siepmann, Modeling of diffusion controlled drug delivery, Journal of Controlled Release. 161 (2012) 351–362. https://doi.org/10.1016/j.jconrel.2011.10.006.

[94] Y. Fu, W.J. Kao, Drug release kinetics and transport mechanisms of non-degradable and degradable polymeric delivery systems, Expert Opin Drug Deliv. 7 (2010) 429–444. https://doi.org/10.1517/17425241003602259.

[95] D. Bikiaris, Karavelidis, Karavas, Giliopoulos, Papadimitriou, Evaluating the effects of crystallinity in new biocompatible polyester nanocarriers on drug release behavior, Int J Nanomedicine. (2011) 3021. https://doi.org/10.2147/ijn.s26016.

[96] M. Omelczuk, J. McGinity, The Influence of Polymer Glass Transition Temperature and Molecular Weight on Drug Release from Tablets Containing Poly(DL-lactic Acid), Pharm Res. 9 (1992) 26–32.

[97] N. Kamaly, B. Yameen, J. Wu, O.C. Farokhzad, Degradable controlled-release polymers and polymeric nanoparticles: Mechanisms of controlling drug release, Chem Rev. 116 (2016) 2602–2663. https://doi.org/10.1021/acs.chemrev.5b00346.

[98] T.D. Reynolds, S.A. Mitchell, K.M. Balwinski, Investigation of the effect of tablet surface area/volume on drug release from hydroxypropylmethylcellulose controlled-release matrix tablets, Drug Dev Ind Pharm. 28 (2002) 457–466. https://doi.org/10.1081/DDC-120003007.

[99] T. Higuchi, Rate of Release of Medicaments from Ointment Bases Containing Drugs in Suspension, J Pharm Sci. 50 (1961) 1047–1047.

[100] J. Siepmann, N.A. Peppas, Higuchi equation: Derivation, applications, use and misuse, Int J Pharm. 418 (2011) 6–12. https://doi.org/10.1016/j.ijpharm.2011.03.051.

[101] M. Padmaa Paarakh, P. Ani Jose, C.M. Setty, G.V.P. Christoper, RELEASE KINETICS-CONCEPTS AND APPLICATIONS, n.d.

[102] T. Higuchi, N. York, Mechanism of Sustained-Action Medication Theoretical Analysis of Rate of Release of Solid Drugs Dispersed in Solid Matrices, n.d.

[103] P.L. Ritger, N.A. Peppas, A simple equation for description of solute release I. Fickian and non-fickian release from non-swellable devices in the form of slabs, spheres, cylinders or disces, Journal of Controlled Release. 5 (1987) 23–36.
[104] P.L. Ritger, N.A. Peppas, A simple equation for description of solute release II. Fickian and anamolous relesase from swellable devices, Journal of Controlled Release. 1 (1987) 37–42.
[105] R.W. Korsmeyer, N.A. Peppas, Solute and penetrant diffusion in swellable polymers. III. Drug release from glassy poly(HEMA-co-NVP) copolymers, Journal of Controlled Release. 1 (1984) 89–98.
[106] T. Sley, P. Cellet, G.M. Pereira, E.C. Muniz, R. Silva, A.F. Rubira, Hydroxyapatite Nanowhiskers Embedded in Chondroitin Sulfate Microspheres as Colon Targeted Drug Delivery System, (2015).
[107] R.W. Baker, H.S. Lonsdale, Controlled Release of Biologically Active Agents, Plenum Press, New York, 1974.
[108] Q. Baoa, Y. Zoub, Y. Wangb, D. Kozakb, S. Choib, D.J. Burgess, Drug release testing of long-acting intrauterine systems, Journal of Controlled Release. 316 (2019) 349–358. https://doi.org/10.1016/j.jconrel.2019.11.015.Drug.
[109] J.A.H. van Laarhoven, M.A.B. Kruft, H. Vromans, In vitro release properties of etonogestrel and ethinyl estradiol from a contraceptive vaginal ring, 2002. www.elsevier.com/locate/ijpharm.
[110] FDA, NEXPLANON (etonogestrel implant) IMPLANON (etonogestrel implant), n.d. www.fda.gov/medwatch.
[111] FDA, Mirena ® (levonorgestrel-releasing intrauterine system), n.d.
[112] Center for Drug Evaluation and Research, Clinical Pharmacology & Biopharmaceutics Review, 2000.
[113] C. Zhao, M. Gunawardana, F. Villinger, M.M. Baum, M. Remedios-Chan, T.R. Moench, L. Zeitlin, K.J. Whaley, O. Bohorov, T.J. Smith, D.J. Anderson, J.A. Moss, Pharmacokinetics and preliminary safety of pod-intravaginal rings delivering the monoclonal antibody VRC01-N for HIV prophylaxis in a macaque model, Antimicrob Agents Chemother. 61 (2017). https://doi.org/10.1128/AAC.02465-16.
[114] J.M. Smith, J.A. Moss, P. Srinivasan, I. Butkyavichene, M. Gunawardana, R. Fanter, C.S. Miller, D. Sanchez, F. Yang, S. Ellis, J. Zhang, M.A. Marzinke, C.W. Hendrix, A. Kapoor, M.M. Baum, Novel multipurpose pod-intravaginal ring for the prevention of HIV, HSV, and unintended pregnancy: Pharmacokinetic evaluation in a macaque model, PLoS One. 12 (2017). https://doi.org/10.1371/journal.pone.0185946.
[115] J.A. Moss, I. Butkyavichene, S.A. Churchman, M. Gunawardana, R. Fanter, C.S. Miller, F. Yang, J.T. Easley, M.A. Marzinke, C.W. Hendrix, T.J. Smith, M.M. Baum, Combination pod-intravaginal ring delivers antiretroviral agents for HIV prophylaxis: Pharmacokinetic evaluation in an ovine model, Antimicrob Agents Chemother. 60 (2016) 3759–3766. https://doi.org/10.1128/AAC.00391-16.

[116] D. de Ziegler, C. Bulletti, B. de Monstier, A.S. Jääskeläinen, The first uterine pass effect, Ann N Y Acad Sci. 828 (1997) 291–299. https://doi.org/10.1111/j.1749-6632.1997.tb48550.x.
[117] R.A. Miles, R.J. Paulson, R.A. Lobo, M.F. Press, L. Dahmoush, M. v. Sauer, Pharmacokinetics and endometrial tissue levels of progesterone after administration by intramuscular and vaginal routes: A comparative study, Fertil Steril. 62 (1994) 485–490. https://doi.org/10.1016/s0015-0282(16)56935-0.
[118] T. Mizutani, S. Nishiyama, I. Amakawa, A. Watanabe, K. Nakamuro, N. Terada, Danazol concentrations in ovary, uterus, and serum and their effect on the hypothalamic-pituitary-ovarian axis during vaginal administration of a danazol suppository*, 1995.
[119] R. Fanchin, C. Righini, L. Maria Schö nauer, F. ois Olivennes, J. Sabino Cunha Filho, R. Frydman, Vaginal versus oral E 2 administration: effects on endometrial thickness, uterine perfusion, and contractility, n.d.
[120] O.S. Tang, K. Gemzell-Danielsson, P.C. Ho, Misoprostol: Pharmacokinetic profiles, effects on the uterus and side-effects, International Journal of Gynecology and Obstetrics. 99 (2007) 160–167. https://doi.org/10.1016/j.ijgo.2007.09.004.
[121] G.M. Yerushalmi, Y. Gilboa, A. Jakobson-Setton, Y. Tadir, C. Goldchmit, D. Katz, D.S. Seidman, Vaginal mifepristone for the treatment of symptomatic uterine leiomyomata: An open-label study, Fertil Steril. 101 (2014) 496–500. https://doi.org/10.1016/j.fertnstert.2013.10.015.
[122] E. Cicinelli, D. De Ziegler, New Hypotheses Transvaginal progesterone: evidence for a new functional “portal system” flowing from the vagina to the uterus, 1999.
[123] C. Bulletti, D. de Ziegler, C. Flamigni, E. Giacomucci, V. Polli, G. Bolelli, F. Franceschetti, Targeted drug delivery in gynaecology: the first uterine pass effect The classical approach to targeted drug delivery relies on the proximity of delivery to the active site such as in the use of, 1997.
[124] L. Wildt, S. Kissler, P. Licht, W. Becker, Sperm transport in the human female genital tract and its modulation by oxytocin as assessed by hysterosalpingoscintigraphy, hysterotonography, electrohysterography and Doppler sonography, 1998.
[125] C. Bulletti, D. de Ziegler, V. Polli, L. Diotallevi, E. del Ferro, C. Flamigni, Uterine contractility during the menstrual cycle, 2000. https://academic.oup.com/humrep/article/15/suppl_1/81/716243.
[126] E. Cicinelli, M. Cignarelli, S. Sabatelli, F. Romano, L. Maria Schonauer, R. Padovano, N. Einer-Jensen, Plasma concentrations of progesterone are higher in the uterine artery than in the radial artery after vaginal administration of micronized progesterone in an oil-based solution to postmenopausal women, n.d.
[127] C. Nilsson, M. Kaukkamaa, H. Vierola, T. Luukkainen, Tissue Concentrations of Levonorgestrel in Women Using a Levonorgestrel-Releasing IUD, (n.d.) 80.
[128] C. Wenham, The gendered impact of the COVID-19 crisis and post-crisis period, (2020).

[129] C. Wenham, J. Smith, S.E. Davies, H. Feng, K.A. Grépin, S. Harman, A. Herten-Crabb, R. Morgan, Women are most affected by pandemics - lessons from past outbreaks, Nature. 583 (2020) 194–198.
[130] T. Riley, E. Sully, Z. Ahmed, A. Biddlecom, Estimates of the potential impact of the covid-19 pandemic on sexual and reproductive health in low-and middle-income countries, Int Perspect Sex Reprod Health. 46 (2020) 73–76. https://doi.org/10.1363/46e9020.
[131] S. Cousins, COVID-19 has "devastating" effect on women and girls, The Lancet. 396 (2020) 301–302.
[132] UNFPA, Impact of COVID-19 on Family Planning: What we know one year into the pandemic, 2021.
[133] K. Church, J. Gassner, M. Elliott, Reproductive health under COVID-19–challenges of responding in a global crisis, Sex Reprod Health Matters. 28 (2020) 1–3. https://doi.org/10.1080/26410397.2020.1773163.
[134] E. Nash, State Policy Trends 2021: The Worst Year for Abortion Rights in Almost Half a Century, 2021.
[135] G. Azcona, A. Bhatt, J. Encarnacion, J. Plazaola-Castaño, P. Seck, S. Staab, L. Turquet, From Insights to Action: Gender Equality in the Wake of COVID-19., United Nations, 2020.
[136] Sophie Barton-Knott/, Forty years into the HIV epidemic, AIDS remains the leading cause of death of women of reproductive age-UNAIDS calls for bold action, 20th International AIDS Conference. (2020).
[137] A.B. Hogan, B.L. Jewell, E. Sherrard-Smith, J.F. Vesga, O.J. Watson, C. Whittaker, A. Hamlet, J.A. Smith, P. Winskill, R. Verity, M. Baguelin, J.A. Lees, L.K. Whittles, K.E.C. Ainslie, S. Bhatt, A. Boonyasiri, N.F. Brazeau, L. Cattarino, L. V. Cooper, H. Coupland, G. Cuomo-Dannenburg, A. Dighe, B.A. Djaafara, C.A. Donnelly, J.W. Eaton, S.L. van Elsland, R.G. FitzJohn, H. Fu, K.A.M. Gaythorpe, W. Green, D.J. Haw, S. Hayes, W. Hinsley, N. Imai, D.J. Laydon, T.D. Mangal, T.A. Mellan, S. Mishra, G. Nedjati-Gilani, K. V. Parag, H.A. Thompson, H.J.T. Unwin, M.A.C. Vollmer, C.E. Walters, H. Wang, Y. Wang, X. Xi, N.M. Ferguson, L.C. Okell, T.S. Churcher, N. Arinaminpathy, A.C. Ghani, P.G.T. Walker, T.B. Hallett, Potential impact of the COVID-19 pandemic on HIV, tuberculosis, and malaria in low-income and middle-income countries: a modelling study, Lancet Glob Health. 8 (2020) e1132–e1141. https://doi.org/10.1016/S2214-109X(20)30288-6.
[138] G. Guaraldi, V. Borghi, J. Milic, F. Carli, G. Cuomo, M. Menozzi, A. Santoro, G. Orlando, C. Puzzolante, M. Meschiari, E. Franceschini, A. Bedini, F. Ferrari, W. Gennari, M. Sarti, C. Mussini, The Impact of COVID-19 on UNAIDS 90-90-90 Targets: Calls for New HIV Care Models, Open Forum Infect Dis. 8 (2021) 1–4. https://doi.org/10.1093/ofid/ofab283.

[139] A. Goga, L.G. Bekker, P. van de Perre, W. El-Sadr, K. Ahmed, M. Malahleha, T. Ramraj, V. Ramokolo, V. Magasana, G. Gray, Centring adolescent girls and young women in the HIV and COVID-19 responses, The Lancet. 396 (2020) 1864–1866. https://doi.org/10.1016/S0140-6736(20)32552-6.
[140] G. Zulaika, M. Bulbarelli, E. Nyothach, A. van Eijk, L. Mason, E. Fwaya, D. Obor, D. Kwaro, D. Wang, S.D. Mehta, P.A. Phillips-Howard, Impact of COVID-19 lockdowns on adolescent pregnancy and school dropout among secondary schoolgirls in Kenya, BMJ Glob Health. 7 (2022). https://doi.org/10.1136/bmjgh-2021-007666.
[141] UN Women, COVID-19 and Ending Violence Against Women and Girls, UN Women Headquaters. (2020) 10.
[142] B. Chmielewska, I. Barratt, R. Townsend, E. Kalafat, J. van der Meulen, I. Gurol-Urganci, P. O'Brien, E. Morris, T. Draycott, S. Thangaratinam, K. Le Doare, S. Ladhani, P. von Dadelszen, L. Magee, A. Khalil, Effects of the COVID-19 pandemic on maternal and perinatal outcomes: a systematic review and meta-analysis, Lancet Glob Health. 9 (2021) e759–e772. https://doi.org/10.1016/S2214-109X(21)00079-6.
[143] B. Kotlar, E. Gerson, S. Petrillo, A. Langer, H. Tiemeier, The impact of the COVID-19 pandemic on maternal and perinatal health: a scoping review, BioMed Central, 2021. https://doi.org/10.1186/s12978-021-01070-6.
[144] O.A. Bolarinwa, B.O. Ahinkorah, A.A. Seidu, E.K. Ameyaw, B.Q. Saeed, J.E. Hagan, U.I. Nwagbara, Mapping evidence of impacts of covid-19 outbreak on sexual and reproductive health: A scoping review, Healthcare (Switzerland). 9 (2021). https://doi.org/10.3390/healthcare9040436.
[145] R. Townsend, B. Chmielewska, I. Barratt, E. Kalafat, J. van der Meulen, I. Gurol-Urganci, P. O'Brien, E. Morris, T. Draycott, S. Thangaratinam, K. Le Doare, S. Ladhani, P. von Dadelszen, L.A. Magee, A. Khalil, Global changes in maternity care provision during the COVID-19 pandemic: A systematic review and meta-analysis, EClinicalMedicine. 37 (2021) 100947. https://doi.org/10.1016/j.eclinm.2021.100947.
[146] N. Kumar, K. Janmohamed, K. Nyhan, L. Forastiere, W.H. Zhang, A. Kagesten, M. Uhlich, A.S. Frimpong, S. van de Velde, J.M. Francis, J.T. Erausquin, E. Larrson, D. Callander, J. Scott, V. Minichiello, J. Tucker, Sexual health (excluding reproductive health, intimate partner violence and gender-based violence) and COVID-19: A scoping review, Sex Transm Infect. (2021) 1–9. https://doi.org/10.1136/sextrans-2020-054896.
[147] T.I. Mukherjee, A.G. Khan, A. Dasgupta, G. Samari, Reproductive justice in the time of COVID-19: a systematic review of the indirect impacts of COVID-19 on sexual and reproductive health, Reprod Health. 18 (2021). https://doi.org/10.1186/s12978-021-01286-6.
[148] L.B. Tolu, G.T. Feyissa, W.G. Jeldu, Guidelines and best practice recommendations on contraception and safe abortion care service provision amid covid-19 pandemic: Scoping review, Ethiopian Journal of Reproductive Health. 13 (2021) 11–20. https://doi.org/10.21203/rs.3.rs-25326/v1.

[149] M.D.J. Peters, C.M. Godfrey, H. Khalil, P. McInerney, D. Parker, C.B. Soares, Guidance for conducting systematic scoping reviews, Int J Evid Based Healthc. 13 (2015) 141–146. https://doi.org/10.1097/XEB.0000000000000050.
[150] A. Tricco, L.E. Zarin, K. O'Brien, H. Colquhoun, D. Levac, Preferred Reporting Items for Systematic reviews and Meta-Analyses extension for Scoping Reviews (PRISMA-ScR) Checklist SECTION, Ann Intern Med. 169 (2018) 11–12. https://doi.org/10.7326/M18-0850.2.
[151] M.D. Peters, C.M. Godfrey, P. McInerney, C.B. Soares, H. Khalil, D. Parker, The Joanna Briggs Institute Reviewers' Manual 2015: Methodology for JBI scoping reviews, 2015.
[152] B. Obrist, N. Iteba, C. Lengeler, A. Makemba, C. Mshana, R. Nathan, S. Alba, A. Dillip, M.W. Hetzel, I. Mayumana, A. Schulze, H. Mshinda, Access to health care in contexts of livelihood insecurity: A framework for analysis and action, PLoS Med. 4 (2007) 1584–1588. https://doi.org/10.1371/journal.pmed.0040308.
[153] J. V. Lazarus, A. Palayew, L.N. Rasmussen, T.H. Andersen, J. Nicholson, O. Norgaard, Searching PubMed to retrieve publications on the COVID-19 pandemic: Comparative analysis of search strings, J Med Internet Res. 22 (2020). https://doi.org/10.2196/23449.
[154] World Bank (World Development Indicators), List of economies (June 2020), 2020.
[155] L. Lindberg, A. VandeVusse, J. Mueller, M. Kirsten, Early Impacts of the COVID-19 Pandemic: Findings from the 2020 Guttmacher Survey of Reproductive Health Experiences, Guttmacher Instutute, New York, 2020. https://doi.org/https://doi.org/10.1363/2020.31482.
[156] L.B. Zapata, K.M. Curtis, R.J. Steiner, J.A. Reeves, A.T. Nguyen, K. Miele, M.K. Whiteman, COVID-19 and family planning service delivery: Findings from a survey of U.S. physicians, Prev Med. 150 (2021) 106664. https://doi.org/10.1016/j.ypmed.2021.106664.
[157] K. White, B. Kumar, V. Goyal, R. Wallace, S.C.M. Roberts, D. Grossman, Changes in Abortion in Texas Following an Executive Order Ban During the Coronavirus Pandemic, JAMA: Journal of the American Medical Association. 325 (2021) 691–693. https://doi.org/10.1001/jama.2020.24096.
[158] L. Wood, R. v Schrag, E. Baumler, D. Hairston, S. Guillot-Wright, E. Torres, J.R. Temple, On the Front Lines of the COVID-19 Pandemic: Occupational Experiences of the Intimate Partner Violence and Sexual Assault Workforce, J Interpers Violence. (2020) 886260520983304. https://doi.org/10.1177/0886260520983304.
[159] B.M. Stifani, K. Avila, E.E. Levi, Telemedicine for contraceptive counseling: An exploratory survey of US family planning providers following rapid adoption of services during the COVID-19 pandemic, Contraception. 103 (2021) 157–162. https://doi.org/10.1016/j.contraception.2020.11.006.
[160] M. Tschann, E.S. Ly, S. Hilliard, H.L.H. Lange, Changes to medication abortion clinical practices in response to the COVID-19 pandemic, Contraception. 104 (2021) 77–81. https://doi.org/10.1016/j.contraception.2021.04.010.

[161] U.D. Upadhyay, R. Schroeder, S.C.M. Roberts, Adoption of no-test and telehealth medication abortion care among independent abortion providers in response to COVID-19, Contracept X. 2 (2020) 100049. https://doi.org/10.1016/j.conx.2020.100049.
[162] S.C.M. Roberts, R. Schroeder, C. Joffe, COVID-19 and Independent Abortion Providers: Findings from a Rapid-Response Survey, Perspect Sex Reprod Health. 52 (2020) 217–225. https://doi.org/10.1363/psrh.12163.
[163] B. Sabri, M. Hartley, J. Saha, S. Murray, N. Glass, J.C. Campbell, Effect of COVID-19 pandemic on women's health and safety: A study of immigrant survivors of intimate partner violence, Health Care Women Int. 41 (2020) 1294–1312. https://doi.org/10.1080/07399332.2020.1833012.
[164] A. Sakowicz, C. Matovina, S. Imeroni, M. Daiter, O. Barry, W.A. Grobman, E.S. Miller, The association between COVID-19 related health services changes and postpartum contraception, Am J Obstet Gynecol. 224 (2021) S372–S372. https://doi.org/10.1016/j.ajog.2020.12.612.
[165] K.A. Muldoon, K.M. Denize, R. Talarico, D.B. Fell, A. Sobiesiak, M. Heimerl, K. Sampsel, COVID-19 pandemic and violence: rising risks and decreasing urgent care-seeking for sexual assault and domestic violence survivors, BMC Med. 19 (2021) 20. https://doi.org/10.1186/s12916-020-01897-z.
[166] M.L. Munro-Kramer, L.M. Cannon, L. Scheiman, A.R. St Ivany, J.M. Bailey, Accessing Healthcare Services During the COVID-19 Pandemic: The Plight of Sexual Assault Survivors, J Forensic Nurs. 17 (2021) 93–97. https://doi.org/10.1097/JFN.0000000000000326.
[167] G. Nagendra, C. Carnevale, N. Neu, A. Cohall, J. Zucker, The Potential Impact and Availability of Sexual Health Services During the COVID-19 Pandemic, Sex Transm Dis. 47 (2020) 434–436. https://doi.org/10.1097/OLQ.0000000000001198.
[168] C.N. Pinto, J.K. Niles, H.W. Kaufman, E.M. Marlowe, D.P. Alagia, G. Chi, B. van der Pol, Impact of the COVID-19 Pandemic on Chlamydia and Gonorrhea Screening in the U.S, Am J Prev Med. (2021). https://doi.org/10.1016/j.amepre.2021.03.009.
[169] T.K. Lin, R. Law, J. Beaman, D.G. Foster, The impact of the COVID-19 pandemic on economic security and pregnancy intentions among people at risk of pregnancy, Contraception. 103 (2021) 380–385. https://doi.org/http://dx.doi.org/10.1016/j.contraception.2021.02.001.
[170] K. Mello, M.H. Smith, B.J. Hill, P. Chakraborty, K. Rivlin, D. Bessett, A.H. Norris, M.L. McGowan, Federal, state, and institutional barriers to the expansion of medication and telemedicine abortion services in Ohio, Kentucky, and West Virginia during the COVID-19 pandemic, Contraception. 104 (2021) 111–116. https://doi.org/10.1016/j.contraception.2021.04.020.
[171] K.A. Johnson, N.O. Burghardt, E.C. Tang, P. Long, R. Plotzker, D. Gilson, R. Murphy, K. Jacobson, Measuring the Impact of the COVID-19 Pandemic on Sexually Transmitted

Diseases (STD) Public Health Surveillance and Program Operations in the State of California, Sex Transm Dis. (2021). https://doi.org/10.1097/olq.0000000000001441.
[172] T. Krishnamurti, A.L. Davis, B. Quinn, A.F. Castillo, K.L. Martin, H.N. Simhan, Mobile Remote Monitoring of Intimate Partner Violence Among Pregnant Patients During the COVID-19 Shelter-In-Place Order: Quality Improvement Pilot Study, J Med Internet Res. 23 (2021) e22790. https://doi.org/10.2196/22790.
[173] B. Gosangi, H. Park, R. Thomas, R. Gujrathi, C.P. Bay, A.S. Raja, S.E. Seltzer, M.C. Balcom, M.L. McDonald, D.P. Orgill, M.B. Harris, G.W. Boland, K. Rexrode, B. Khurana, Exacerbation of Physical Intimate Partner Violence during COVID-19 Pandemic, Radiology. 298 (2021) E38-e45. https://doi.org/10.1148/radiol.2020202866.
[174] J. Clement, M. Jacobi, B.N. Greenwood, Patient access to chronic medications during the Covid-19 pandemic: Evidence from a comprehensive dataset of US insurance claims, PLoS One. 16 (2021) e0249453. https://doi.org/10.1371/journal.pone.0249453.
[175] S.B. Sorenson, L. Sinko, R.A. Berk, The Endemic Amid the Pandemic: Seeking Help for Violence Against Women in the Initial Phases of COVID-19, J Interpers Violence. 36 (2021) 4899–4915. https://doi.org/10.1177/0886260521997946.
[176] M.D. Creinin, H. Tougas, M. Wilson, M.C. Matulich, Coronavirus disease 2019 impact on abortion care at a Northern California tertiary family planning program, Am J Obstet Gynecol. (2021). https://doi.org/10.1016/j.ajog.2021.03.007.
[177] A.R.A. Aiken, J.E. Starling, R. Gomperts, M. Tec, J.G. Scott, C.E. Aiken, Demand for Self-Managed Online Telemedicine Abortion in the United States During the Coronavirus Disease 2019 (COVID-19) Pandemic, Obstetrics and Gynecology. 136 (2020) 835–837. https://doi.org/10.1097/aog.0000000000004081.
[178] T. Adelekan, B. Mihretu, W. Mapanga, S. Nqeketo, L. Chauke, Z. Dwane, L. Baldwin-Ragaven, Early effects of the COVID-19 pandemic on family planning utilisation and termination of pregnancy services in Gauteng, South Africa : March–April 2020, Wits J Clin Med. 2 (2020) 145–152. https://doi.org/10.18772/26180197.2020.v2n2a7.
[179] L. Belay, T. Hurisa, F. Abbas, M. Daba, B. Abebe, B. Nigatu, S. Prager, Effect of COVID-19 pandemic on safe abortion and contraceptive services and mitigation measures: a case study from a tertiary facility in Ethiopia, Ethiopian Journal of Reproductive Health. 12 (2020) 51–57. https://ejrh.org/index.php/ejrh/article/view/418/131.
[180] S.B. Mambo, F.K. Sikakulya, R. Ssebuufu, Y. Mulumba, H. Wasswa, K. Thompson, J.C. Rusatira, F. Bhondoekhan, L.K. Kamyuka, S.O. Akib, C. Kirimuhuzya, J. Nakawesi, P. Kyamanywa, Factors that influences access and utilisation of sexual and reproductive health services among Ugandan youths during the COVID-19 pandemic lockdown: An online cross-sectional survey, (2020). https://doi.org/10.21203/rs.3.rs-48529/v4.
[181] S.N. Wood, C. Karp, F. Olaolorun, A.Z. Pierre, G. Guiella, P. Gichangi, L.A. Zimmerman, P. Anglewicz, E. Larson, C. Moreau, Need for and use of contraception by women before and during COVID-19 in four sub-Saharan African geographies: results

from population-based national or regional cohort surveys, Lancet Global Health. 9 (2021) e793–e801. https://doi.org/http://dx.doi.org/10.1016/S2214-109X(21)00105-4.

[182] P. Thekkur, K.C. Takarinda, C. Timire, C. Sandy, T. Apollo, A.M. v Kumar, S. Satyanarayana, H.D. Shewade, M. Khogali, R. Zachariah, I.D. Rusen, S.D. Berger, A.D. Harries, Operational Research to Assess the Real-Time Impact of COVID-19 on TB and HIV Services: The Experience and Response from Health Facilities in Harare, Zimbabwe, Trop Med Infect Dis. 6 (2021). https://doi.org/10.3390/tropicalmed6020094.

[183] P. Thekkur, H. Tweya, S. Phiri, J. Mpunga, T. Kalua, A.M. v Kumar, S. Satyanarayana, H.D. Shewade, M. Khogali, R. Zachariah, I.D. Rusen, S.D. Berger, A.D. Harries, Assessing the Impact of COVID-19 on TB and HIV Programme Services in Selected Health Facilities in Lilongwe, Malawi: Operational Research in Real Time, Trop Med Infect Dis. 6 (2021). https://doi.org/10.3390/tropicalmed6020081.

[184] M.J. Siedner, J.D. Kraemer, M.J. Meyer, G. Harling, T. Mngomezulu, P. Gabela, S. Dlamini, D. Gareta, N. Majozi, N. Ngwenya, J. Seeley, E. Wong, C. Iwuji, M. Shahmanesh, W. Hanekom, K. Herbst, Access to primary healthcare during lockdown measures for COVID-19 in rural South Africa: a longitudinal cohort study, MedRxiv. (2020). https://doi.org/10.1101/2020.05.15.20103226.

[185] M.J. Siedner, J.D. Kraemer, M.J. Meyer, G. Harling, T. Mngomezulu, P. Gabela, S. Dlamini, D. Gareta, N. Majozi, N. Ngwenya, J. Seeley, E. Wong, C. Iwuji, M. Shahmanesh, W. Hanekom, K. Herbst, Access to primary healthcare during lockdown measures for COVID-19 in rural South Africa: an interrupted time series analysis, BMJ Open. 10 (2020) e043763. https://doi.org/10.1136/bmjopen-2020-043763.

[186] M. Nyashanu, R. Chireshe, F. Mushawa, M.S. Ekpenyong, Exploring the challenges of women taking antiretroviral treatment during the COVID-19 pandemic lockdown in peri-urban Harare, Zimbabwe, Int J Gynaecol Obstet. (2021). https://doi.org/10.1002/ijgo.13771.

[187] M. Ponticiello, J. Mwanga-Amumpaire, P. Tushemereirwe, G. Nuwagaba, R. King, R. Sundararajan, “Everything is a Mess”: How COVID-19 is Impacting Engagement with HIV Testing Services in Rural Southwestern Uganda, in: AIDS Behav, Cornell University, Ithaca, NY, USA. Department of Pediatrics, Mbarara University of Science and Technology, Mbarara, Uganda. Global Health Sciences, University of California, San Francisco, San Francisco, CA, USA. Weill Cornell Center for Global Health, , 2020: pp. 3006–3009. https://doi.org/10.1007/s10461-020-02935-w.

[188] H. Lagat, M. Sharma, E. Kariithi, G. Otieno, D. Katz, S. Masyuko, M. Mugambi, B. Wamuti, B. Weiner, C. Farquhar, Impact of the COVID-19 Pandemic on HIV Testing and Assisted Partner Notification Services, Western Kenya, in: AIDS Behav, PATH, Kisumu, Kenya. Department of Global Health, University of Washington, Seattle, USA. msharma1@uw.edu. International Clinical Research Center (ICRC), Department of Global Health, University of Washington, 908 Jefferson St, Seattle, WA, 98104, USA. msh, 2020: pp. 3010–3013. https://doi.org/10.1007/s10461-020-02938-7.

[189] S.L. Lecher, M. Naluguza, C. Mwangi, J. N'Tale, D. Edgil, G. Alemnji, H. Alexander, Notes from the Field: Impact of the COVID-19 Response on Scale-Up of HIV Viral Load Testing - PEPFAR-Supported Countries, January-June 2020, MMWR Morb Mortal Wkly Rep. 70 (2021) 794–795. https://doi.org/10.15585/mmwr.mm7021a3.

[190] J. Leight, C. Hensly, M. Chissano, L. Ali, Short-term effects of the COVID-19 state of emergency on contraceptive access and utilization in Mozambique, PLoS One. 16 (2021) e0249195. https://doi.org/10.1371/journal.pone.0249195.

[191] S. Linnemayr, L. Jennings Mayo-Wilson, U. Saya, Z. Wagner, S. MacCarthy, S. Walukaga, S. Nakubulwa, Y. Karamagi, HIV Care Experiences During the COVID-19 Pandemic: Mixed-Methods Telephone Interviews with Clinic-Enrolled HIV-Infected Adults in Uganda, AIDS Behav. 25 (2021) 28–39. https://doi.org/10.1007/s10461-020-03032-8.

[192] J.E. Mantell, J. Franks, M. Lahuerta, D. Omollo, A. Zerbe, M. Hawken, Y. Wu, D. Odera, W.M. El-Sadr, K. Agot, Life in the Balance: Young Female Sex Workers in Kenya Weigh the Risks of COVID-19 and HIV, AIDS Behav. 25 (2021) 1323–1330. https://doi.org/10.1007/s10461-020-03140-5.

[193] I. Mbithi, P. Thekkur, J.M. Chakaya, E. Onyango, P. Owiti, N.C. Njeri, A.M. v Kumar, S. Satyanarayana, H.D. Shewade, M. Khogali, R. Zachariah, I.D. Rusen, S.D. Berger, A.D. Harries, Assessing the Real-Time Impact of COVID-19 on TB and HIV Services: The Experience and Response from Selected Health Facilities in Nairobi, Kenya, Trop Med Infect Dis. 6 (2021). https://doi.org/10.3390/tropicalmed6020074.

[194] C. Karp, S.N. Wood, G. Guiella, P. Gichangi, S.O. Bell, P. Anglewicz, E. Larson, L. Zimmerman, C. Moreau, Contraceptive dynamics during COVID-19 in sub-Saharan Africa: longitudinal evidence from Burkina Faso and Kenya, BMJ Sex Reprod Health. (2021). https://doi.org/10.1136/bmjsrh-2020-200944.

[195] A. Kassie, A. Wale, W. Yismaw, Impact of Coronavirus Diseases-2019 (COVID-19) on Utilization and Outcome of Reproductive, Maternal, and Newborn Health Services at Governmental Health Facilities in South West Ethiopia, 2020: Comparative Cross-Sectional Study, Int J Womens Health. 13 (2021) 479–488. https://doi.org/10.2147/ijwh.s309096.

[196] J. Dorward, T. Khubone, K. Gate, H. Ngobese, Y. Sookrajh, S. Mkhize, A. Jeewa, C. Bottomley, L. Lewis, K. Baisley, C.C. Butler, N. Gxagxisa, N. Garrett, The impact of the COVID-19 lockdown on HIV care in 65 South African primary care clinics: an interrupted time series analysis, Lancet HIV. 8 (2021) e158–e165. https://doi.org/10.1016/s2352-3018(20)30359-3.

[197] J. Dyer, K. Wilson, J. Badia, K. Agot, J. Neary, I. Njuguna, J. Kibugi, E. Healy, K. Beima-Sofie, G. John-Stewart, P. Kohler, The Psychosocial Effects of the COVID-19 Pandemic on Youth Living with HIV in Western Kenya, AIDS Behav. 25 (2021) 68–72. https://doi.org/10.1007/s10461-020-03005-x.

[198] S. Gichuna, R. Hassan, T. Sanders, R. Campbell, M. Mutonyi, P. Mwangi, Access to Healthcare in a time of COVID-19: Sex Workers in Crisis in Nairobi, Kenya, Glob Public Health. 15 (2020) 1430–1442. https://doi.org/10.1080/17441692.2020.1810298.
[199] D.L.J. Davey, L.G. Bekker, N. Mashele, P. Gorbach, T.J. Coates, L. Myer, PrEP retention and prescriptions for pregnant women during COVID-19 lockdown in South Africa, Lancet HIV. 7 (2020) e735. https://doi.org/10.1016/s2352-3018(20)30226-5.
[200] S.G. Abdela, A.B. Berhanu, L.M. Ferede, J. van Griensven, Essential Healthcare Services in the Face of COVID-19 Prevention: Experiences from a Referral Hospital in Ethiopia, Am J Trop Med Hyg. 103 (2020) 1198–1200. https://doi.org/10.4269/ajtmh.20-0464.
[201] S. Davidge, A Perfect Storm: The impact of the Covid-19 pandemic on domestic abuse survivors and the services supporting them, Women's Aid, Bristol, UK, 2020. https://www.womensaid.org.uk/a-perfect-storm-the-impact-of-the-covid-19-pandemic-on-domestic-abuse-survivors-and-the-services-supporting-them/.
[202] R. Thomson-Glover, H. Hamlett, D. Weston, J. Ashby, Coronavirus (COVID-19) and young people's sexual health, Sex Transm Infect. 96 (2020) 473–474. https://doi.org/http://dx.doi.org/10.1136/sextrans-2020-054699.
[203] C. Vives-Cases, D. la Parra-Casado, J.F. Estevez, J. Torrubiano-Dominguez, B. Sanz-Barbero, Intimate Partner Violence against Women during the COVID-19 Lockdown in Spain, Int J Environ Res Public Health. 18 (2021) 9. https://doi.org/10.3390/ijerph18094698.
[204] R. Rodriguez-Jimenez, N.E. Fares-Otero, L. García-Fernández, Gender-based violence during COVID-19 outbreak in Spain, Psychol Med. (2020) 1–2. https://doi.org/10.1017/s0033291720005024.
[205] N. Roland, J. Drouin, D. Desplas, F. Cuenot, R. Dray-Spira, A. Weill, M. Zureik, Effects of the Coronavirus Disease 2019 (COVID-19) Lockdown on the Use of Contraceptives and Ovulation Inductors in France, in: Obstet Gynecol, EPI-PHARE, a scientific cooperation between The French National Health Insurance Fund (CNAM) and the French National Agency for Medicines and Health Products Safety (ANSM)., 2021: pp. 415–417. https://doi.org/10.1097/aog.0000000000004281.
[206] D. Simoes, A.R. Stengaard, L. Combs, D. Raben, Impact of the COVID-19 pandemic on testing services for HIV, viral hepatitis and sexually transmitted infections in the WHO European Region, March to August 2020, Eurosurveillance. 25 (2020). https://doi.org/http://dx.doi.org/10.2807/1560-7917.ES.2020.25.47.2001943.
[207] C. Moreau, M. Shankar, A. Glasier, S. Cameron, K. Gemzell-Danielsson, Abortion regulation in Europe in the era of COVID-19: a spectrum of policy responses, BMJ Sex Reprod Health. (2020). https://doi.org/10.1136/bmjsrh-2020-200724.
[208] G. Nittari, G.G. Sagaro, A. Feola, M. Scipioni, G. Ricci, A. Sirignano, First Surveillance of Violence against Women during COVID-19 Lockdown: Experience from "Niguarda" Hospital in Milan, Italy, Int J Environ Res Public Health. 18 (2021). https://doi.org/10.3390/ijerph18073801.

[209] I. Lete, J. Novalbos, E. de la Viuda, F. Lugo, M. Herrero, M. Obiol, J. Perelló, R. Sanchez-Borrego, Impact of the Lockdown Due to COVID-19 Pandemic in the Use of Combined Hormonal Oral Contraception in Spain - Results of a National Survey: Encovid, Open Access J Contracept. 12 (2021) 103–111. https://doi.org/10.2147/oajc.s306580.

[210] R. Lewis, C. Blake, M. Shimonovich, N. Coia, J. Duffy, Y. Kerr, J. Wilson, C.A. Graham, K.R. Mitchell, Disrupted prevention: condom and contraception access and use among young adults during the initial months of the COVID-19 pandemic. An online survey, BMJ Sex Reprod Health. (2021). https://doi.org/10.1136/bmjsrh-2020-200975.

[211] R. Lundin, B. Armocida, P. Sdao, S. Pisanu, I. Mariani, A. Veltri, M. Lazzerini, Gender-based violence during the COVID-19 pandemic response in Italy, J Glob Health. 10 (2020) 20359. https://doi.org/10.7189/jogh.10.020359.

[212] J.D. Kowalska, A. Skrzat-Klapaczyńska, D. Bursa, T. Balayan, J. Begovac, N. Chkhartishvili, D. Gokengin, A. Harxhi, D. Jilich, D. Jevtovic, K. Kase, B. Lakatos, R. Matulionyte, V. Mulabdic, A. Nagit, A. Papadopoulos, M. Stefanovic, A. Vassilenko, M. Vasylyev, N. Yancheva, O. Yurin, A. Horban, HIV care in times of the COVID-19 crisis - Where are we now in Central and Eastern Europe?, Int J Infect Dis. 96 (2020) 311–314. https://doi.org/10.1016/j.ijid.2020.05.013.

[213] C. Ebert, J.I. Steinert, Prevalence and risk factors of violence against women and children during COVID-19, Germany, Bull World Health Organ. 99 (2021) 429–438. https://doi.org/10.2471/blt.20.270983.

[214] K. Gibelin, A. Agostini, M. Marcot, H. Piclet, F. Bretelle, L. Miquel, COVID-19 impact in abortions' practice, a regional French evaluation, J Gynecol Obstet Hum Reprod. 50 (2021) 102038. https://doi.org/10.1016/j.jogoh.2020.102038.

[215] S. Caruso, A.M.C. Rapisarda, P. Minona, Sexual activity and contraceptive use during social distancing and self-isolation in the COVID-19 pandemic, Eur J Contracept Reprod Health Care. 25 (2020) 445–448. https://doi.org/10.1080/13625187.2020.1830965.

[216] L. de Kort, E. Wouters, S. van de Velde, Obstacles and opportunities: a qualitative study of the experiences of abortion centre staff with abortion care during the first COVID-19 lockdown in Flanders, Belgium, Sex Reprod Health Matters. 29 (2021) 1921901. https://doi.org/10.1080/26410397.2021.1921901.

[217] A.R.A. Aiken, J.E. Starling, R. Gomperts, J.G. Scott, C.E. Aiken, Demand for self-managed online telemedicine abortion in eight European countries during the COVID-19 pandemic: A regression discontinuity analysis, BMJ Sex Reprod Health. (2021) 1–8. https://doi.org/10.1136/bmjsrh-2020-200880.

[218] S.B. Rose, S.M. Garrett, E.M. McKinlay, S.J. Morgan, Access to sexual healthcare during New Zealand's COVID-19 lockdown: cross-sectional online survey of 15–24-year-olds in a high deprivation region, BMJ Sexual & Reproductive Health. (2021) bmjsrh-2020-200986. https://doi.org/10.1136/bmjsrh-2020-200986.

[219] S. Qiao, X. Yang, S. Sun, X. Li, T. Mi, Y. Zhou, Z. Shen, Challenges to HIV service delivery and the impacts on patient care during COVID-19: perspective of HIV care providers in Guangxi, China, AIDS Care. 33 (2021) 559–565. https://doi.org/10.1080/09540121.2020.1849532.
[220] G. Li, D. Tang, B. Song, C. Wang, S. Qunshan, C. Xu, H. Geng, H. Wu, X. He, Y. Cao, Q. Shen, Impact of the COVID-19 Pandemic on Partner Relationships and Sexual and Reproductive Health: Cross-Sectional, Online Survey Study, J Med Internet Res. 22 (2020) N.PAG-N.PAG. https://doi.org/10.2196/20961.
[221] O. Htun Nyunt, N.M.A. Wan, P. Soan, O. Tawil, M.K. Lwin, M.T.A. Hsan, K.M. Win, F. Mesquita, How Myanmar Is Working to Maintain Essential Services for People Living With HIV and Key Populations During the Covid-19 Pandemic, J Int Assoc Provid AIDS Care. 20 (2021) 23259582211017744. https://doi.org/10.1177/23259582211017742.
[222] S. Janyam, D. Phuengsamran, J. Pangnongyang, W. Saripra, L. Jitwattanapataya, C. Songsamphan, P. Benjarattanaporn, D. Gopinath, Protecting sex workers in Thailand during the COVID-19 pandemic: opportunities to build back better, WHO South East Asia J Public Health. 9 (2020) 100–103. https://doi.org/10.4103/2224-3151.294301.
[223] E.P.F. Chow, J.S. Hocking, J.J. Ong, T.R. Phillips, C.K. Fairey, Sexually Transmitted Infection Diagnoses and Access to a Sexual Health Service Before and After the National Lockdown for COVID-19 in Melbourne, Australia, Open Forum Infect Dis. 8 (2021) 10. https://doi.org/10.1093/ofid/ofaa536.
[224] J. Coombe, F. Kong, H. Bittleston, H. Williams, J. Tomnay, A. Vaisey, S. Malta, J. Goller, M. Temple-Smith, L. Bourchier, A. Lau, J.S. Hocking, Contraceptive use and pregnancy plans among women of reproductive age during the first Australian COVID-19 lockdown: findings from an online survey, Eur J Contracept Reprod Health Care. (2021) 1–14. https://doi.org/10.1080/13625187.2021.1884221.
[225] S.M. Perez-Vincent, E. Carreras, M.A. Gibbons, T.E. Murphy, M. Rossi, COVID-19 Lockdowns and Domestic Violence: Evidence from Two Studies in Argentina, Inter-American Development Bank, 2020. https://doi.org/http://dx.doi.org/10.18235/0002490.
[226] A. Silverio-Murillo, L. Hoehn-Velasco, J.R. Balmori de la Miyar, A. Rodríguez, COVID-19 and women's health: Examining changes in mental health and fertility, Econ Lett. 199 (2021) 109729. https://doi.org/10.1016/j.econlet.2021.109729.
[227] K. Celestin, A. Allorant, M. Virgin, E. Marinho, K. Francois, J.G. Honore, C. White, J.S. Valles, G. Perrin, N. de Kerorguen, J. Flowers, J.G. Balan, J.B.T. Koama, S. Barnhart, N. Puttkammer, Short-Term Effects of the COVID-19 Pandemic on HIV Care Utilization, Service Delivery, and Continuity of HIV Antiretroviral Treatment (ART) in Haiti, AIDS Behav. 25 (2021) 1366–1372. https://doi.org/10.1007/s10461-021-03218-8.
[228] J.M. Aguero, COVID-19 and the rise of intimate partner violence, World Dev. 137 (2021) 7. https://doi.org/10.1016/j.worlddev.2020.105217.
[229] A. Pattojoshi, A. Sidana, S. Garg, S.N. Mishra, L.K. Singh, N. Goyal, S.K. Tikka, Staying home is NOT "staying safe": A rapid 8-day online survey on spousal violence against

women during the COVID-19 lockdown in India, in: Psychiatry Clin Neurosci, Department of Psychiatry, Hi-Tech Medical College & Hospital, Bhubaneswar, India. Prerna De-addiction and Rehabilitation Centre, Sriganga Nagar, Rajasthan, India. Department of Psychiatry, Shri Guru Ram Rai Institute of Medical & Health Sciences, Dehradun, 2021: pp. 64–66. https://doi.org/10.1111/pcn.13176.

[230] S. Aryal, S. Nepal, S. Ballav Pant, Safe abortion services during the COVID -19 pandemic: a cross-sectional study from a tertiary center in Nepal, F1000Res. 10 (2021) 112. https://doi.org/10.12688/f1000research.50977.1.

[231] I. Aolymat, A Cross-Sectional Study of the Impact of COVID-19 on Domestic Violence, Menstruation, Genital Tract Health, and Contraception Use among Women in Jordan, Am J Trop Med Hyg. 104 (2020) 519–525. https://doi.org/10.4269/ajtmh.20-1269.

[232] Impact of COVID-19 on violence against women and girls and service provision: UN Women rapid assessment and findings, United Nations Women Headquarters, 2020. https://www.unwomen.org/-/media/headquarters/attachments/sections/library/publications/2020/impact-of-covid-19-on-violence-against-women-and-girls-and-service-provision-en.pdf?la=en&vs=0.

[233] A.J. Restar, H.M. Garrison-Desany, T. Adamson, C. Childress, G. Millett, B.A. Jarrett, S. Howell, J.L. Glick, S.W. Beckham, S. Baral, HIV treatment engagement in the context of COVID-19: an observational global sample of transgender and nonbinary people living with HIV, BMC Public Health. 21 (2021) 901. https://doi.org/10.1186/s12889-021-10977-5.

[234] M. Lyons, G. Brewer, Experiences of Intimate Partner Violence during Lockdown and the COVID-19 Pandemic, J Fam Violence. (2021) 1–9. https://doi.org/10.1007/s10896-021-00260-x.

[235] M.S. Khan, S. Rego, J.B. Rajal, V. Bond, R.K. Fatima, A.K. Isani, J. Sutherland, K. Kranzer, Mitigating the impact of COVID-19 on tuberculosis and HIV services: A cross-sectional survey of 669 health professionals in 64 low and middle-income countries, PLoS One. 16 (2021) e0244936. https://doi.org/10.1371/journal.pone.0244936.

[236] M. Endler, T. Al-Haidari, C. Benedetto, S. Chowdhury, J. Christilaw, F. el Kak, D. Galimberti, C. Garcia-Moreno, M. Gutierrez, S. Ibrahim, S. Kumari, C. McNicholas, D. Mostajo Flores, J. Muganda, A. Ramirez-Negrin, H. Senanayake, R. Sohail, M. Temmerman, K. Gemzell-Danielsson, How the coronavirus disease 2019 pandemic is impacting sexual and reproductive health and rights and response: Results from a global survey of providers, researchers, and policy-makers, Acta Obstet Gynecol Scand. 100 (2021) 571–578. https://doi.org/10.1111/aogs.14043.

[237] A.C. Flynn, K. Kavanagh, A.D. Smith, L. Poston, S.L. White, The Impact of the COVID-19 Pandemic on Pregnancy Planning Behaviors, Womens Health Rep (New Rochelle). 2 (2021) 71–77. https://doi.org/10.1089/whr.2021.0005.

[238] A.R.A. Aiken, J.E. Starling, R. Gomperts, J.G. Scott, C.E. Aiken, Demand for self-managed online telemedicine abortion in eight European countries during the COVID-19

pandemic: a regression discontinuity analysis, BMJ Sex Reprod Health. (2021). https://doi.org/10.1136/bmjsrh-2020-200880.
[239] T. Hale, N. Angrist, R. Goldszmidt, B. Kira, A. Petherick, T. Phillips, S. Webster, E. Cameron-Blake, L. Hallas, S. Majumdar, H. Tatlow, A global panel database of pandemic policies (Oxford COVID-19 Government Response Tracker), Nat Hum Behav. 5 (2021) 529–538. https://doi.org/10.1038/s41562-021-01079-8.
[240] J. Bearak, A. Popinchalk, B. Ganatra, A.B. Moller, Ö. Tunçalp, C. Beavin, L. Kwok, L. Alkema, Unintended pregnancy and abortion by income, region, and the legal status of abortion: estimates from a comprehensive model for 1990–2019, Lancet Glob Health. 8 (2020) e1152–e1161. https://doi.org/10.1016/S2214-109X(20)30315-6.
[241] A.O. Tsui, R. McDonald-Mosley, A.E. Burke, Family planning and the burden of unintended pregnancies, Epidemiol Rev. 32 (2010) 152–174. https://doi.org/10.1093/epirev/mxq012.
[242] T. Riley, E. Sully, Z. Ahmed, A. Biddlecom, Estimates of the Potential Impact of the COVID-19 Pandemic on Sexual and Reproductive Health in Low- and Middle-Income Countries, Int Perspect Sex Reprod Health. 46 (2020) 73–76. https://doi.org/10.33314/jnhrc.v18i2.2747.
[243] M. Berer, National Laws and Unsafe Abortion: The Parameters of Change, (2004) 1–8.
[244] A.M. Gresham, B.J. Peters, G. Karantzas, L.D. Cameron, J.A. Simpson, Examining associations between COVID-19 stressors, intimate partner violence, health, and health behaviors, J Soc Pers Relat. 38 (2021) 2291–2307. https://doi.org/10.1177/02654075211012098.
[245] A.R. Piquero, W.G. Jennings, E. Jemison, C. Kaukinen, F.M. Knaul, Domestic violence during the COVID-19 pandemic - Evidence from a systematic review and meta-analysis, J Crim Justice. 74 (2021) 101806. https://doi.org/10.1016/j.jcrimjus.2021.101806.
[246] A. Banke-Thomas, S. Yaya, Looking ahead in the COVID-19 pandemic: emerging lessons learned for sexual and reproductive health services in low- and middle-income countries, Reprod Health. 18 (2021). https://doi.org/10.1186/s12978-021-01307-4.
[247] M. Amiri, I.M. El-Mowafi, T. Chahien, H. Yousef, L.H. Kobeissi, An overview of the sexual and reproductive health status and service delivery among Syrian refugees in Jordan, nine years since the crisis: a systematic literature review, Reprod Health. 17 (2020) 1–20. https://doi.org/10.1186/s12978-020-01005-7.
[248] A.M. Starrs, A.C. Ezeh, G. Barker, A. Basu, J.T. Bertrand, R. Blum, A.M. Coll-Seck, A. Grover, L. Laski, M. Roa, Z.A. Sathar, L. Say, G.I. Serour, S. Singh, K. Stenberg, M. Temmerman, A. Biddlecom, A. Popinchalk, C. Summers, L.S. Ashford, Accelerate progress—sexual and reproductive health and rights for all: report of the Guttmacher–Lancet Commission, The Lancet. 391 (2018) 2642–2692. https://doi.org/10.1016/S0140-6736(18)30293-9.

[249] G.D. Meckler, M.N. Elliott, D.E. Kanouse, K.P. Beals, M.A. Schuster, Nondisclosure of Sexual Orientation to a Physician Among a Sample of Gay, Lesbian, and Bisexual Youth, n.d.
[250] J.E. Ehrenpreis, E.D. Ehrenpreis, A Historical Perspective of Healthcare Disparity and Infectious Disease in the Native American Population, 2022. www.amjmedsci.com.
[251] J.A. Summers, M.G. Baker, N. Wilson, New Zealand's experience of the 1918-19 inn uenza pandemic: a systematic review after 100 years, NZMJ. 131 (2018) 1487. www.nzma.org.nz/journal.
[252] A.K. Boggild, L. Yuan, D.E. Low, A.J. McGeer, The Impact of Influenza on the Canadian First Nations, Canadian Journal of Public Health. (2011) 345–349.
[253] A. v. Groom, T.W. Hennessy, R.J. Singleton, J.C. Butler, S. Holve, J.E. Cheek, Pneumonia and influenza mortality among American Indian and Alaska native people, 1990û2009, Am J Public Health. 104 (2014). https://doi.org/10.2105/AJPH.2013.301740.
[254] R. Alsalem, Violence against indigenous women and girls, 2022. https://www.ohchr.org/en/calls-for-input/calls-input/call-inputs-report-violence-against-indigenous-.
[255] Marie Stopes International, Resilience, Adaptation, and Action: MSI's Response to COVID-19, 2020.
[256] Serving Sara During the COVID-19 Pandemic: Lessons Learned in Family Planning Adaptations, 2021.
[257] P.D. United Nations, Department of Economic and Social Affairs, Contraceptive Use by Method 2019, 2019.
[258] D. Bartz, J.A. Greenberg, Sterilization in the United States., Rev Obstet Gynecol. 1 (2008) 147–152. https://doi.org/10.2307/2134232.
[259] F. U.S. Department of Health and Human Services, Labeling for Permanent Implants Intended for Sterilization, 2016.
[260] A.L. Givan, H.D. White, J.E. Stern, E. Colby, E.J. Gosselin, P.M. Guyre, C.R. Wira, Flow cytometric analysis of leukocytes in the human female reproductive tract: Comparison of fallopian tube, uterus, cervix, and vagina, American Journal of Reproductive Immunology. 38 (1997) 350–359. https://doi.org/10.1111/j.1600-0897.1997.tb00311.x.
[261] P. Muenzner, V. Bachmann, W. Zimmermann, J. Hentschel, C.R. Hauck, Human-Restricted Bacterial Pathogens Block Shedding of Epithelial Cells by Stimulating Integrin Activation, Science (1979). 329 (2010) 1197–1202.
[262] Z. McGee, R.L. Jensen, C.M. Clemens, D. Taylor-Robinson, A.P. Johnson, C.R. Gregg, Gonococcal infection of human fallopian tube mucosa in organ culture: Relationship of mucosal tissue TNF-α concentration to sloughing of ciliated cells, Sex Transm Dis. 26 (1999) 160–165. https://doi.org/10.1097/00007435-199903000-00007.
[263] C.A. Eddy, C.J. Paljerstein, Anatomic and physiologic factors affecting the development of transcervical sterilization techniques. I-7, in: Female Transcervical Sterilization, 1983: pp. 8–22.

[264] R.F. Valle, C.S. Carignan, T.C. Wright, Tissue response to the STOP microcoil transcervical permanent contraceptive device: Results from a prehysterectomy study, Fertil Steril. 76 (2001) 974–980. https://doi.org/10.1016/S0015-0282(01)02858-8.
[265] R.G. Growe, M.I. Luster, P.A. Fail, J. Lippes, Quinacrine-induced occlusive fibrosis in the human fallopian tube is due to a unique inflammatory response and modification of repair mechanisms, J Reprod Immunol. 97 (2013) 159–166. https://doi.org/10.1016/j.jri.2012.12.003.
[266] S. Rezai, M. LaBine, H.A. Gomez Roberts, I. Lora Alcantara, C.E. Henderson, M. Elmadjian, D. Nuritdinova, Essure Microinsert Abdominal Migration after Hysteroscopic Tubal Sterilization of an Appropriately Placed Essure Device: Dual Case Reports and Review of the Literature, Case Rep Obstet Gynecol. 2015 (2015) 1–5. https://doi.org/10.1155/2015/402197.
[267] E. Swider, O. Koshkina, J. Tel, L.J. Cruz, I.J.M. de Vries, M. Srinivas, Customizing poly(lactic-co-glycolic acid) particles for biomedical applications, Acta Biomater. 73 (2018) 38–51. https://doi.org/10.1016/j.actbio.2018.04.006.
[268] H. Pan, H. Jiang, W. Chen, The Biodegradability of Electrospun Dextran/PLGA Scaffold in a Fibroblast/Macrophage Co-culture, Biomaterials. 29 (2008) 1583–1592.
[269] M. Caliendo, D. Lee, R. Queiroz, D. Waldman, Sclerotherapy with use of doxycycline after percutaneous drainage of postoperative lymphoceles, Journal of Vascular and Interventional Radiology. 12 (2001) 73–77.
[270] K.M. AlGhamdi, A.E. Ashour, A.C. Rikabi, N.A. Moussa, Phenol as a novel sclerosing agent: A safety and efficacy study on experimental animals, Saudi Pharmaceutical Journal. 22 (2014) 71–78. https://doi.org/10.1016/j.jsps.2013.01.007.
[271] A.N. Hurewitz, Chien Liang Wu, P. Mancuso, S. Zucker, Tetracycline and doxycycline inhibit pleural fluid metalloproteinases: A possible mechanism for chemical pleurodesis, Chest. 103 (1993) 1113–1117. https://doi.org/10.1378/chest.103.4.1113.
[272] M. Sourdeval, C. Lemaire, C. Brenner, E. Boisvieux-Ulrich, F. Marano, Mechanisms of doxycycline-induced cytotoxicity on human bronchial epithelial cells., Frontiers in Bioscience. 11 (2006) 3036–48.
[273] A. Halverson, Hemorrhoids, 1 (2007) 77–85. https://doi.org/10.1055/s-2007-977485.
[274] G. Pedersen, J. Brynskov, T. Saermark, Phenol toxicity and conjugation in human colonic epithelial cells, Scand J Gastroenterol. 37 (2002) 74–79. https://doi.org/10.1080/003655202753387392.
[275] Y. Zhao, G. Wang, W. Li, Z. liang Zhu, Determination of reaction mechanism and rate constants of alkaline hydrolysis of phenyl benzoate in ethanol-water medium by nonlinear least squares regression, Chemometrics and Intelligent Laboratory Systems. 82 (2006) 193–199. https://doi.org/10.1016/j.chemolab.2005.06.023.
[276] K.Y.B. Ng, R. Mingels, H. Morgan, N. Macklon, Y. Cheong, In vivo oxygen, temperature and pH dynamics in the female reproductive tract and their importance in human

conception: A systematic review, Hum Reprod Update. 24 (2018) 15–34. https://doi.org/10.1093/HUMUPD/DMX028.
[277] J.C. Chow, D.W. Young, D.T. Golenbock, W.J. Christ, F. Gusovsky, Toll-like Receptor-4 Mediates Lipopolysaccharide-induced Signal Transduction, Journal of Biological Chemistry. 274 (1999) 10689–10692.
[278] D. Hopwood, W. Slidders, G.R. Yeaman, Tissue fixation with phenol-formaldehyde for routine histopathology, Histochem J. 21 (1989) 228–234.
[279] M. V. Natu, H.C. de Sousa, M.H. Gil, Effects of drug solubility, state and loading on controlled release in bicomponent electrospun fibers, Int J Pharm. 397 (2010) 50–58. https://doi.org/10.1016/j.ijpharm.2010.06.045.
[280] S. Cao, Y. Jiang, H. Zhang, N. Kondza, K.A. Woodrow, Core-shell nanoparticles for targeted and combination antiretroviral activity in gut-homing T cells, Nanomedicine. 14 (2018) 2143–2153. https://doi.org/10.1016/j.nano.2018.06.005.
[281] W. Chen, A. Palazzo, W.E. Hennink, R.J. Kok, Effect of particle size on drug loading and release kinetics of gefitinib-loaded PLGA microspheres, Mol Pharm. 14 (2017) 459–467. https://doi.org/10.1021/acs.molpharmaceut.6b00896.
[282] N. Rasenack, B.W. Müller, Micron-Size Drug Particles: Common and Novel Micronization Techniques, Pharm Dev Technol. 9 (2004) 1–13. https://doi.org/10.1081/PDT-120027417.
[283] G.W. Radebaugh, J.L. Murtha, T.N. Julian, J.N. Bondi, Methods for evaluating the puncture and shear properties of pharmaceutical polymeric films, Int J Pharm. 45 (1988) 39–46.
[284] R.A. Sheth, S. Sabir, S. Krishnamurthy, R.K. Avery, Y.S. Zhang, A. Khademhosseini, R. Oklu, Endovascular Embolization by Transcatheter Delivery of Particles : Past , Present , and Future, (n.d.). https://doi.org/10.3390/jfb8020012.
[285] D. Carson, Y. Jiang, K. Woodrow, Tunable release of multiclass anti-HIV drugs that are water- soluble and loaded at high drug content in polyester blended electrospun fibers Daniel, Pharm Res. 33 (2016) 125–136. https://doi.org/10.1007/s11095-015-1769-0.
[286] A. Laurent, Microspheres and Nonspherical Particles for Embolization, Tech Vasc Interv Radiol. 10 (2007) 248–256. https://doi.org/10.1053/j.tvir.2008.03.010.
[287] C. Eddy, C. Pauerstein, Anatomy and Physiology of the Fallopian Tube, Clin Obstet Gynecol. 23 (1980) 1177–1193.
[288] T.G. Park, Degradation of poly(lactic-co-glycolic acid) microspheres: effect of copolymer composition, Biomaterials. 16 (1995) 1123–1130. https://doi.org/10.1016/0142-9612(95)93575-X.
[289] T. Wynn, Cellular and molecular mechanisms in fibrosis, Journal of Pathology. 214 (2008) 199–210. https://doi.org/10.1111/exd.14193.
[290] J. Bell, E. Liechty, I. Bergin, Animal models of contraception: utility and limitations, Open Access J Contracept. (2015) 27. https://doi.org/10.2147/oajc.s58754.

[291] F.J. Al-Saffar, H.N.H. Al-Ebbadi, Histomorphological and Histochemical Study of the Uterus of the Adult Guinea Pigs (Cavica porcellus), Indian J Sci Technol. 12 (2019) 01–09. https://doi.org/10.17485/ijst/2019/v12i46/148620.
[292] O. Shynlova, A. Dorogin, S.J. Lye, Stretch-induced uterine myocyte differentiation during rat pregnancy: Involvement of caspase activation, Biol Reprod. 82 (2010) 1248–1255. https://doi.org/10.1095/biolreprod.109.081158.
[293] R.S. Neuwirth, K. Ryu, R.M. Richart, Further studies on chemical closure of the Fallopian tubes in the monkey, Am J Obstet Gynecol. 119 (1974) 463–465.
[294] S. Humphreys, P. Routledge, The toxicology of silver nitrate, Adverse Drug React Toxicol Rev. 17 (1998) 115–143.
[295] J.T. Jensen, C. Hanna, S. Yao, E. Micks, A. Edelman, L. Holden, O.D. Slayden, Blockade of tubal patency following transcervical administration of polidocanol foam: initial studies in rhesus macaques, 89 (2015) 540–549. https://doi.org/10.1016/j.contraception.2013.11.017.Blockade.
[296] J.T. Jensen, M.I. Rodriguez, Transcervical polidocanol as a nonsurgical method of female sterilization : a pilot study, 70 (2004) 111–115. https://doi.org/10.1016/j.contraception.2004.03.005.
[297] J.T. Jensen, C. Hanna, S. Yao, E. Thompson, C. Bauer, O.D. Slayden, Transcervical administration of polidocanol foam prevents pregnancy in female baboons, Contraception. 94 (2016) 527–533. https://doi.org/10.1016/j.contraception.2016.07.008.
[298] S.L. Shenoy, W.D. Bates, H.L. Frisch, G.E. Wnek, Role of chain entanglements on fiber formation during electrospinning of polymer solutions: Good solvent, non-specific polymer-polymer interaction limit, Polymer (Guildf). 46 (2005) 3372–3384. https://doi.org/10.1016/j.polymer.2005.03.011.
[299] O. Veiseh, J.C. Doloff, M. Ma, A.J. Vegas, H. Hei, A.R. Bader, J. Li, E. Langan, J. Wyckoff, W.S. Loo, S. Jhunjhunwala, A. Chiu, S. Siebert, K. Tang, S. Aresta-dasilva, M. Bochenek, J. Mendoza-elias, Y. Wang, M. Qi, D.M. Lavin, M. Chen, N. Dholakia, I. Lacík, G.C. Weir, J. Oberholzer, D.L. Greiner, Size- and shape-dependent foreign body immune response to materials implanted in rodents and non-human primates, 14 (2015) 643–651. https://doi.org/10.1038/nmat4290.Size-.
[300] J.L. Hernandez, J. Park, S. Yao, A.K. Blakney, H. v. Nguyen, B.H. Katz, J.T. Jensen, K.A. Woodrow, Effect of tissue microenvironment on fibrous capsule formation to biomaterial-coated implants, Biomaterials. 273 (2021) 120806. https://doi.org/10.1016/j.biomaterials.2021.120806.
[301] ParaGard ® T 380A Intrauterine Copper Contraceptive, n.d.
[302] B. Young Holt, J.A. Turpin, J. Romano, Multipurpose Prevention Technologies: Opportunities and Challenges to Ensure Advancement of the Most Promising MPTs, Frontiers in Reproductive Health. 3 (2021). https://doi.org/10.3389/frph.2021.704841.

[303] A. Nokhodchi, S. Raja, P. Patel, K. Asare-Addo, The role of oral controlled release matrix tablets in drug delivery systems, BioImpacts. 2 (2012) 175–187. https://doi.org/10.5681/bi.2012.027.
[304] A. Akil, B. Devlin, M. Cost, L.C. Rohan, Increased dapivirine tissue accumulation through vaginal film codelivery of dapivirine and tenofovir, Mol Pharm. 11 (2014) 1533–1541. https://doi.org/10.1021/mp4007024.
[305] A.S. Ham, L.C. Rohan, A. Boczar, L. Yang, K. W. Buckheit, R.W. Buckheit, Vaginal film drug delivery of the pyrimidinedione IQP-0528 for the prevention of HIV infection, Pharm Res. 29 (2012) 1897–1907. https://doi.org/10.1007/s11095-012-0715-7.
[306] M.E. Cam, A.N. Hazar-Yavuz, S. Cesur, O. Ozkan, H. Alenezi, H. Turkoglu Sasmazel, M. Sayip Eroglu, F. Brako, J. Ahmed, L. Kabasakal, G. Ren, O. Gunduz, M. Edirisinghe, A novel treatment strategy for preterm birth: Intra-vaginal progesterone-loaded fibrous patches, Int J Pharm. 588 (2020). https://doi.org/10.1016/j.ijpharm.2020.119782.
[307] N. Nematpour, P. Moradipour, M.M. Zangeneh, E. Arkan, M. Abdoli, L. Behbood, The application of nanomaterial science in the formulation a novel antibiotic: Assessment of the antifungal properties of mucoadhesive clotrimazole loaded nanofiber versus vaginal films, Materials Science and Engineering C. 110 (2020). https://doi.org/10.1016/j.msec.2020.110635.
[308] M.T.C. Mc Crudden, E. Larrañeta, A. Clark, C. Jarrahian, A. Rein-Weston, B. Creelman, Y. Moyo, S. Lachau-Durand, N. Niemeijer, P. Williams, H.O. McCarthy, D. Zehrung, R.F. Donnelly, Design, Formulation, and Evaluation of Novel Dissolving Microarray Patches Containing Rilpivirine for Intravaginal Delivery, Adv Healthc Mater. 8 (2019). https://doi.org/10.1002/adhm.201801510.
[309] J. das Neves, B. Sarmento, Precise engineering of dapivirine-loaded nanoparticles for the development of anti-HIV vaginal microbicides, Acta Biomater. 18 (2015) 77–87. https://doi.org/10.1016/j.actbio.2015.02.007.
[310] J. das Neves, F. Araújo, F. Andrade, M. Amiji, M.F. Bahia, B. Sarmento, Biodistribution and pharmacokinetics of Dapivirine-loaded nanoparticles after vaginal delivery in mice, Pharm Res. 31 (2014) 1834–1845. https://doi.org/10.1007/s11095-013-1287-x.
[311] L.M. Ensign, B.C. Tang, Y.-Y. Wang, T.A. Tse, T. Hoen, R. Cone, J. Hanes, Mucus-Penetrating Nanoparticles for Vaginal Drug Delivery Protect Against Herpes Simplex Virus, n.d. https://www.science.org.
[312] J.T. Clark, T.J. Johnson, M.R. Clark, J.S. Nebeker, J. Fabian, A.L. Tuitupou, S. Ponnapalli, E.M. Smith, D.R. Friend, P.F. Kiser, Quantitative evaluation of a hydrophilic matrix intravaginal ring for the sustained delivery of tenofovir, Journal of Controlled Release. 163 (2012) 240–248. https://doi.org/10.1016/j.jconrel.2012.08.033.
[313] A. Externbrink, K. Eggenreich, S. Eder, S. Mohr, K. Nickisch, S. Klein, Development and evaluation of accelerated drug release testing methods for a matrix-type intravaginal ring, European Journal of Pharmaceutics and Biopharmaceutics. 110 (2017) 1–12. https://doi.org/10.1016/j.ejpb.2016.10.012.

[314] I. Koutsamanis, A. Paudel, K. Nickisch, K. Eggenreich, E. Roblegg, S. Eder, Controlled-release from high-loaded reservoir- type systems—a case study of ethylene-vinyl acetate and progesterone, Pharmaceutics. 12 (2020). https://doi.org/10.3390/pharmaceutics12020103.
[315] W.W. Yang, E. Pierstorff, Reservoir-based polymer drug delivery systems, J Lab Autom. 17 (2012) 50–58. https://doi.org/10.1177/2211068211428189.
[316] M.B. Lowinger, S.E. Barrett, F. Zhang, R.O. Williams, Sustained release drug delivery applications of polyurethanes, Pharmaceutics. 10 (2018). https://doi.org/10.3390/pharmaceutics10020055.
[317] J.Y. Cherng, T.Y. Hou, M.F. Shih, H. Talsma, W.E. Hennink, Polyurethane-based drug delivery systems, Int J Pharm. 450 (2013) 145–162. https://doi.org/10.1016/j.ijpharm.2013.04.063.
[318] Development of a Hybrid Artificial Pancreas with a Dense Polyurethane Membrane, (n.d.).
[319] M.-C. Bé langer, Y. Marois, R. Roy, Y. Mehri, E. Wagner, Z. Zhang, M.W. King, M. Yang, C. Hahn, R. Guidoin, Selection of a Polyurethane Membrane for the Manufacture of Ventricles for a Totally Implantable Artificial Heart: Blood Compatibility and Biocompatibility Studies, 2000.
[320] K. Gorna, S. Gogolewski, Preparation, degradation, and calcification of biodegradable polyurethane foams for bone graft substitutes, 2003.
[321] B. Li, K. v. Brown, J.C. Wenke, S.A. Guelcher, Sustained release of vancomycin from polyurethane scaffolds inhibits infection of bone wounds in a rat femoral segmental defect model, Journal of Controlled Release. 145 (2010) 221–230. https://doi.org/10.1016/j.jconrel.2010.04.002.
[322] Q. Guo, P.T. Knight, P.T. Mather, Tailored drug release from biodegradable stent coatings based on hybrid polyurethanes, Journal of Controlled Release. 137 (2009) 224–233. https://doi.org/10.1016/j.jconrel.2009.04.016.
[323] E.H. Seo, K. Na, Polyurethane membrane with porous surface for controlled drug release in drug eluting stent, Biomater Res. 18 (2014). https://doi.org/10.1186/2055-7124-18-15.
[324] S.A.L. Moura, L.D.C. Lima, S.P. Andrade, A. da Silva-Cunha Junior, R.L. Órefice, E. Ayres, G.R. da Silva, Local drug delivery system: Inhibition of inflammatory angiogenesis in a murine sponge model by dexamethasone-loaded polyurethane implants, J Pharm Sci. 100 (2011) 2886–2895. https://doi.org/10.1002/jps.22497.
[325] P. Basak, B. Adhikari, I. Banerjee, T.K. Maiti, Sustained release of antibiotic from polyurethane coated implant materials, in: J Mater Sci Mater Med, 2009. https://doi.org/10.1007/s10856-008-3521-3.
[326] A. Martinelli, L. D'Ilario, I. Francolini, A. Piozzi, Water state effect on drug release from an antibiotic loaded polyurethane matrix containing albumin nanoparticles, Int J Pharm. 407 (2011) 197–206. https://doi.org/10.1016/j.ijpharm.2011.01.029.

[327] T.J. Johnson, K.M. Gupta, J. Fabian, T.H. Albright, P.F. Kiser, Segmented polyurethane intravaginal rings for the sustained combined delivery of antiretroviral agents dapivirine and tenofovir, European Journal of Pharmaceutical Sciences. 39 (2010) 203–212. https://doi.org/10.1016/j.ejps.2009.11.007.
[328] J.T. Su, S. Sung, P. Kulkarni, E. Draganoiu, P. Kiser, Permeability and Diffusion of Pharmaceuticals through Thermoplastic Polyurethanes, n.d.
[329] G. Verstraete, J. Van Renterghem, P.J. Van Bockstal, S. Kasmi, B.G. De Geest, T. De Beer, J.P. Remon, C. Vervaet, Hydrophilic thermoplastic polyurethanes for the manufacturing of highly dosed oral sustained release matrices via hot melt extrusion and injection molding, Int J Pharm. 506 (2016) 214–221. https://doi.org/10.1016/j.ijpharm.2016.04.057.
[330] Y. Jiang, S. Cao, D.K. Bright, A.M. Bever, A.K. Blakney, I.T. Suydam, K.A. Woodrow, Nanoparticle-Based ARV Drug Combinations for Synergistic Inhibition of Cell-Free and Cell-Cell HIV Transmission, Mol Pharm. 12 (2015) 4363–4374. https://doi.org/10.1021/acs.molpharmaceut.5b00544.
[331] Lubrizol LifeSciences, Solvent Effects Pathway™ TPU Excipients Overview, 2017.
[332] M. Shoaib, A. Bahadur, S. Iqbal, M.S.U. Rahman, S. Ahmed, G. Shabir, M.A. Javaid, Relationship of hard segment concentration in polyurethane-urea elastomers with mechanical, thermal and drug release properties, J Drug Deliv Sci Technol. 37 (2017) 88–96. https://doi.org/10.1016/j.jddst.2016.12.003.
[333] A. Baldan, Review Progress in Ostwald ripening theories and their applications to nickel-base superalloys Part I: Ostwald ripening theories, n.d.
[334] K. Tietz, S. Klein, In vitro methods for evaluating drug release of vaginal ring formulations—a critical review, Pharmaceutics. 11 (2019). https://doi.org/10.3390/pharmaceutics11100538.
[335] K.M. Gupta, S.M. Pearce, A.E. Poursaid, H.A. Aliyar, P.A. Tresco, M.A. Mitchnik, P.F. Kiser, Polyurethane intravaginal ring for controlled delivery of dapivirine, a nonnucleoside reverse transcriptase inhibitor of HIV-1, J Pharm Sci. 97 (2008) 4228–4239. https://doi.org/10.1002/jps.21331.
[336] M. Kaur, K.M. Gupta, A.E. Poursaid, P. Karra, A. Mahalingam, H.A. Aliyar, P.F. Kiser, Engineering a degradable polyurethane intravaginal ring for sustained delivery of dapivirine, Drug Deliv Transl Res. 1 (2011) 223–237. https://doi.org/10.1007/s13346-011-0027-1.
[337] D.J. Murphy, D. Lim, R. Armstrong, C.F. McCoy, Y.H.D. Bashi, P. Boyd, T. Derrick, P. Spence, B. Devlin, R.K. Malcolm, Refining the in vitro release test method for a dapivirine-releasing vaginal ring to match in vivo performance, Drug Deliv Transl Res. (2021). https://doi.org/10.1007/s13346-021-01081-7.
[338] J.L. Duda, Molecular diffusion in polymeric systems, 1985.
[339] L. Masaro, X.X. Zhu, Physical models of diffusion for polymer solutions, gels and solids, n.d.

[340] D.M. Moss, M. Siccardi, M. Murphy, M.M. Piperakis, S.H. Khoo, D.J. Back, A. Owen, Divalent metals and pH alter raltegravir disposition in vitro, Antimicrob Agents Chemother. 56 (2012) 3020–3026. https://doi.org/10.1128/AAC.06407-11.
[341] D. Zhou, Y. Qiu, Understanding Biopharmaceutics Properties for Pharmaceutical Product Development and Manufacturing II: Dissolution and In Vitro-In Vivo Correlation, 2010.
[342] Clinical Pharmacology & Biopharmaceutics Review, 2000.
[343] C. Celum, PrEP Adherence and Effect of Drug Level Feedback Among Young African Women in HPTN 082, in: 10th IAS Conference on HIV Science, Mexico City, 2019.
[344] A. Ferenczy, T.C. Wright, Anatomy and Histology of the Cervix, n.d.
[345] D.W. Ludovici, B.L. De Corte, M.J. Kukla, H. Ye, C.Y. Ho, M.A. Lichtenstein, R.W. Kavash, K. Andries, M.-P. De Be´thunebe´thune, H. Azijn, R. Pauwels, P.J. Lewi, J. Heeres, L.M.H. Koymans, M.R. De Jonge, K.J.A. Van Aken, F.F.D. Daeyaert, K. Das, E. Arnold, P.A.J. Janssen, Evolution of Anti-HIV Drug Candidates. Part 3: Diarylpyrimidine (DAPY) Analogues, n.d.
[346] L.C. Rohan, R.P. Edwards, L.A. Kelly, K.A. Colenello, F.P. Bowman, P.A. Crowley-Nowick, Optimization of the Weck-Cel Collection Method for Quantitation of Cytokines in Mucosal Secretions, 2000.
[347] C. Bauer, The baboon (Papio sp.) as a model for female reproduction studies, Contraception. 92 (2015) 120–123. https://doi.org/10.1016/j.contraception.2015.06.007.
[348] J.D. Bell, I.L. Bergin, M.F. Natavio, F. Jibrel, M.K. Zochowski, W.J. Weadock, S.D. Swanson, D.M. Aronoff, D.L. Patton, Feasibility of LNG-IUS in a baboon model, in: Contraception, 2013: pp. 380–384. https://doi.org/10.1016/j.contraception.2012.08.032.
[349] D.J. Anderson, J. Marathe, J. Pudney, The Structure of the Human Vaginal Stratum Corneum and its Role in Immune Defense, American Journal of Reproductive Immunology. 71 (2014) 618–623. https://doi.org/10.1111/aji.12230.
[350] A.M. Carias, T.J. Hope, Barriers of Mucosal Entry of HIV/SIV, Curr Immunol Rev. 15 (2018) 4–13. https://doi.org/10.2174/1573395514666180604084404.
[351] K.A. Woodrow, K.M. Bennett, D.D. Lo, Mucosal vaccine design and delivery, Annu Rev Biomed Eng. 14 (2012) 17–46. https://doi.org/10.1146/annurev-bioeng-071811-150054.
[352] D. Serfatyl, H. Yaneva, The Endometrium and the IUD Mechanism of Action of IUDS, n.d.
[353] NT Cu380 NT Cu380 Mini, n.d. www.besinshealthcare.ca.
[354] K. Heinemann, S. Reed, S. Moehner, T. Do Minh, Risk of uterine perforation with levonorgestrel-releasing and copper intrauterine devices in the European Active Surveillance Study on Intrauterine Devices, Contraception. 91 (2015) 274–279. https://doi.org/10.1016/j.contraception.2015.01.007.
[355] A. Nel, S. Smythe, K. Young, K. Malcolm, C. Mccoy, Z. Rosenberg, J. Romano, Safety and Pharmacokinetics of Dapivirine Delivery From Matrix and Reservoir Intravaginal Rings to HIV-Negative Women, J Acquir Immune Defic Syndr. 51 (2009) 416–423. www.jaids.com.

[356] P. Fletcher, S. Harman, H. Azijn, N. Armanasco, P. Manlow, D. Perumal, M.P. De Bethune, J. Nuttall, J. Romano, R. Shattock, Inhibition of human immunodeficiency virus type 1 infection by the candidate microbicide dapivirine, a nonnucleoside reverse transcriptase inhibitor, Antimicrob Agents Chemother. 53 (2009) 487–495. https://doi.org/10.1128/AAC.01156-08.
[357] M. Elstein, Cervical Mucus: Its Physiological Role and Clinical Significance, n.d.